UCLA
UCLA Electronic Theses and Dissertations

Title
Mechanisms of Phosphoinositide-Mediated Clathrin Adaptor Progression at the trans-Golgi Network

Permalink
https://escholarship.org/uc/item/4j69q4h0

Author
Daboussi, Lydia

Publication Date
2013

Peer reviewed|Thesis/dissertation

eScholarship.org Powered by the California Digital Library
University of California

UNIVERSITY OF CALIFORNIA
Los Angeles

Mechanisms of Phosphoinositide-Mediated Clathrin Adaptor Progression at the *trans*-Golgi Network

A dissertation submitted in partial satisfaction of the requirements for the degree Doctor of Philosophy in Biological Sciences

by

Lydia Daboussi

2013

ABSTRACT OF THE DISSERTATION

Mechanisms of Phosphoinositide-Mediated Clathrin Adaptor Progression at the *trans*-Golgi Network

by

Lydia Daboussi

Doctor of Philosophy in Biological Sciences

University of California, Los Angeles, 2013

Professor Gregory S. Payne, Chair

Clathrin-mediated trafficking is a conserved process during which clathrin coated vesicles transport cargo between the trans-Golgi Network (TGN) and the endosomes, and during the process of endocytosis. These studies identify a previously unrecognized sequence of assembly between adaptor-specific clathrin coated vesicles. At the TGN, we found that GGA-enriched vesicles form first, followed by the biogenesis of AP-1 enriched vesicles. We then identified the mechanism by which this process is temporally controlled. We have identified a novel direct physical interaction between the VHS domain of Gga2 and the yeast PI(4)-Kinase, Pik1p, that is important for the recruitment of Pik1p to the TGN membrane. Deletion of GGA proteins results in the delay of PI(4)P accumulation and Pik1p recruitment. Furthermore, we have mapped the regions through which Pik1p interacts with Gga2 and demonstrate that these binding sites are important for the Pik1p-GGA interaction in vivo. Disruption of these binding sites through mutation results in delayed PI(4)P accumulation, mislocalized Ent5p and delayed AP-1 recruitment. We also provide evidence that this Pik1/GGA interaction is regulated by GTP-

Arf1. Arf1 binds to the GAT domain of GGA2, enabling Pik1p to directly bind to the VHS domain of Pik1p. We also find that this network of physical interactions is conserved in mammals.

The dissertation of Lydia Daboussi is approved.

Alex Van der Bliek

Kelsey C. Martin

Carla Kohler

Gregory S. Payne, Committee Chair

University of California, Los Angeles

2013

This thesis is dedicated to my beautiful children and wonderful husband.

TABLE OF CONTENTS

Preface	List of Figures	viii
Preface	List of Tables	xi
Preface	Acknowledgements	xii
Preface	Vita	xiv
Chapter 1	Introduction	1
Chapter 2	Phosphoinositide-mediated clathrin adaptor progression at the *trans*-Golgi network	25
Chapter 3	Mapping of the Pik1 binding site to Gga2 VHS domain in vitro	51
Chapter 4	The *trans*-Golgi Network in *S. cerevisiae* shares characteristics with Early Endosomes	111
Chapter 5	Yeast Irc6p is a novel type of conserved clathrin coat accessory factor related to small G proteins	135
Chapter 6	Genome-wide analysis of AP-3-dependent protein transport in yeast	159
Chapter 7	Conclusions and future directions	177

LIST OF FIGURES

Figure 2-1	Sequential assembly of clathrin adaptors	28
Figure 2-2	Spatial relationships of clathrin adaptors by SIM.	30
Figure 2-3	Adaptor and clathrin dynamics at the TGN.	31
Figure 2-4	TGN PtdIns(4)P dynamics depend on Arf1p and Gga proteins.	32
Figure 2-5	Depletion of PtdIns(4)P alters localization of AP-1 and Ent5p.	33
Figure 2-6	Pik1p/Frq1p overexpression enhances co-localization of sequentially recruited clathrin adaptors with functional consequences.	34
Figure 2-7	Gga2p acts in Pik1p recruitment and binds Pik1p.	35
Figure 2-S1	GFP-Clc1p Chc1p-mRFP colocalize in living yeast cells and the distribution of peak to peak fluorescence times.	39
Figure 2-S2	Structured illumination microscopy of clathrin and clathrin adaptors.	40
Figure 2-S3	Deletion of the β1 subunit of AP-1 does not affect the relative assembly kinetics of Gga2p and Chc1p.	41
Figure 2-S4	Inactivation of Pik1p decreases PtdIns(4)P but not PtdIns(3)P levels.	42
Figure 2-S5	Clathrin adaptor localization in lipid kinase mutants.	43
Figure 2-S6	Complete autoradiographs and immunoblots used in Figures 6 and 7.	44
Figure 2-S7	Sequential adaptor-enriched clathrin-coated vesicle formation at the TGN.	45
Figure 3-1.	Predicted Domain Architecture of Pik1 and Pik1p fragments used for in vitro experiments	56
Figure 3-2	Pik1 283-300 interacts with the VHS domain in vitro.	57
Figure 3-3.	Pik1p (283-291) mediates an interaction with the VHS domain of Gga2p.	59
Figure 3-4	Pik1 286-291^{acidic} does not interact with the VHS domain	61
Figure 3-5	Strategy to introduce Pik1 286-291^{acidic} in vivo	62
Figure 3-6	Pik1p 286-291^{acidic} does not affect binding to Gga2p VHS in yeast extracts.	64
Figure 3-7	Constructs to identify a second Pik1p-VHS interaction site	65
Figure 3-8	Residues 220-230 of Pik1p interact weakly with the VHS domain of	67

	Gga2p	
Figure 3-9	Acidic mutations in Pik1p abolish interaction with the VHS domain.	68
Figure 3-10	Alanine mutations in Pik1p 218-220 and 224-226 reduce interaction with the VHS domain.	70
Figure 3-11	Alanine mutations are better than acidic mutations at parsing which Pik1p residues are important for VHS binding in Pik1 (218-221).	74
Figure 3-12	Alanine Screen through VBS1 reveals that basic residues are important forbinding to the VHS domain.	76
Figure 3-13	Single Amino Acid mutations to Alanine do not affect VBS2 binding to the VHS domain.	78
Figure 3-14	Pik1^{GGA} exhibits reduced binding to the VHS domain	80
Figure 3-15	Introduction of *pik1^{GGA}* inhibits growth	81
Figure 3-16	Pik1^{GGA} causes a delay in PI4P accumulation,and AP-1 recruitment	84
Figure 3-17	pik1p^{GGA} causes Ent5p mislocalization	86
Figure 3-18	Both VHS and VHS-GAT domains bind to Pik1p	88
Figure 3-19	The VHS domain of Gga2p interacts more robustly with Pik1 than does the VHS-GAT domain.	89
Figure 3-20	VHS and GAT domains of Gga2 interact in vitro in *S. cerevisiae*	90
Figure 3-21	Gga2 VHS domain interacts with its GAT domain in trans from *mus musculus*	91
Figure 3-22	GTP-Arf1p enhances the interaction between VHS-GAT of Gga2p and Pik1p	92
Figure 3-23	PI4KIIIb interacts with the VHS domain of Gga2 in *M. musculus*	94
Figure 4-1	Model of Mup1p-pHluorin transport to the vacuole	114
Figure 4-2	Mup1p-Phluorin colocalizes with Gga2p-mRFP	119
Figure 4-3	Mup1p-Phluorin that colocalizes with Gga2-mRFP originates from biosynthetic events	122
Figure 4-4	Abp1p positive puncta are transported towards Gga2p positive	123
Figure 4-5	Gga2p positive puncta are transported towards Abp1p positive puncta	125
Figure 5-1	Irc6p function is associated with clathrin-mediated transport between the TGN and endosomes	139
Figure 5-2	A G-like domain in Irc6p	141
Figure 5-3	Mammalian p34 substitutes for Irc6p in vivo.	143
Figure 5-4	The Irc6/p34 G-protein–like family	144
Figure 5-5	Irc6p physically interacts with AP complexes and Rab proteins	145
Figure 5-6	Irc6p functionally interacts with Ypt31p	146
Figure 5-7	Irc6p links Ypt31p to AP-1	147
Figure 5-S1	Irc6p does not function in AP-2-dependent endocytosis	151
Figure 5-S2	Irc6p contains a novel G-like domain	152
Figure 5-S3	Mammalian p34 has a predicted N-terminal Rossmann-fold domain, can be expressed in yeast and binds yeast AP-1 and AP-2	153
Figure 6-1	Example of results from analysis of ALP maturation instrains from the *MAT*a deletion library	165
Figure 6-2	Specific defect in ALP transport in *yck3*Δ cells. (A) Pulsechaseimmunoprecipitation of ALP	166

Figure 6-3	Mislocalization of GFP-ALP in *yck3*Δbut not *vac17*Δcells	167
Figure 6-4	Selective defects in type II membrane protein transportin *svp26*Δcells	167
Figure 6-5	ALP and CPS maturation is delayed in *vac8*Δand *vac17*Δcells	168
Figure 6- 6	Accumulated pALP in *vac17*Δcells matures after 120 min delay	169
Figure 6-7	Model for Yck3p function	169
Figure 6-S1	*Overexpression of VPS41 does not rescue the ALP maturation defect in yck3Δ cells*	174

LIST OF TABLES

Table 2-1	Dynamics of clathrin adaptors, phosphoinositide binding reporters and Golgi markers at the TGN	29
Table 2-2	List of strains used in this study	49
Table 2-3	List of Primers used in study	51
Table 3-1	List of strains used in this study	104
Table 3-2.	List of Plasmids used in this study	105
Table 4-1	Strain Table	128
Table 5-1	Data collection, processing, and refinement statistics	140
Table 5--S1	P-loop NTPase/adaptin-binding family	154-155
Table 5-S2	Strains used in this study	156-157
Table 6-1	ALP maturation defects in strains from gene deletion libraries	164

ACKNOWLEDGEMENTS

I would like to thank my mentor Gregory S. Payne, first for taking me as a rotation student when he wasn't planning on taking any students that year. And second, for letting me join his lab. The Payne Lab has been a fantastic place to learn science. I'm really grateful that his creativity and nose for a good project. I'm really happy that he let me work on this microscopy project during my rotation, and then continue on it during the duration of my time in his lab. I'm really grateful that I started out with a mentor who is careful, detailed orientated and crazy about controls.

The department of Biological Chemistry has been a wonderful, collaborative space to talk with collegues about science. I'm really grateful for the opportunities to present that I've been given. They've really helped me to be a better scientist.

The technical support staff at 3i have made my ability to do microscopy so much easier

Ric Grambo for all of his help in figuring out how to make figures. Without Ric, I wouldn't have been able to make the supplementary movies for Chapter 2 in which the arrows follow the puncta through time. I really his support with Adobe and the BCIF, without which I would not have any data.

I'd like to thank Esteban Fernandez for training me on the microscope and sitting with me in the dark room speculating on whether AP-1 and GGA puncta were showing any interesting dynamics.

Toh Hean has helped me so many times fix the microscope when things weren't working, and let me complain indefinitely when components couldn't easily be fixed. We serendipitously co-hosted Roger Y. Tsien in 2006, and we've been working together to train users on the microscope ever since.

I would like to especially thank Giancarlo Costaguta for first being such a wonderful person to be around in lab, then for being such a wonderful husband and father.

I would like to thank Isabella Costaguta for keeping me young with her late nights, early mornings, and no slowing down attitude. She is always the high point of my day (and frequently the high point of my middle of the night).

I'd also like to thank my parents for teaching me to count ants in line, teeth on a fish and clouds in the sky. Thank you for taking me to eat breakfast in the parks on weekends and never squelching my love of Disney. Most of all, thank you for believing in my ability to be a scientist.

Chapter 2 is reprinted from *Nature Cell Biology* (volume 14, February 2012, pages 239-248) with permission from Nature Publishing Group

Chapter 5 is reprinted from *Molecular Biology of the Cell* (volume 23, November 2012, pages 4416-4429) with permission from the American Society for Cell Biology

Chapter 6 is reprinted from *Molecular Biology of the Cell* (volume 20, March 2009, pages 1592-1604) with permission from the American Society for Cell Biology

VITA

September, 2001 - June, 2005	Stanford University B.S. in Biological Sciences with Honors
September, 2010 - June, 2011	Dissertation Year Fellowship, University of California, Los Angeles
September, 2006 - June, 2010	NIH T32 Genetics Training Grant, University of California, Los Angeles
June, 2005	Lauren D. Weinstein Award, for undergraduate instruction of a course, Stanford University
June, 2004 - September 2004	Howard Hughes Summer Research Fellowship, Stanford University

PUBLICATIONS AND PRESENTATIONS

Daboussi, L., Costaguta, G. and Payne, G.S. (2012) Phosphoinositide-mediated clathrin adaptor progression at the trans-Golgi network. Nature Cell Biol., 14(3):239-48

Anand, V.C., Daboussi, L., Lorenz, T.C. and Payne, G.S. (2009) Genome-wide Analysis of AP-3-dependent Protein Transport in Yeast. Mol. Biol. Cell 20: 1592-1604

Gorynia S., Lorenz T.C., Costaguta G., Daboussi L., Cascio D., and Payne G.S. (2012) Yeast Irc6p is a novel type of conserved clathrin accessory factor related to G proteins. Mol. Biol. Cell.

Daboussi L., Ghukasian R., Costaguta G., Payne G.P. (2012) *Mechanisms regulating PtdIns(4)phosphate-mediated clathrin adaptor progression at the TGN*. Gordon Research Conference- Lysosomes and Endocytosis (Oral Presentation)

Daboussi L., Costaguta G., Payne G.P. (2012) Phosphoinositide-mediated clathrin adaptor progression at the *trans* Golgi network. Sigman Symposium, UCLA. (Poster Presentation)

Daboussi L., Costaguta G., Payne G.P. (2010) *PI4P Controls Sequential Assembly of Clathrin Adaptors at the TGN*. Gordon Research Conference-Lysosomes and Endocytosis. (Poster Presentation)

Daboussi L., Costaguta G., Payne G.P. (2009) *Dynamics of Clathrin Coat Assembly at the TGN in S. cerevisiae.* The American Society for Cell Biology (Poster Presentation)

Chapter 1

Introduction

Abstract:

In eukaryotic cells, clathrin-coated vesicles (ccvs) mediate trafficking at the plasma membrane during the process of endocytosis and between the trans-Golgi network and endosomes. Clathin is a conserved protein as are the adaptor proteins which facilitate ccv biogenesis. There are two main intracellular clathrin adaptors, the monomeric GGA proteins and the heterotetrameric complex AP-1. Each of these proteins share some recruitment factors, but are recruited to membranes by distinct mechanisms. Both of these adaptors play important roles in mediating cell polarity and development. Aberrant function of AP-1 and GGA can result in developmental defects and lethality.

Introduction:

A major form of membrane trafficking in the endocytic and secretory systems is mediated by clathrin. Clathrin assembles into triskelia, each one composed of three clathrin heavy chains (Chc1p) and three clathrin light chains (Clc1p). These triskelia then in turn assemble into higher order hexagons and pentagons which form the outer coat of the vesicle (McMahon and Boucrot, 2011). In mammalian cells, the ratio of heavy chains to light chains in some cases may be greater than 1:1 (Girard et al., 2005). However, this point is still under debate. In vertebrates, a recent duplication of the clathrin heavy chain gene generated CHC17 and CHC22 (named for the chromosome on which they were located). CHC17 is ubiquitously expressed, while CHC22 is expressed in muscle tissues. In mammals, CHC17 forms several types of structures at cellular membranes, as determined by electron microscopy and fluorescence microscopy (Brodsky, 2012; Saffarian et al., 2009). The best characterized structures are 80-200nm coated vesicles at the plasma membrane. The second, more recently

identified structures are larger flat lattices found on the basal surface of attached cells in culture (Saffarian et al., 2009). The physiological function of these large lattices is still under debate ((den Otter and Briels, 2011; Heuser et al., 1987)).

Clathrin can form a wide variety of cage types in vitro and in vivo, but it does not have affinity for membranes on its own. Clathrin requires several additional factors for ccv biogenesis. Some of these additional factors, known as adaptor proteins, serve as a link between clathrin and the membrane and provide additional specificity for location of the clathrin coat. These adaptor proteins also recruit accessory factors required for membrane invagination, vesicle scission and vesicle uncoating (Traub, 2005). The process of clathrin-mediated endocytosis is well characterized compared to the intracellular trafficking pathways which rely on clathrin. However, several recent studies have revealed new insights into the molecular mechanisms of clathrin trafficking between the TGN and endosomes, including mechanisms of adaptor recruitment, and how adaptor proteins mediate cell polarity and cell development (Reales et al., 2011; Ren et al., 2012; Shafaq-Zadah et al., 2012; Xu et al., 2012). New research detailing how aberrant trafficking results in humoral response defects, tissue deformation, and lethality is also now available (Schreiner et al., 2010; Takahashi et al., 2011; Xu et al., 2012). The fidelity of membrane trafficking supports the integrity of membrane bound organelles, thereby contributing to the health of the cell, tissue and general organization of the cell (Mellman and Nelson, 2008; Schreiner et al., 2010). This chapter will focus on the factors that contribute to normal clathrin adaptor localization, proper ccv biogenesis and the abnormalities observed in tissues and organisms that arise when these processes are disrupted.

An Introduction to AP-1

There are five adaptor protein complexes in mammals: AP-1, A(Gan et al., 2002)P-2, AP-3, AP-4, and AP-5 (Canagarajah et al., 2013). Only AP-1, AP-2, and possibly AP-3 interact with clathrin in mammals (Canagarajah et al., 2013). In yeast, there are three AP complexes: AP-1, AP-2, and AP-3. Only AP-1 and AP-2 interact with clathrin (Vowels and Payne, 1998; Yeung et al., 1999). All AP complexes are heterotetrameric complexes composed of four subunits: two large subunits (β1-β5; α/ γ/ε/δ/ζ), one medium subunit (μ1-μ5), and one small subunit (σ1-σ5). In the case of yeast AP-1, two genes encode μ1 isoforms, (Yeung et al., 1999) . These two alleles of the μ-adaptin of AP-1 subunit are conserved in mammals and the AP-1 complex is then termed AP-1A and AP-1B as determined by the incorportation of either the μ1A or μ1B subunit. Although, these two μ-adaptin subunits share 80% sequence identity, in mammals they mediate differential AP-1 localization, and cargo binding profiles of the AP-1 complex. AP-1A is ubiquitously expressed, and AP-1B is expressed in epithelial cells (Boehm and Bonifacino, 2002; Folsch et al., 2003; Ohno et al., 1999). The β and γ subunits contain appendage or 'ear' domains which interact with accessory factors that are important for ccv biogenesis. Accessory factors participate in membrane invagination, vesicle scission and vesicle uncoating (Duncan and Payne, 2003; Owen et al., 1999). The ear domains of the β1 and γ1 subunits of AP-1 both directly bind to clathrin through clathrin box motifs however only the β1 subunit interacts with clathrin through motifs that are also present in the hinge region. The core domain of AP-1 interacts with ARF, lipids and cargo.

AP-1 Localization Factors

Several factors are known to be important for localization of AP-1 to the TGN. These factors include Arf1p which interacts with β1 subunit in the AP-1 core, and recently has been shown in a crystal structure to also potentially interact with the γ subunit (Ren et al., 2012). Brefelden A, inhibits Arf GTP exchange activity, redistributing AP-1 from the TGN to the cytosol (Donaldson et al., 1992; Fernandez and Payne, 2006; Stamnes and Rothman, 1993). Amazingly, comparable phenotypes can be detected in whole animals. In vivo application of BFA in awake rats disrupts AP-1- dependent synaptic vesicle budding (Körber et al., 2012). Arf1 may not be the only Arf molecule required for proper AP-1 recruitment. Two other molecules have recently been implicated. First, depletion of Arf6, like depletion of AP-1B, results in missorting of AP-1B dependent cargo, implying that Arf6 may play a role in localizing AP-1B (Shteyn et al., 2011). Second, the Arf1-like protein, Arfrp1 directly interacts with AP-1 through the μ1 subunit and also recruits AP-1 to liposomes in vitro (Yusong et al., 2013).

There are also factors other than ARF which play essential roles in AP-1 localization. In yeast, Laa1p was identified as an AP-1 interacting factor essential for AP-1 localization in cells at high density (post-diauxic shift). Interestingly, Laa1p localization is reliant on ARF function, suggesting that Laa1p and ARF coordinate to regulate AP-1 localization (Fernandez and Payne, 2006). PI(4)P is also a crucial determinant for AP-1 localization to membranes in vivo and to liposomes in vitro. (Daboussi et al., 2012; Ren et al., 2012; Wang et al., 2003).

In addition to those factors most studied, recent evidence has emerged for localization factors that are shared between AP-1 and AP-2. One such family of proteins is the amphiphysin proteins; largely characterized as functioning at the plasma membrane. However, recent studies

have implicated amphiphysin in AP-1 recruitment to membranes. AP-1 stabilization on liposomes was shown to depend on purified amphiphysin 2 or amphiphysin 1 / 2 heterodimer. A physical interaction between AP-1 and amphiphysin could also be detected in vivo, after crosslinking (Huser et al., 2013). Future experiments need to be conducted with respect to whether this protein has the potential to localize AP-1 at the TGN and endosomes but this work has alluring possibilities for function in vivo.

AP-1 Accessory Factors

Several AP-1 accessory factors have been described through the years and are reviewed in (Duncan and Payne, 2003). Recently identified AP-1 interacting factors facilitate AP-1 ccv biogenesis and their absence has consequences on sorting of AP-1 cargo. Eps15, one such factor that normally functions with AP-2 in endocytosis was localized to the TGN (Ioannou and Marat, 2012). It also contains a binding site that is specific for AP-1 (and not AP-2) as determined by co-immunoprecipitation from cell extracts. Expression of Eps15 that contained a mutant AP-1 binding region resulted in a decrease of protein secretion from the TGN (Chi et al., 2008). Additionally, a flurry of recent papers have identified the AP-1 accessory factor, Irc6p. This protein is conserved from yeast (Irc6p) to humans (p34) and has been implicated as an important regulator of AP-1 trafficking. In humans, mutations in p34 causes keratodermia, a skin disorder with manifestations typically on palms and soles with varying severity. (Babu et al., 2012; Gorynia et al., 2012; Pohler et al.).

AP-1: Role in Development

AP-1 plays an essential role during the development of higher order eukaryotes. In mice, loss of the μ1A or γ subunits results in embryonic lethality, (Meyer et al., 2000; Zizioli et al.,

1999) presumably because μ1A and γ are essential for the stable assembly of the AP-1 complex. In fact, in the absence of μ1A the remaining AP-1 subunits fail to localize to the TGN, suggestive of an AP-1 complex that is not formed or is not functional. (Meyer et al., 2000). While the absence of an entire subunit affects the assembly of the whole AP-1 complex, milder mutations can be tolerated. In humans a premature stop codon in the σ subunit of AP-1 can be viable, but results in mental retardation, enteropathy, deafness, peripheral neuropathy, ichthyosis, and keratodermia (Montpetit et al., 2008).

The absence of AP-1B, which is specifically expressed in epithelial cells, has differing consequences. Knockdown of the epithelial specific μ1B is not lethal in mice (Takahashi et al., 2011). Nevertheless, disruption of AP-1B in polarized epithelial cells that cover the intestinal mucosal surface results in several phenotypes. In these cells lacking AP-1B the cytokine receptors that are dependent on AP-1B for normal trafficking to the basolateral surface are misdirected to the apical plasma membrane resulting in colitis (Takahashi et al., 2011). In addition to aberrant trafficking in the intestine, AP-1B has also been implicated in normal kidney function and development (Schreiner et al., 2010).

The requirement of AP-1 for normal development of multicellular organisms is conserved in metazoans. In *C. elegans*, AP-1 deficiency results in embryonic lethality (Shim et al., 2000). In *D. melanogaster* the exact phenotypic consequences of deleting AP-1 are not known during embryogenesis. However, there are some clues that AP-1 does play a significant role in development. For example, AP-1 deficiency in ommitidia during development results in aberrant Notch signaling, causing a disordered array of photoreceptor neurons, and aberrant ommatidia formation (Kametaka et al., 2012).

AP-1: Role in Cell Polarity

Establishment and maintenance of cellular polarity is generated through the polarized sorting of proteins and lipids, primarily from intracellular organelles to the plasma membrane (Ang et al., 2004; Griffiths and Simons, 1986). The role that trafficking proteins play in the transport of polarity modules is beginning to be understood. Several proteins that are transported to the basolateral surface of epithelial cells do so through canonical AP sorting motifs such as YXXφ, NPXY, and di-hydrophobic based sorting signals (Bonifacino, 2003; Mellman and Nelson, 2008). This raises the possibility that a clathrin-dependent sorting mechanism might be involved in the polarization of these proteins. Indeed it has been established that clathrin is critical for proper maintenance of basolateral polarity in MDCK cells (Deborde et al., 2008). AP-1 has also been identified in several studies as an important regulator of cell polarity. (Gravotta et al., 2012; Xu et al., 2012; Zhang et al., 2012).

Both AP-1A and AP-1B play roles in establishing cell polarity. AP-1A is ubiquitously expressed in mammals and localizes to both the TGN and to a post TGN compartment (Boehm and Bonifacino, 2002; Folsch et al., 2003). Depletion of AP-1A can missort basolateral proteins from the TGN into the sorting endosome in MDCK cells (Reales et al., 2011). The coxsackie adenovirus receptor (CAR) is normally sorted to the basolateral membrane where it interacts with junctional adhesion molecule L, which facilitates tight junction integrity (Verdino et al., 2010; Witherden et al., 2010). CAR is sorted to the basolateral membrane via a YXXφ motif that interacts with AP-1A (Witherden et al., 2010). Depletion of AP-1A causes a concomitant mislocalization of this cargo protein, which has potential consequences for the integrity of tight junctions (Carvajal-Gonzalez et al., 2012). In rat hippocampal neurons µ1A plays a direct role in

the selective delivery of cargo to dendrites, inhibiting delivery to the axons. Various transmembrane receptors are sorted by recognition of sorting signals in the cytosolic domains by the μ1A subunit AP-1 complex. Mutation of the μ1A subunit affects dendritic spine morphology and decreases the number of synapses (Farias et al., 2012).

The AP-1B adaptor complex is specifically expressed in polarized epithelial cells and also plays a role in maintaining apical-basolateral polarity (Ohno et al., 1999). Current genetic and biochemical data support a model in which AP-1B sorts cargo from a recycling endosome to the basolateral surface of polarized epithelial cells by recognizing tyrosine based motifs (Fölsch et al., 1999; Ohno et al., 1999). Cells which lack μ1B, missort AP-1B cargo to the apical surface. Interestingly, expression of exogenous μ1B in LLC-PK1 cells, which lack μ1B, is sufficient to reroute LDLR and TfR from the apical to the basolateral membrane of the cell (Gan et al., 2002).

The PAR protein module is one of three protein modules critical for apical-basal polarity (St Johnston and Ahringer, 2010). The PAR module is composed of PAR-3/PAR-6/PKC-3 (aPKC) and localizes to the apical domain of polarized cells. In *C. elegens,* the role that clathrin-mediated trafficking plays in the localization of these polarity modules was difficult to ascertain because AP-1 is required for viability (Shim et al., 2000). To identify the pathways affected during development, two organs have been well studied: the intestine, and the brain. First, in the intestine, depletion of AP-1 affects the maintenance of the lumen and the proper localization of the PAR-3 polarity protein (Zhang et al., 2012). Another member of the aPKC module, PAR-6, was also recently found to be mislocalized to the basal surface when AP-1 is depleted in the intestine (Shafaq-Zadah et al., 2012). These results support the idea that AP-1 is important for

mediating polarized exocytosis to the apical membrane, and also plays a role in the localization of polarity modules in polarized epithelia.

Second, during neuron formation in *C. elegans,* depleting AP-1 leads to the disorganization of neuronal tissue. Evidence now supports the idea that AP-1 is an important trafficking factor in maintaining basal cell polarity of dendritically polarized receptors in interneurons. AP-1 plays a role in enabling proper cilium structure and function, and cooperates with RAB-8 to coordinate distinct steps in neuronal ciliary membrane sorting and trafficking (Dwyer et al., 2001; Kaplan et al., 2010). The absence of AP-1 redistributes AP-1 dependent receptors between the axons and the dendritic compartments (Margeta et al., 2009). This mechanism seems largely conserved through metazoans, as recent studies have confirmed similar finding in mouse neurons as well (Farias et al., 2012).

Polarization of cells relies heavily on the effective sorting of cargo from intracellular organelles to the correct membrane surface. Clathrin and AP-1 play an important role in the polarized trafficking of polarity modules, and components needed for tight junctions among several other types of cargo. The correct localization of these proteins have a significant impact on tissue morphology, ultimately affecting the development of the organism being examined.

AP-1: Implications for Disease

The human immunodeficiency virus (HIV) establishes chronic infection by evading the host immune system through the suppression of CD4. HIV-1 Nef protein is believed to contain several protein-protein interaction domains which enable the downregulation of MHC-I and CD4 (Aiken et al., 1994; Fölsch et al., 1999; Greenberg et al., 1998; Mangasarian et al., 1999). Nef has been shown to escape antigen presentation in HIV-infected primary T-cells by the

recruitment of AP-1 to the cytosolic tail of MHC-I. This interaction is important for routing biosynthetic MHC-I from the TGN into the endolysosomal pathway where it is eventually degraded (Roeth et al., 2004). Recently a noncanonical hydrophobic motif in Nef has been identified as important critical for binding to μ1A (Iijima et al., 2012).

Another recent study has implicated AP-1 in the lysosomal targeting of Niemann-Pick type C 1 and 2 (NPC1, and 2). Mutation in NPC1 or NPC2 genes results in the accumulation of cholesterol and glycosphingolipids in the late endosomes/lysosomes. In humans, this can result in a fatal neurodegenerative disorder (Poirier et al., 2013).

AP-1, and AP-3, have also been implicated in the trafficking of Batten disease protein, CLN3. Batten disease is a severe neurodegenerative disorder and the most common cause of juvenile dementia. Despite the conservation of CLN3 from yeast to humans, the exact function is not known. It is best characterized by a predominant localization in the vacuole/lysosome. Interesting, both AP-1 and AP-3 interact with distinct dileucine motifs present in CLN3 that are required for proper CLN3 sorting to the lysosome in mouse fibroblasts (Kyattala et al., 2005; Kyttala et al., 2004) .

An Introduction to GGA:

The Golgi-localized γ-ear containing ARF binding protein (GGA) proteins were initially identified based on sequence homology to the γ1-adaptin subunit of AP-1 (Dell'Angelica et al., 2000; Hirst et al., 2000) . GGA proteins are monomeric clathrin adaptors that participate in CCV formation and are conserved among eukaryotic organisms. *S. cerevisiae* express two GGA proteins (Gga1p, and Gga2p), *Drosophila* have only a single GGA protein and mammalian cells express three GGA proteins (Gga1-3) (Dell'Angelica et al., 2000; Kametaka et al., 2010). Each

of the GGA proteins have similar architectures. The amino terminal VHS domain (VPS27, HRS, STAM) mediates binding to cargo proteins, and in yeast interacts with PI(4)P (Demmel et al., 2008). The central GAT domain (GGA and Tom1) interacts with GTP bound Arf1. Importantly, the GAT domain is also involved in membrane association and recognizes Ubiquitin as a mechanism to sort cargo (Puertollano and Bonifacino, 2004) (Scott et al., 2004; Shiba et al., 2004). The hinge and C-terminal 'ear' regions of GGA contain binding motifs for clathrin, the γ-ear of AP-1 and the epsin-like adaptors (Costaguta et al., 2001; Duncan and Payne, 2003).

GGA enriched CCVs have been localized to the TGN by immunoelectron microscopy (Doray et al., 2002). Most genetic and biochemical data suggests that GGAs have roles in cargo packaging into ccvs which bud from the TGN and deliver cargo to either early or late endosomes (Black and Pelham, 2000; Costaguta et al., 2001; Puertollano et al., 2001). In yeast, there is also evidence that GGA participates in forward traffic from the TGN to late endosomes (Deng et al., 2009). GGA proteins are generally thought to be involved solely in clathrin coated vesicle formation, however there are some exceptions. GGA1 has also been found on tubular-vesicular structures emanating away from the TGN into the cytoplasm where they presumably interact with endosomes in mammalian cells (Puertollano et al., 2003). There may be some instances in which GGA does not participate in forward trafficking from the TGN, recently GGA3 was localized to recycling endosomes (RE) and shown to play a role in the recycling of at least some receptors between RE and the plasma membrane (Parachoniak et al., 2011).

GGA: Recruitment Factors

A network of complex interactions is important for proper GGA localization. In mammalian cells, membrane association of GGA is believed to occur through the GAT domain

interacting with PI(4)P (Wang et al., 2007). PI(4)P is enriched at the Golgi and acts a regulator of GGA recruitment in animal cells (Behnia and Munro, 2005; Carlton and Cullen, 2005). Residues R276, R281 and Y310 are particularly important for mediating interaction with PI(4)P, when these residues are mutated, GGA is partially defective in its recruitment to the TGN (Wang et al., 2007). There are also additional modes through which GGA proteins interact with PI(4)P. In yeast, PI(4)P has been implicated in Gga2 recruitment to membranes through a low affinity interaction between the lipid and the N-terminal VHS domain. In vitro, Gga2 recruitment to liposomes is stimulated by the addition of PI(4)P as well as the addition of GTP-bound Arf1p. (Demmel et al., 2008). In yeast, Arf1p plays a role, but is not essential for GGA recruitment. GGA in the presence of Brefelden A is still localized to the TGN (Fernandez and Payne, 2006). In mammals Arf plays a more critical role in GGA localization (Boman et al., 2000; Takatsu et al., 2002).

Other interactions have also been identified as important for GGA localization. Gga recruitment relies on a network of interactions between the scaffold Ysl2p/Mon2p, Arl1, and the lipid flippase Neo1p. Ysl2/Mon2 functions at the TGN in the maintenance of vacoule integrity (Jochum et al., 2002). Deletion of either Ysl2/Mon2 or Arl1 mislocalizes Gga2p. Gga2p's dependency on these proteins for correct localization is conserved in humans (Singer-Kruger et al., 2008).

Another contributing factor for GGA localization are the cargo proteins present at the TGN. Cargo proteins have been shown to be important in a somewhat dose dependant manner for GGA recruitment in animal cells (Hirst et al., 2007).

GGA proteins: A Role in Development

Gga proteins are important adaptors for many cargo proteins that traffic between the TGN and endosomes in *S. cerevisiae*, *D. melanogaster* and mammals. Recent work has begun to characterize the molecular mechanisms that GGA orchestrates and the developmental defects observed in the absence of GGA.

In *S. cerevisiae* deletion of either *GGA1* or *GGA2* leads to minor defects due to cargo rerouting. However, combining both deletions impairs proteolytic processing of the inactive precursors of the vacuolar hydrolases caryboxypeptidase Y (CPY) and carboxypeptidase S (Bonifacino, 2004). These phenotypes denote defective transport from the TGN to the vacuole. Additionally, in yeast GGA proteins directly interact with, and are important for localization of the yeast PI4Kinase, Pik1p. Pik1p is an essential gene, and is critical for anterograde trafficking from the TGN (Hama et al., 1999; Walch-Solimena and Novick, 1999). Deletion of the GGA genes results in the delayed recruitment of Pik1p to the TGN, resulting in the delayed accumulation of PI(4)P. Depletion of PI(4)P has several strong consequences for secretion, cell polarization and cell growth (Hama et al., 1999)

The requirement for GGA proteins during development varies by organism. In *D. melanogaster,* the literature is conflicting as to the requirement of GGA. Knockdowns of dGGA using RNAi generate conflicting results ranging from complete lethality, semi-lethality to no obvious phenotypes, or defects in viability or fertility (Eissenberg et al., 2011; Hirst and Carmichael, 2011; Kametaka et al., 2012). A recent study tried to address this variability by generating two null alleles of dGGA, the first by P-element excision and a second through targeted homologous recombination. Both of these independently generated dGGA null flies

were viable and showed no obvious fertility defects. There were however more subtle phenotypes, such as hypersensitivity to dietary chloroquine (an indication that the lysosome is not properly mediating proteolysis). This phenotype is in agreement with the function of mammalian and yeast GGA.

Despite the resilience of *D. melanogaster*, disruption of GGA in mammals can result in severe phenotypic consequences. GGA2 null mice showed high rates of embryonic or neonatal lethality (depending on the strain background). GGA1 and GGA3 seem to share some redundant function. The absence of either GGA1 or GGA3 was well tolerated by the mice. However, the absence of both is lethal (Govero et al., 2012). Interestingly, expression of GGA2 is highest in the brain during development suggesting this as its most important function is during development, and not post-natally. In contrast, GGA1 and GGA3 expression remained steady from late embryogenesis through adulthood (Govero et al., 2012).

GGA proteins: Implications for Disease

Alzheimer's Disease (AD) is a complex neurodegenerative disease influenced by several genes and environmental risk factors (Reitz et al., 2011). One marker for AD brains is BACE1, a stress-related protease that is upregulated in AD neural tissue and affects the trafficking of Amyloid Precursor Protein (APP) (Cole and Vassar, 2008). BACE1 interacts with GGA proteins by means of a DXXLL-motif sequence, DISLL. (Prabhu et al.) GGA1 and GGA3 have been shown to regulate the degradation of BACE1 in traumatic brain injury (TBI), an environmental risk factor for Alzheimer's Disease. In mouse models of TBI, GGA1 and GGA3 depletion in the acute phase after injury results in the rapid elevation of BACE1 (Walker et al., 2012). One possible mechanism for the rapid decrease in GGA proteins following TBI may be attributable to

caspase-3 mediated degradation of GGA (Lefort et al., 2012). In cell culture, similar effects are observed. Knockdown of GGA proteins by RNAi results in the increased accumulation of BACE1 in the endosomes (He et al., 2005; Tesco et al., 2007; Wahle et al., 2005; Wahle et al., 2006) Some studies suggest that the increase in BACE1 is not a result of increase in expression, but rather the increased stability of existing BACE1because of decreased proteolysis (Lefort et al., 2012).

Concluding Remarks

AP-1 and GGA are both intracellular adaptors that mediate clathrin trafficking. In the past several years a great amount of research has been conducted to identify AP-1 and GGA localization factors, accessory proteins and the mechanism of binding to each as a potential means to better understand the role that they play in development and disease. However, several questions are still being debated; chief among them is whether GGA and AP-1 are codependent. Is it possible that both AP-1 and GGA are incorporated into the same ccvs? AP-1 and GGA can interact in vitro, however the functional significance has yet to be determined. Most research argues against a single coat containing both adaptors. AP-1 and GGA localize to distinct compartments in *S. cerevisiae*, *D. melanogaster*, and mammals by standard fluorescence microscopy, structured illumination microscopy, and electron microscopy. Also unclear are the exact causes of lethality in mammals when AP-1A , GGA2 and both GGA1 and GGA3 are deleted. Tissue specific knockouts have been very useful in understanding the role that AP-1 and GGA play during development. However, more work will need to be conducted, making this area of research worthy of attention for years to come.

Aiken, C., Konner, J., Landau, N. R., Lenburg, M. E., and Trono, D. (1994). Nef induces CD4 endocytosis: Requirement for a critical dileucine motif in the membrane-proximal CD4 cytoplasmic domain. Cell *76*, 853-864.

Ang, A. L., Taguchi, T., Francis, S., Folsch, H., Murrells, L. J., Pypaert, M., Warren, G., and Mellman, I. (2004). Recycling endosomes can serve as intermediates during transport from the

Golgi to the plasma membrane of MDCK cells. The Journal of Cell Biology *167*, 531-543.
Babu, M., Vlasblom, J., Pu, S., Guo, X., Graham, C., Bean, B. D. M., Burston, H. E., Vizeacoumar, F. J., Snider, J., Phanse, S*., et al.* (2012). Interaction landscape of membrane-protein complexes in Saccharomyces cerevisiae. Nature *489*, 585-589.

Behnia, R., and Munro, S. (2005). Organelle identity and the signposts for membrane traffic. Nature *438*, 597-604.

Black, M. W., and Pelham, H. R. (2000). A selective transport route from Golgi to late endosomes that requires the yeast GGA proteins. J Cell Biol *151*, 587 - 600.

Boehm, M., and Bonifacino, J. S. (2002). Genetic analyses of adaptin function from yeast to mammals. Gene *286*, 175-186.

Boman, A. L., Zhang, C., Zhu, X., and Kahn, R. A. (2000). A family of ADP-ribosylation factor effectors that can alter membrane transport through the trans-Golgi. Mol Biol Cell *11*, 1241 - 1255.

Bonifacino, J. S. (2003). Signals for sorting of transmembrane proteins to endosomes and lysosomes. Annu Rev Biochem *72*, 395 - 447.

Bonifacino, J. S. (2004). The GGA proteins: adaptors on the move. Nat Rev Mol Cell Biol *5*, 23-32.

Brodsky, F. M. (2012). Diversity of Clathrin Function: New Tricks for an Old Protein. Annual Review of Cell and Developmental Biology *28*, 309-336.

Canagarajah, B. J., Ren, X., Bonifacino, J. S., and Hurley, J. H. (2013). The clathrin adaptor complexes as a paradigm for membrane-associated allostery. Protein Science, [ahead of print].
Carlton, J. G., and Cullen, P. J. (2005). Coincidence detection in phosphoinositide signaling. Trends in Cell Biology *15*, 540-547.

Carvajal-Gonzalez, J. M., Gravotta, D., Mattera, R., Diaz, F., Perez Bay, A., Roman, A. C., Schreiner, R. P., Thuenauer, R., Bonifacino, J. S., and Rodriguez-Boulan, E. (2012). Basolateral sorting of the coxsackie and adenovirus receptor through interaction of a canonical YXXφ motif with the clathrin adaptors AP-1A and AP-1B. Proceedings of the National Academy of Sciences *109*, 3820-3825.

Chi, S., Cao, H., Chen, J., and McNiven, M. A. (2008). Eps15 Mediates Vesicle Trafficking from the trans-Golgi Network via an Interaction with the Clathrin Adaptor AP-1. Molecular Biology of the Cell *19*, 3564-3575.

Cole, S. L., and Vassar, R. (2008). The Role of Amyloid Precursor Protein Processing by BACE1, the β-Secretase, in Alzheimer Disease Pathophysiology. Journal of Biological Chemistry *283*, 29621-29625.

Costaguta, G., Stefan, C. J., Bensen, E. S., Emr, S. D., and Payne, G. S. (2001). Yeast Gga Coat Proteins Function with Clathrin in Golgi to Endosome Transport. Molecular Biology of the Cell *12*, 1885-1896.

Daboussi, L., Costaguta, G., and Payne, G. S. (2012). Phosphoinositide-mediated clathrin adaptor progression at the trans-Golgi network. Nat Cell Biol *14*, 239-248.

Deborde, S., Perret, E., Gravotta, D., Deora, A., Salvarezza, S., Schreiner, R., and Rodriguez-Boulan, E. (2008). Clathrin is a key regulator of basolateral polarity. Nature *452*, 719-723.

Dell'Angelica, E. C., Puertollano, R., Mullins, C., Aguilar, R. n. C., Vargas, J. D., Hartnell, L. M., and Bonifacino, J. S. (2000). Ggas: A Family of Adp Ribosylation Factor-Binding Proteins Related to Adaptors and Associated with the Golgi Complex. The Journal of Cell Biology *149*, 81-94.

Demmel, L., Gravert, M., Ercan, E., Habermann, B., MÃ¼ller-Reichert, T., Kukhtina, V., Haucke, V., Baust, T., Sohrmann, M., Kalaidzidis, Y.*, et al.* (2008). The Clathrin Adaptor Gga2p Is a Phosphatidylinositol 4-phosphate Effector at the Golgi Exit. Molecular Biology of the Cell *19*, 1991-2002.

den Otter, W. K., and Briels, W. J. (2011). The Generation of Curved Clathrin Coats from Flat Plaques. Traffic *12*, 1407-1416.

Deng, Y., Guo, Y., Watson, H., Au, W.-C., Shakoury-Elizeh, M., Basrai, M. A., Bonifacino, J. S., and Philpott, C. C. (2009). Gga2 Mediates Sequential Ubiquitin-independent and Ubiquitin-dependent Steps in the Trafficking of ARN1 from the trans-Golgi Network to the Vacuole. Journal of Biological Chemistry *284*, 23830-23841.

Donaldson, J. G., Finazzi, D., and Klausner, R. D. (1992). Brefeldin A inhibits Golgi membrane-catalysed exchange of guanine nucleotide onto ARF protein. Nature *360*, 350-352.

Doray, B., Ghosh, P., Griffith, J., Geuze, H. J., and Kornfeld, S. (2002). Cooperation of GGAs and AP-1 in packaging MPRs at the trans-Golgi network. Science *297*, 1700 - 1703.

Duncan, M. C., and Payne, G. S. (2003). ENTH/ANTH domains expand to the Golgi. Trends in Cell Biology *13*, 211-215.

Dwyer, N. D., Adler, C. E., Crump, J. G., L'Etoile, N. D., and Bargmann, C. I. (2001). Polarized Dendritic Transport and the AP-1 mu1 Clathrin Adaptor UNC-101 Localize Odorant Receptors to Olfactory Cilia. Neuron *31*, 277-287.

Eissenberg, J. C., Ilvarsonn, A. M., Sly, W. S., Waheed, A., Krzyzanek, V., Pohlmann, R., Waschkau, D., Kretzschmar, D., and Dennes, A. C. (2011). Drosophila GGA Model: An Ultimate Gateway to GGA Analysis. Traffic *12*, 1821-1838.

Farias, G. G., Cuitino, L., Guo, X., Ren, X., Jarnik, M., Mattera, R., and Bonifacino, Juan S. (2012). Signal-Mediated, AP-1/Clathrin-Dependent Sorting of Transmembrane Receptors to the Somatodendritic Domain of Hippocampal Neurons. Neuron *75*, 810-823.

Fernandez, G. E., and Payne, G. S. (2006). Laa1p, a Conserved AP-1 Accessory Protein Important for AP-1 Localization in Yeast. Molecular Biology of the Cell *17*, 3304-3317.

Fölsch, H., Ohno, H., Bonifacino, J. S., and Mellman, I. (1999). A Novel Clathrin Adaptor Complex Mediates Basolateral Targeting in Polarized Epithelial Cells. Cell *99*, 189-198.

Folsch, H., Pypaert, M., Maday, S., Pelletier, L., and Mellman, I. (2003). The AP-1A and AP-1B clathrin adaptor complexes define biochemically and functionally distinct membrane domains. The Journal of Cell Biology *163*, 351-362.

Gan, Y., McGraw, T. E., and Rodriguez-Boulan, E. (2002). The epithelial-specific adaptor AP1B mediates post-endocytic recycling to the basolateral membrane. Nat Cell Biol *4*, 605-609.

Girard, M., Allaire, P. D., McPherson, P. S., and Blondeau, F. (2005). Non-stoichiometric relationship between clathrin heavy and light chains revealed by quantitative comparative proteomics of clathrin-coated vesicles from brain and liver. Molecular & Cellular Proteomics *4*, 1145-1154.

Gorynia, S., Lorenz, T. C., Costaguta, G., Daboussi, L., Cascio, D., and Payne, G. S. (2012). Yeast Irc6p is a novel type of conserved clathrin coat accessory factor related to small G proteins. Molecular Biology of the Cell *23*, 4416-4429.

Govero, J., Doray, B., Bai, H., and Kornfeld, S. (2012). Analysis of *Gga* Null Mice Demonstrates a Non-Redundant Role for Mammalian GGA2 during Development. PLoS ONE *7*, e30184.
Gravotta, D., Carvajal-Gonzalez, JoseÂ M., Mattera, R., Deborde, S., Banfelder, JasonÂ R., Bonifacino, Juan S., and Rodriguez-Boulan, E. (2012). The Clathrin Adaptor AP-1A Mediates Basolateral Polarity. Developmental Cell *22*, 811-823.

Greenberg, M. E., Iafrate, A. J., and Skowronski, J. (1998). The SH3 domain-binding surface and an acidic motif in HIV-1 Nef regulate trafficking of class I MHC complexes. EMBO J *17*, 2777-2789.

Griffiths, G., and Simons, K. (1986). The trans Golgi network: sorting at the exit site of the Golgi complex. Science *234*, 438-443.
Hama, H., Schnieders, E. A., Thorner, J., Takemoto, J. Y., and DeWald, D. B. (1999). Direct Involvement of Phosphatidylinositol 4-Phosphate in Secretion in the Yeast Saccharomyces cerevisiae. Journal of Biological Chemistry *274*, 34294-34300.

He, X., Li, F., Chang, W.-P., and Tang, J. (2005). GGA Proteins Mediate the Recycling Pathway of Memapsin 2 (BACE). Journal of Biological Chemistry *280*, 11696-11703.

Heuser, J. E., Keen, J. H., Amende, L. M., Lippoldt, R. E., and Prasad, K. (1987). Deep-etch visualization of 27S clathrin: a tetrahedral tetramer. The Journal of Cell Biology *105*, 1999-2009.

Hirst, J., and Carmichael, J. (2011). A potential role for the clathrin adaptor GGA in Drosophila spermatogenesis. BMC Cell Biology *12*, 22.

Hirst, J., Lui, W. W., Bright, N. A., Totty, N., Seaman, M. N., and Robinson, M. S. (2000). A family of proteins with gamma-adaptin and VHS domains that facilitate trafficking between the trans-Golgi Network and the vacuole/lysosome. J Cell Biol *149*, 67 - 80.

Hirst, J., Seaman, M. N., Buschow, S. I., and Robinson, M. S. (2007). The role of cargo proteins in GGA recruitment. Traffic *8*, 594 - 604.

Huser, S., Suri, G., Crottet, P., and Spiess, M. (2013). Interaction of amphiphysins with AP-1 clathrin adaptors at the membrane. Biochemical Journal *450*, 73-83.

Iijima, S., Lee, Y.-J., Ode, H., Arold, S. T., Kimura, N., Yokoyama, M., Sato, H., Tanaka, Y., Strebel, K., and Akari, H. (2012). A Noncanonical mu-1A-Binding Motif in the N Terminus of HIV-1 Nef Determines Its Ability To Downregulate Major Histocompatibility Complex Class I in T Lymphocytes. Journal of Virology *86*, 3944-3951.

Ioannou, M. S., and Marat, A. L. (2012). The Role of EHD Proteins at the Neuronal Synapse. Sci Signal *5*, jc1-.

Jochum, A., Jackson, D., Schwarz, H., Pipkorn, R. d., and Singer-KrÃ¼ger, B. (2002). Yeast Ysl2p, Homologous to Sec7 Domain Guanine Nucleotide Exchange Factors, Functions in Endocytosis and Maintenance of Vacuole Integrity and Interacts with the Arf-Like Small GTPase Arl1p. Molecular and Cellular Biology *22*, 4914-4928.

Kametaka, S., Kametaka, A., Yonekura, S., Haruta, M., Takenoshita, S., Goto, S., and Waguri, S. (2012). AP-1 clathrin adaptor and CG8538/Aftiphilin are involved in Notch signaling during eye development in Drosophila melanogaster. Journal of Cell Science *125*, 634-648.
Kametaka, S., Sawada, N., Bonifacino, J. S., and Waguri, S. (2010). Functional characterization of protein-sorting machineries at the trans-Golgi Network in Drosophila melanogaster. J Cell Sci *123*, 460 - 471.

Kaplan, O. I., Molla-Herman, A., Cevik, S., Ghossoub, R., Kida, K., Kimura, Y., Jenkins, P., Martens, J. R., Setou, M., Benmerah, A., and Blacque, O. E. (2010). The AP-1 clathrin adaptor facilitates cilium formation and functions with RAB-8 in C. elegans ciliary membrane transport. Journal of Cell Science *123*, 3966-3977.

Körber, C., Horstmann, H., Sätzler, K., and Kuner, T. (2012). Endocytic Structures and Synaptic Vesicle Recycling at a Central Synapse in Awake Rats. Traffic *13*, 1601-1611.
Kyattala, A., Yliannala, K., Schu, P., Jalanko, A., and Luzio, J. P. (2005). AP-1 and AP-3 Facilitate Lysosomal Targeting of Batten Disease Protein CLN3 via Its Dileucine Motif. Journal of Biological Chemistry *280*, 10277-10283.

Kyttala, A., Ihrke, G., Vesa, J., Schell, M. J., and Luzio, J. P. (2004). Two Motifs Target Batten Disease Protein CLN3 to Lysosomes in Transfected Nonneuronal and Neuronal Cells. Molecular Biology of the Cell *15*, 1313-1323.

Lefort, R., Pozueta, J., and Shelanski, M. (2012). Cross-Linking of Cell Surface Amyloid Precursor Protein Leads to Increased Î²-Amyloid Peptide Production in Hippocampal Neurons: Implications for Alzheimer's Disease. The Journal of Neuroscience *32*, 10674-10685.

Mangasarian, A., Piguet, V., Wang, J.-K., Chen, Y.-L., and Trono, D. (1999). Nef-Induced CD4 and Major Histocompatibility Complex Class I (MHC-I) Down-Regulation Are Governed by Distinct Determinants: N-Terminal Alpha Helix and Proline Repeat of Nef Selectively Regulate MHC-I Trafficking. Journal of Virology *73*, 1964-1973.

Margeta, M. A., Wang, G. J., and Shen, K. (2009). Clathrin adaptor AP-1 complex excludes multiple postsynaptic receptors from axons in C. elegans. Proceedings of the National Academy of Sciences *106*, 1632-1637.

McMahon, H. T., and Boucrot, E. (2011). Molecular mechanism and physiological functions of clathrin-mediated endocytosis. Nat Rev Mol Cell Biol *12*, 517-533.
Mellman, I., and Nelson, W. J. (2008). Coordinated protein sorting, targeting and distribution in polarized cells. Nat Rev Mol Cell Biol *9*, 833-845.

Meyer, C., Zizioli, D., Lausmann, S., Eskelinen, E.-L., Hamann, J., Saftig, P., von Figura, K., and Schu, P. (2000). [mu]1A-adaptin-deficient mice: lethality, loss of AP-1 binding and rerouting of mannose 6-phosphate receptors. EMBO J *19*, 2193-2203.

Montpetit, A., Cote, S. p., Brustein, E., Drouin, C. A., Lapointe, L., Boudreau, M. l., Meloche, C., Drouin, R. g., Hudson, T. J., Drapeau, P., and Cossette, P. (2008). Disruption of *AP1S1*, Causing a Novel Neurocutaneous Syndrome, Perturbs Development of the Skin and Spinal Cord. PLoS Genet *4*, e1000296.

Ohno, H., Tomemori, T., Nakatsu, F., Okazaki, Y., Aguilar, R. C., Foelsch, H., Mellman, I., Saito, T., Shirasawa, T., and Bonifacino, J. S. (1999). μ1B, a novel adaptor medium chain expressed in polarized epithelial cells. FEBS Letters *449*, 215-220.

Owen, D. J., Vallis, Y., Noble, M. E. M., Hunter, J. B., Dafforn, T. R., Evans, P. R., and McMahon, H. T. (1999). A Structural Explanation for the Binding of Multiple Ligands by the alpha-Adaptin Appendage Domain. Cell *97*, 805-815.

Parachoniak, Christine A., Luo, Y., Abella, Jasmine V., Keen, James H., and Park, M. (2011). GGA3 Functions as a Switch to Promote Met Receptor Recycling, Essential for Sustained ERK and Cell Migration. Developmental Cell *20*, 751-763.

Pohler, E., Mamai, O., Hirst, J., Zamiri, M., Horn, H., Nomura, T., Irvine, A. D., Moran, B., Wilson, N. J., Smith, F. J. D.*, et al.* (2012). Haploinsufficiency for AAGAB causes clinically heterogeneous forms of punctate palmoplantar keratoderma. Nat Genet *44*, 1272-1276.

Poirier, S., Mayer, G., Murphy, S. R., Garver, W. S., Chang, T. Y., Schu, P., and Seidah, N. G. (2013). The Cytosolic Adaptor AP-1A Is Essential for the Trafficking and Function of Niemann-Pick Type C Proteins. Traffic *14*, 458-469.

Prabhu, Y., Burgos, P. V., Schindler, C., Farias, G. G., Magadin, J. G., and Bonifacino, J. S. Adaptor protein 2-mediated endocytosis of the β-secretase BACE1 is dispensable for amyloid precursor protein processing. Molecular Biology of the Cell *23*, 2339-2351.

Puertollano, R., and Bonifacino, J. S. (2004). Interactions of GGA3 with the ubiquitin sorting machinery. Nat Cell Biol *6*, 244-251.

Puertollano, R., Randazzo, P. A., Presley, J. F., Hartnell, L. M., and Bonifacino, J. S. (2001). The GGAs Promote ARF-Dependent Recruitment of Clathrin to the TGN. Cell *105*, 93-102.

Puertollano, R., van der Wel, N. N., Greene, L. E., Eisenberg, E., Peters, P. J., and Bonifacino, J. S. (2003). Morphology and Dynamics of Clathrin/GGA1-coated Carriers Budding from the Trans-Golgi Network. Molecular Biology of the Cell *14*, 1545-1557.

Reales, E., Sharma, N., Low, S. H., Folsch, H., and Weimbs, T. (2011). Basolateral Sorting of Syntaxin 4 Is Dependent on Its N-terminal Domain and the AP1B Clathrin Adaptor, and Required for the Epithelial Cell Polarity. PLoS ONE *6*, e21181.

Reitz, C., Brayne, C., and Mayeux, R. (2011). Epidemiology of Alzheimer disease. Nat Rev Neurol *7*, 137-152.

Ren, X., Farias, Ginny G., Canagarajah, Bertram J., Bonifacino, Juan S., and Hurley, James H. (2012). Structural Basis for Recruitment and Activation of the AP-1 Clathrin Adaptor Complex by Arf1. Cell *152*, 755-767.

Roeth, J. F., Williams, M., Kasper, M. R., Filzen, T. M., and Collins, K. L. (2004). HIV-1 Nef disrupts MHC-I trafficking by recruiting AP-1 to the MHC-I cytoplasmic tail. The Journal of Cell Biology *167*, 903-913.

Saffarian, S., Cocucci, E., and Kirchhausen, T. (2009). Distinct Dynamics of Endocytic Clathrin-Coated Pits and Coated Plaques. PLoS Biol *7*, e1000191.

Schreiner, R., Frindt, G., Diaz, F., Carvajal-Gonzalez, J. M., Perez Bay, A. E., Palmer, L. G., Marshansky, V., Brown, D., Philp, N. J., and Rodriguez-Boulan, E. (2010). The absence of a clathrin adapter confers unique polarity essential to proximal tubule function. Kidney Int *78*, 382-388.

Scott, P. M., Bilodeau, P. S., Zhdankina, O., Winistorfer, S. C., Hauglund, M. J., Allaman, M. M., Kearney, W. R., Robertson, A. D., Boman, A. L., and Piper, R. C. (2004). GGA proteins bind ubiquitin to facilitate sorting at the trans-Golgi network. Nat Cell Biol *6*, 252-259.

Shafaq-Zadah, M., Brocard, L., Solari, F., and Michaux, G. g. (2012). AP-1 is required for the maintenance of apico-basal polarity in the C. elegans intestine. Development *139*, 2061-2070.

Shiba, Y., Katoh, Y., Shiba, T., Yoshino, K., Takatsu, H., Kobayashi, H., Shin, H.-W., Wakatsuki, S., and Nakayama, K. (2004). GAT (GGA and Tom1) Domain Responsible for Ubiquitin Binding and Ubiquitination. Journal of Biological Chemistry *279*, 7105-7111.

Shim, J., Sternberg, P. W., and Lee, J. (2000). Distinct and Redundant Functions of mu1 Medium Chains of the AP-1 Clathrin-Associated Protein Complex in the Nematode Caenorhabditis elegans. Molecular Biology of the Cell *11*, 2743-2756.

Shteyn, E., Pigati, L., and Folsch, H. (2011). Arf6 regulates AP-1B-dependent sorting in polarized epithelial cells. The Journal of Cell Biology *194*, 873-887.

Singer-Kruger, B., Lasic, M., Burger, A.-M., Hauszer, A., Pipkorn, R., and Wang, Y. (2008). Yeast and human Ysl2p/hMon2 interact with Gga adaptors and mediate their subcellular distribution. EMBO J *27*, 1423-1435.

St Johnston, D., and Ahringer, J. (2010). Cell Polarity in Eggs and Epithelia: Parallels and Diversity. Cell *141*, 757-774.

Stamnes, M. A., and Rothman, J. E. (1993). The binding of AP-1 clathrin adaptor particles to Golgi membranes requires ADP-ribosylation factor, a small GTP-binding protein. Cell *73*, 999-1005.

Takahashi, D., Hase, K., Kimura, S., Nakatsu, F., Ohmae, M., Mandai, Y., Sato, T., Date, Y., Ebisawa, M., Kato, T.*, et al.* (2011). The Epithelia-Specific Membrane Trafficking Factor AP-1B Controls Gut Immune Homeostasis in Mice. Gastroenterology *141*, 621-632.

Takatsu, H., Yoshino, K., Toda, K., and Nakayama, K. (2002). GGA proteins associate with Golgi membranes through interaction between their GGAH domains and ADP-ribosylation factors. Biochem J *365*, 369-378.

Tesco, G., Koh, Y. H., Kang, E. L., Cameron, A. N., Das, S., Sena-Esteves, M., Hiltunen, M., Yang, S.-H., Zhong, Z., Shen, Y.*, et al.* (2007). Depletion of GGA3 Stabilizes BACE and Enhances β-Secretase Activity. Neuron *54*, 721-737.

Traub, L. M. (2005). Common principles in clathrin-mediated sorting at the Golgi and the plasma membrane. Biochimica et Biophysica Acta (BBA) - Molecular Cell Research *1744*, 415-437.

Verdino, P., Witherden, D. A., Havran, W. L., and Wilson, I. A. (2010). The Molecular Interaction of CAR and JAML Recruits the Central Cell Signal Transducer PI3K. Science *329*, 1210-1214.

Vowels, J. J., and Payne, G. S. (1998). A dileucine-like sorting signal directs transport into an AP-3-dependent, clathrin-independent pathway to the yeast vacuole. EMBO J *17*, 2482-2493.

Wahle, T., Prager, K., Raffler, N., Haass, C., Famulok, M., and Walter, J. (2005). GGA proteins regulate retrograde transport of BACE1 from endosomes to the trans-Golgi network. Molecular and Cellular Neuroscience *29*, 453-461.

Wahle, T., Thal, D. R., Sastre, M., Rentmeister, A., Bogdanovic, N., Famulok, M., Heneka, M. T., and Walter, J. (2006). GGA1 Is Expressed in the Human Brain and Affects the Generation of Amyloid Î²-Peptide. The Journal of Neuroscience *26*, 12838-12846.

Walch-Solimena, C., and Novick, P. (1999). The yeast phosphatidylinositol-4-OH kinase Pik1 regulates secretion at the Golgi. Nat Cell Biol *1*, 523-525.

Walker, K. R., Kang, E. L., Whalen, M. J., Shen, Y., and Tesco, G. (2012). Depletion of GGA1 and GGA3 Mediates Postinjury Elevation of BACE1. The Journal of Neuroscience *32*, 10423-10437.

Wang, J., Sun, H.-Q., Macia, E., Kirchhausen, T., Watson, H., Bonifacino, J. S., and Yin, H. L. (2007). PI4P Promotes the Recruitment of the GGA Adaptor Proteins to the Trans-Golgi

Network and Regulates Their Recognition of the Ubiquitin Sorting Signal. Molecular Biology of the Cell *18*, 2646-2655.

Wang, Y. J., Wang, J., Sun, H. Q., Martinez, M., Sun, Y. X., Macia, E., Kirchhausen, T., Albanesi, J. P., Roth, M. G., and Yin, H. L. (2003). Phosphatidylinositol 4 Phosphate Regulates Targeting of Clathrin Adaptor AP-1 Complexes to the Golgi. Cell *114*, 299-310.

Witherden, D. A., Verdino, P., Rieder, S. E., Garijo, O., Mills, R. E., Teyton, L., Fischer, W. H., Wilson, I. A., and Havran, W. L. (2010). The Junctional Adhesion Molecule JAML Is a Costimulatory Receptor for Epithelial T Cell Activation. Science *329*, 1205-1210.

Xu, J., Toops, K. A., Diaz, F., Carvajal-Gonzalez, J. M., Gravotta, D., Mazzoni, F., Schreiner, R., Rodriguez-Boulan, E., and Lakkaraju, A. (2012). Mechanism of polarized lysosome exocytosis in epithelial cells. Journal of Cell Science.

Yeung, B. G., Phan, H. L., and Payne, G. S. (1999). Adaptor Complex-independent Clathrin Function in Yeast. Molecular Biology of the Cell *10*, 3643-3659.

Yusong, G., Giulia, Z., and Randy, S. (2013). A novel GTP-binding protein adaptor protein complex responsible for export of Vangl2 from the trans Golgi network. eLife *2*.

Zhang, H., Kim, A., Abraham, N., Khan, L. A., Hall, D. H., Fleming, J. T., and Gobel, V. (2012). Clathrin and AP-1 regulate apical polarity and lumen formation during C. elegans tubulogenesis. Development *139*, 2071-2083.

Zizioli, D., Meyer, C., Guhde, G., Saftig, P., von Figura, K., and Schu, P. (1999). Early Embryonic Death of Mice Deficient in gamma-Adaptin. Journal of Biological Chemistry *274*, 5385-5390.

Chapter 2

Phosphoinositide-Mediated Clathrin Adaptor Progression at the *trans*-Golgi Network

nature cell biology

ARTICLES

Phosphoinositide-mediated clathrin adaptor progression at the *trans*-Golgi network

Lydia Daboussi[1], Giancarlo Costaguta[1] and Gregory S. Payne[1,2,3]

Clathrin-coated vesicles mediate endocytosis and transport between the *trans*-Golgi network (TGN) and endosomes in eukaryotic cells. Clathrin adaptors play central roles in coat assembly, interacting with clathrin, cargo and membranes. Two main types of clathrin adaptor act in TGN–endosome traffic: GGA proteins and the AP-1 complex. Here we characterize the relationship between GGA proteins, AP-1 and other TGN clathrin adaptors using live-cell and super-resolution microscopy in yeast. We present evidence that GGA proteins and AP-1 are recruited sequentially in two waves of coat assembly at the TGN. Mutations that decrease phosphatidylinositol 4-phosphate (PtdIns(4)P) levels at the TGN slow or uncouple AP-1 coat assembly from GGA coat assembly. Conversely, enhanced PtdIns(4)P synthesis shortens the time between adaptor waves. Gga2p binds directly to the TGN PtdIns(4)-kinase Pik1p and contributes to Pik1p recruitment. These results identify a PtdIns(4)P-based mechanism for regulating progressive assembly of adaptor-specific clathrin coats at the TGN.

The last subcompartment of the Golgi complex, the TGN, sorts proteins into distinct transport carriers that are targeted to different destinations, including the plasma membrane and the endosome–lysosome system. A major class of TGN-derived transport carriers are clathrin-coated vesicles (CCVs), which select cargo for delivery to endosomes. CCVs form through the concerted action of three types of highly conserved proteins: clathrin, which forms the outer coat scaffold; adaptors, which link clathrin to membranes by binding to clathrin, phosphoinositides and/or cargo proteins; and accessory proteins, which contribute to coat assembly, membrane invagination, scission and uncoating[1].

The principal adaptors that participate in TGN CCV formation are GGA proteins, epsin-related proteins and the heterotetrameric AP-1 complex (β1, γ1, μ1 and σ1; refs 1,2). Yeast cells express AP-1, two GGA proteins (Gga1p and Gga2p) and two Golgi-localized epsin-related proteins (Ent3p and Ent5p; ref. 2). Physical and genetic interaction studies indicate that these adaptors are part of an extended clathrin-based network in which AP-1 and Gga proteins seem to constitute distinct network hubs[3–8].

The relationship between AP-1 and Gga proteins during TGN CCV formation is uncertain. Both proteins seem to rely on similar sets of low-affinity (low micromolar dissociation constant) multivalent interactions for recruitment to the TGN, including binding to the activated form of the ADP-ribosylation factor 1 (ARF1) GTPase, PtdIns(4)P and cargo[1,9]. However, whether the adaptors act sequentially, in parallel or in distinct pathways remains unresolved, and the extent of co-localization has varied in different studies[1]. Here we have taken advantage of the dispersed nature of Golgi cisternae in the yeast *Saccharomyces cerevisiae* to assess the distribution and relative dynamics of fluorescently tagged AP-1 and Gga proteins expressed at endogenous levels. Our results provide evidence for sequential waves of adaptor-specific coat assembly, coupled by synthesis of PtdIns(4)P.

RESULTS

Gga2p and AP-1 assemble sequentially

Movies of cells expressing clathrin coat proteins fused to GFP or mRFP were acquired by spinning-disc confocal microscopy. Clathrin coat protein fusions, expressed from the normal chromosomal loci, localized as heterogeneous puncta throughout the cell, similar to patterns observed by immunofluorescence microscopy of fixed cells[6,10]. Fluorescently tagged clathrin heavy chain (Chc1p–mRFP) localized as transient puncta at the plasma membrane and at internal sites (Supplementary Movie S1) as observed by others[11], normally persisting for 2 min or less. Internal clathrin foci grew to relatively large sizes (0.3–1.5 μm), assumed irregular and often changing shapes, and moved in random directions. TGN clathrin adaptors formed puncta with characteristics of the internal clathrin structures (Fig. 1).

The relative dynamics of specific protein pairs were assessed in two-colour movies of single optical sections by tracking individual puncta. In cells expressing Gga2p–mRFP and β1–GFP (β1 subunit of AP-1), Gga2p foci appeared first, increased in intensity, and then

[1]Department of Biological Chemistry, David Geffen School of Medicine, University of California, Los Angeles, California 90095, USA. [2]Molecular Biology Institute, University of California, Los Angeles, California 90095, USA.
[3]Correspondence should be addressed to G.S.P. (e-mail: gpayne@mednet.ucla.edu)

Received 22 June 2011; accepted 3 December 2011; published online 19 February 2012; DOI: 10.1038/ncb2427

© 2012 Macmillan Publishers Limited. All rights reserved.

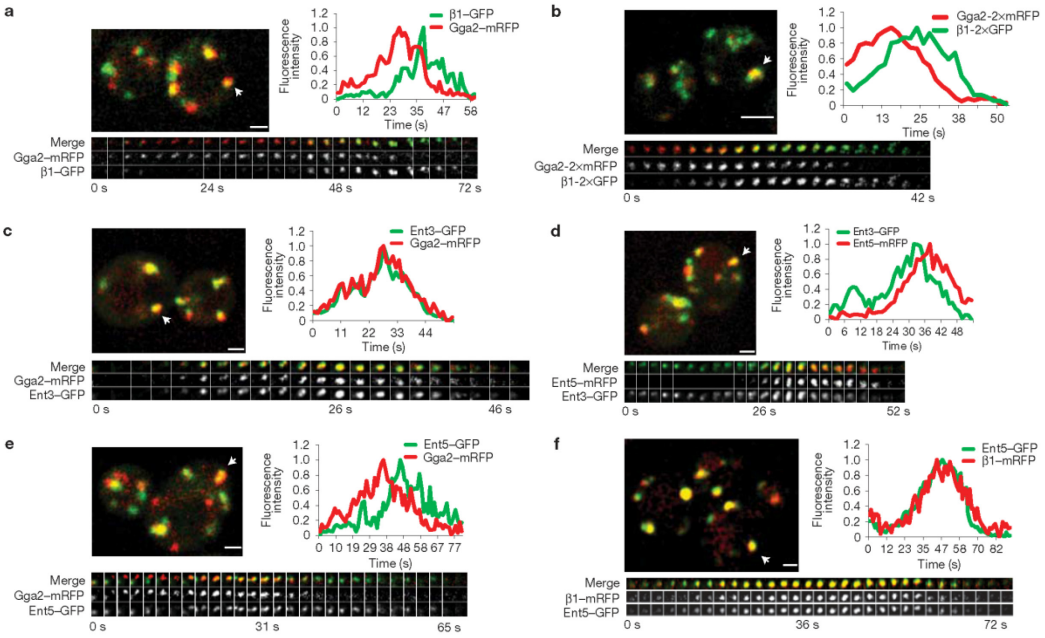

Figure 1 Sequential assembly of clathrin adaptors. (**a**–**f**) Pairs of clathrin coat proteins were assessed in two-colour movies of single optical sections (**a**,**c**–**f**) or in three dimensions (**b**) by tracking puncta that remained separate from other puncta throughout their lifetimes and were present for at least seven frames (~8.4 s). The top left image in **a** and **c**–**f** shows a merged image of live cells co-expressing GFP- and mRFP-tagged versions of the indicated clathrin adaptors; the arrowhead indicates a puncta selected for the kymograph below. Scale bars, 1 μm. The top left image in **b** shows an image of five optical sections along the *z* axis that were imaged at 0.3 μm intervals. One *z*-stack was collected every 2.1 s. Scale bar, 2 μm. The bottom panel in **a**–**f** shows a three-channel kymograph (merged, mRFP and GFP) of the selected puncta; the time to acquire one image pair was 1.2 s. Every other image pair is shown in the kymograph. The graphs show the normalized level of GFP and mRFP fluorescence intensity in the puncta as a function of time. (**a**) GPY3109. (**b**) GPY4974. (**c**) GPY3954. (**d**) GPY3912. (**e**) GPY3962. (**f**) GPY3900.

became AP-1 positive as the Gga2p intensity declined (Fig. 1a and Supplementary Movie S2). A total of 98% of Gga2p puncta transitioned to AP-1 ($n = 101$, 38 cells). Conversely, 95.8% of AP-1 puncta were preceded by the appearance of Gga2p ($n = 142$, 51 cells). In contrast, imaging of cells expressing clathrin light chain (GFP–Clc1p) and heavy chain (Chc1p–mRFP) revealed complete co-localization and coincident profiles, as expected for subunits of the same protein complex (Supplementary Fig. S1a). We presume that declines in coat protein fluorescence intensity reflect budding of CCVs. Infrequently we observed release of smaller puncta, but were unable to effectively track budding events.

The Gga2p to AP-1 sequence was also observed by three-dimensional live-cell imaging where optical sections were collected along the *z* axis over time (Fig. 1b), indicating that the appearance of puncta in single optical sections probably represents coat assembly rather than movement of pre-existing coats into the focal plane. On the basis of better temporal and spatial resolution and reduced photobleaching, subsequent analyses were carried out with single optical sections.

We determined the times between peak intensities of Gga2p–mRFP and β1–GFP in puncta (peak-to-peak time). Gga2p–mRFP fluorescence intensity peaked 10.4 s ± 0.55 s before AP-1 reached peak fluorescence intensity (Table 1, row 1, and Supplementary Fig. S1b). Similar results were obtained when the σ1 subunit was tagged with GFP and compared with Gga2p–mRFP (L.D., unpublished observations).

Chemically fixed cells were imaged by structured illumination microscopy (SIM), a super-resolution technique[12]. Gga2p–GFP or β1–GFP was localized as clusters of ≈100–200 nm structures, consistent with the size expected for individual or closely spaced coated pits (Fig. 2a,b). This indicates that puncta observed by confocal microscopy can be composed of multiple individual coats below the resolution limit of the microscope. In SIM images of cells expressing both Gga2p–mRFP and β1–GFP, most of the Gga2p structures were adjacent to, but distinct from, the β1 structures (Fig. 2e). Our data provide evidence that the consecutive fluorescence peaks of Gga2p and AP-1 represent a wave of semi-synchronous Gga2p coat formation followed by a wave of AP-1 coats. Multiple coated structures in each fluorescent puncta probably accounts for the heterogeneity in peak-to-peak values.

Two waves of clathrin adaptor assembly

Ent3p binds to Gga2p and depends on Gga2p for localization[4,6]. Ent3p and Gga2p fluorescence intensities peaked simultaneously (Fig. 1c and Table 1, row 2, and Supplementary Fig. S1c and Movie S3). Moreover,

© 2012 Macmillan Publishers Limited. All rights reserved.

Table 1 Dynamics of clathrin adaptors, phosphoinositide binding reporters and Golgi markers at the TGN.

Row	Strain		Number of puncta (n) in total cells (c)		Peak-to-peak time (s)
	Mutations	Labelled proteins	n	c	
1	Wild type	Gga2–mRFP β1–GFP	102	59	10.4±0.55
2	Wild type	Gga2–mRFP Ent3–GFP	91	38	0.01±0.16
3	Wild type	Ent3–GFP β1–mRFP	30	21	10.2±1.40
4	Wild type	Ent3–GFP Ent5–mRFP	99	52	8.4±0.70
5	Wild type	Gga2–mRFP Ent5–GFP	91	46	8.0±0.14
6	Wild type	Ent5–GFP β1–mRFP	58	30	1.3±0.62
7	Wild type	Gga2–GFP Sec7–mRFP	97	25	0.29±0.39
8	Wild type	Sec7–mRFP β1–GFP	76	48	10.4±1.18
9	Wild type	Gga2–GFP Chc1–mRFP	95	49	1.3±0.4
10	Wild type	Chc1–mRFP β1–GFP	59	34	8.0±0.7
11	*gga1*Δ *gga2*Δ	Chc1–mRFP β1–GFP	71	36	0.79 ± 0.73
12	*β1*Δ (*apl2*Δ)	Chc1–mRFP Gga2–GFP	22	40	0.9±0.64
13	Wild type	Sec7–mRFP β1–GFP	76	48	10.4±1.18
14	*gga1*Δ *gga2*Δ	Sec7–mRFP β1–GFP	49	25	26.1±1.9
15	Wild type	Gga2–mRFP β1–GFP	102	59	10.4±0.55
16	*arf1*Δ	Gga2–mRFP β1–GFP	47	41	20.5±2.7
17	Wild type	Gga2–mRFP GFP–PH^{OSH1}	104	52	5.3±0.44
18	Wild type	GFP–PH^{OSH1} β1–mRFP	87	52	4.1±0.4
19	Wild type	Sec7–mRFP GFP–PH^{OSH1}	103	61	3.8±0.54
20	*gga1*Δ *gga2*Δ	Sec7–mRFP GFP–PH^{OSH1}	117	68	11.3±0.86
21	*arf1*Δ	Sec7–mRFP GFP–PH^{OSH1}	45	33	11.0±2.1
22	Wild type	Gga2–mRFP GFP–PH^{OSH1}	104	52	5.3±0.6
23	*GPD–PIK1 GPD–FRQ1*	Gga2–mRFP GFP–PH^{OSH1}	48	27	0.0±0.81
24	Wild type	Gga2–mRFP β1–GFP	102	59	10.4±0.55
25	*GPD–PIK1 GPD–FRQ1*	Gga2–mRFP β1–GFP	67	35	5.7±0.77
26	Wild type	Ent3–GFP Ent5–mRFP	99	52	8.4±0.70
27	*GPD–PIK1 GPD–FRQ1*	Ent3–GFP Ent5–mRFP	30	17	3.9±1.5
28	Wild type	Sec7–mRFP GFP–Pik1	75	47	4.1±0.6
29	*gga1*Δ *gga2*Δ	Sec7–mRFP GFP–Pik1	61	36	12.6±1.3
30	Wild type	Frq1–GFP Sec7–mRFP	55	38	1.5±0.8
31	*gga1*Δ *gga2*Δ	Frq1–GFP Sec7–mRFP	73	48	0.4±0.9

Haploid cells expressing the indicated fluorescent proteins were imaged using live-cell microscopy. Multiple puncta from each strain were analysed for changes in fluorescence intensity of the indicated proteins over time. The time between the points of peak fluorescence intensity for each protein was determined and the mean peak-to-peak time was calculated for all of the analysed puncta in a given strain. The data are presented as the mean±s.e.m. for each strain. The order of tagged proteins in each row represents the order of assembly. Some rows are repeated to facilitate comparison (1,15,24; 4,26; 8,13; 17,22). Light blue shading separates groups that share a common wild type control.

Ent3p localized as 100–200 nm puncta that substantially co-localized with Gga2p by SIM (Fig. 2c,f). In comparison with AP-1 (either β1 (Table 1, row 3) or σ1 (L.D., unpublished observations)), Ent3p peaked on average 10.2 s earlier, similarly to Gga2p. Little co-localization between Ent3p and AP-1 was evident by SIM (Supplementary Fig. S2a).

Ent5p binds clathrin, Gga2p and AP-1 (refs 4,6). Genetic interactions indicate that Ent5p function is more important for AP-1-mediated transport[4]. Ent5p appeared as puncta after Ent3p (Fig. 1d); 98.2% of Ent3p puncta became positive for Ent5p ($n = 114$, 38 cells) and almost all Ent5p puncta derived from Ent3p puncta (98.5%, $n = 67$, 23 cells). The peak-to-peak time between Ent3p and Ent5p was 8.4 s (Table 1, row 4), slightly shorter than that observed between Gga2p/Ent3p and AP-1. This difference can be attributed to a small population (≈20%) of puncta in which Ent5p intensity peaked close to that of Ent3p (Supplementary Fig. S1d), and a main population that peaked 9.8 s after Ent3p. Similar results were obtained with Gga2p–mRFP and Ent5p–GFP (Fig. 1e and Table 1, row 5, and Supplementary Movie S4). In accord with these findings, most but not all Ent5p peaked coincidentally with AP-1 (Fig. 1f and Table 1, row 6, and Supplementary Fig. S1e). By SIM, 100–200 nm Ent5p puncta infrequently co-localized with Gga2p and more commonly overlapped with β1 (Fig. 2d,g and Supplementary Fig. S2d).

Together, our results reveal two waves of adaptor assembly: Gga2p and Ent3p assemble first, peaking along with a minor fraction of Ent5p, followed 10 s later by a spatially distinct peak of AP-1 assembly and most of Ent5p. These relationships correspond well with known physical and genetic interactions[4].

Sequential adaptor assembly occurs at the TGN

Sec7p, an ARF GTPase nucleotide exchange factor, is a TGN peripheral membrane protein[13–15]. Sec7p–mRFP and Gga2p–GFP fluorescence profiles were coincident (Fig. 3a and Table 1, row 7), providing evidence that the main site of Gga2p assembly is the TGN. Sec7p–mRFP peaked 10.4 s before β1–GFP, the same time separation observed between Gga2p and AP-1 (Fig. 3b and Table 1, rows 1 and 8). A total of 95.4% of Sec7p–mRFP puncta became positive for AP-1 ($n = 154$, 68 cells) and 94.4% of AP-1 puncta arose from Sec7p puncta ($n = 108$, 53 cells). These data indicate that the process of sequential clathrin adaptor assembly originates at the TGN.

Clathrin and AP-1 dynamics depend on Gga proteins

Clathrin assembly, monitored with Chc1p–mRFP, peaked at about the same time as Gga2p (Fig. 3d and Table 1, row 9). In static images of cells, 56% of Gga2p co-localized with Chc1p and significant overlap was observed by SIM, as expected for assembly of individual Gga2p-containing clathrin coats (Fig. 2h). In cells expressing Chc1p–mRFP and β1–GFP, the peak of Chc1p preceded the AP-1 peak by 8 s (Table 1, row 10), consistent with the relative timing of Gga2p and AP-1 assembly. However, in contrast to Gga2p, substantial clathrin fluorescence signal persisted through the AP-1 peak (Fig. 3e). AP-1 co-localization with

© 2012 Macmillan Publishers Limited. All rights reserved.

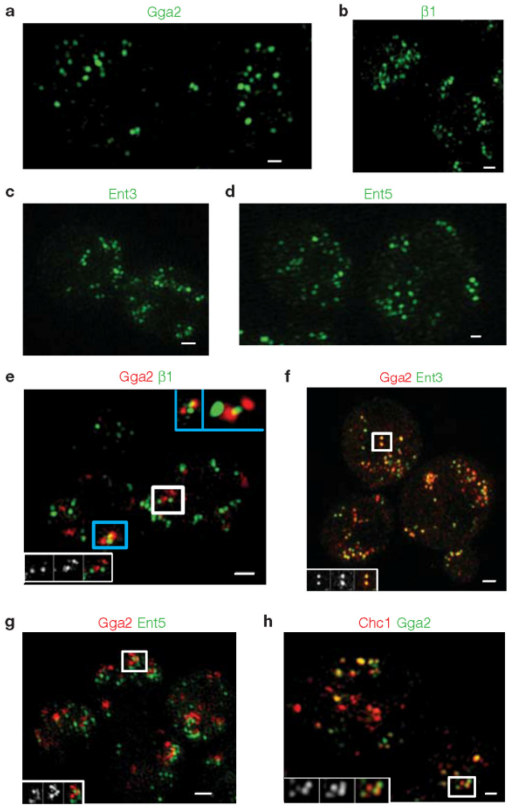

Figure 2 Spatial relationships of clathrin adaptors by SIM. Cells expressing the GFP- and mRFP-tagged adaptors were imaged by SIM. (**a–d**) Maximum image projection of the GFP channel for strains *GGA2–GFP CHC1–mRFP* (GPY4931; **a**), *β1–GFP CHC1–mRFP* (GPY4932; **b**), *ENT3–GFP ENT5–mRFP* (GPY3912; **c**) and *ENT5–GFP β1–mRFP* (GPY3900; **d**). (**e–h**) Maximum image projection of the merged channel for *GGA2–mRFP β1–GFP* (GPY3109; **e**), *GGA2–mRFP ENT3–GFP* (GPY3954; **f**), *GGA2–2xmRFP ENT5–2xGFP* (GPY4962; **g**) and *CHC1–mRFP GGA2-GFP* (GPY4931; **h**). In **e**, the blue-bordered inset (top right) shows the three-dimensional volume view of the blue-outlined region below with no rotation (left) and with rotation around the *x* and *z* axes (right). In **e–h**, the white-bordered insets (bottom left) show (left to right) the GFP, mRFP and merged maximum image projection for the puncta outlined in white above. Scale bars, 400 nm.

Chc1p in static images was lower than that observed for Gga2p; 44% ($n = 75$ cells) versus 56% ($n = 99$ cells), $P = 0.002$. Similarly, the overlap between AP-1 and clathrin was less apparent by SIM, indicating that at steady state clathrin is preferentially associated with Gga2p-enriched coats (Supplementary Fig. S2b).

In contrast to wild-type cells, cells lacking Gga proteins exhibited Chc1p peak intensity at virtually the same time as AP-1 (0.79 s; Fig. 3f and Table 1, row 11) and co-localization between AP-1 and clathrin increased from 44% ($n = 75$ cells) to 58% ($n = 78$ cells), $P = .001$. Similar results were obtained in cells lacking Ent3p and Gga proteins (L.D., unpublished observations). As expected from these findings, SIM analysis of *gga1*Δ*gga2*Δ *ent3*Δ cells revealed greater co-localization between clathrin and AP-1 (Supplementary Fig. S2c). Thus, Gga proteins seem to establish the initial timing and localization of clathrin assembly at the TGN. Consistent with this interpretation, inactivation of AP-1 (*β1*Δ) did not alter the relative timing of Gga2p and Chc1p assembly, except to eliminate the shoulder of clathrin fluorescence signal that corresponds to the peak of AP-1 in wild-type cells (Table 1, row 12, and Supplementary Fig. S3).

In *gga1*Δ *gga2*Δ cells, AP-1 assembly relative to Sec7p–mRFP was delayed by ≈2.5-fold when compared with wild-type cells (Fig. 3b,c and Table 1, rows 13 and 14). Thus, the timing of AP-1 assembly depends on Gga proteins, providing evidence that AP-1 recruitment is coupled to prior assembly of Gga/clathrin coats.

Arf1p influences adaptor dynamics

Arf GTPases are associated with Gga- and AP-1-mediated protein transport from the TGN (ref. 1). There are two Golgi-localized Arf proteins in yeast, Arf1p and Arf2p. Both yeast Gga proteins bind to Arf–GTP but this interaction is not absolutely required for Gga protein localization and function[7,10]. In contrast, AP-1 localization is more dependent on Arf–GTP (ref. 7). Adaptor dynamics were investigated in cells carrying a deletion of *ARF1*, which is expressed at ten times the level of *ARF2* (*arf1*Δ *arf2*Δ cells are inviable[16]). Although Golgi elements coalesce into a limited number of large structures in *arf1*Δ cells[17], there was a clear progression from Gga2p to AP-1 (Fig. 4a and Supplementary Movie S5). However, AP-1 peak fluorescence signal was delayed by twofold when compared with wild-type cells (Table 1, rows 15 and 16, and Supplementary Fig. S1f).

Temporal modulation of PtdIns(4)P levels by Gga and Arf1 proteins

PtdIns(4)P binds to, and promotes localization of, GGA proteins and AP-1 in mammalian cells[18,19]. A similar low-affinity interaction between PtdIns(4)P and Gga protein occurs in yeast[20]. To monitor PtdIns(4)P levels, we used GFP fused to the PtdIns(4)P-binding PH domain of Osh1p (GFP–PH^{OSH1}; ref. 21). GFP–PH^{OSH1} reached maximum intensity 5.3 s after the peak of Gga2p and 4.1 s before the peak of AP-1 (Table 1, rows 17 and 18). Consistent with this sequence, GFP–PH^{OSH1} also peaked after Sec7p–mRFP (Fig. 4b and Table 1, row 19). In *gga1*Δ*gga2*Δ cells, GFP–PH^{OSH1} exhibited a ≈3-fold delay in maximum recruitment when compared with Sec7p–mRFP (Fig. 4c and Table 1, rows 19 and 20). Similarly, GFP–PH^{OSH1} recruitment was slowed in *arf1*Δ cells (Fig. 4d and Table 1, row 21), known to have reduced PtdIns(4)P levels[22]. Thus, PtdIns(4)P increases at the TGN after recruitment of Sec7p and Gga2p and seems to peak before the maximum levels of AP-1. As for AP-1, the normal kinetics of PtdIns(4)P accumulation depends on Gga and Arf1 proteins.

Depletion of PtdIns(4)P inhibits sequential assembly of clathrin adaptors

PtdIns(4)P levels at the Golgi were lowered using a temperature-sensitive allele of *PIK1* (*pik1-83^{ts}*), encoding the PtdIns(4)-kinase associated with Golgi function in yeast[22,23]. At the permissive

© 2012 Macmillan Publishers Limited. All rights reserved.

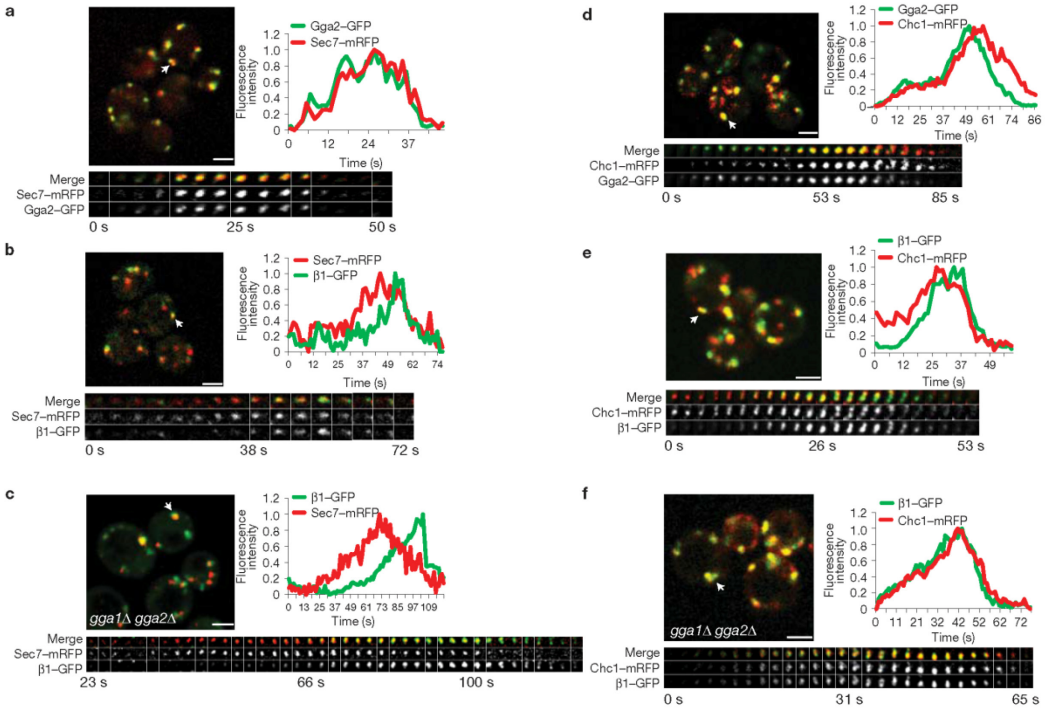

Figure 3 Adaptor and clathrin dynamics at the TGN. (**a–f**) Panels presenting the indicated proteins as in Fig. 1. Scale bars, 2 μm. The time to acquire one image pair was 1.1–1.3 s. (**a**) GPY4933. (**b**) GPY4934. (**c**) GPY4935. (**d**) GPY4931. (**e**) GPY4932. (**f**) GPY4936.

temperature, GFP–PH^{OSH1} exhibited a wild-type localization pattern. After 30 min at 37 °C, the reporter was primarily cytoplasmic (Supplementary Fig. S4a–d), indicative of reduced PtdIns(4)P levels. There was no significant effect of Pik1p inactivation on localization of a PtdIns(3)P reporter, GFP–FYVE (Supplementary Fig. S4e–h).

In *pik1-83^{ts}* cells shifted to 37 °C, Gga2p and Ent3p maintained punctate co-localization (Fig. 5a,b). By comparison, a significant fraction of Ent5p was redistributed to the cytoplasm (Fig. 5c,d). Under the same conditions, AP-1 assembled, although little AP-1 was recruited to Gga2p puncta (Fig. 5e–g and Supplementary Movie S6). This uncoupling resulted in a significant decrease in Gga2p/AP-1 co-localization in static images whereas there was little change in Gga2p/Ent3p co-localization (Fig. 5h). Gga2p/AP-1 co-localization was not restored by introducing an enzymatically inactive Pik1p mutant[24] (Supplementary Fig. S5a). In *ent5*Δ cells, the relative co-localization of Gga2p and AP-1 was equivalent to that in wild-type cells (G.C., unpublished observations), making it unlikely that the effect of Pik1p inactivation on the relationship between Gga2p and AP-1 was due to Ent5p mislocalization.

PtdIns(3)P synthesis was eliminated by deleting *VPS34*, which encodes the only PtdIns(3)-kinase in yeast[25]. The PtdIns(3)P reporter GFP–FYVE, but not GFP–PH^{OSH1}, was primarily cytoplasmic in *vps34*Δ cells, demonstrating a specific loss of PtdIns(3)P (Supplementary Fig. S5b,c). In *vps34*Δ cells, we detected punctate localization and sequential assembly of Gga2p and AP-1 as well as Ent3p and Ent5p, similar to wild-type cells (Supplementary Fig. S5d,e and Movie S7). Together our findings support a specific role for PtdIns(4)P in recruitment of Ent5p and AP-1 to Gga2p/Ent3p-positive Golgi membranes.

Pik1p overexpression increases the rate of adaptor progression

To elevate PtdIns(4)P levels, we used strong constitutive promoters to drive expression of *PIK1* and *FRQ1*, an adaptor necessary for Pik1p localization[26]. In these cells, GFP–PH^{OSH1} peaked simultaneously with Gga2p, about 5 s earlier than in wild-type cells, providing evidence for increased rates of PtdIns(4)P synthesis at the TGN (Table 1, rows 22 and 23). Under these conditions, we observed significantly higher Gga2p/AP-1 co-localization and a twofold reduction in the peak-to-peak separation (Fig. 6a,d and Table 1, rows 24 and 25, and Supplementary Fig. S1g). Similar results were obtained with Ent3p and Ent5p (Fig. 6b,d and Table 1, rows 26 and 27). Levels of co-localization between Ent3p and Gga2p were not altered (Fig. 6c,d). The diametric effects of elevating or reducing PtdIns(4)P levels identify this phosphoinositide as a critical factor controlling TGN clathrin adaptor progression.

To assess the fidelity of clathrin-mediated transport between the TGN and endosomes in Pik1p/Frq1p-overexpressing cells, maturation

© 2012 Macmillan Publishers Limited. All rights reserved.

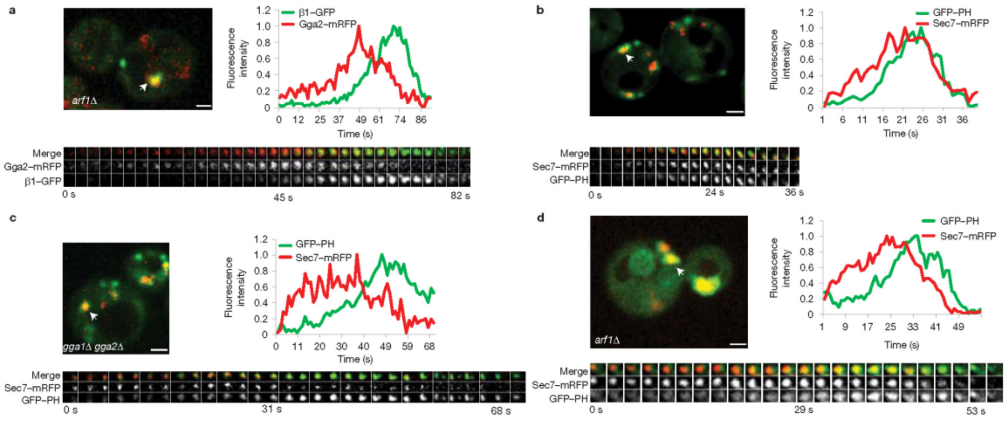

Figure 4 TGN PtdIns(4)P dynamics depend on Arf1p and Gga proteins. (**a**–**d**) Panels presenting the indicated strains as described for Fig. 1. Scale bars, 1 μm. The time to acquire one image pair was between 1.0 and 1.2 s. GFP–PH (GFP–PH^{OSH1}). (**a**) GPY4937. (**b**) GPY4938. (**c**) GPY4939. (**d**) GPY4955.

of the mating pheromone α-factor was evaluated. Pheromone maturation is initiated in the TGN by the Kex2p protease, which relies on clathrin-, AP-1- and Gga-dependent cycling between the TGN and endosomes for localization[5,27–29]. Compared with wild-type cells, Pik1p/Frq1p-overexpressing cells exhibited partial α-factor maturation defects ($8.6 \pm 1.3\%$ ($n = 4$) precursor forms in Pik1p/Frq1p-overexpressing cells versus $3.2 \pm 1.2\%$ ($n = 4$) in wild-type cells ($P < 0.01$); Fig. 6e). This result provides evidence that clathrin-mediated TGN localization of Kex2p is perturbed in Pik1p/Frq1p-overexpressing cells.

We also observed a defect in glycosylation of carboxypeptidase Y (CPY). The core oligosaccharides added to CPY in the endoplasmic reticulum (p1 CPY) are extended in the Golgi apparatus (p2 CPY). p2 CPY is proteolytically matured in the vacuole (mCPY). The Golgi α1–3 mannosyltransferase Mnn1p adds the final sugars to generate p2 CPY (ref. 30). Localization of Mnn1p to the TGN, as for Kex2p, depends on clathrin[31]. In pulse-chase experiments, p2 and mCPY in Pik1p/Frq1p-overexpressing cells were slightly smaller than in wild-type cells (Fig. 6f,g and Supplementary Fig. S6a,b). The p1 forms in the two strains were identical (Fig. 6f) and endoglycosidase H treatment eliminated the difference between mCPY species (Fig. 6g), indicating that the smaller sizes of p2 and mCPY in Pik1p/Frq1p-overexpressing cells are due to incomplete glycosylation in the Golgi. The defects in α-factor maturation and CPY glycosylation indicate that increased synthesis of PtdIns(4)P and shortened adaptor progression times are associated with compromised clathrin-mediated TGN–endosome traffic, probably because precocious AP-1 assembly sorts Kex2p and Mnn1p away from their substrates in the TGN.

Gga2p acts in Pik1p recruitment and directly binds Pik1p

In wild-type cells, Frq1p–GFP peaked at nearly the same time as Sec7p–mRFP whereas GFP–Pik1p reached maximum levels 4.1 s later, similar to the peak of PtdIns(4)P (Fig. 7a and Table 1, rows 19, 28 and 30). In *gga1*Δ *gga2*Δ cells, Pik1p recruitment was delayed, similarly to PtdIns(4)P levels, by threefold when compared with Sec7p (12.6 s; Fig. 7b and Table 1, rows 28 and 29). The profile of Frq1p was not altered (Table 1, rows 30 and 31). Pik1p and Frq1p in cell extracts bound to full-length Gga2p (Fig. 7c and Supplementary Fig. S6c,d). Moreover, Pik1p from cell extracts interacted specifically with the Gga2p VHS domain (Fig. 7d and Supplementary Fig. S6e) and the Gga2p VHS domain bound directly to a recombinant Pik1p fragment (Fig. 7e and Supplementary Fig. S6f). Together these results provide evidence that direct physical interactions between Gga proteins and Pik1p contribute to Pik1p recruitment to the TGN.

DISCUSSION

Our results demonstrate two sequential waves of clathrin coat assembly that originate at the TGN and are distinguished by adaptor type. Gga2p, Ent3p and a minor population of Ent5p assemble in the first wave. AP-1 and most Ent5p are recruited in the second wave. The relative timing of AP-1-enriched coat assembly is dependent on Gga proteins and Arf1p, and the progression between coat types is controlled by PtdIns(4)P. This coupled progression of adaptor-specific clathrin coat formation reveals a hitherto unrecognized process of TGN maturation.

The relationship between Gga and AP-1 adaptor function has not been clearly defined. Although the two adaptors share a number of interaction partners, including Arf, PtdIns(4)P and clathrin, they recognize different cargo sorting signals and certain accessory proteins, and only partially co-localize in static images[1,4,9]. We observed that the major populations of Gga2p and AP-1 were separated in time and space. These results indicate that most clathrin coats forming at the TGN consist primarily of one or the other type of adaptor, and so would be enriched with the corresponding cargo selectivity. This organization provides a simple mechanism to generate CCVs at the TGN targeted to different compartments based on adaptor-directed incorporation of targeting/fusion proteins. In accord with this view, Gga proteins recruit Ent3p, which in

© 2012 Macmillan Publishers Limited. All rights reserved.

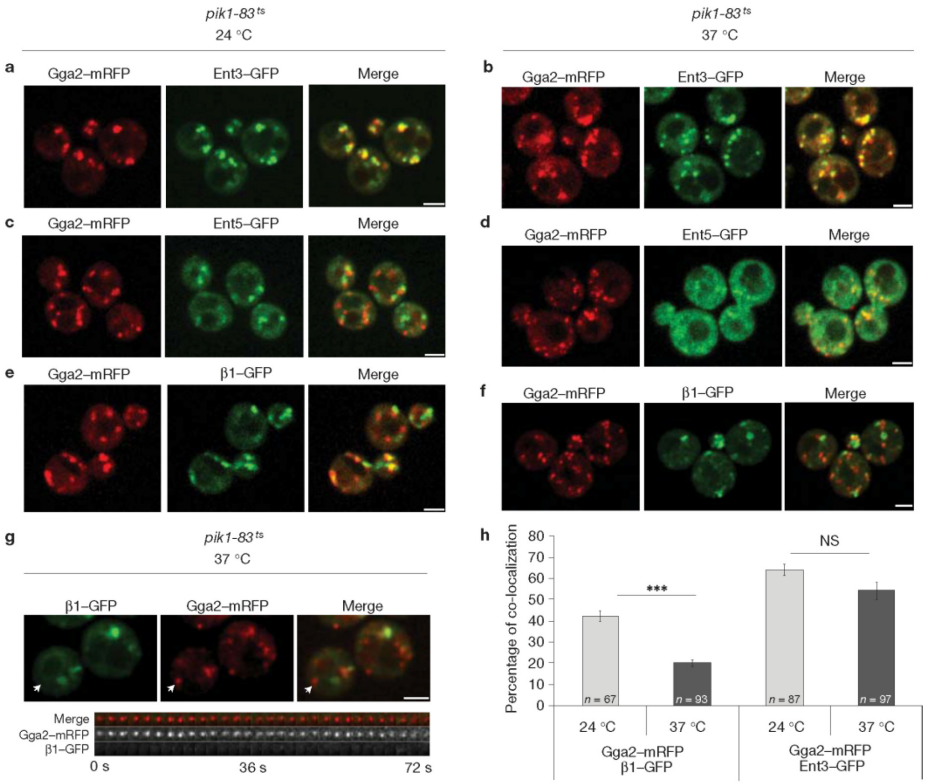

Figure 5 Depletion of PtdIns(4)P alters localization of AP-1 and Ent5p. (**a**–**f**) Representative still images from live cells of *GGA2–mRFP ENT3–GFP pik1-83^{ts}* (GPY4940; **a**,**b**), *GGA2–mRFP ENT5–GFP pik1-83^{ts}* (GPY4941; **c**,**d**) and *GGA2–mRFP β1–GFP pik1-83^{ts}* (GPY4942; **e**,**f**) incubated at 24 °C (**a**,**c**,**e**) or shifted for 30 min to 37 °C (**b**,**d**,**f**). (**g**) The top panel shows still images from live cells of GPY4942 shifted to 37 °C for 30 min. The white arrowhead highlights puncta in the kymograph below. Scale bars, 2 μm. The bottom panel shows a three-channel kymograph of the selected puncta; the time to acquire one image pair was 1.2 s. Every other image pair is shown in the kymograph. (**h**) Gga2p–mRFP co-localization with β1–GFP (GPY4942) or Ent3–GFP (GPY4940) was quantified in *pik1-83^{ts}* cells at 24 °C (light grey bars) or after a shift to 37 °C for 30 min (dark grey bars). Error bars, s.e.m.; *n*, number of events; $^{***}P < 0.001$; NS, not significant (two-tailed *t*-test).

turn binds SNAREs (soluble NSF attachment protein receptors) involved in targeting/fusion to late endosomes, thereby specifying the destination of Gga-enriched CCVs (refs 32–34). Thus, temporally regulated genesis of adaptor-specific coats represents a means to diversify the trafficking repertoire of coated vesicles budding from a particular compartment.

Our results indicate that PtdIns(4)P is a key regulator of the TGN adaptor assembly sequence. Changes in PtdIns(4)P levels that alter adaptor progression are accompanied by defects associated with adaptor function. For example, in combination with *pik1^{ts}* alleles that lower PtdIns(4)P levels, deletions of Gga proteins or AP-1 subunits result in synthetic growth and/or partial α-factor maturation defects[20] (L.D. and G.C., unpublished observations). Importantly, increased PtdIns(4)P synthesis due to Pik1p/Frq1p overexpression also leads to incomplete α-factor maturation and CPY glycosylation. These findings support the view that adaptor progression contributes to optimal function of clathrin-mediated traffic from the TGN.

The effects of PtdIns(4)P on adaptor assembly are likely to be, at least in part, direct. Mammalian AP-1 binds PtdIns(4)P and the residues in the mammalian AP-1 γ subunit necessary for phosphoinositide binding are conserved in the yeast protein[19]. Ent5p contains an amino-terminal domain homologous to phosphoinositide-binding ANTH domains. Binding of Ent5p (and Ent3p) to PtdIns(3)P and PtdIns(3,5)P_2 has been reported[36–38]; however, the specificity of this interaction has been questioned[39]. Our findings are most consistent with a primary role for PtdIns(4)P in Ent5p localization *in vivo*.

Similarly to AP-1, Gga2p binds to PtdIns(4)P and Arf1p through low-affinity interactions that cooperate to enhance Gga2p membrane association[20]. However, Gga2p does not absolutely require Arf interaction for localization[10] and our findings indicate that acute

© 2012 Macmillan Publishers Limited. All rights reserved.

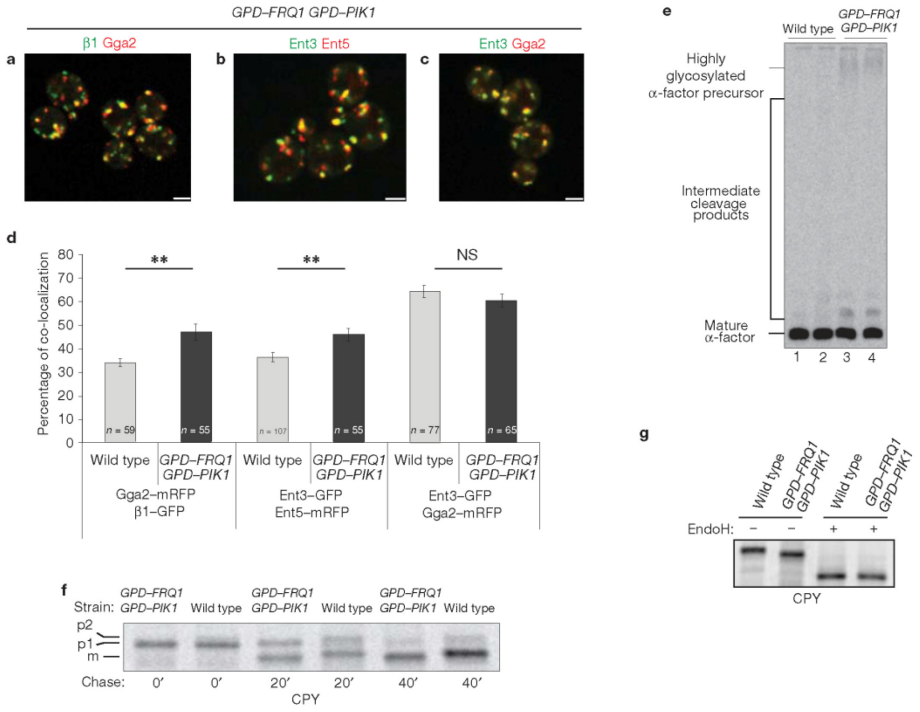

Figure 6 Pik1p/Frq1p overexpression enhances co-localization of sequentially recruited clathrin adaptors with functional consequences. (**a–c**) Representative still images from live cells of strains *GPD–PIK1 GPD–FRQ1 β1–GFP GGA2–mRFP* (GPY4943; **a**), *GPD–PIK1 GPD–FRQ1 ENT3–GFP ENT5–mRFP* (GPY4944; **b**) and *GPD–PIK1 GPD–FRQ1 ENT3–GFP GGA2–mRFP* (GPY4945; **c**). Scale bars, 2 μm. (**d**) Co-localization of the indicated adaptors was quantified in wild-type and Pik1p/Frq1p-overexpressing strains. Left two bars, GPY3109 (light grey bar) versus GPY4943 (dark grey bar); middle two bars, GPY3912 (light grey bar) versus GPY4944 (dark grey bar); right two bars, GPY3954 (light grey bar) versus GPY4945 (dark grey bar). Error bars, s.e.m.; *n*, the number of events; $^{**}P < 0.005$; NS, not significant (two-tailed *t*-test). (**e**) Secreted α-factor immunoprecipitated from the media of radiolabelled cells. Lane 1, wild type (SEY6210); lane 2, *GGA2–mRFP β1–GFP* (GPY3109; wild type); lane 3, *GPD–PIK1 GPD–FRQ1* (GPY4961); lane 4, *GPD–PIK1 GPD–FRQ1 GGA2–mRFP β1–GFP* (GPY4943). (**f**) Pulse-chase immunoprecipitation of CPY. Cells from wild-type (SEY6210) and *GPD–PIK1 GPD–FRQ1* (GPY4961) strains were metabolically labelled with [^{35}S]methionine–cysteine for 10 min at 24 °C and then labelling was quenched with non-radioactive amino acids. Samples of cells were removed at the indicated time points and CPY was immunoprecipitated and analysed by SDS–PAGE and autoradiography. (**g**) Endoglycosidase H treatment of CPY. CPY was immunoprecipitated from a 40 min time point of a pulse-chase as in (**f**) and analysed directly (EndoH –) or treated with endoglycosidase H (EndoH +). Uncropped images of autoradiographs are shown in Supplementary Fig. S6a,b.

PtdIns(4)P reduction does not markedly alter Gga2p recruitment. Thus, our *in vivo* analyses reveal differential dependencies of Gga2p and AP-1 on shared interaction partners, providing a basis for the observed temporal separation of adaptor assembly. Adaptor-specific interactions may also contribute to the spatial and temporal patterns of assembly[7,40]. We favour the view that spatial separation of adaptor-specific coats reflects temporally distinct assembly events (Supplementary Fig. S7).

The Gga2p VHS domain directly binds Pik1p and deletion of the *GGA* genes delayed recruitment of Pik1p to the TGN, providing evidence that binding of Pik1p to Gga proteins contributes to Pik1p recruitment. A defect in Gga-mediated Pik1p recruitment accounts for our finding that cells lacking Gga proteins or Arf1p accumulated PtdIns(4)P more slowly and exhibited a corresponding delay in AP-1 assembly. These results support a model in which assembly of Gga-enriched coats with Arf1p at the TGN stimulates Pik1p recruitment and the attendant increase in PtdIns(4)P synthesis in turn promotes assembly of AP-1/Ent5p coats (Fig. 7f). Notably, recruitment of Pik1p by the VHS domain of Gga proteins, and the combined contribution of Pik1p-generated PtdIns(4)P and Arf1p to Gga2p localization, constitute a positive feedback pathway to drive PtdIns(4)P accumulation at the TGN (Fig. 7g). Thus, our model posits a regulatory network converging on Pik1p to generate a temporal gradient of PtdIns(4)P that controls adaptor progression.

PtdIns(4)P-coupled progression of Gga2p- to AP-1-enriched coats represents a previously unrecognized maturation process at the TGN (Fig. 7f and Supplementary Fig. S7). Although there are some differences in localization mechanisms of yeast and mammalian

© 2012 Macmillan Publishers Limited. All rights reserved.

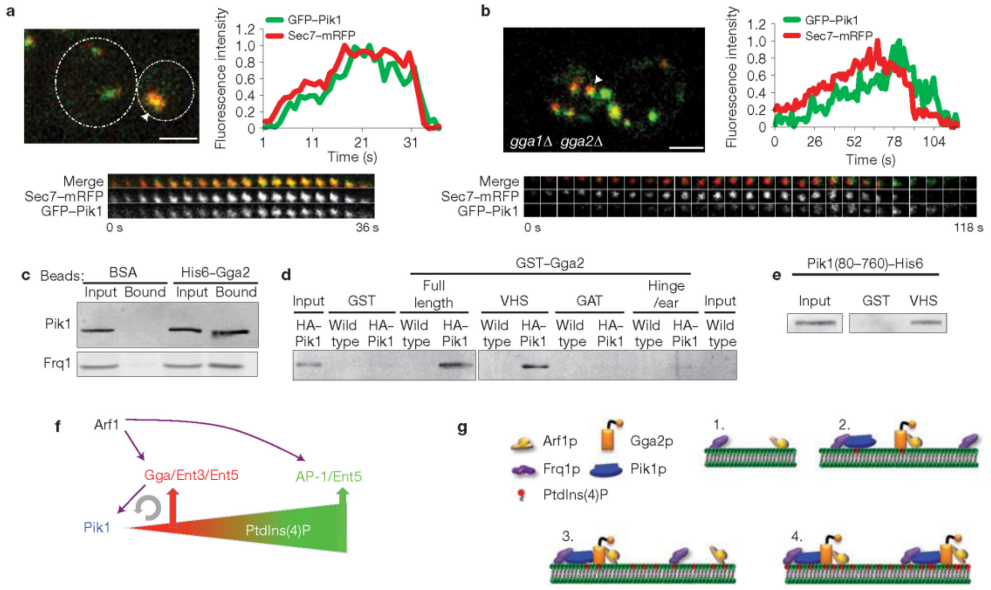

Figure 7 Gga2p acts in Pik1p recruitment and binds Pik1p. (**a**,**b**) Panels presenting the indicated proteins and strains as for Fig. 1. The time to acquire one image pair was 1.0–1.3 s. (**a**) GPY4968. The dot–dash lines in the upper left panel indicate cell boundaries. (**b**) GPY4969. Scale bars, 2 μm. (**c**) Extracts from cells expressing HA–Pik1p (GPY4966, top panel) or Frq1p–GFP (GPY4967, bottom panel) were incubated with BSA-conjugated or His6–Gga2p-conjugated Sepharose. Bound proteins were eluted and analysed by SDS–PAGE and immunoblotting. (**d**) Extracts of cells expressing HA–Pik1p (GPY4966) were applied to glutathione beads coupled to GST, the indicated GST–Gga2p domains or to GST–Gga2p full length. Bound proteins were analysed as in **c**. (**e**) Recombinant Pik1(80–760)–His6 was incubated with glutathione–Sepharose coupled to GST or to GST–Gga2pVHS (VHS). Bound proteins were analysed as in **c**. (**f**) Model for regulation of PtdIns(4)P and adaptor progression at the TGN. The arrows represent known regulatory interactions. The grey arrow indicates a positive-feedback loop. See text for details. (**g**) Model for the positive feedback between Pik1p and Gga2p. (1) Arf1p and Frq1p are recruited to TGN membranes. (2) Frq1p recruits Pik1p, initiating low levels of PtdIns(4)P production. Arf1p and PtdIns(4)P (and cargo, not shown) recruit Gga2p. (3) The VHS domain of Gga2p interacts with Pik1p, helping to recruit or stabilize Pik1p at TGN membranes, thereby promoting PtdIns(4)P production. (4) Increased PtdIns(4)P stimulates recruitment of additional Gga2p, which in turn further enhances Pik1p association with the TGN. Uncropped images of blots are shown in Supplementary Fig. S6c–f.

GGA proteins and AP-1, the strong conservation of binding partners, including ARF and PtdIns(4)P, favours the view that a similar progression occurs in mammalian cells. Supporting this possibility, mammalian GGA proteins often localize with a more compact perinuclear distribution than AP-1, and by immuno-electron microscopy are more prevalent than AP-1 on uncoated TGN membranes, consistent with assembly of GGA proteins at an earlier TGN stage than AP-1 (refs 35,41,42).

A PtdIns(3)P-controlled maturation process occurs in the endocytic pathway at early endosomes[43] that, although mechanistically distinct, is analogous to what we describe for the TGN. Taken together, these findings reveal phosphoinositide-based maturation as a mechanism that allows temporal subspecialization within major organelles in both the secretory and endocytic pathways. □

METHODS

Methods and any associated references are available in the online version of the paper at http://www.nature.com/naturecellbiology

Note: Supplementary Information is available on the Nature Cell Biology website

ACKNOWLEDGEMENTS

We thank J.Thorner, S. Emr and T. Levine for plasmids and strains, J. Atkins for help with SIM, and members of the laboratory for helpful discussions. We are especially grateful to K. Kilborn for advice and assistance with confocal microscopy and K. Martin, G. Weinmaster and A. van der Bliek for comments on the manuscript. This work was supported by NIH NRSA T32 GM-007104 and a UCLA Dissertation Year Fellowship to L.D. and NIH GM39040 to G.P.

AUTHOR CONTRIBUTIONS

L.D. and G.S.P. conceived the experiments. L.D. carried out all microscopy, protein interaction and CPY experiments. G.C. carried out the α-factor experiments, and generated recombinant expression and integration constructs. L.D. and G.S.P. wrote the manuscript.

COMPETING FINANCIAL INTERESTS

The authors declare no competing financial interests.

Published online at http://www.nature.com/naturecellbiology
Reprints and permissions information is available online at http://www.nature.com/reprints

1. Traub, L. M. Common principles in clathrin-mediated sorting at the Golgi and the plasma membrane. *Biochim. Biophys. Acta* **1744**, 415–437 (2005).
2. Duncan, M. C. & Payne, G. S. ENTH/ANTH domains expand to the Golgi. *Trends Cell Biol.* **13**, 211–215 (2003).

© 2012 Macmillan Publishers Limited. All rights reserved.

3. Black, M. W. & Pelham, H. R. B. A selective transport route from Golgi to late endosomes that requires the yeast GGA proteins. *J. Cell Biol.* **151**, 587–600 (2000).
4. Costaguta, G., Duncan, M. C., Fernandez, G. E., Huang, G. H. & Payne, G. S. Distinct roles for TGN/endosome epsin-like adaptors Ent3p and Ent5p. *Mol. Biol. Cell* **17**, 3907–3920 (2006).
5. Costaguta, G., Stefan, C. J., Bensen, E. S., Emr, S. D. & Payne, G. S. Yeast Gga coat proteins function with clathrin in Golgi to endosome transport. *Mol. Biol. Cell* **12**, 1885–1896 (2001).
6. Duncan, M. C., Costaguta, G. & Payne, G. S. Yeast epsin-related proteins required for Golgi-endosome traffic define a γ-adaptin ear-binding motif. *Nat. Cell Biol.* **5**, 77–81 (2003).
7. Fernandez, G. E. & Payne, G. S. Laa1p, a conserved AP-1 accessory protein important for AP-1 localization in yeast. *Mol. Biol. Cell* **17**, 3304–3317 (2006).
8. Ha, S. A. *et al.* The synaptojanin-like protein Inp53/Sjl3 functions with clathrin in a yeast TGN-to-endosome pathway distinct from the GGA protein-dependent pathway. *Mol. Biol. Cell* **14**, 1319–1333 (2003).
9. Graham, T. R. & Burd, C. G. Coordination of Golgi functions by phosphatidylinositol 4-kinases. *Trends Cell Biol.* **21**, 113–121 (2011).
10. Boman, A. L. *et al.* ADP-ribosylation factor (ARF) interaction is not sufficient for yeast GGA protein function or localization. *Mol. Biol. Cell* **13**, 3078–3095 (2002).
11. Newpher, T. M., Smith, R. P., Lemmon, V. & Lemmon, S. K. *In vivo* dynamics of clathrin and its adaptor-dependent recruitment to the actin-based endocytic machinery in yeast. *Dev. Cell* **9**, 87–98 (2005).
12. Schermelleh, L. *et al.* Subdiffraction multicolor imaging of the nuclear periphery with 3D structured illumination microscopy. *Science* **320**, 1332–1336 (2008).
13. Franzusoff, A., Redding, K., Crosby, J., Fuller, R. S. & Schekman, R. Localization of components involved in protein transport and processing through the yeast Golgi apparatus. *J. Cell Biol.* **112**, 27–37 (1991).
14. Rossanese, O. W. *et al.* A role for actin, Cdc1p, and Myo2p in the inheritance of late Golgi elements in *Saccharomyces cerevisiae*. *J. Cell Biol.* **153**, 47–62 (2001).
15. Losev, E. *et al.* Golgi maturation visualized in living yeast. *Nature* **441**, 1002–1006 (2006).
16. Stearns, T., Kahn, R. A., Botstein, D. & Hoyt, M. A. ADP ribosylation factor is an essential protein in *Saccharomyces cerevisiae* and is encoded by two genes. *Mol. Cell Biol.* **10**, 6690–6699 (1990).
17. Gaynor, E. C., Chen, C. Y., Emr, S. D. & Graham, T. R. ARF is required for maintenance of yeast Golgi and endosome structure and function. *Mol. Biol. Cell* **9**, 653–670 (1998).
18. Wang, J. *et al.* PI4P promotes the recruitment of the GGA adaptor proteins to the trans-Golgi network and regulates their recognition of the ubiquitin sorting signal. *Mol. Biol. Cell* **18**, 2646–2655 (2007).
19. Wang, Y. J. *et al.* Phosphatidylinositol 4 phosphate regulates targeting of clathrin adaptor AP-1 complexes to the Golgi. *Cell* **114**, 299–310 (2003).
20. Demmel, L. *et al.* The clathrin adaptor Gga2p is a phosphatidylinositol 4-phosphate effector at the Golgi exit. *Mol. Biol. Cell* **19**, 1991–2002 (2008).
21. Loewen, C. J., Roy, A. & Levine, T. P. A conserved ER targeting motif in three families of lipid binding proteins and in Opi1p binds VAP. *EMBO J.* **22**, 2025–2035 (2003).
22. Audhya, A., Foti, M. & Emr, S. D. Distinct roles for the yeast phosphatidylinositol 4-kinases, Stt4p and Pik1p, in secretion, cell growth, and organelle membrane dynamics. *Mol. Biol. Cell* **11**, 2673–2689 (2000).
23. Walch-Solimena, C. & Novick, P. The yeast phosphatidylinositol-4-OH kinase pik1 regulates secretion at the Golgi. *Nat. Cell Biol.* **1**, 523–525 (1999).
24. Strahl, T., Hama, H., DeWald, D. B. & Thorner, J. Yeast phosphatidylinositol 4-kinase, Pik1, has essential roles at the Golgi and in the nucleus. *J. Cell Biol.* **171**, 967–979 (2005).
25. Schu, P. V. *et al.* Phosphatidylinositol 3-kinase encoded by yeast VPS34 gene essential for protein sorting. *Science* **260**, 88–91 (1993).
26. Hendricks, K. B., Wang, B. Q., Schnieders, E. A. & Thorner, J. Yeast homologue of neuronal frequenin is a regulator of phosphatidylinositol-4-OH kinase. *Nat. Cell Biol.* **1**, 234–241 (1999).
27. Fuller, R. S., Sterne, R. E. & Thorner, J. Enzymes required for yeast prohormone processing. *Annu. Rev. Physiol.* **50**, 345–362 (1988).
28. Payne, G. S. & Schekman, R. Clathrin—a role in the intracellular retention of a Golgi membrane protein. *Science* **245**, 1358–1365 (1989).
29. Phan, H. L. *et al.* The *Saccharomyces cerevisiae APS1* gene encodes a homolog of the small subunit of the mammalian clathrin AP-1 complex: evidence for functional interaction with clathrin at the Golgi complex. *EMBO J.* **13**, 1706–1717 (1994).
30. Dean, N. Asparagine-linked glycosylation in the yeast Golgi. *Biochim. Biophys. Acta* **1426**, 309–322 (1999).
31. Graham, T. R., Seeger, M., Payne, G. S., MacKay, V. L. & Emr, S. D. Clathrin-dependent localization of α1,3 mannosyltransferase to the Golgi complex of *Saccharomyces cerevisiae*. *J. Cell Biol.* **127**, 667–678 (1994).
32. Black, M. W. & Pelham, H. R. A selective transport route from Golgi to late endosomes that requires the yeast GGA proteins. *J. Cell Biol.* **151**, 587–600 (2000).
33. Chidambaram, S., Zimmermann, J. & von Mollard, G. F. ENTH domain proteins are cargo adaptors for multiple SNARE proteins at the TGN endosome. *J. Cell Sci.* **121**, 329–338 (2008).
34. Wang, J. *et al.* Epsin N-terminal homology domains bind on opposite sides of two SNAREs. *Proc. Natl Acad. Sci. USA* **108**, 12277–12282 (2011).
35. Doray, B., Ghosh, P., Griffith, J., Geuze, H. J. & Kornfeld, S. Cooperation of GGAs and AP-1 in packaging MPRs at the trans-Golgi network. *Science* **297**, 1700–1703 (2002).
36. Chidambaram, S., Mullers, N., Wiederhold, K., Haucke, V. & von Mollard, G. F. Specific interaction between SNAREs and epsin N-terminal homology (ENTH) domains of epsin-related proteins in trans-Golgi network to endosome transport. *J. Biol. Chem.* **279**, 4175–4179 (2004).
37. Eugster, A. *et al.* Ent5p is required with Ent3p and Vps27p for ubiquitin-dependent protein sorting into the multivesicular body. *Mol. Biol. Cell* **15**, 3031–3041 (2004).
38. Friant, S. *et al.* Ent3p is a PtdIns(3,5)P2 effector required for protein sorting to the multivesicular body. *Dev. Cell* **5**, 499–511 (2003).
39. Narayan, K. & Lemmon, M. A. Determining selectivity of phosphoinositide-binding domains. *Methods* **39**, 122–133 (2006).
40. Singer-Kruger, B. *et al.* Yeast and human Ysl2p/hMon2 interact with Gga adaptors and mediate their subcellular distribution. *EMBO J.* **27**, 1423–1435 (2008).
41. Hirst, J. *et al.* A family of proteins with γ-adaptin and VHS domains that facilitate trafficking between the trans-Golgi network and the vacuole/lysosome. *J. Cell Biol.* **149**, 67–80 (2000).
42. Poussu, A., Lohi, O. & Lehto, V. P. Vear, a novel Golgi-associated protein with VHS and γ-adaptin 'ear' domains. *J. Biol. Chem.* **275**, 7176–7183 (2000).
43. Zoncu, R. *et al.* A phosphoinositide switch controls the maturation and signaling properties of APPL endosomes. *Cell* **136**, 1110–1121 (2009).

© 2012 Macmillan Publishers Limited. All rights reserved.

METHODS

Media and strains. The strains used in this study are listed in Supplementary Table S1 (refs 4,7,22,44,45). Yeast strains were grown in standard rich medium (YPD) or synthetic dextrose medium (SD) with the appropriate supplements. Fluorescent tags and deletions were introduced at endogenous loci using standard PCR-based homologous recombination. All tagged genes were fully functional as assessed by growth of cells harbouring a tagged gene in a genetic background where deletion of the gene causes severe growth defects.

Except where noted here, all strains were generated from diploid cells by mating, sporulation and isolation of haploid spores. Strains expressing GFP–PH^{OSH1} under the control of the *PHO5* promoter were generated by integrating pGFP–PH^{OSH1} at the *URA3* locus of haploid cells[21]. FYVE–GFP-expressing strains were obtained by transformation of haploid cells with pRS316–FYVE–GFP. Strains overexpressing Pik1p and Frq1p were generated by integrating the glucose phosphate dehydrogenase promoter at the 5′ end of both *PIK1* and *FRQ1* (ref. 46) and then carrying out the appropriate crosses. The *VPS34* gene disruption was generated by replacing the first 2190 base pairs of the coding region with *TRP1* in diploid cells, which were then sporulated for isolation of haploids. All integrations were confirmed by PCR. All primers used for integrations and deletions are described in Supplementary Table S2.

Plasmids. pFA6a–2×GFP^{S65T}–HIS3MX6 was generated using primers 5′-gctgcaggtcgacggatccccgggctaattaacagtaaaggagaagaacttttc-3′ and 5′-gtattcgttaattaaagatctgagtccggatttgtatagttcatccatgccatgtgtaatcccagcagctgt-3′ to amplify GFP^{S65T} from pFA6a–GFP^{S65T}–HIS3MX6 (ref. 47), introducing restriction sites for SalI and PacI. The PCR product was then treated with SalI and PacI and introduced into the same sites in front of GFP^{S65T} on pFA6a–GFP^{S65T}–HIS3MX6 to create pFA6a–2×GFP^{S65T}–HIS3MX6. The construct was confirmed by sequencing. pFA6a–2×mRFP–TRP1 was generated using primers 5′-aattcacaccggcgcctccggactcagatctatggcctcctccgaggacgtcatcaaggagttcatgcgc-3′ and 5′-agaagtggcgcgccttaggcgccggttgagtggcggccctcggcgcgctcg-3′ to amplify mRFP from pFA6a–mRFP–TRP1 (ref. 48), introducing restriction sites for SgrAI and AscI. The PCR product was then treated with SgrAI and AscI and introduced into the same sites at the end of mRFP on pFA6a–mRFP–TRP1 to create pFA6a–2×mRFP–TRP1. The construct was confirmed by sequencing. To generate pRS316–GFP–FYVE, a BamH1 fragment encompassing GFP–FYVE from pGFP–FYVE^{EEA1}–URA3 (ref. 49) was inserted into the BamHI sites of pRS316 (ref. 50). To generate pPik1–GFP(A8)–PIK1, a BamHI and EcoRI fragment from pFA6a–natNT2 (Euroscarf, accession number p30346) was ligated into pBluescript KS(+) to generate pB–natNT2. Then, *PIK1* PCR fragments containing nucleotides −550 to −351, digested with SacII and NotI, and nucleotides −350 to +96, digested with EcoRI, were inserted into the respective sites of pB–natNT2 to generate pB–natNT2–PIK1(−550 + 97). The EcoRI fragment was checked by sequencing. Finally, a PCR fragment containing GFP from pGFP–FYVE and nucleotides coding for an 8-alanine-linker insertion at the 3′ was cloned into an existing NsiI site at the ATG start site of *PIK1* to generate pB–natNT2–GFP(A8)–PIK1. To integrate into the *PIK1* genomic locus, pB–natNT2–GFP(A8)–PIK1 was cut with SacII and EcoRV before transformation. To generate pGex4T1–Gga2(1–169), pGex4T1–Gga2(170–336), pGex4T1–Gga2(337–585), the relevant regions of GGA2 (amino acids 1–169 (VHS), 170–336 (GAT) and 337–585 (hinge/ear)) were amplified by PCR and inserted into the BamHI and SalI sites of pGex-4T-1 (GE Healthcare). The plasmids were checked by restriction enzyme analysis and DNA sequencing. pRS316–pik1^{D918A} was generated by inserting a NheI and SacI fragment from pRS314–GAL1–mycPIK1^{D918A} (PTS12; ref. 27) into pRS316–PIK1 (pJB11; ref. 26). The plasmid was checked by restriction analysis and DNA sequencing. pET28a–Pik1(80–760) was generated by PCR amplification of a fragment encoding amino acids 250–760 of Pik1p followed by cleavage with NcoI and SalI and insertion into pET28a (Novagen, EMD Biosciences) in frame with the carboxy-terminal His6 tag, creating pET28a–Pik1(250–760). The plasmid was checked by restriction analysis and DNA sequencing. A NcoI and NheI fragment from pRS316–PIK1 was then inserted into pET28a–Pik1(250–760) to generate pET28a–Pik1(80–760), which was checked by restriction analysis.

Cell fixation and SIM. Cells were grown overnight in YPD media to 0.4–0.8 × 10^7 cells ml^{-1}. Cells were sedimented at 750*g* for 3 min and resuspended in 4% paraformaldehyde, 42 mM NaOH, 100 mM KH_2PO_4, 100 mM sucrose and 1 mM $MgCl_2$ at pH 5.5 at room temperature for 15 min. Fixed cells were sedimented, washed once in 1.2 M sorbitol and 0.1 M KPO_4 at pH 7.4 and resuspended in 1.2 M sorbitol and 0.1 M KPO_4 at pH 7.4.

SIM achieves resolution of fluorescent objects below the diffraction limit by passing structured light through a diffraction grating to generate multiple interfering beams of light, collecting images and then repeating the process twice with the diffraction grating rotated 60° from the previous position[12]. The resulting super-resolution image is computationally reconstructed on the basis of changes in the fluorescence patterns between images[12]. Images were captured using a ×60, 1.42 NA objective on an OMX microscope (Applied Precision) equipped with two Photometrics Cascade II 512 cameras for the GFP and mRFP channels. Each channel was acquired simultaneously by excitation at 488 and 561.5 nm, respectively. A diffraction grating illuminated samples at the indicated wavelengths at 125 nm intervals, at three different 60° angles[12]. Three-dimensional images were reconstructed using SoftWoRx (Applied Precision).

Live-cell microscopy. Cells were grown in SD complete or SD–uracil at room temperature to a density of 0.1–0.3 × 10^7 cells ml^{-1}. Cells were sedimented by centrifugation at 750 *g* for 2 min, resuspended in 100 µl of the appropriate media and then imaged at room temperature. GFP and mRFP channels were exposed for between 100 and 500 ms per frame, and a mRFP/GFP frame pair was collected every 1–2 s. Typically 100–200 GFP/mRFP frame pairs were collected per time-lapse movie.

Image acquisition and analysis. Images were captured using a 100×/1.45 NA objective on a 3i Marianas SDC confocal microscope equipped with a Zeiss AxioObserver Z1, Yokogawa CSU-22 confocal head and a Hamamatsu EMCCD C9100-13 camera, all controlled by Slidebook 4.2 software. GFP and mRFP images were acquired by excitation at 488 nm and 561 nm from a high-speed AOTF laser launch line.

Time-lapse movies were analysed using Slidebook 4.2. Movies were first photobleach-corrected and then the average fluorescence intensity of a tracked puncta was measured for each frame over its lifetime. The time point with the highest average value was taken as the time point of peak fluorescence and the time point with the lowest average value was taken as the minimum. Normalized fluorescence intensity at time point X = (intensity at time point X − minimum intensity)/(maximum intensity − minimum intensity). Two criteria were applied to select puncta for data collection: the structure had to be present for more than seven frames (~8.4 s); each structure had to remain distinct from other puncta.

Co-localization was quantified by creating masks from the GFP and mRFP channels after sequential Gaussian and Laplacian filtering. The accuracy of each mask was checked by visual comparison to the original image. Co-localization between proteins was expressed as the percentage of pixels from the corresponding channel that overlap with the other channel from the same image[7].

Statistical analysis. Statistical significance of peak-to-peak and co-localization data was tested using the unpaired, Student *t*-test. Significance of the α-factor data was tested using the chi-squared test. Results are expressed as the mean ± s.e.m.

Metabolic labelling, immunoprecipitation and affinity binding. Metabolic labelling and immunoprecipitation of α-factor from the media was carried out at 24 °C as described previously[5]. Pulse-chase immunoprecipitation of CPY was carried out as described for carboxypeptidase S (ref. 4) except that antibody to CPY was used. EndoH treatment was carried out as described previously[51].

For binding experiments, N-terminal GST fusions of the Gga2p VHS domain, GAT domain, hinge/ear domain, full-length Gga2, full-length His6–Gga2 and Pik1(80–760)–His6 were expressed in BL21–DE3 (Codon+) *Escherichia coli*. Bacteria were lysed in PBS at pH 7.4 (and 30 mM imidazole for Pik1 fragments) with a protease inhibitor mixture (Roche Diagnostics GmbH) by sonication. The resulting lysates were cleared by centrifugation for 20 min at 12,000*g*. Glutathione–Sepharose (Gga2 fragments) or Ni-NTA beads (Pik1 fragment or His6–Gga2) were added to the supernatant and allowed to bind for 1 h at 4 °C. GST fusions bound to glutathione were used directly. The bound Pik1 fragment or His6–Gga2p was washed four times with PBS, then three times with 50 mM HEPES at pH 7.4, 50 mM NaCl and 30 mM imidazole, and then eluted in 50 mM HEPES at pH 7.4, 50 mM NaCl and 300 mM imidazole. His6–Gga2p and BSA were coupled to CNBr-activated Sepharose following the manufacturer's instructions (GE Healthcare). Proteins were analysed by SDS–polyacrylamide gel electrophoresis (SDS–PAGE) and immunoblotting with anti-HA antibody (Covance) at a 1:1,000 dilution.

For affinity binding, yeast cells were grown to mid-logarithmic phase in YPD medium. A total of 15 × 10^8 cells per sample were converted to spheroplasts and lysed by resuspension in a final volume of 1 ml of lysis buffer: 100 mM MES–NaOH at pH 6.5, 1.5 mM $MgCl_2$, 2 mM $CaCl_2$, 0.2 mM dithiothreitol, 2 mM NaN_3 containing 1% Triton X-100 and a protease inhibitor mixture[5]. The extract was clarified by centrifugation for 30 min at 16,000*g* at 4 °C. The supernatant was incubated for 30 min in the presence of Protein A Sepharose (Amersham Pharmacia Biotech) followed by centrifugation for 20 s at 16,000*g*. The resulting supernatant was brought to 1 ml in lysis buffer and BSA-conjugated or His6–Gga2-conjugated Sepharose was added; the samples were incubated for 1.5 h at 4 °C, washed twice in lysis buffer, then twice in lysis buffer without Triton X-100, and eluted with sample buffer at 100 °C for 3 min (2% SDS, 10% glycerol, 62.4 mM Tris–HCl at pH 6.8, 0.1 mg ml^{-1} bromophenol blue and 0.4% β-mercaptoethanol). Proteins were analysed by SDS–PAGE and immunoblotting with anti-GFP (Scantibodies, 1:1,000)

© 2012 Macmillan Publishers Limited. All rights reserved.

DOI: 10.1038/ncb2427

or anti-HA (Covance, 1:1,000) antibody and goat anti-rabbit IgG conjugated with alkaline phosphatase (Bio-Rad). Yeast lysates for affinity binding experiments with N-terminal GST fusions of Gga2 were carried out as described above except that yeast cells were lysed in 50 mM HEPES, 50 mM NaCl and 1% Triton X-100. Beads containing GST alone or GST–Gga2 fragments were incubated with the yeast lysate for 2 h at 4 °C. Washing and elution of the beads were carried out as described above.

Direct binding experiments were carried out by incubating purified Pik1(80–760)–His6 with GST- or GST–Gga2p(VHS)-bound glutathione–Sepharose in 50 mM HEPES at pH 7.4, 50 mM NaCl and 300 mM imidazole for 1 h at 4 °C. Washing and elution were carried out as described above. To detect Pik1(80–760)–His6, penta His monoclonal antibody (Qiagen) was used for immunoblot analysis (1:1,000 dilution).

44. Robinson, J. S., Klionsky, D. J., Banta, L. M. & Emr, S. D. Protein sorting in *Saccharomyces cerevisiae*: isolation of mutants defective in the delivery and processing of multiple vacuolar hydrolases. *Mol. Cell Biol.* **8**, 4936–4948 (1988).
45. Yeung, B. G., Phan, H. L. & Payne, G. S. Adaptor complex-independent clathrin function in yeast. *Mol. Biol. Cell* **10**, 3643–3659 (1999).
46. Janke, C. *et al.* A versatile toolbox for PCR-based tagging of yeast genes: new fluorescent proteins, more markers and promoter substitution cassettes. *Yeast* **21**, 947–962 (2004).
47. Longtine, M. S. *et al.* Additional modules for versatile and economical PCR-based gene deletion and modification in *Saccharomyces cerevisiae*. *Yeast* **14**, 953–961 (1998).
48. Huh, W. K. *et al.* Global analysis of protein localization in budding yeast. *Nature* **425**, 686–691 (2003).
49. Burd, C. G. & Emr, S. D. Phosphatidylinositol(3)-phosphate signaling mediated by specific binding to RING FYVE domains. *Mol. Cell* **2**, 157–162 (1998).
50. Sikorski, R. S. & Hieter, P. A system of shuttle vectors and yeast host strains designed for efficient manipulation of DNA in *Saccharomyces cerevisiae*. *Genetics* **122**, 19–27 (1989).
51. Vowels, J. J. & Payne, G. S. A role for the lumenal domain in Golgi localization of the *Saccharomyces cerevisiae* guanosine diphosphatase. *Mol. Biol. Cell* **9**, 1351–1365 (1998).

© 2012 Macmillan Publishers Limited. All rights reserved.

DOI: 10.1038/ncb2427

nature cell biology

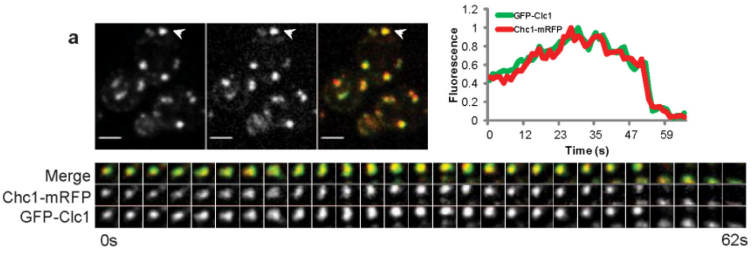

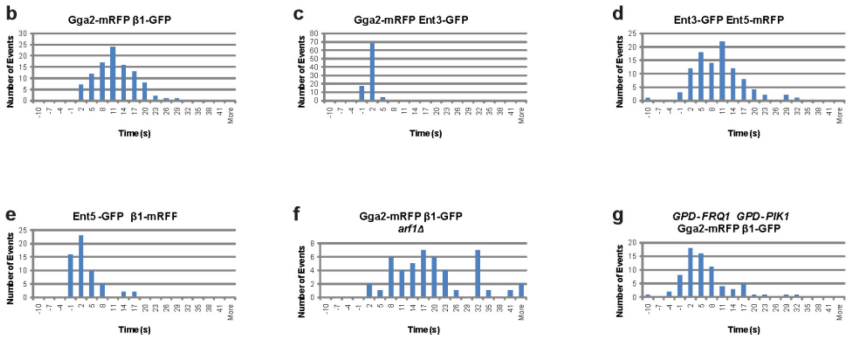

Figure S1 GFP-Clc1p Chc1p-mRFP colocalize in living yeast cells and the distribution of peak to peak fluorescence times. (a) Colocalization of GFP-Clc1p and Chc1p-mRFP. Upper panel: Merged image of cells expressing GFP-Clc1p Chc1p-mRFP (GPY3252); arrowhead indicates puncta selected for kymograph in the bottom panel. Time to acquire one image pair was 1.2s. Scale bar = 2μm. Bottom panel: three channel kymograph (merged, mRFP and GFP) of the selected puncta. Every other image pair is shown in the kymograph. Graph: normalized level of GFP and mRFP fluorescence intensity in the puncta as a function of time. (b-g) Distribution of peak to peak fluorescence times. Selected histograms of the time between peaks of fluorescent intensity for the indicated adaptors used to calculate average peak-to-peak times in Table 1. Events are binned in 3 second intervals. Strains used are: (b) GPY3109 (c) GPY3954 (d) GPY3912 (e) GPY3900 (f) GPY4937 (g) GPY4943.

© 2012 Macmillan Publishers Limited. All rights reserved.

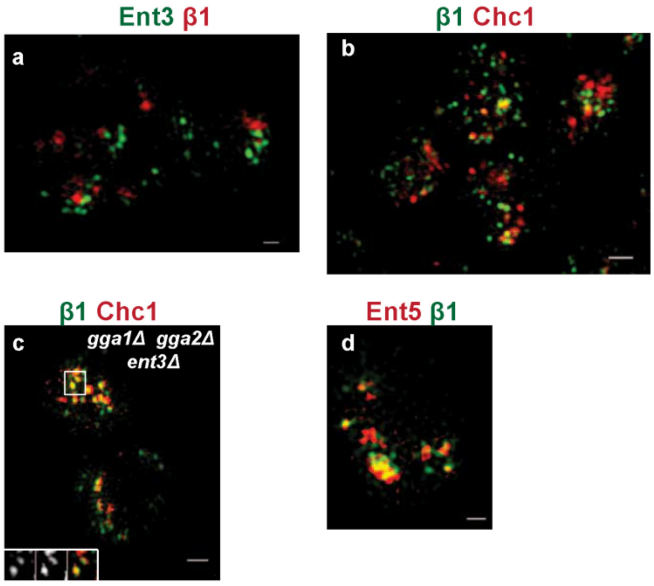

Figure S2 Structured illumination microscopy of clathrin and clathrin adaptors. (a) GPY3974 (b) GPY4932 (c) GPY 4946 (d) GPY4963 cells were imaged by structured illumination microscopy. Maximum projection image is shown. Inset in C contains (left to right) the GFP, mRFP and merged maximum image projection for the puncta in the white box. Scale bar = 400 nm.

© 2012 Macmillan Publishers Limited. All rights reserved.

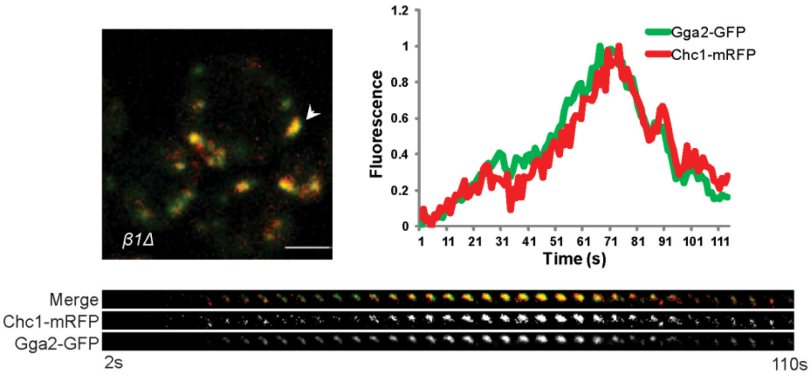

Figure S3 Deletion of the β1 subunit of AP-1 does not affect the relative assembly kinetics of Gga2p and Chc1p. Upper panel: Merged image of cells expressing Chc1p-mRFP and Gga2p-GFP in a β1Δ strain (GPY4975); arrowhead indicates puncta selected for kymograph in the bottom panel. Scale bar = 2μm. Bottom panel: three channel kymograph (merged, mRFP and GFP) of the selected puncta; time to acquire one image pair was 1.2s. Every other image pair is shown in the kymograph. Graph: normalized level of GFP and mRFP fluorescence intensity in the puncta as a function of time.

© 2012 Macmillan Publishers Limited. All rights reserved.

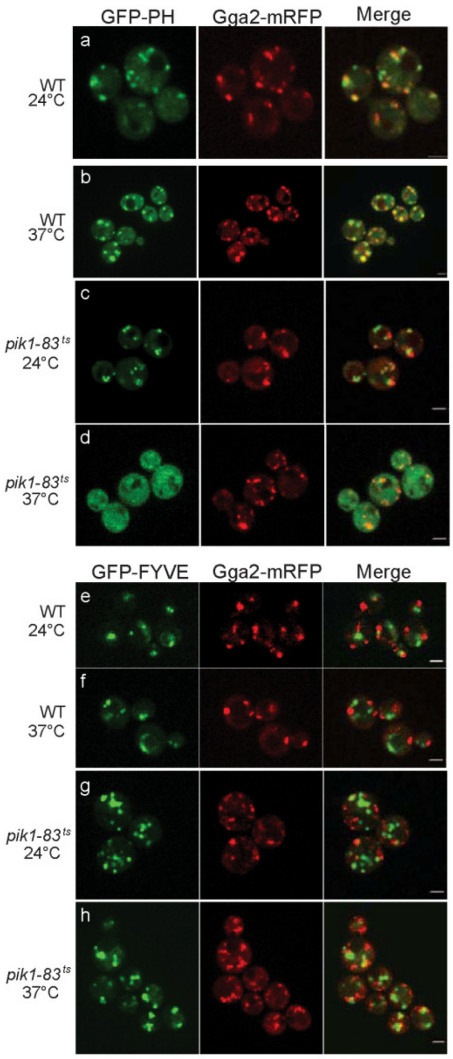

Figure S4 Inactivation of Pik1p decreases PtdIns(4)P but not PtdIns(3)P levels. Still images were acquired from wild-type or *pik1-83*^{ts} cells grown at 24°C or shifted to 37°C for 30 minutes. Representative still images of the following strains: (a, b) *GFP-PH*^{OSH1} *GGA2-mRFP* (GPY4948), (c, d) *GFP-PH*^{OSH1} *GGA2-mRFP pik1-83*^{ts} (GPY4947), (e, f) *GFP-FYVE GGA2-mRFP* (GPY4949), (g, h) *GFP-FYVE GGA2-mRFP pik1-83*^{ts} (GPY4950). Scale bar = 2 μm.

© 2012 Macmillan Publishers Limited. All rights reserved.

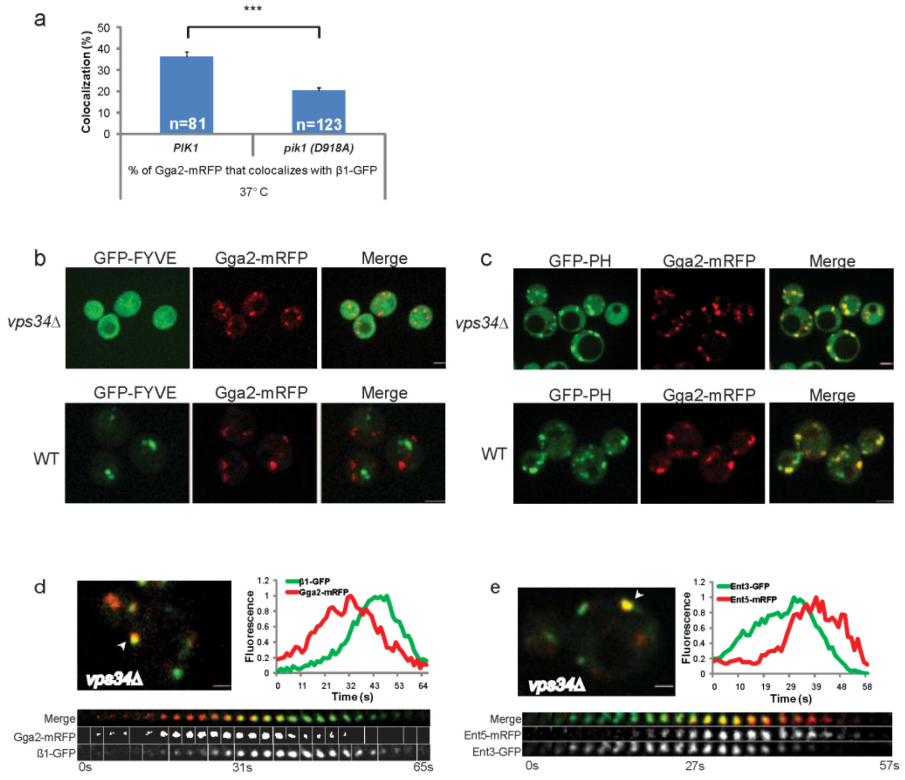

Figure S5 Clathrin adaptor localization in lipid kinase mutants. Wild-type (pRS316-*PIK1*; GPY4976) or kinase-inactive (pRS316-*pik1D918A*; GPY4977) Pik1p were expressed from low copy plasmids in *pik1-83*^{ts} cells. Colocalization between Gga2p-mRFP and β1-GFP at 37°C is shown where (n) = number of cells. Error bars show S.E.M ($p << 0.001$). (b, c) Representative still images of (b) *GFP-FYVE GGA2-mRFP vps34Δ* (GPY4951); *GFP-FYVE GGA2-mRFP* (GPY4949) (c) *GFP-PH*^{OSH1} *GGA2-mRFP vps34Δ* (GPY 4952); *GFP-PH*^{OSH1} *GGA2-mRFP* (GPY4948). Scale bar = 2 μm. (d, e) Upper panel: merged image of live cells co-expressing the indicated GFP- and mRFP-tagged intracellular clathrin adaptors; arrowhead indicates puncta selected for kymograph in the bottom panel. Scale bar = 1 **μm**. Bottom panel: three channel kymograph (merged, mRFP and GFP) of the selected puncta; time to acquire one image pair was between 1.1-1.3 s. Every other image pair is shown in the kymograph. Graph: normalized level of GFP and mRFP fluorescence intensity in the puncta as a function of time. (d) *ENT3-GFP ENT5-mRFP vps34Δ* (GPY4953) and (e) **β1-GFP GGA2-mRFP** *vps34Δ* (GPY4954).

© 2012 Macmillan Publishers Limited. All rights reserved.

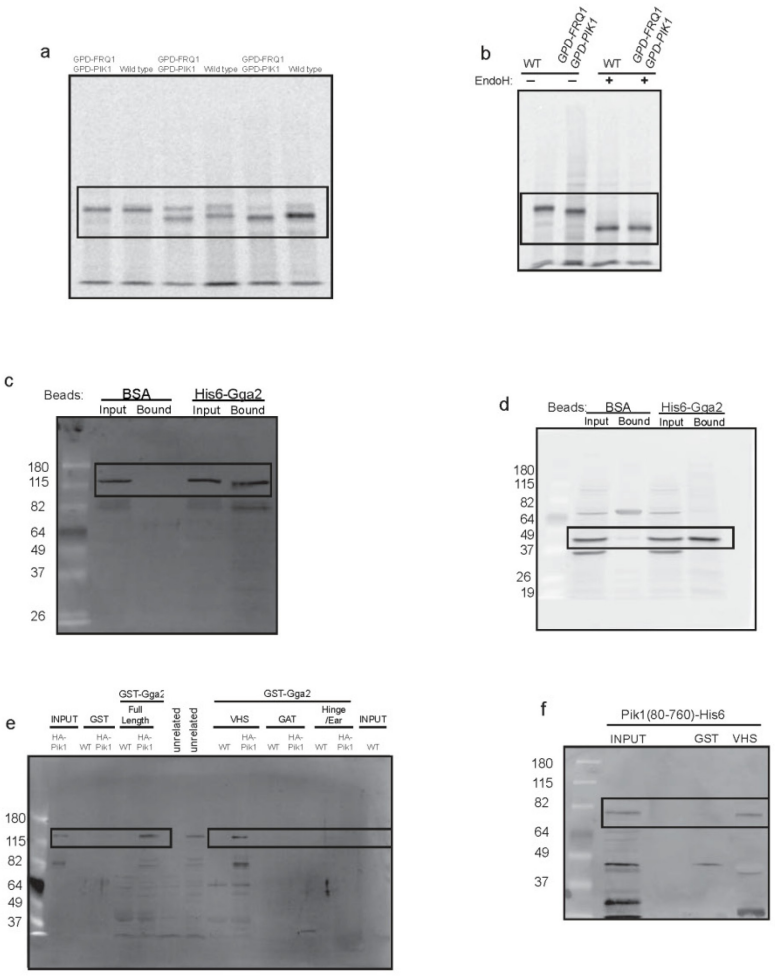

Figure S6 Complete autoradiographs and immunoblots used in Figures 6 and7. Regions of interest are boxed.

© 2012 Macmillan Publishers Limited. All rights reserved.

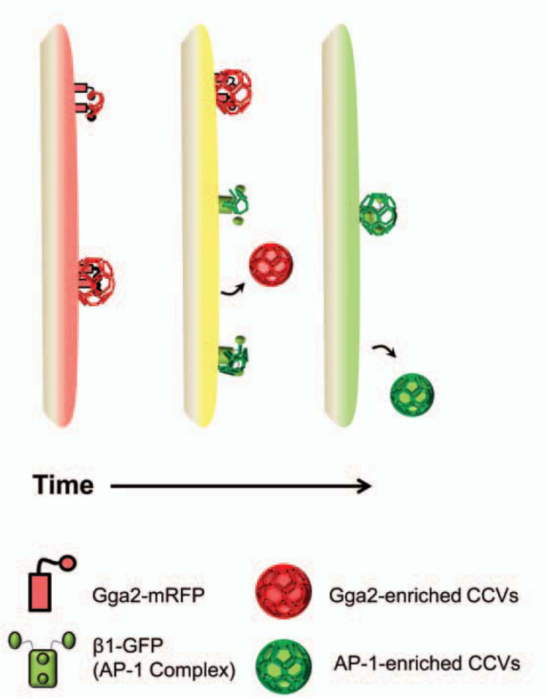

Figure S7 Sequential adaptor-enriched clathrin-coated vesicle formation at the TGN. Initially, low PtdIns(4)P concentrations favor recruitment of Gga proteins and assembly of Gga-enriched ccv without significant AP-1 recruitment. This stage could manifest as a red (Gga2p-mRFP) focus in live cell images and as individual, closely spaced red puncta in SIM images. As PtdIns(4)P levels increase Gga ccv mature and concomitantly AP-1 is recruited, initiating formation of distinct AP-1-enriched ccv. This intermediate stage would manifest as a yellow focus (Gga2p-mRFP and β1-GFP overlapping) in live cell images and adjacent, spatially distinct red and green puncta by SIM. The spatial separation of Gga and AP-1 signals in SIM images reflects formation of individual ccv that are enriched in one or the other adaptor. Finally, the temporal separation of Gga and AP-1 recruitment would lead to a last stage in which Gga ccv have budded and no additional Gga recruitment occurs (likely due in part to the depletion of Gga-dependent cargo collected into the Gga-enriched ccv). As a consequence, only the maturing AP-1-enriched ccv would remain, manifesting as a green focus in live cell images and closely spaced green puncta by SIM.

© 2012 Macmillan Publishers Limited. All rights reserved.

Supplementary Movie Legends

Movie S1 Clathrin dynamics. Time-lapse movie of Chc1p-mRFP in live cells (GPY3100-20D). Interval between frames is 1.5 s. Playback rate is 7 frames per second.

Movie S2 Transition from Gga2-mRFP to β1-GFP (AP-1). Merged time-lapse movie depicts the kinetics of Gga2-mRFP (red) and β1-GFP (green) fluorescence at selected puncta (arrows) in GPY3109 cells. Interval between frames is 1.3s. Playback rate is 7 frames per second.

Movie S3 Ent3p-GFP and Gga2p-mRFP assemble together. Merged time-lapse movie depicts the kinetics of Gga2p-mRFP (red) and Ent3p-GFP (green) fluorescence at a selected puncta (arrow) in GPY3954 cells. Interval between frames is 1.2s. Playback rate is 7 frames per second.

Movie S4 Transition from Gga2p-mRFP to Ent5-GFP. The merged time-lapse image depicts the kinetics of Gga2p-mRFP (red) and Ent5p-GFP (green) fluorescence at selected puncta (arrows) in GPY3962 cells. Interval between frames is 1.2 s. Playback rate is 7 frames per second.

Movie S5 Transition of Gga2p-mRFP to β1-GFP at the TGN in *arf1Δ* cells. The merged time-lapse image depicts the kinetics of Gga2p-mRFP (red) and β1-GFP (green) fluorescence at selected TGN puncta (arrow) in *arf1Δ* cells (GPY4937). Interval between frames is 1.2 s Playback rate is 7 frames per second.

Movie S6 Uncoupling of Gga2p-mRFP and β1-GFP localization in *pik1-83^{ts}* cells. The merged time-lapse image depicts the kinetics of Gga2p-mRFP (red) and β1-GFP (green) fluorescence at selected puncta (arrows) in *pik1-ts^{83}* cells (GPY4942) shifted for 30 min. at 37°C. Interval between frames is 1.2 s. Playback rate is 7 frames per second.

Movie S7 Transition of Ent3p-GFP to Ent5p-mRFP in *vps34Δ* cells. The merged time-lapse image depicts the kinetics of Ent3p-GFP (green) and Ent5p-mRFP (red) fluorescence at selected puncta (arrows) in *vps34Δ* cells (GPY4953). Interval between frames is 1.2 s. Playback rate is 7 frames per second.

© 2012 Macmillan Publishers Limited. All rights reserved.

Supplementary Table Legends.

Table S1 Strains used in this study. All strains were derived from SEY6210 or GPY404 as indicated in the table. Only differences from the parental genotypes are indicated.

Table S2 Primers used in this study.

Supplementary References

4. Costaguta, G., Duncan, M.C., Fernandez, G.E., Huang, G.H. & Payne, G.S. Distinct roles for TGN/endosome epsin-like adaptors Ent3p and Ent5p. Mol Biol Cell *17*, 3907-3920 (2006)..
7. Fernandez, G.E. & Payne, G.S. Laa1p, a conserved AP-1 accessory protein important for AP-1 localization in yeast. Mol Biol Cell *17*, 3304-3317. (2006).
22. Audhya, A., Foti, M. & Emr, S.D. Distinct roles for the yeast phosphatidylinositol 4-kinases, Stt4p and Pik1p, in secretion, cell growth, and organelle membrane dynamics. Mol Biol Cell *11*, 2673-2689 (2000).
44. Robinson, J.S., Klionsky, D.J., Banta, L.M. & Emr, S.D. Protein sorting in *Saccharomyces cerevisiae*: isolation of mutants defective in the delivery and processing of multiple vacuolar hydrolases. Mol Cell Biol *8*, 4936-4948 (1988).
45. Yeung, B.G., Phan, H.L. & Payne, G.S. Adaptor complex-independent clathrin function in yeast. Mol Biol Cell *10*, 3643-3659. (1999).

© 2012 Macmillan Publishers Limited. All rights reserved.

Daboussi et al.,
Supplemental Table 1.

Strain Table:

Strain	Genotype	Reference
SEY6210	*MATα ura3–52 leu2-3112 his3- Δ 200 trp1-Δ 901 lys2-801 suc2- Δ 9*	44
GPY404	*MAT**a** ura3–52 leu2-3112 his3- Δ 200 trp1-Δ 901 lys2-801 suc2-Δ 9*	45
GPY3100-20D	SEY6210 *CHC1-mRFP::KANMX6*	This study
GPY3109	SEY6210 *GGA2-mRFP::KANMX6 APL2-GFP(S65T)::HIS3MX6*	7
GPY 3252	GPY404 *GFP-CLC1 CHC1-mRFP::KanMX6*	This study
GPY3900	SEY6210 *ENT5-GFP (S65T)::KANMX6 APL2-mRFP::TRP1*	4
GPY3912	SEY6210 *ENT3-GFP(S65T)::KANMX6 ENT5-mRFP::HIS3MX6*	4
GPY3954	SEY6210 *ENT3-GFP(S65T)::KANMX6 GGA2-mRFP::KANMX6*	4
GPY3962	SEY6210 *ENT5-GFP(S65T)::KANMX6 GGA2-mRFP::KANMX6*	4
GPY3974	SEY6210 *ENT3-GFP(S65T)::KANMX6 APL2-mRFP::TRP1*	4
GPY4931	SEY6210 *GGA2-GFP(S65T)::HIS3MX6 CHC1-mRFP::KANMX6*	This study
GPY4932	SEY6210 *APL2-GFP(S65T)::HIS3MX6 CHC1-mRFP::KANMX6*	This study
GPY4933	SEY404 *GGA2-GFP(S65T)::HIS3MX6 SEC7-mRFP::KANMX6*	This study
GPY4934	GPY404 *SEC7-mRFP:: KANMX6 APL2-GFP(S65T)::HIS3MX6*	This study
GPY4935	GPY404 *SEC7-mRFP::KANMX6 APL2-GFP(S65T)::HIS3MX6 gga1Δ::HIS3 gga2Δ::HIS3*	This study
GPY4936	*SEY6210 APL2-GFP(S65T)::HIS3MX6 CHC1-mRFP::KANMX6 gga1Δ::HIS3 gga2Δ::HIS3*	This study
GPY4937	*SEY6210 APL2-GFP(S65T)::HIS3MX6 GGA2-mRFP::KANMX6 arf1Δ::HIS3*	This study
GPY4938	*GPY404 SEC7-mRFP::KANMX6 ura3–52::pPHO5-GFP-myc-PH^{OSH1}::URA3*	This study
GPY4939	SEY6210 *SEC7-mRFP::KANMX6 gga1Δ::HIS3 gga2Δ::HIS3 ura3–52::pPHO5-GFP-myc-PH^{OSH1}::URA3*	This study
GPY4940	GPY404 *GGA2-mRFP::KANMX6 ENT3-GFP(S65T)::KANMX6 pik1Δ::HIS3* pRS314-pik1-83^{ts} (*TRP1 CEN6 pik1-83^{ts}*)	This study
GPY4941	GPY404 *GGA2-mRFP::KANMX6 ENT5-GFP(S65T)::KANMX6 pik1Δ::HIS3* pRS314-pik1-83^{ts} (*TRP1 CEN6 pik1-83^{ts}*)	This study
GPY4942	GPY404 *GGA2-mRFP::KANMX6 APL2-GFP(S65T)::HIS3MX6 pik1Δ::HIS3* pRS314-pik1-83^{ts} (*TRP1 CEN6 pik1-83^{ts}*)	This study
GPY4943	SEY6210 *NATNT2::GPD-PIK1 NATNT2::GPD-FRQ1 APL2-GFP(S65T)::HIS3MX6 GGA2-mRFP::KANMX6*	This study
GPY4944	SEY6210 *NATNT2::GPD-PIK1 NATNT2::GPD-FRQ1 ENT3-GFP(S65T):: KANMX6 ENT5-mRFP::HIS3MX6*	This study
GPY4945	SEY6210 *NATNT2::GPD-PIK1 NATNT2::GPD-FRQ1 ENT3-GFP(S65T)::KANMX6 GGA2-mRFP::KANMX6*	This study
GPY4946	SEY6210 *APL2-GFP(S65T)::HIS3MX6 CHC1-mRFP::KANMX6 gga1Δ::HIS3 gga2Δ::HIS3 ent3Δ::TRP1*	This study
GPY4947	SEY6210 *GGA2-mRFP::KANMX6 ura3-52::PH-GFP^{OSH1}::URA3 pik1Δ::HIS3* pRS314-pik1-83^{ts} (*TRP1 CEN6 pik1-83^{ts}*)	This study
GPY4948	SEY6210 *GGA2-mRFP::KANMX6 ura3–52::pPHO5-GFP-myc-PH^{OSH1}::URA3*	This study
GPY4949	SEY6210 *GGA2-mRFP::KANMX6* pRS316-GFP-FYVE (*URA3 CEN GFP-FYVE*)	This study
GPY4950	SEY6210 *GGA2-mRFP::KANMX6* pRS316-GFP-FYVE (URA3 CEN GFP-	This study

GPY4951	SEY404 *GGA2-mRFP::KANMX6 vps34Δ::TRP1* pRS316-GFP-FYVE (*URA3 CEN6 GFP-FYVE*)	This study
GPY4952	SEY404 *GGA2-mRFP::KANMX6 vps34Δ::TRP1 ura3–52::pPHO5-GFP-myc-PH^{OSH1}::URA3*	This study
GPY4953	GPY404 *ENT3-GFP(S65T)::KANMX6 ENT5-mRFP::HIS3MX6 vps34Δ::TRP1*	This study
GPY4954	GPY404 *APL2-GFP(S65T)::HISMX3 GGA2-mRFP::KANMX6 vps34Δ::TRP1*	This study
GPY4955	SEY6210 *SEC7-mRFP::TRP1 ura3–52::pPHO5-GFP-myc-PH^{OSH1}::URA3 arf1Δ::HIS3*	This study
GPY4958	GPY 404 *NATNT2::GPD-PIK1 NATNT2::GPD-FRQ1 ura3–52::pPHO5-GFP-myc-PH^{OSH1}::URA3 GGA2-mRFP::KANMX6*	This study
GPY4961	SEY6210 *NATNT2::GPD-FRQ1 NATNT2::GPD-PIK1*	This study
GPY4962	SEY6210 *ENT5-2XGFP(S65T)::HIS3MX6 GGA2-2XmRFP::TRP1*	This study
GPY4963	SEY6210 *APL2-2XGFP(S65T)::HIS3MX6 ENT5-2XmRFP::TRP1*	This study
GPY4964	SEY6210 *APL2-2XGFP(S65T)::HIS3MX6 ENT3-2XmRFP::TRP1*	This study
GPY4965	SEY6210 *APL2-2XmRFP::HIS3MX6 ura3–52::pPHO5-GFP-myc-PH^{OSH1}::URA3*	This study
GPY4966	GPY404 *NATNT2::GPD-HA-PIK1*	This study
GPY4967	GPY404 *FRQ1-GFP::KANMX6*	This study
GPY4968	SEY6210 *NATNT2::pPIK1-GFP(A8)-PIK1 SEC7-mRFP::KANMX6*	This study
GPY4969	SEY6210 *NATNT2::pPIK1-GFP(A8)-PIK1 SEC7-mRFP::KANMX6 gga1Δ::HIS3 gga2Δ::HIS3*	This study
GPY4970	SEY6210 *FRQ1-GFP::KANMX6 SEC7-mRFP::TRP1*	This study
GPY4973	GPY404.2 *FRQ1-GFP::KANMX6 SEC7-mRFP::TRP1 gga1Δ::NATNT2 gga2Δ::HIS3*	This study
GPY4974	SEY6210 *APL2-2XGFP(S65T)::HIS3MX6 GGA2-2XmRFP::TRP1*	This study
GPY4975	GPY6210 *GGA2-GFP::KANMX6 CHC1-mRFP::KANMX6 apl2Δ-6::TRP1*	This study
GPY4976	GPY404 *GGA2-mRFP::KANMX6 APL2-GFP(S65T)::HIS3MX6 pik1Δ::HIS3* pRS314-pik1-83^{ts} (*TRP1 CEN6 pik1-83^{ts}*) pJB11 *(URA3 CEN6 PIK1)*	This study
GPY4977	GPY404 *GGA2-mRFP::KANMX6 APL2-GFP(S65T)::HIS3MX6 pik1Δ::HIS3* pRS314-pik1-83^{ts} (*TRP1 CEN6 pik1-83^{ts}*) pRS316-pik1(D918A) (*URA3 CEN6 pik1-D918A*)	This study
AAY104	SEY6210 *pik1Δ::HIS3* pRS314-pik1-83^{ts} (*TRP1 CEN6 pik1-83^{ts}*)	22

Daboussi et al.,

Supplemental Table 2

For strain construction:

Gene	Sequence
	GCTGATGAACAGCGCGATGAACGTTCAACCCACAGGATTTCGGA
CHC1	*TCCCCGGGTTAATTAA*
	ACACGATGGGGTACAGCAAACGAATTATTTTATCCACGTCGAATT
CHC1	*CGAGCTCGTTTAAAC*
	GGGCGGCAATATAGTGTCACAGGATCTCCTCGATTTATTC CGG
β1	*ATCCCCGGGTTAATT AA*
	ATGGTATAATACTTAAGTTCACTACAACGGACGTTTATAG
β1	*GAATTCGAGCTCGTTTAAAC*
	GGGCGGCAATATAGTGTCACAGGATCTCCTCGATTTATTCCGGA
β1	*TCCCCGGGCTAATTAA*
	GACAAGTCACTACTTCAAGTATAACCCAGACAAGAGTCTTTTAAA
GGA1	*CGTACGCTGCAGGTCGAC*
	ATAATATGGCATCTACTTTTTTTTCAACTTCTCTACCGAATTTGAA
GGA1	*TCGATGAATTCGAGCTCG*
	CCAAGCTGAAGAAACTGCTGTTTTTACGTTACCTAATGTACGGAT
GGA2	*CCCCGGGTTAATTAA*
	ACATAGAGAAGAGAAAGGATTGATAAGAAACGCCAGAGGAGAAT
GGA2	*TCGAGCTCGTTTAAAC*
	CCAATAATAACCATACATCATCCAAAGAAATCGATTTACTTTCCTT
ENT3	*TCGGATCCCCGGGTTAATTAA*
	TTATAAAACATTTACATATTGTGTAAACCAATAATATCACGAATTC
ENT3	*GAGCTCGTTTAAAC*
	TGCATTTTCCGACTTATTCTCTTACTCCAAGTCGTTGGTCCGGAT
ENT5	*CCCCGGGTTAATTAA*
	CTGTATTGAATGTATTGGGAGATGAAGGGGTATTTGGTGAGAATT
ENT5	*CGAGCTCGTTTAAAC*
	TGCATTTTCCGACTTATTCTCTTACTCCAAGTCGTTGGTCCGGAT
ENT5	*CCCCGGGCTAATTAA*
	GAGAGTTATTTTGTGCTTGAAAACTGTTTTTGATTCAAAAAAAAAC
FRQ1	*GTACGCTGCAGGTCGAC*
	CAAACATGTCAGGTCATCTTTGGAAAGCTTTGACGTCTTGGCTCC
FRQ1	*CATCGATGAATTCTCTGTCG*
	CTCTATTATTGGTGCCTTAAACCTTTACGATGGCTTAATACGGAT
FRQ1	*CCCCGGGTTAATTAA*
	TGTTATAACATCCAATCCATAAGAAGCAAAAACAAAGTTTGAATTC
FRQ1	*GAGCTCGTTTAAAC*

	TTCATTGCGAGCGTTCGTTTTCATTAAGCATTCGTTCTCTTCACTA
PIK1	*TGCGTACGCTGCAGGTCGAC*
PIK1	*TTCAATAGTAATCATCAAAGCTTTTCTTTGAACTGGATGCTTTATG*
	ATTTCTAAGCAGAGTTGGTGAATTATACCTTTCTACTGATCGGAT
SEC7	*CCCCGGGTTAATTAA*
	ACTAAGCATATTTTAATCTGCTGGACCATTCAACAAAGCCGAATT
SEC7	*CGAGCTCGTTTAAAC*
	CCGGTGAAGGTTTGTATGAAGGTTTGGAATGGTTAAGTAACAGTT
ARF1	*TGAAACGGATCCCCGGGTTAATTAA*
	TATGTTTCATTTAGTTTATACAAGCGTATTTGATCCATATTCTAGA
ARF1	*ATTCGAGCTCGTTTAAAC*
	ATGTCACTGAACAACATAACATTCTGTGTCTCACAGGAATCCGGA
VPS34	*TCCCCGGGTTAATTAA*
	CCCATCTGGCGTGACTAGTAAGTTGTCTAAATGCCTATCGGAATT
VPS34	*CGAGCTCGTTTAAAC*

For Plasmid Construction:

ppik1-GFP(A8)-PIK1

SacII-Pik1(-550)	*GCTCCACCGCGGTTTGGGAAGACGACGAGCCTAAGAATTTATGG*
Pik1(-351)-NotI	*TCTAGAGCGGCCGCCTATGAATAGTGAATAATAAGTGGTG*
EcoRI-Pik1(-350)	*GAGCTCGAATTCTATGTTACATCATAAGGCCATTGTCAC*
Pik1(251)-ClaI	*GACGGTATCGATTCTGTCTCCATGGTGACGAGGACCTG*
NsiI-GFP(1)	*GCTTCAATGCATATATGTCTTTAATTAACAGTAAAGGAGAAG*
	AAGGCTATGCATTGCAGCTGCAGCAGCGGCAGCTGCTCGTGATC
GFP(725)-LiA8-NsiI	*TGAGTCCGGATTTGTATAGTTCATCCATGCCATGTGTAATCC*

pGex4T1-Gga2(1-169)

BamHI-Gga2(1)	*ACGCGGATCCATGTCCCATCCGCACTCACATAGCATA*
Gga2(507)-SalI	*ACGCGTCGACTTAGGGGAATGCATAACCCTTATATTTCAAC*

pGex4T1-Gga2(170-336)

BamHI-Gga2(508)	*ACGCGGATCCAAAATCAGTGAATCCGACCTAGCAGTTTTG*
Gga2(1008)-SalI	*ACGCGTCGACTTAAGAAACATGACTTGGATGTATCTGCGAAGC*

pGex4T1-Gga2(337-585)

BamHI-Gga2(1009)	*ACGCGGATCCGCTCCGTTACAACAATCTTCTGGTGCTTTAACG*
Gga2(1758)-SalI	*ACGCGTCGACTTATACATTAGGTAACGTAAAAACAGCAGTTTC*

pET28a-Pik1(80-760)

NcoI-Pik1(748)	*CATGCCATGGGTGCATCCTTCAGGAAATCCAGACATAGTG*
Pik1(2280)-SalI	*ACGCGTCGACAATACCACCCGTCATTAAATCGTTTTCC*

Chapter 3

Mechanisms of Phosphoinositide-Mediated Clathrin Adaptor Localization

Clathrin-mediated trafficking is an evolutionarily conserved transport mechanism from the plasma membrane to the endosomes and between the *trans*-Golgi Network (TGN) and endosomes. Clathrin forms a hexamer, composed of three clathrin heavy chains and three clathrin light chains. Clathrin hexamers polymerize into higher order polyhedrals, forming the outer coat of the vesicle. Clathrin has no affinity for membrane and therefore relies on adaptor proteins to serve as a link between it and the membrane (Brodsky, 2012). Adaptor proteins serve two additional functions: binding to cargo and recruiting accessory proteins. Accessory proteins play a key role in vesicle biogenesis by facilitating membrane invagination, vesicle scission and vesicle uncoating (Traub, 2005).

There are two classes of clathrin adaptor protein: the multimeric adaptors, and the monomeric adaptors. In yeast, at the TGN, there is a single heterotetrameric adaptor AP-1, which is composed of two large subunits (β1 and γ1; 83kD and 95kD respectively) a medium subunit (μ1; 53kD) and a small subunit (σ1; 19kD). Monomeric TGN adaptors are the GGA proteins (Golgi-localized γ-ear containing ARF binding protein), and the epsin-related proteins (Ent3p and Ent5p). Yeast cells express two homologous GGA proteins (Gga1p and Gga2p) which share ~70% sequence similarity. The amino terminal VHS domain (VPS27, HRS, STAM) mediates binding to lipids. The central GAT domain (GGA and Tom1) also interacts with lipids as well as with GTP-bound Arf1 and ubiquitin (Puertollano and Bonifacino, 2004; Scott et al., 2004; Shiba et al., 2004). The hinge and C-terminal 'ear' regions of GGA contain binding motifs for clathrin, the γ-ear of AP-1 and the epsin-like adaptors (Duncan and Payne, 2003).

In yeast, there are two primary rounds of CCV biogenesis at the TGN. First, GGA is recruited to the TGN through polyvalent interactions with GTP-bound Arf1p, lipids and cargo (Bonifacino, 2004; Traub, 2005), and other factors . After recruitment to the TGN GGA/Ent3p enriched CCVs can be formed. Recently, we have shown that a direct interaction between Gga

and the yeast PI(4)-Kinase, Pik1p, promotes the production of PI(4)P in vivo, thereby inducing the second wave of recruitment of AP-1 and Ent5p to the TGN (Daboussi et al., 2012).

Pik1p is the primary source of intracellular PI(4)P and localizes to the TGN in yeast (Daboussi et al., 2012; Graham and Burd, 2011). It is composed of several domains important for protein-protein interactions and catalytic activity. The N-terminal LKU domain (Lipid Kinase Unique) is immediately adjacent to the Frq1p interaction site. Frq1p (frequenin), is a myristolyated EF-hand domain protein, important for Pik1p recruitment to the membrane (Strahl et al., 2003; Strahl et al., 2007). The central PI4K Homology domain contains a region of homology between Pik1 and its mammalian homolog (PI4KIIIb). In mammals this region interacts with Rab11 (the yeast homologs of Rab11 are Ypt31p and Ypt32p). The C-terminal domain of Pik1p contains an ATP-binding catalytic domain essential to the production of PI4P (Figure 3-1A) (Balla and Balla, 2006).

Frq1p is important for Pik1p localization to the TGN in yeast. However it is unclear as to whether this mechanism of recruitment is conserved in higher order eukaryotes. Mammalian cells express several PI4-Kinases, however there is only one *PIK1* homologue, PI4KIIIb (Balla and Balla, 2006; Graham and Burd, 2011). PI4KIIIB localizes predominately to the TGN and is ubiquitously expressed. Intriguingly, the *FRQ1* homologue, *ncs-1* (Neuronal Calcium Sensor 1) is primarily expressed in neuronal tissues. There is no clear evidence that ncs-1 serves as a recruitment factor for PI4KIIIB in non-neuronal tissues (Balla and Balla, 2006). Additionally, the only known clue for PI4KIIIB recruitment to membranes is that it occurs through an Arf1p dependent mechanism (Godi et al., 1999). The manner in which PI4KIIIB is recruited to the TGN remains unsolved.

The focus of this work is to define the mechanism of interaction between GGA and Pik1p. We have found that Pik1p binds directly to the VHS domain of Gga2p via two interaction

sites. Our results support a model in which the Pik1p-Gga2p interaction occurs solely at the TGN membrane regulated by GTP-bound Arf1. We also present data that suggests this mechanism may be conserved in mammals.

RESULTS

Direct binding of the Gga2p VHS domain to residues 286-291 of Pik1p

Gga proteins have been shown to play a role in the recruitment of Pik1p to the TGN in vivo. Additionally, Pik1p interacts directly with the Gga2p VHS domain in vitro (Daboussi et al., 2012). We have further mapped the region of interaction between Pik1 and the Gga2p VHS domain using recombinant proteins in vitro. Fragments of Pik1p between the Frq1p binding domain and the catalytic domain (Figure 3-1A), delimited the region of Pik1p that interacts with the VHS domain to a short fragment between residues 283-300 on Pik1p (Figures 3-1; Figure 3-2). Next, to understand which residues contributes most to binding to the VHS domain, we performed an alanine scan of Pik1p (283-300), mutating each three adjacent residues to alanine (Figure 3-3A). Three separate Pik1p mutants showed reduced binding to the VHS domain: the most dramatic effects were demonstrated by mutations in residues 286-288 and 289-291 (Figure 3-3B: Lanes 5-8). Additionally, the Pik1p mutant with alanine mutations from 283-285 showed some decrease in interaction with the VHS domain relative to the wildtype (Figure 3-3B: Lane 3,4). However, these mutations were less severe than mutations in the region between 286-291. Even though mutations in 286-288 and 289-291 resulted in the largest decrease in binding, the interaction was not completely eliminated. Mutations in residues 292-300 did not affect the Pik1p-VHS interaction (Figure 3-3B: Lanes 9-14). These data indicate that a significant region of interaction with the VHS domain lies between residues 286 and 291 of Pik1p.

A

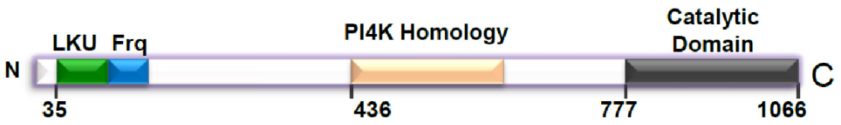

B

Pik1 Fragments	Interacts with VHS?
80-760	yes
420-760	no
250-581	yes
250-548	yes
250-503	yes
250-425	yes
250-380	yes
250-330	yes
330-410	no
350-425	no
350-503	no
350-548	no
290-380	no
283-329	yes

Figure 3-1. Predicted Domain Architecture of Pik1 and Pik1p fragments used for in vitro experiments

A.) Pik1 is 1066 amino acids in length and is composed of a Lipid Kinase Unique (LKU) domain, a Frq1 binding site, a PI4K homology region which in mammalian cells interacts with Rab11. (Rab11 has two homologues in yeast Ypt31p and Ypt32.) The C-terminus of Pik1is composed of an ATP-binding catalytic domain which places phosphate at the 4-position of phosphatidylinositol. (Adapted from (Balla and Balla, 2006)). **B.)** Schematic of each of the fragments used to map the first VHS binding site. The left column indicates the residues contained in each fragment. The center column is a schematic of each fragment with its relative position on full length Pik1p (above). Green indicates that the recombinantely expressed and purified fragment of Pik1p interacted with a purified, recombinantely expressed GST-VHS domain. Red indicates that there was not a significant interaction. Additionally, the right column denotes whether each Pik1p fragment does or does not interact with the VHS domain.

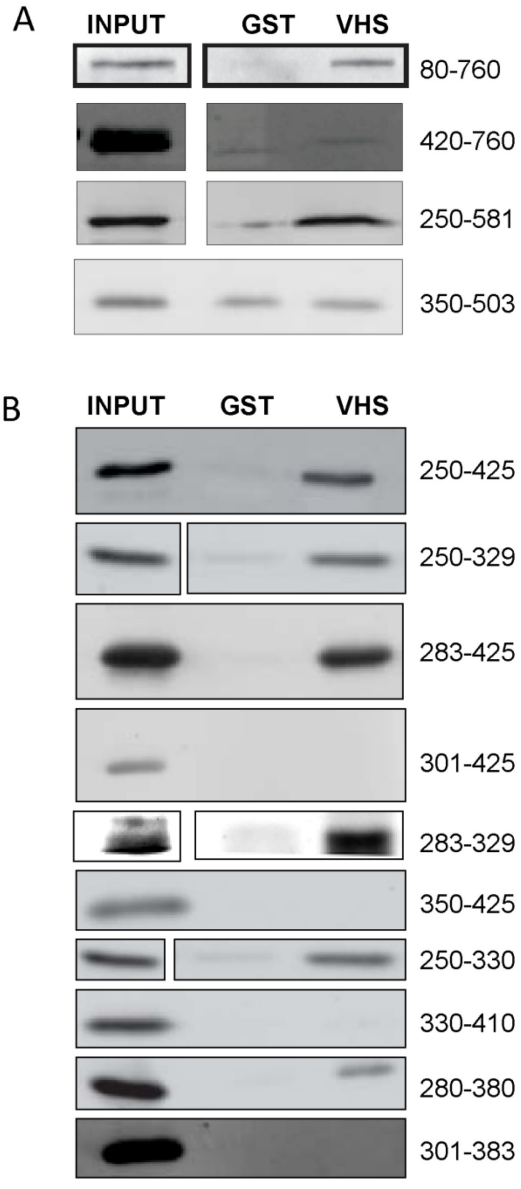
A
INPUT
GST
VHS
80-760
420-760
250-581
350-503
B
INPUT
GST
VHS
250-425
250-329
283-425
301-425
283-329
350-425
250-330
330-410
280-380
301-383

Figure 3-2. Pik1 283-300 interacts with the VHS domain in vitro.

A and B.) The indicated Pik1 constructs (right column) were recombinantly expressed as His6 fusions and purified. Samples were then incubated with glutathione-sepharose coupled to GST or GST-VHS (Gga2). Bound proteins were eluted with by sample buffer before being applied to an SDS-PAGE gel and subjected to a western blot analysis. Input=2% (anti-HIS 1:1000; QIAGEN)

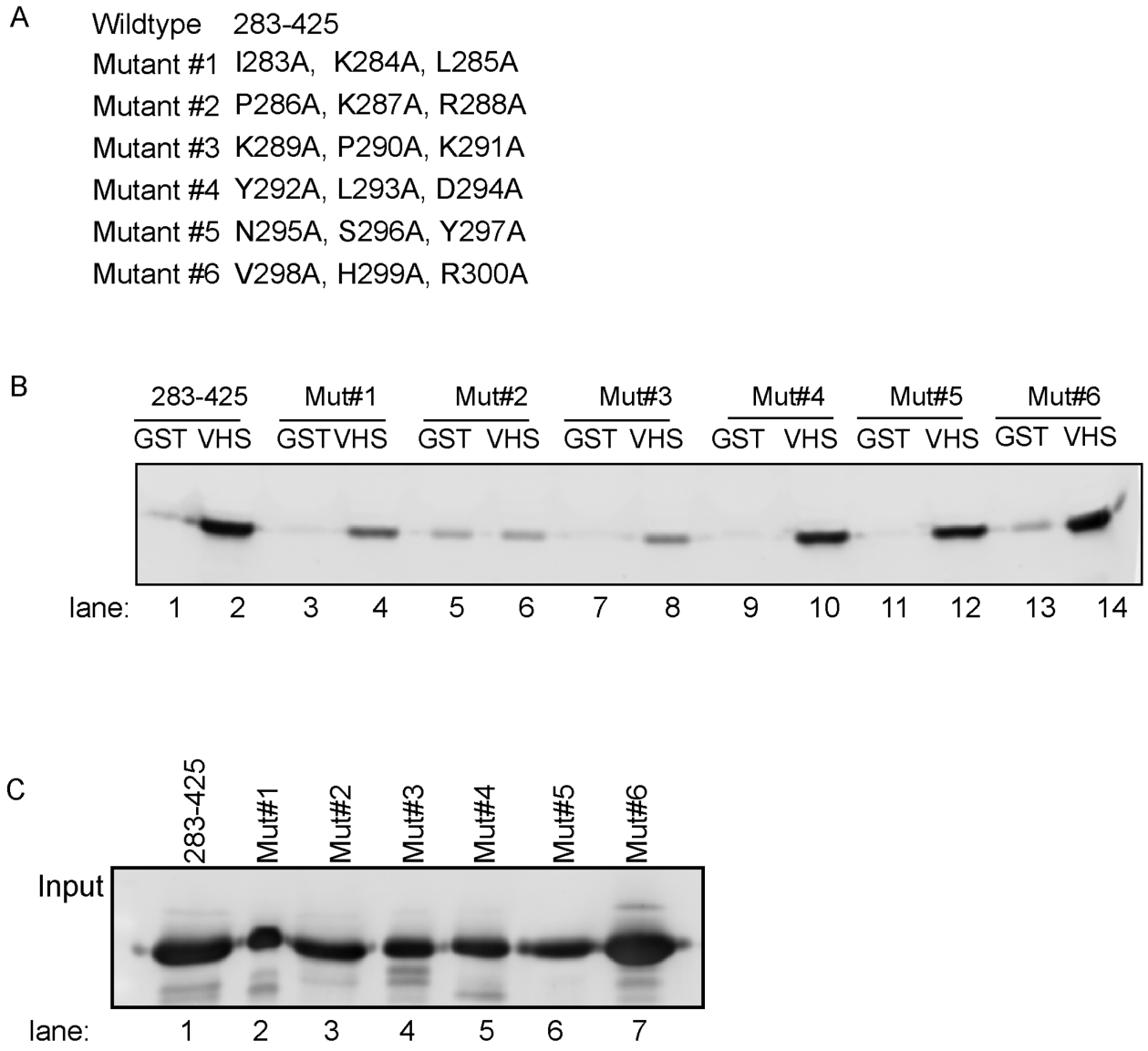

Figure 3-3. Pik1p (283-291) mediates an interaction with the VHS domain of Gga2p.

A fragment of Pik1p containing residues 283-425 was C-terminally HIS tagged, expressed from a pet28a vector and purified as described in Figure 3-2. This WT construct served as the template to introduce alanine mutations in the first 18 residues. **A.)** List of constructs used for the experiment. **B.)** Pulldown experiment using recombinately expressed, purified proteins of the given WT or mutant Pik1p fragments, GST and GST-VHS. Pulldown was conducted as described in figure 3-2. **C.)** Contains the inputs for each of the constructs used in the pulldown experiments. Input=2%. (anti-HIS 1:1000; QIAGEN)

To determine if we could completely eliminate binding of Pik1p to the VHS domain, we mutated 286-291 to either alanine or acidic residues (Figure 3-4: A-C). Solubility of the 286-291^{alanine} mutant was decreased relative to wildtype and the other mutants (Figure 3-4C: Lane 5). However, expression of the 286-291^{acidic} mutation was similar to wildtype (Figure 3-4C: Lane 1, 6). In this acidic mutant, binding of the Pik1p fragment to the VHS domain was no longer detectable (Figure 3-4B: Lanes 11, 12). These results reveal an interacting sequence in Pik1p (286-291) with the Gga2p VHS domain.

286-291 ^{acidic} mutation does not affect binding to the VHS domain, in the context of full length Pik1p

286-291 ^{acidic} mutations were introduced into the full length *PIK1* gene in vivo as described in Figure 3-5. The 286-291 ^{acidic} mutation was inserted into an allele of *PIK1* under the GPD promoter and N-terminally tagged with HA. Pik1p containing 286-291 ^{acidic} bound to Gga2p VHS domain. There was no change in binding of Pik1p containing 286-291 ^{acidic} compared to the wildtype Pik1p (Figure 3-6). This result raises the possibility additional bindings sites on Pik1p mediate an interaction with the VHS domain of Gga2p.

Additional VHS binding site in Pik1p

Given the domain architecture of Pik1p (Figure 3-1A), we hypothesized that a second potential VHS interaction site may be nearby to residues 286-291. To test this hypothesis we constructed several new Pik1p fragments (Figure 3-7). The N-terminus of the protein (residues 1-258), despite low solubility, interacted specifically with the VHS domain (Figure 3-7A, 3-8A). Expression of fragments from aa 1-200 resulted in low solubility, therefore we designed fragments of Pik1p that excluded aa 1-200. Each of these constructs contained 286-291 ^{acidic}

A

Wildtype 283-425
Mutant #1 I283A, K284A, L285A
Mutant #2 P286A, K287A, R288A
Mutant #3 K289A, P290A, K291A
Mutant #7 P286A, K287A, R288A, K289A, P290A, K291A
Mutant #8 P286E, K287E, R288D, K289E, P290D, K291E

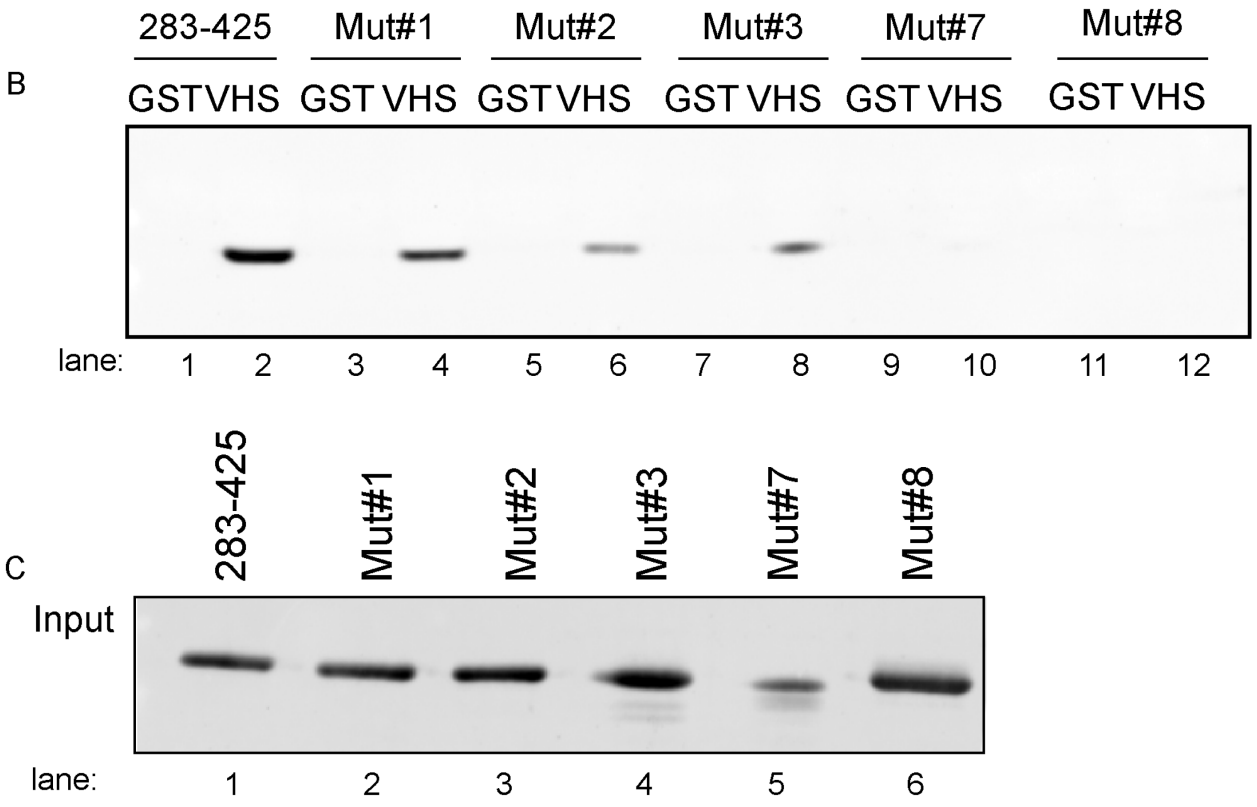

Figure 3-4. Pik1 286-291^{acidic} does not interact with the VHS domain

A fragment of Pik1 containing residues 283-425 is C-terminally HIS tagged, expressed from a pet28a vector and purified as described in Figure 3-3. This WT construct served as the template to introduce subsequent alanine mutations. **A.**) List of constructs used for the experiment. **B.)** Pulldown experiment using recombinately expressed, purified proteins of the given WT or mutant Pik1p fragments, GST and GST-VHS. Pulldown was conducted as described in figure 3-3. C.) Contains the inputs for each of the constructs used in the pulldown experiments. Input=2%. (anti-HIS 1:1000; QIAGEN)

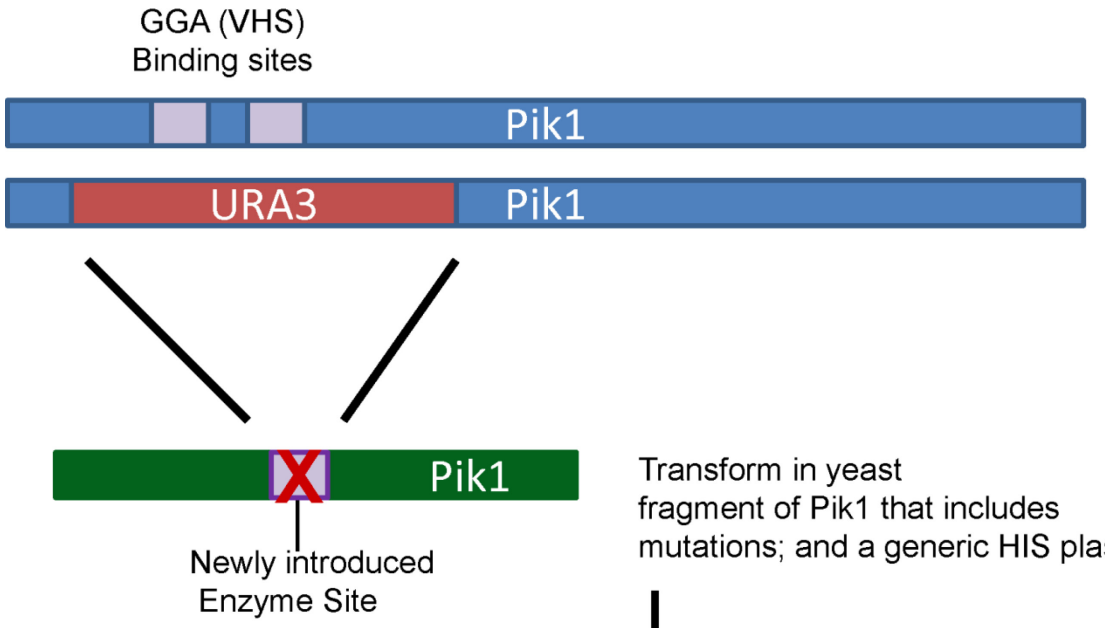

Transform in yeast
fragment of Pik1 that includes
mutations; and a generic HIS plasmid

↓

Select on SD-HIS plates

↓

Replica plate onto 5-FOA

↓

PCR amplify region with mutation

↓

Digest PCR product with PvuII
to identify clones wtih mutations

Figure 3-5. Strategy to introduce Pik1 286-291^{acidic} in vivo

DNA containing a *URA3* cassette was recombined into the region of *PIK1* that contained the putative VHS-binding site in a diploid, wildtype strain. **2.)** A fragment of DNA containing *pik1 286-291*^{acidic} with a PvuII site (the enzyme site was introduced with a single silent mutation) was co-transformed with a pRS423 which contains a HIS marker. Cells were then selected on SD-HIS plates and then replica plated onto 5-Fluoroortic acid plates (5-FOA). Under these conditions, cells that have successfully recombined Pik1 286-291^{acidic} allele can grow**.** Colonies that grew on 5-FOA were restruck onto a fresh 5-FOA plate and subsequently onto YPD. Single colony PCR was then conduced to generate a fragment from nucleotide 4-1620. PCR product was then digested with PvuII. Positive clones were then sporulated, dissected and subjected to tetrad analysis by PCR and PvuII digestion to obtain haploid cells with the*286-291*^{acidic} allele.

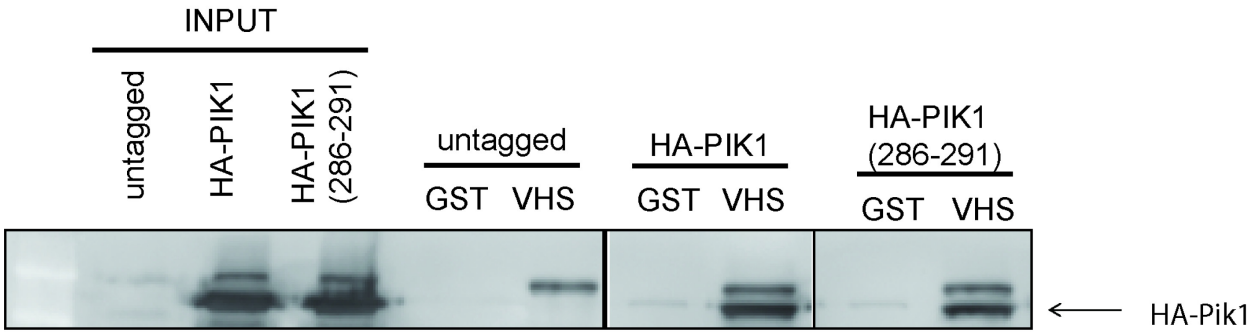

Figure 3-6. Pik1p 286-291^{acidic} does not affect binding to Gga2p VHS in yeast extracts.

Yeast cells containing untagged Pik1p, or HA-tagged Pik1p (wildtype, and Pik1p 286-291^{acidic}) were lysed and applied to glutathione-sepharose coupled to GST or GST-VHS. Bound proteins were eluted and then analyzed by SDS-PAGE and subsequent western blot analysis. Arrow denotes HA-Pik1p (anti-HA 1:1000; Sigma)

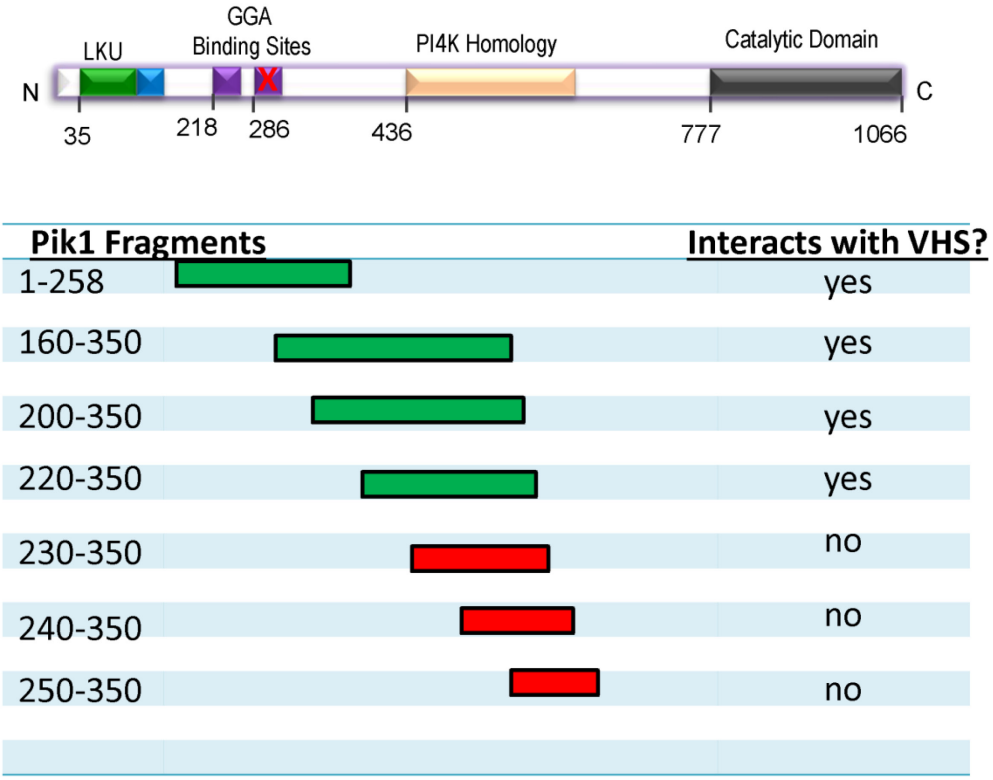

Figure 3-7. Constructs to identify a second Pik1p-VHS interaction site.

The left column indicates the residues of Pik1p that each fragment contains. The center column is a schematic of each fragment with its relative position on full length Pik1 (above). Green indicates that the recombinantly expressed and purified fragment of Pik1 interacted with a purified, recombinantly expressed GST-VHS domains. Red indicates that there was not a significant interaction between the Gga2 VHS domain and Pik1p. The right column denotes whether each Pik1p construct does or does not interact with the VHS domain.

mutations. Interaction of these newly generated fragments with the VHS domain is therefore only attributable to additional interacting residues on Pik1p. Using purified recombinantly expressed constructs, we narrowed the site of interaction between residues 220 and 230 (Figure 3-8, 3-9). These results indicate that there are at least two VHS interacting regions in Pik1p.

Pik1p 218-226 is a basic region that interacts with the VHS domain

Visual inspection of the Pik1p region between residues 200-230 revealed a basic sequence (^{218}KKTSRSKR^{225}) that is similar to the binding site identified at residues 285-291 of Pik1. Pik1(215-350) more robustly interacted with the VHS domain compared to Pik1(220-350), supporting the hypothesis that residues upstream of 220 play a role in mediating the Pik1-VHS interaction (data not shown). To characterize which residues are important for binding, we mutated sets of three adjacent residues from 218-229 to either aspartic acid or glutamic acid (Figure 3-9: A-C). Each of these mutants lost detectable binding to the Gga2p VHS domain. This result suggests one of two possibilities. First, that many residues in this region are important for binding to the VHS domain and that mutation of any three adjacent residues results in lost binding. Second, acidic residues, to which the endogenous amino acids are mutated, can in this context, affect the binding of neighboring residues. To test between these hypotheses, we mutated adjacent sets of three amino acids, in Pik1p between 218-229, to alanine (Figure 3-10A). Constructs containing mutations in 218-220 or 224-226 exhibited decreased affinity for the VHS domain relative to wildtype (Figure 3-10B: Lanes 7,8,11,12). Interestingly, both mutants normally contain multiple basic residues. When we mutated all of the basic residues in this area to alanine we reduced the Pik1-VHS interaction further (Figure 3-10C, lane 8 and 9). Alanine mutation in residues 221-223, 227-229 and to a lesser extent 230-232 did not greatly affect binding to the VHS domain.

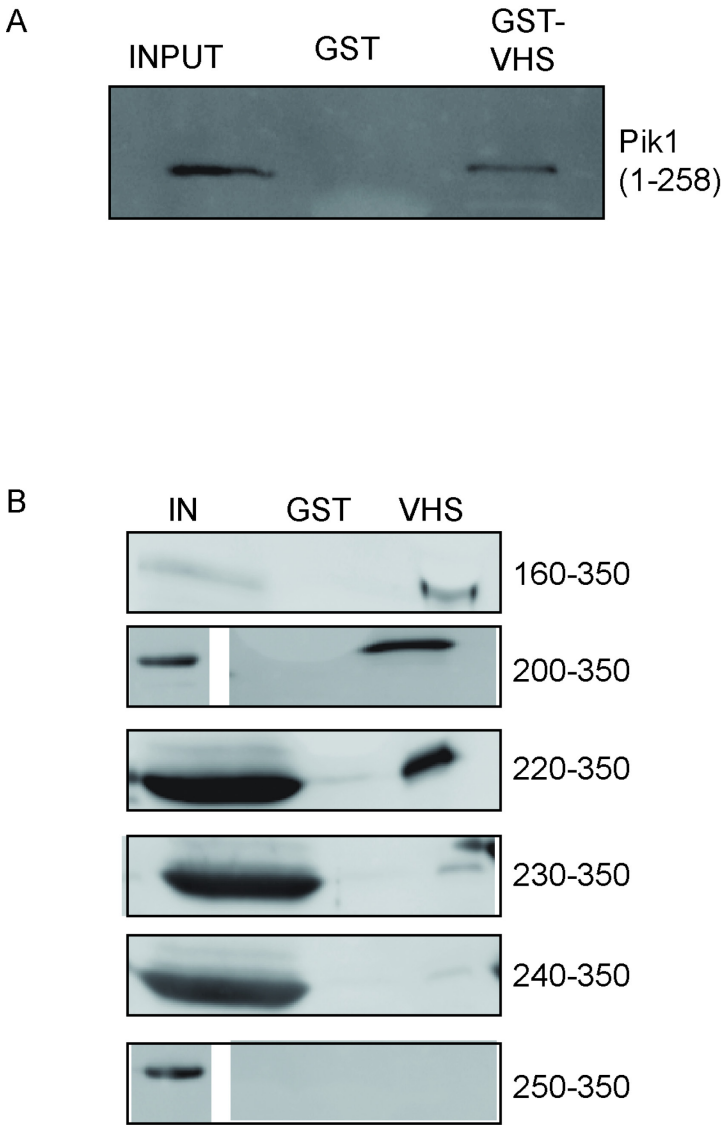

Figure 3-8. Residues 220-230 of Pik1p interact weakly with the VHS domain of Gga2p

Purified, recombinant His6-tagged Pik1(1-258) was incubated with glutathione-sepharose coupled to GST or GST-Gga2pVHS (VHS). Bound proteins were eluted and analyzed by SDS-PAGE and immunoblotting. **A.)** Pulldown using the wildtype Pik1p residues 1-258. B.) Purified recombinant His6-tagged Pik1p 160-350, 200-350, 220-350, 230- 350, 240-350, and 250-350 were incubated with gluthathione sepharose coupled to GST or GST-VHS and then analyzed as described above . Each of these constructs contains the 286-291^{acidic} mutation**.** (anti-HIS 1:1000, QIAGEN)

A

Explanation of Constructs

215-325 215-325

218-220 K218E, K219E, T220A

221-223 S221E, R222E, S223D

227-229 S227D, S228E, S229D

218-225 K218E, K219E, R222E, K224E, R225E,

B

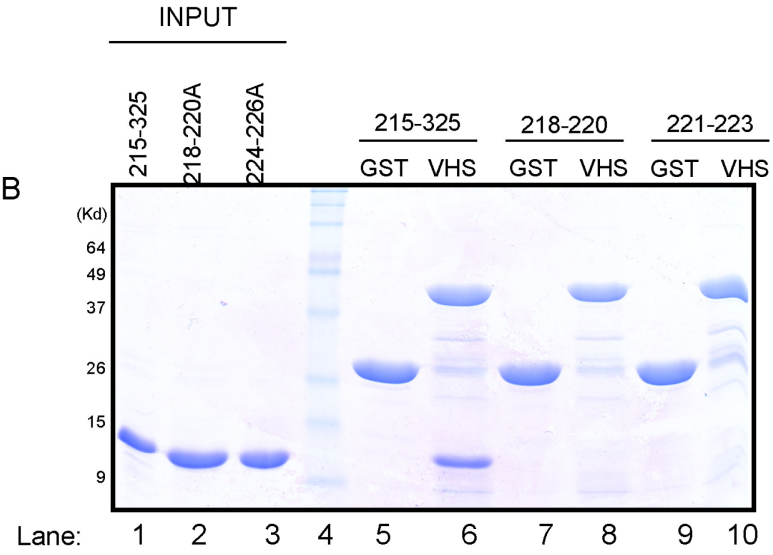

C

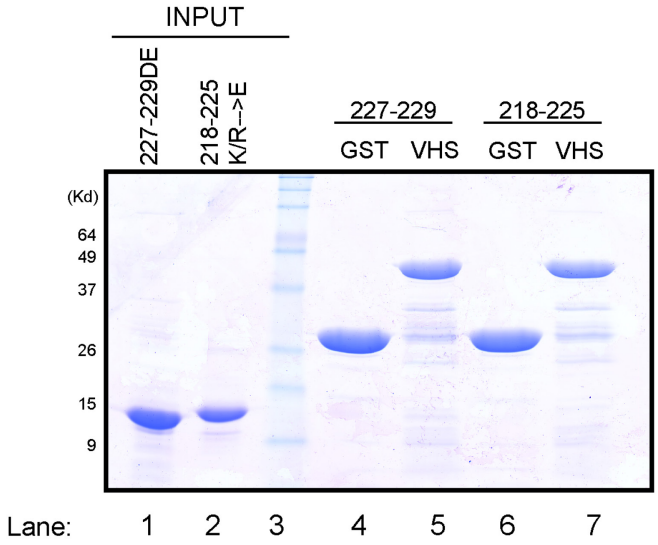

Figure 3-9. Acidic mutations in Pik1p abolish interaction with the VHS domain.

A.) List of constructs used for the experiment. A fragment of His6-Pik1 encompassing residues 215-325 contains the 286-291^{acidic} mutation. This construct served as the template to introduce acidic residues in sets of three from 218-229 of Pik1. **B.)** Recombinantly expressed, purified Pik1p constructs described in A were incubated with glutathione-sepharose and bound protein were analyzed by SDS-PAGE and coommassie blue staining. **C.)** Recombinantly expressed, purified Pik1p constructs described in A were incubated with glutathione-sepharose and analyzed as in **B**. Input=2%.

A

Explanation of Constructs

215-325 215-325 Wildtype

218-220 K218A, K219A, T220A

221-223 S221A, R222A, S223A

224-226 K224A, R225A, V226A

218-225 K218A, K219A, R222A, K224A, R225A,

B

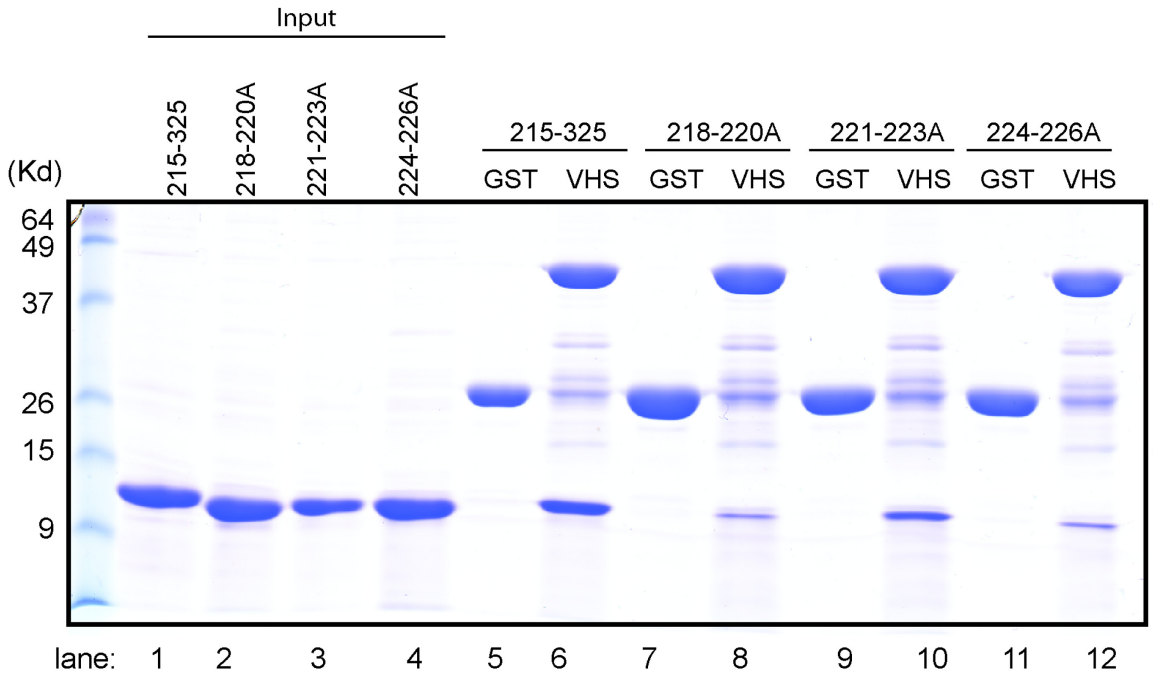

C

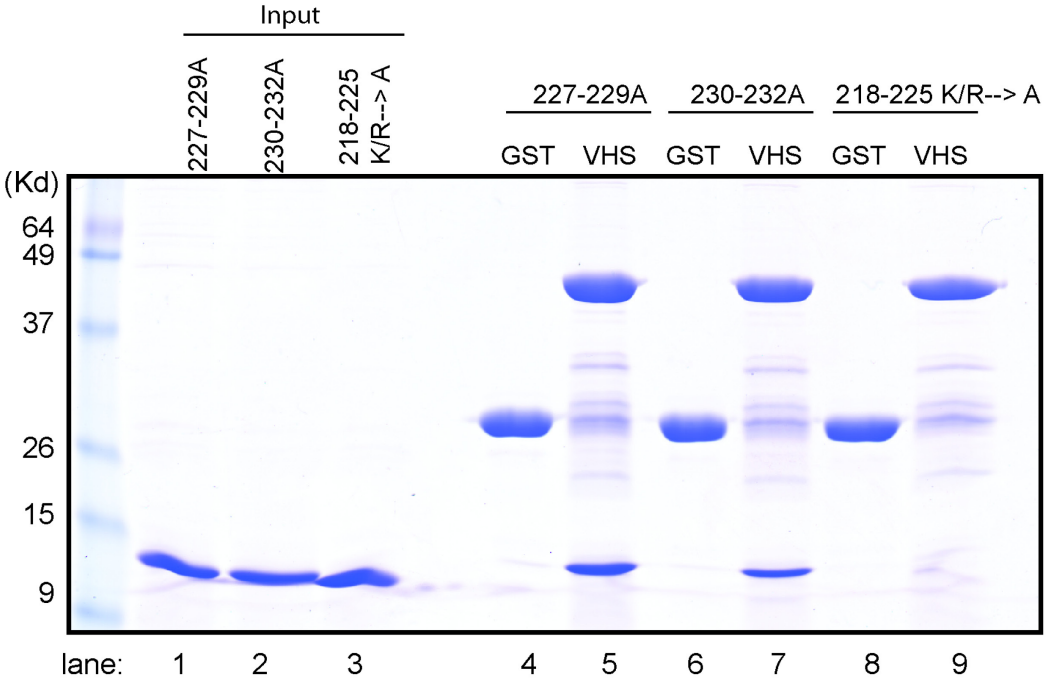

Figure 3-10. Alanine mutations in Pik1p 218-220 and 224-226 reduce interaction with the VHS domain.

A.) List of constructs used for the experiment. A fragment of His6-Pik1 encompassing residues 215-325 also contains the 286-291^{acidic} mutations. This construct served as the template to introduce acidic residues in sets of three from 218-229 of Pik1. **B.)** Recombinantly expressed, purified Pik1p constructs described in A were incubated with glutathione-sepharose and bound protein were analyzed by SDS-PAGE and coommassie blue staining. **C.)** Recombinantly expressed, purified Pik1p constructs described in A were incubated with glutathione-sepharose and analyzed as in **B**. Input=2%.

To distinguish which residues of Pik1p between 218-226 are important for mediating the interaction with the Gga2p VHS domain, we created several fragments of Pik1 that contained single amino acid substitutions. First, we compared single alanine or acidic mutations in residues from 218-221 (Figure 3-11 A-C). Mutation of K218E, K219E, T220D, and S221D ablated binding to the VHS domain (Figure 3-11: A, Lanes 7-12; B, Lanes 7,8). Alanine mutations in this context yielded milder phenotypes (Figure 3-11B, C). The K218A, K219A mutations reduced binding relative to wildtype, however not as significantly as the acidic mutations. Conversely, the T220A and S221A mutations did not have any significant effect on the Pik1p-VHS interaction. These results imply that alanine mutations are better to differentiate between those Pik1p residues that are important for binding to the VHS domain and those that are not. Based on these results, we chose to continue our mutational analysis using alanine substitutions (Figure 3-12, 3-13).

Alanine mutations differentially affect the two Pik1p Binding sites.

We have described the presence of two VHS binding sites in Pik1p, and heretofore we will refer to Pik1 (218-225) as VBS1 and Pik1 (286-291) as VBS2 (VHS Binding Site). Alanine scanning of VBS1 revealed that five basic residues (positions K218, K219, R221, K224, and R225) when mutated to alanine, resulted in a significant decrease in binding between the VHS domain and the corresponding Pik1p fragment. Conversely, only mild effects, if any were observed when non-basic residues were mutated (Figure 3-12 A, B). We then conducted an alanine scan of VBS2 to specifically identify those residues which contribute to the Pik1p -VHS interaction (Figure 3-13). When any single residue in the second binding site is mutated to alanine, there is no significant affect on the interaction with the VHS domain. These results indicate that, despite similarity in primary sequence between the two VHS binding sites of Pik1p, they differentially interact with the Gga2 VHS domain. This raises two possibilities: either they

differ in their affinity to the VHS domain and/or they interact with different sites on the VHS domain.

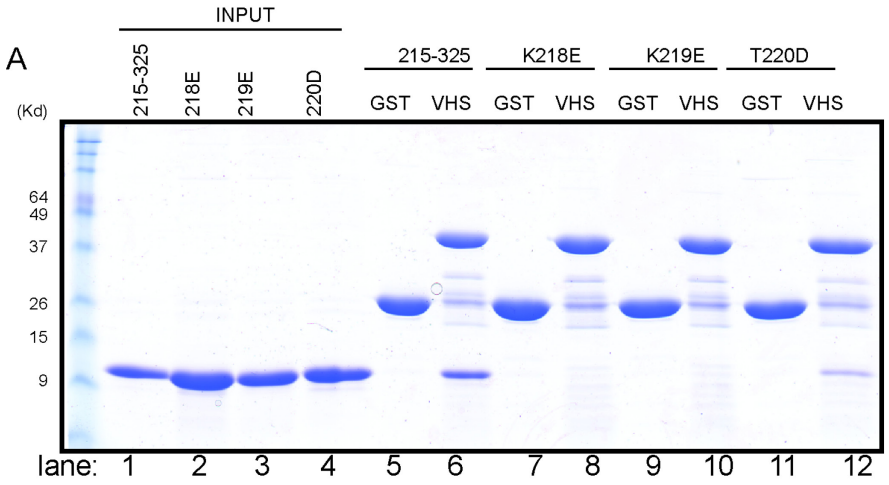
A
INPUT
215-325
218E
219E
220D
215-325
K218E
K219E
T220D
GST
VHS
GST
VHS
GST
VHS
GST
VHS
(Kd)
64
49
37
26
15
9
lane: 1 2 3 4 5 6 7 8 9 10 11 12

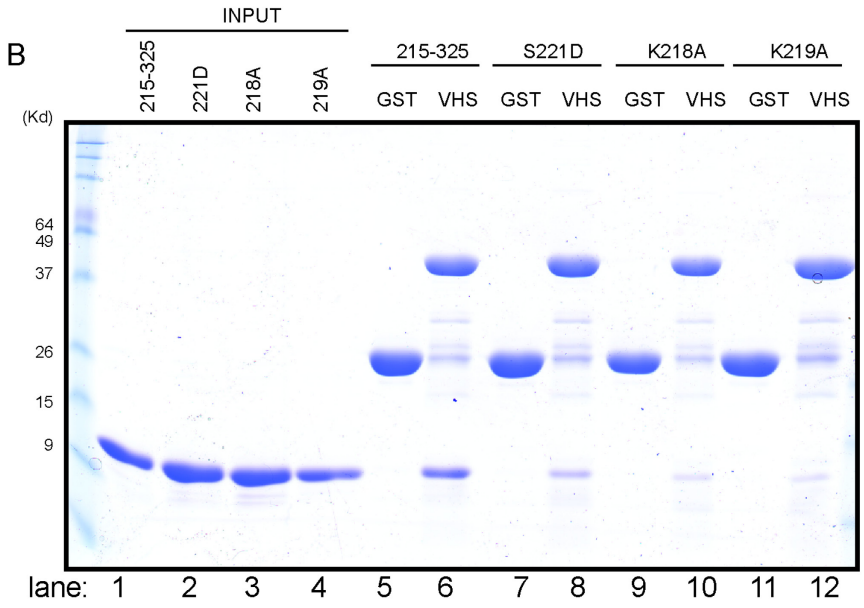
B
INPUT
215-325
221D
218A
219A
215-325
S221D
K218A
K219A
GST
VHS
GST
VHS
GST
VHS
GST
VHS
(Kd)
64
49
37
26
15
9
lane: 1 2 3 4 5 6 7 8 9 10 11 12

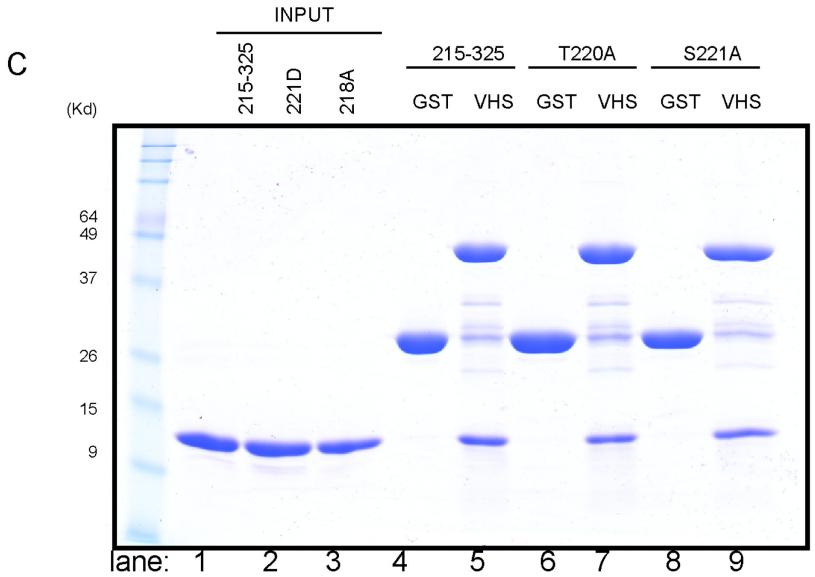
C
INPUT
215-325
221D
218A
215-325
T220A
S221A
GST
VHS
GST
VHS
GST
VHS
(Kd)
64
49
37
26
15
9
lane: 1 2 3 4 5 6 7 8 9

Figure 3-11. Alanine mutations are better than acidic mutations at parsing which Pik1p residues are important for VHS binding in Pik1 (218-221).

A fragment of His6 Pik1p encompassing residues 215-325, contains acidic mutations in residues 286-291. The Pik1p 215-325$^{286\text{-}291}$ construct served as the template into which single acidic or alanine mutations were introduced. **A.)** Recombinantly expressed, purified proteins Pik1 215-325, K218E, K219E, or T220D were incubated with glutathione-sepharose coupled to GST or GST-VHS and analyzed by SDS-PAGE and Coomassie Blue staining. **B.)** His6-Pik1 215-325$^{286\text{-}291}$ (S221D, K218A, or K219A) were incubated with glutathione-sepharose coupled to GST or GST-VHS and analyzed as described in A. **C.)** Pik1 215-325$^{286\text{-}291}$ T220A, or S221A were incubated with glutathione-sepharose coupled to GST or GST-VHS and analyzed as described in **A**. Input=2%.

A



B

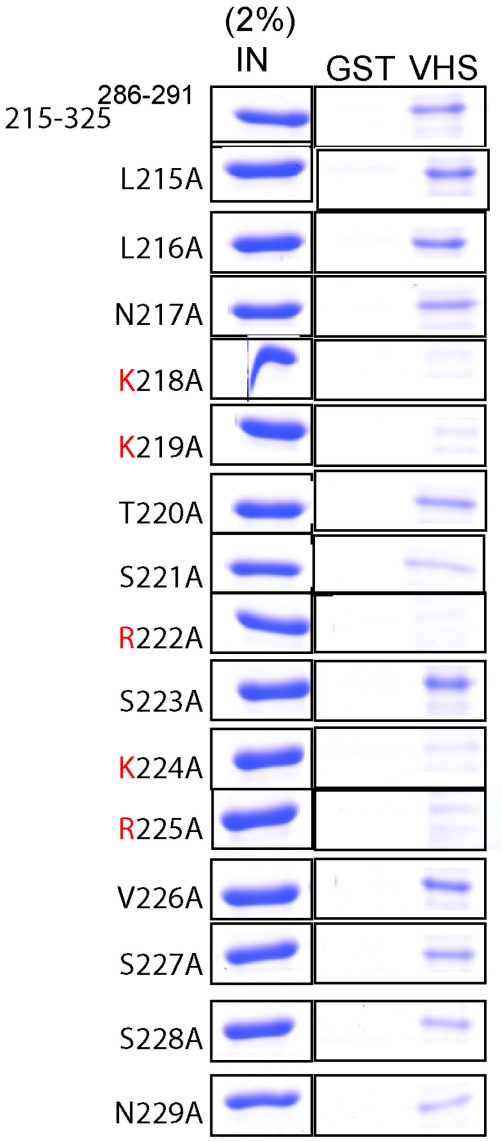

Figure 3-12. Alanine Screen through VBS1 reveals that basic residues are important for binding to the VHS domain.

A.) Alanine scan of VBS1 and surrounding residues. Those residues which exhibit decreased binding upon alanine substitution are shown in red. **B.)** His6-Pik1p 215-325$^{286\text{-}291}$ or His6- Pik1p

containing single alanine substitutions spanning from residue 215-229 were incubated with glutathione-sepharose coupled to GST or GST-VHS and analyzed by SDS-PAGE and Coomassie Blue Staining. Input=2%.

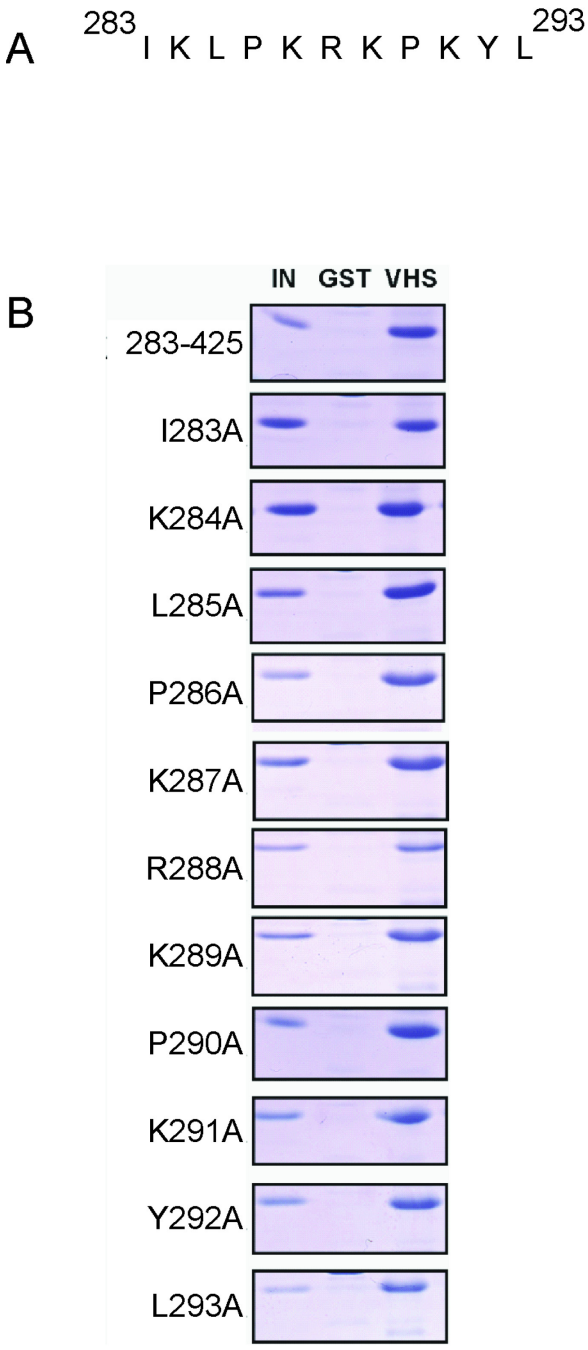

Figure 3-13 Single Amino Acid mutations to Alanine do not affect VBS2 binding to the VHS domain.

A .) Alanine scan of VBS2 and surrounding residues. B.) Recombinantly expressed, purified His6-Pik1p (283-425) or constructs of His6-Pik1p containing single alanine substitutions

spanning from residue 283-293 were incubated with glutathione-sepharose coupled to GST or GST-VHS and analyzed by SDS-PAGE and Coomassie Blue staining. Input= 2%.

Pik1^{GGA} exhibits reduced binding to the VHS domain.

To analyze the contribution of the VHS binding sites on Pik1, both VBS1 and VBS2 were mutated in the context of the full length gene in vivo (K218E, K219E, S220A, P286E, K287E, R288D, K289E, P290D, and K291E). These mutations will be referred to as pik1^{GGA}. Mutations were introduced in vivo using a similar strategy to that described in Figure 3-6. HA-Pik1p^{GGA}, from cell extracts, interacted less well with the Gga2p VHS domain than did wildtype HA-Pik1p (Figure 3-14). This result provides evidence that mutation of VBS1 and 2 inhibits the Pik1p-Gga2p interaction in vitro.

pik1^{GGA} affects cell growth.

Cells expressing Pik1^{GGA} were grown to exponential phase in a liquid culture and then plated onto rich media (YPD). After 2 days of growth at 37°C, *pik1^{GGA}* cells exhibited a temperature sensitive phenotype. They grew more slowly compared to wildtype (Figure 3-15). Previous studies have shown that mutations in either the AP-1 or GGA pathway result in very mild growth defects (Costaguta et al., 2006; Costaguta et al., 2001). However mutation in both pathways is near lethal. When we combined the *pik1^{GGA}* mutation with *gga2*Δ, we detected a synthetic growth phenotype compared to either of the single mutations. This serves as a genetic indication that the AP-1 pathway is being affected by the *pik1^{GGA}* mutations.

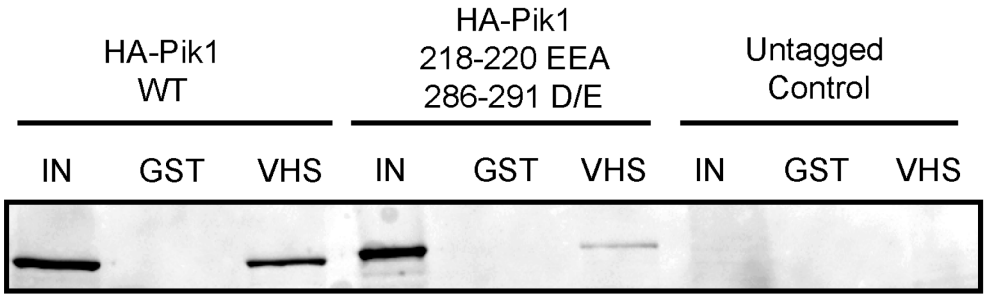

Figure 3-14 Pik1^{GGA} exhibits reduced binding to the VHS domain.

Extracts from cells containing untagged Pik1p, HA-Pik1p (WT) or HA-Pik1^{GGA} were incubated with glutathione-sepharose beads coupled to purified GST or GST-VHS. Bound proteins were analyzed by SDS-PAGE and immunoblotting. Input=1%. (polyclonal anti-HA 1:250, Clontech).

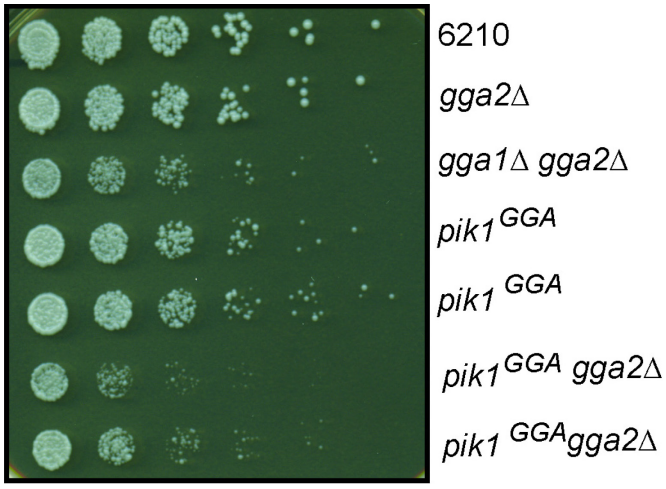

Figure 3-15. Introduction of *pik1*^{GGA} inhibits growth.

Using a strategy similar to the one described in Figure 3-6, mutations in both VHS binding sites were introduced in vivo into an untagged allele of *PIK1* that is under its endogenous promoter. VBS1 contains the mutations 218E, 219E, 220A and VBS2 contains the mutations, 287E, 288D, 289E, 290D, 291E (GPY 5047 and GPY 5048). These strains along with a wild-type strain (SEY6210), *gga2*Δ (GPY 2149), *gga1*Δ*gga2*Δ (GPY 3431.1), *pik1*^{GGA} *gga2*Δ (GPY 5049 and GPY 5050) were grown to exponential phase on rich media at room temperature and then spotted onto YPD +AUT plates. This plate was grown at 37°C for 1 day.

pik1^{GGA} affects PI4P, Ent5p and AP-1 localization in vivo.

Movies of cells expressing GFP or mRFP tagged clathrin coat fusion proteins, or the TGN marker Sec7p were acquired by spinning disc confocal microscopy. Each fusion protein was expressed from its endogenous locus, as the only source of that protein in the cell, and has been assayed for functionality as described in (Daboussi et al., 2012). Each fusion protein localized as puncta throughout the cell, frequently near the plasma membrane, as normally obsesrved of TGN localization in yeast.

Sec7p-mRFP and a PI(4)P marker (GFP-PH^{OSH1}) were expressed in cells (Loewen et al., 2003). Sec7p-mRFP is recruited first to the membrane and reaches its peak fluorescence intensity 3.8s ± 1.1s (n=18 puncta) before GFP-PH. This result is in agreement with previous studies (Daboussi et al., 2012). However, in cells that contained *pik1^{GGA}*, GFP-PH^{OSH1} was delayed in its accumulation at the TGN and did not reach peak fluorescence intensity until 8.8s ± 1.5s after Sec7p-mRFP (n=25 puncta, p=0.003; Figure 3-16A) .

AP-1 has been shown to rely on the phosphoinositide, PI(4)P, as a localization signal. In previous studies, when PI(4)P was depleted AP-1 was mislocalized and when PI(4)P accumulation was delayed AP-1 was delayed in its recruitment to the TGN (Daboussi et al., 2012). pik1p^{GGA} cells exhibit delays in AP-1 assembly. In wildtype cells AP-1 reached its maximum fluorescence intensity 11.3s ± 1.1s (n=22 puncta) after Gga2p-mRFP. In *pik1^{GGA}* cells AP-1 reached maximum fluorescence after Gga2p-mRFP 25.5s ± 1.9s (n=41 puncta; p= 2.0 X $10^{-7;}$ Figure 3-16B).

In wildtype cells expressing Ent5p-mRFP, puncta are bright and localized to areas near the plasma membrane. However, in *pik1^{GGA}* cells, Ent5p-mRFP is partially mislocalized. Ent5p-mRFP mislocalization makes analysis with time-lapse movies technically challenging because of difficulties with exacerbated bleaching of a weak Ent5p-mRFP signal (Figure 3-17A). We also

detected that there were fewer observable puncta per cell, in cells expressing pik1p^{GGA} versus wildtype. We calculated an average of 3.4 puncta per cell (n= 82 cells) in wildtype cells versus1.5 puncta per cell in *pik1^{GGA}* cells (Figure 3-17B; n= 126 cells; p= 3.8 X 10^{-15}). These results indicate that the pik1p^{GGA} mutations affect PI4P accumulation and those adaptors Ent5p and AP-1 which rely on PI(4)P as a signal for recruitment to the TGN.

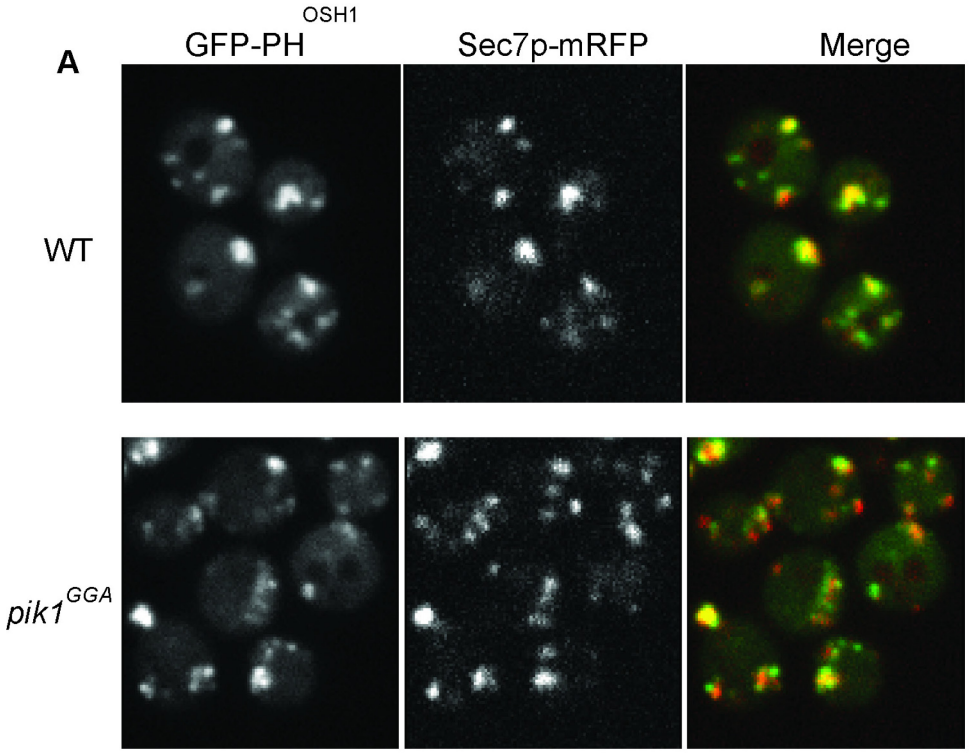
A
OSH1
GFP-PH
Sec7p-mRFP
Merge
WT
pik1GGA

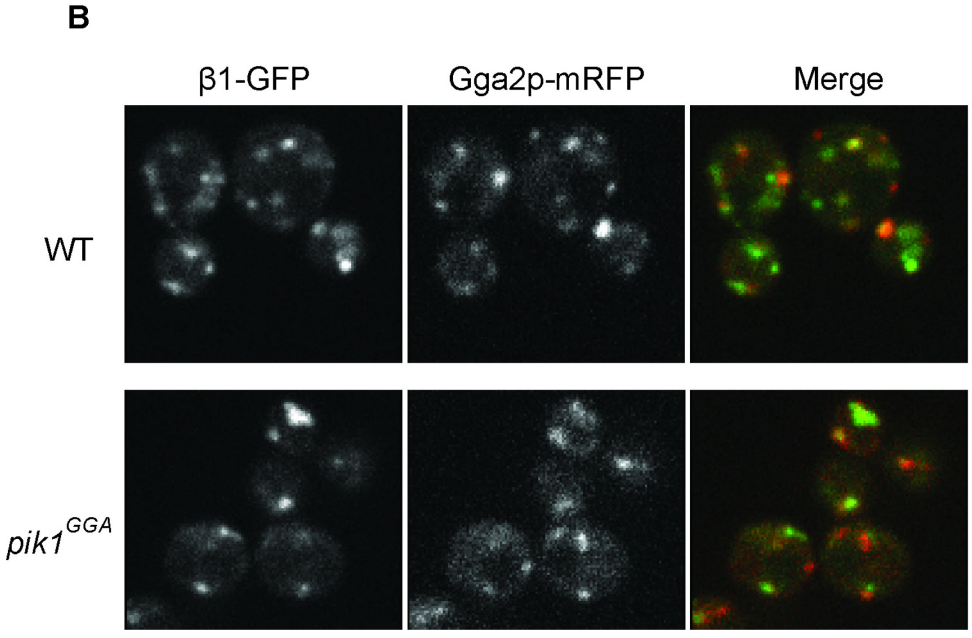
B
β1-GFP
Gga2p-mRFP
Merge
WT
pik1GGA

Figure 3-16. Pik1^{GGA} causes a delay in PI4P accumulation,and AP-1 recruitment

Using a strategy similar to the one described in Figure 3-6, mutations in both VHS binding sites were introduced in vivo. Binding site #1 contains the mutations 218E, 219E, 220A and binding site #2 contains the mutations 286-291286E, 287E, 288D, 289E, 290D, 291E. **A)** Cells expressing GFP-PH^{OSH1} Sec7p-mRFP (Upper Panel; GPY 4938) or GFP-PH^{OSH1} Sec7p-mRFP *pik1^{GGA}* (Lower Panel; GPY 5052) were imaged by spinning disc confocal microscopy **B.)** β1-GFP Gga2p-mRFP (Upper Panel; GPY 3109) or β1-GFP Gga2p-mRFP *pik1^{GGA}* (Lower Panel; GPY 5053) Cells expressing the indicated GFP- and mRFP-tagged proteins were imaged by confocal time-lapse movies. The time to acquire one image pair was 1.2s.

A

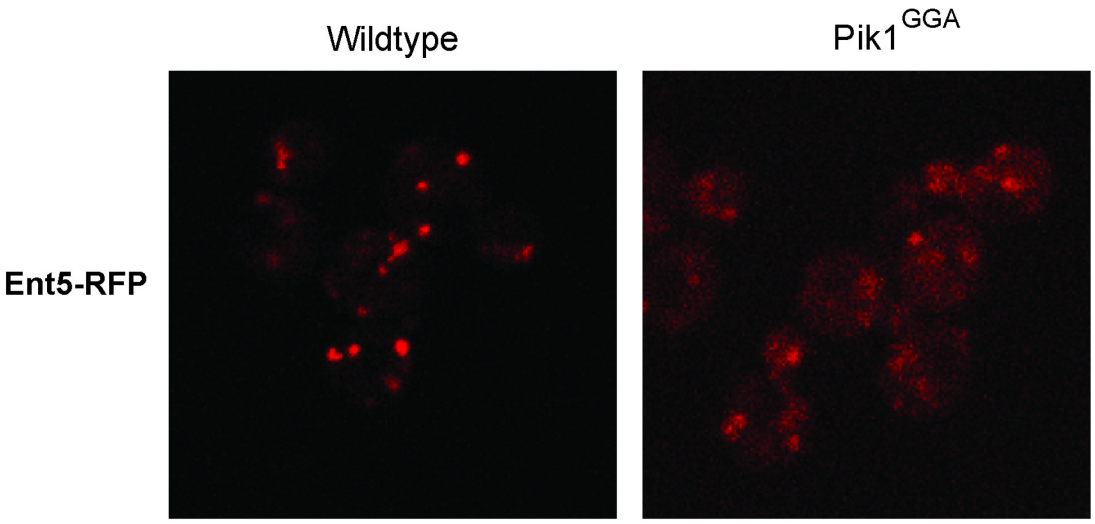

B

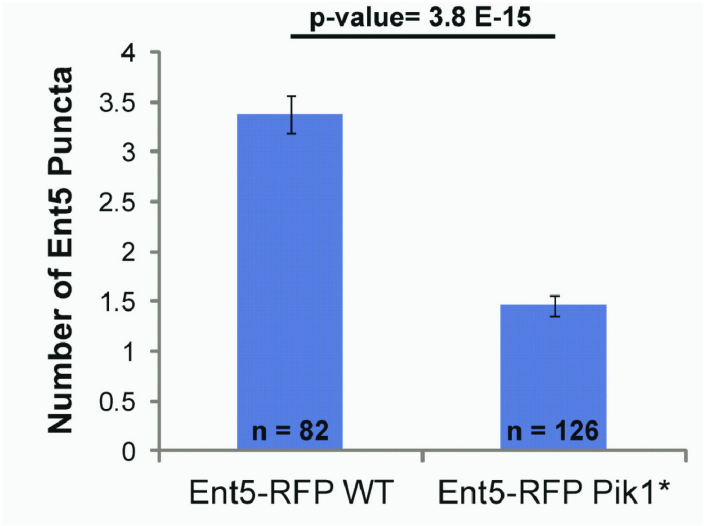

Figure 3-17. pik1p^{GGA} causes Ent5p mislocalization

A.) Live cell imaging by spinning disc confocal of cells expressing Ent5p-mRFP in wildtype (left panel) or *pik1*^{GGA} cells (right panel). **B.)** The number of Ent5-mRFP puncta in each cell were counted, summed, and then divided by the total number of cell counted for each population (wildtype versus *pik1*^{GGA} cells). p=3.8 X 10^{-15}, n= number of cells.

Direct binding between the VHS and GAT domains of Gga2

During our analysis with whole cell extracts (WCE) we found that Gga2p fragments containing either the VHS domain or the VHS-GAT domain interacted equally well with full length Pik1p (Figure 3-18). However, during our analysis with purified Pik1p fragments, we observed a consistently stronger interaction with the VHS domain than with the VHS-GAT domain over a range of concentrations of Pik1p, and under different buffer conditions (Figure 3-19A and B and data not shown). This raises the possibility that an interaction between the VHS and GAT domains prevents Pik1p from interacting in vitro with Gga2p. We tested this possibility by first assaying whether the VHS and GAT domains could interact in vitro. We found that we could reliably detect a specific and direct interaction between soluble GAT domain and the VHS domain (Figure 3-20). We conducted a similar experiment using the VHS and GAT domains of Gga2 from *mus musculus*, and found that the interaction between the Gga2 VHS and GAT domains is conserved (Figure 3-21).

We hypothesized that an unknown VHS or GAT binding protein may be supplied from the WCE, that when bound would be competent to open the VHS and GAT domains such that Pik1p would then be able to interact with the VHS domain. We took a candidate approach and first tested the ability of Arf1p to fulfill this role in vitro. In the absence of GTP-bound Arf1p, Pik1p does not detectably interact with the VHS-GAT domain. However, when Pik1p is applied to glutathione-sepharose coupled to VHS-GAT that had been prebound with GTP-Arf1p, Pik1p now interacts with the VHS-GAT construct similarly to VHS alone (Figure 3-22). These data indicate that GTP-Arf1p bound to the VHS-GAT facilitates Pik1p binding to the VHS domain.

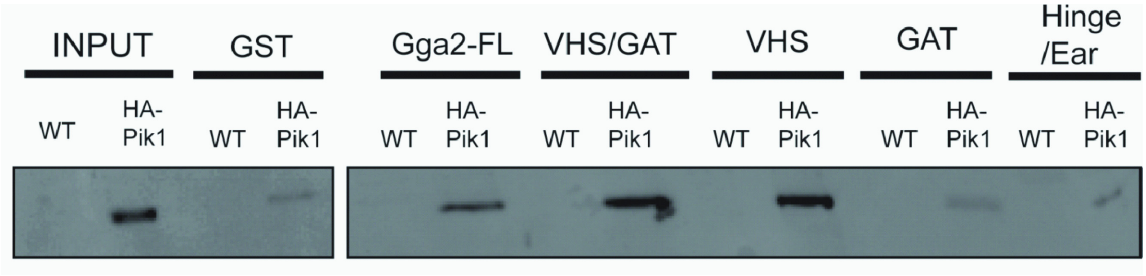

Figure 3-18. Both VHS and VHS-GAT domains bind to Pik1p

Extracts from cells containing untagged Pik1p, or HA-Pik1p (WT) were incubated with glutathione-sepharose beads coupled to purified GST, GST-Gga2p, GST-VHS-GAT, GST-VHS, GST-GAT, GST-Hinge/Ear. Bound proteins were analyzed by SDS-PAGE and immunoblotting. Input= 1%. (polyclonal anti-HA 1:250, Clontech).

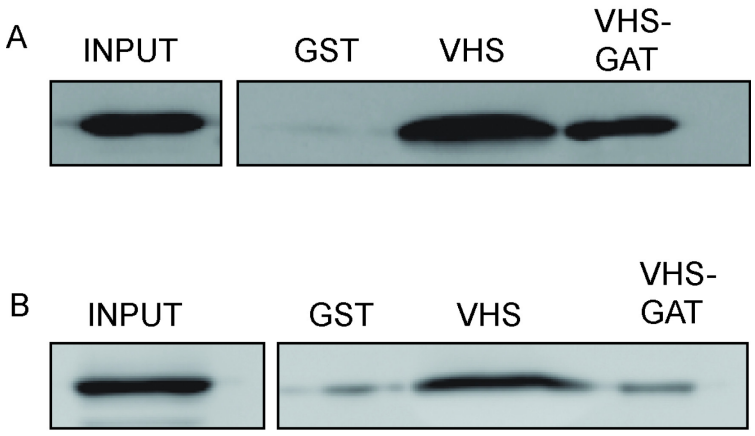

Figure 3-19. The VHS domain of Gga2p interacts more robustly with Pik1 than does the VHS-GAT domain.

Affinity binding of yeast Gga2p VHS or VHS-GAT domains. Purified, recombinantly expressed His6-Pik1 (250-590) was incubated with glutathione-sepharose coupled to GST, GST-VHS, or GST-VHS-GAT in a buffer containing **A.)** 50mM Hepes pH 7.4, 50mM NaCl or **B.)** 50mM Hepes pH 7.4, 150mM NaCl. **(A, B)** Bound proteins were analyzed by SDS-PAGE and immunoblotting Input= 5%. (anti-HIS6 1:1000, QIAGEN).

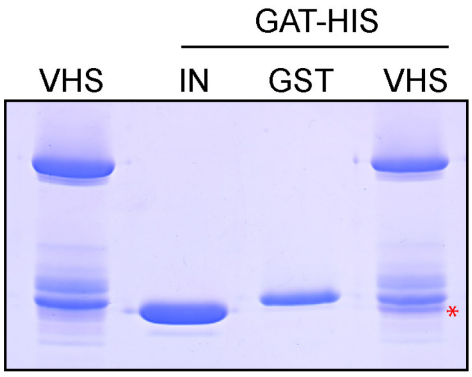

Figure 3-20 VHS and GAT domains of Gga2 interact in vitro in *S. cerevisiae*

Affinity binding of the Gga2p VHS domain from yeast. Purified, soluble GAT-HIS from *S. cerevisiae* Gga2p was incubated with glutathione-sepharose beads coupled to either GST or GST-VHS and allowed to bind. Bound samples were eluted and analyzed by SDS-page, and Coomassie Blue staining. INPUT=2% (*) denotes bound Gga2 GAT-HIS.

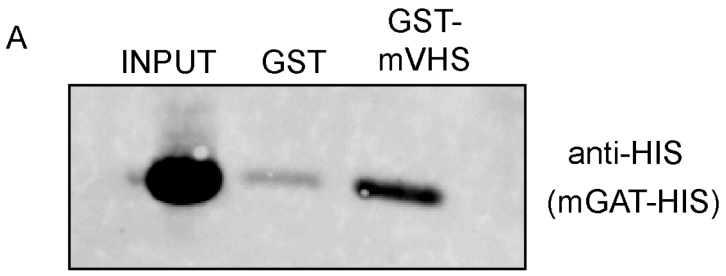

Figure 3-21 Gga2 VHS domain interacts with its GAT domain in trans from *mus musculus*.

Affinity binding of the Gga2p VHS domain from mouse. Recombinantly expressed, purified GAT-HIS6 was then applied to glutathione sepharose coupled to either GST or GST-VHS from mouse Gga2 and allowed to bind. Samples were eluted and analyzed by SDS-page and western blot analysis.

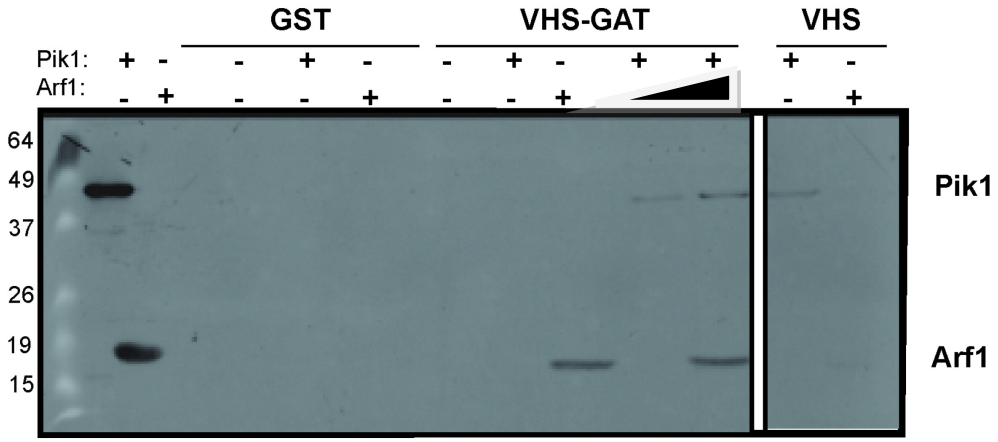

Figure 3-22 GTP-Arf1p enhances the interaction between VHS-GAT of Gga2p and Pik1p.

Affinity binding of yeast VHS-GAT. Pik1p (250-590)-HIS and Arf1p (Δ1-17, Q71L) were recombinantly expressed, and purified. Arf1p was preincubated with GTP. Arf1p and Pik1p were added as indicated to glutathione-sepharose coupled to GST, GST-VHS or GST-VHS. Bound proteins were analyzed by SDS-PAGE and immunoblotting (anti-HIS6 1:1000, QIAGEN).

Binding of Pik1p to the VHS domain of Gga2p is conserved

Through a homology search of Pik1p with potential mammalian homologues we identified PI4KIIIb as the closest homologue of Pik1p, in agreement with previous studies (Balla and Balla, 2006; Graham and Burd, 2011). Two fragments of PI4KIIIb were then generated that encompassed a region containing the homologous Pik1p-VHS binding sites. PI4KIIIb (195-308) specifically interacted with the VHS domain of mammalian Gga2 (Figure 3-23 A). This result raises the possibility that a mechanism for recruitment of Pik1p to the TGN via the VHS domain of Gga2, similar to the one observed in yeast, is conserved in mammalian cells.

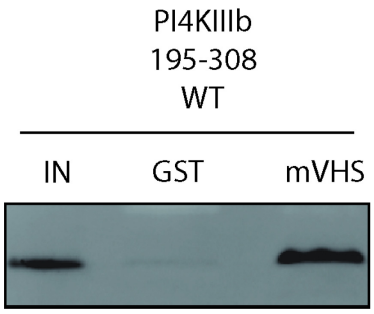

Figure 3-23 PI4KIIIb interacts with the VHS domain of Gga2 in *M. musculus*

A.) Affinity binding of GST-VHS from mouse Gga2. PI4KIIIb (195-308) was recombinantly expressed, purified and incubated with glutathione-sepharose coupled to GST or to GST-VHS from *mus musculus***.** Bound proteins from both experiments were analyzed by SDS-PAGE and immunoblot (anti-HIS 1:1000, QIAGEN).

DISCUSSION

We have found two binding sites on Pik1p that interact with the VHS domain of Gga2. The ability of Gga2p to interact with Pik1p is regulated by GTP-Arf1p binding to the GAT domain of Gga2p. The interaction of Pik1p and Gga2p promote PI4P production at the Golgi, and this PI4P production promotes the recruitment of two downstream clathrin adaptors: Ent5p and AP-1. This crucial sequence of events describes how GGA proteins contribute to AP-1 and Ent5 vesicle biogenesis.

Mapping the Pik1p-GGA interaction motifs

We have identified two linear motifs in Pik1p, enriched with basic residues, that directly interact with the VHS domain of Gga2p. We have mapped the region of interaction of Pik1p between residues 200-760, omitting the N- and C-terminus. These two domains were very insoluble, difficult to purify, and generally so little protein was obtained that the results were difficult to interpret. Pik1 (1-258) did yield some protein so that we could determine that there was a binding determinant in this region, however when additional constructs delimiting the region (1-200) were constructed, they were generally insoluble and all showed some level of weak binding to the VHS domain. It was difficult to determine whether this result represented a real interaction of Pik1p with the VHS domain, or whether these highly insoluble proteins were also just binding nonspecifically to the VHS domain. The kinase domain (aa 761-1066) also showed a similar pattern, very little protein could be successfully purified, however Pik1 (761-1066) showed some small level of interaction with the VHS domain. 761-1066 contains the basic sequence ^{855}KKALTKKM^{902} which resides within the catalytic domain of Pik1p, and may overlap with residues thought to be involved in the coordination of ATP. There are no obvious basic stretches found in Pik1 (1-200). It is possible that if this fragment interacts with the VHS domain, it does so through a different type of motif.

Differences between the two VHS binding sites in Pik1p

In vitro, both binding sites behave differently. VBS1, (^{218}KKTSRSKR^{225}) is sensitive to even single alanine mutations of the basic residues. Acidic mutation of any residue in this region completely eliminates binding to the VHS, as detected by Coomassie blue staining. VBS2 (^{283}IKLPKRKPK^{291}), by contrast, requires the concerted mutation of several residues before there is a significant decrease in binding to the VHS domain. Both VBS1 and VBS2 contain 5 basic residues, however their spacing is different. VBS2 contains two proline residues which could introduce kinks into this region, acting as a stabilizing force for this fragment so that it could securely interlock with the VHS domain. VBS1 (and VBS2) is predicted to be unstructured; it may be more flexible, less adherent to the VHS domain and thereby more sensitive to mutation.

A more definitive understanding of the basis of differential interaction between VBS1 and VBS2 can be obtained in two ways. First, measure the affinity coefficients (K_D) of each motif to the VHS domain through Biacore experimentation. Second, determine whether each of the Pik1p motifs interacts with the same or different regions of the VHS domain. Mapping the binding site(s) on the VHS domain that interacts with Pik1p would increase our understanding as to whether these two motifs interact with the same site of different Gga2p molecules in a 1:2 stoichiometry, or whether they interact with different sites of the same Gga2p molecule in a 1:1 stoichiometry. Knowledge of this difference could indicate differences in clustering of these two proteins (discussed in more detail in Chapter 7).

When VBS1 and VBS2 were mutated together in vivo in the context of the full length protein, interaction with the VHS domain was not completely ablated as observed by a pulldown assay. This may indicate that there are other regions of Pik1p that interact with the VHS domain, possibly residues at the N- and C-terminal regions. Otherwise, it is possible that there

is a network of indirect interactions between Gga2p and Pik1p. For example, Pik1p has been shown to directly interact with Sec7p, an ARF-GEF for Arfp1. Arf1p in turn directly interacts with the GAT domain of Gga2p and we have shown that the GAT domain of Gga2p directly interacts with the VHS domain of Gga2p. Therefore it is possible that the residual interaction seen in pulldown experiments when both Pik1p interaction sites are mutated is the result of these binding networks.

Conservation of the Pik1p-Gga2p interaction to mammalian cells

The mammalian homologue of Pik1p is PI4KIIIb, so we chose the region of PI4KIIIb that contained potential VBS1 and VBS2 along with surrounding residues. The region of PI4KIIIβ aa (195-308), contain two basic motifs similar to VBS1 and VBS2. These regions of PI4KIIIb also directly interacts with the VHS domain of mammalian Gga2p. These two motifs are: ^{228}RHSRGTKLRK^{237} and ^{246}LKAHRKR^{252}. I mutated each of the basic residues in both sequences to acidic residues in the context of the 195-308 fragment, and in each case the resulting construct did not show dramatically decreased interaction with the VHS domain (data not shown). It is possible that if these in vitro interaction represent truly conserved interactions that there may either be additional determinants in this fragment that bind to the VHS domain, or that the mechanism of binding may be different. Even if the motifs are different from yeast to mammals, the region of binding appears to be the same.

In in vitro experiments, I have found that PI4KIIIb binding to the VHS domain of mGga2 is greater than to mGga1. The VHS domains of both proteins are highly homologous, exhibiting 78% sequence similarity. The highest region of dissimilarity between the two proteins involves a stretch of 18 residues at the N-terminus that are present in mGga2 but not found in mGga1. The sequence found in mGga2p is ^{11}G**S**PAGT**ES**A**E**GGPGAAAL^{28}. This sequence contains two

acidic residues and two polar residues which could possibly contribute to binding basic residues in PI4KIIIb.

Effects of pik1p^{GGA} in vivo

pik1p^{GGA} does have an effect on cell growth. Pik1p^{GGA} also significantly affect the accumulation of PI(4)P at the TGN, and consequently the recruitment of AP-1 and Ent5p. Genetic disruption of AP-1 and Ent5p function however, does not have significant effects on growth, or effects on maturation of the mating pheromone α-factor (Costaguta et al., 2006). In fact, mutation in either the AP-1 or GGA pathway does not significantly affect cell growth. However, mutation in both pathways has near lethal results (Costaguta et al., 2006; Costaguta et al., 2001). By fluorescence microscopy, AP-1 recruitment is delayed in the *pik1^{GGA}* mutant, and Ent5p is partially mislocalized. Because pik1^{GGA} mutant is affecting the AP-1/Ent5p trafficking pathway, it was possible that there may also be a synthetic interaction with mutations in the GGA pathway. If true, this would present a genetic argument that the pool of PI(4)P that is delayed at the TGN in the Pik1^{GGA} mutant, is likely PI(4)P that is specifically generated for the recruitment of AP-1 and Ent5.

AP-1 and the lipid marker GFP-PH^{OSH1} are significantly delayed in the *pik1^{GGA}* mutant. The delays are nearly comparable with full deletions of both *GGA1* and *GGA2* genes. We hypothesize that the mutations in *pik1^{GGA}* are specifically affecting the direct interaction between Pik1p and Gga2p, however it may be possible that Pik1p interacts with other recruiting proteins via these basic motifs. Without doing a whole genome screen to identify additional possible interacting partners in this region, we can still test for specificity of GGA function. In the future, GGA should be overexpressed in a strain background that contains Pik1^{GGA} to determine if forcing an interaction between Gga2p and Pik1p can at least partially rescue the *pik1^{GGA}*

phenotype. This experiment, could confirm that the Pik1^{GGA} mutant phenotype is due primarily to the loss of the Pik1-GGA interaction.

To biochemically and genetically ascertain the effects of the pik1^{GGA} mutation in vivo we should identify which cargo, and which trafficking pathways, if any, are being disrupted by the *pik1^{GGA}* mutation. AP-1 and Ent5p are thought to be involved in anterograde and retrograde trafficking between the TGN and early endosomes (Costaguta et al., 2006; Duncan and Payne, 2003). However, the distruption of these two proteins (through mutation or full gene deletion) does not have strong effects on growth or trafficking alone. The GGA proteins are thought to be involved in anterograde trafficking from the TGN to the late endosome. Disruption of both AP-1 and GGA pathways is lethal in yeast. This synthetic effect can be used to identify possible synthetic phenotypes between *pik1^{GGA}* and the adaptors. Likewise, the sorting of the mating pheromone α-factor relies on clathrin trafficking of its main protease, Kex2p, for proper phereomone maturation. Both AP-1 and GGA play a role in the fidelity of Kex2p receptor recycling (Costaguta et al., 2001; Fuller, 1988; Payne and Schekman, 1989). By assessing the potential synthetic defects of Kex2p recycling, we would be able to independently evaluate the role that *pik1^{GGA}* plays in the AP-1 pathway.

Conservation of the Pik1-GGA interaction as a means to recruit AP-1

The significance of this interaction is based on the premise that these proteins are each conserved in humans. The mechanism identified in yeast may have some significance for the recruitment of PI4KIIIβ to the Golgi and the role that GGA potentially plays in this recruitment together with the biogenesis of AP-1 enriched vesicles. A recent study using inhibitors of TOR signaling to retarget AP-1 and GGA2 to the mitochondria (which could potentially also disrupt intracellular clathrin localization) identified AP-1 as a “lynchpin,” necessary for the recruitment of

GGA into AP-1 vesicles (Hirst et al., 2012). This data is directly opposed to several studies which identify large populations of AP-1 and GGA at different locations of the TGN and endosomal network in animal cells (Doray et al., 2002; Hirst et al., 2009; Puertollano et al., 2003). Determining whether a sequence of assembly also exists between AP-1 and GGA in animal cells would help to clarify the conflicting literature. If such a sequence exists, it would be useful to understand the mechanism of this sequence. Is it possible that GGA proteins recruit PI4KIIIb as a means to recruit AP-1 to the TGN? If this is the case, then specific questions that need to be addressed are: Does ARF1 play a similar role in opening up the VHS-GAT domains to allow for PI4KIIIb to interact with the VHS domain? In yeast deletion of *ARF1* leads to a decrease in global PI(4)P levels in vivo, likewise we can measure a delay in PI4P accumulation at the TGN by live-cell microscopy. Another outstanding question which needs to be addressed in further studies is whether GGA proteins play a role in recruiting or stabilizing PI4KIIIβ at the TGN membrane. What are the effects of knocking down GGA proteins in cell culture? Is there a decrease in PI(4)P, is there a delay in AP-1 recruitment? Some previous work indicates that this question may be difficult to address because knockdown of GGA or AP-1 in cultured cells may lead to an eventual recovery of trafficking in these cells through pathways which are unknown. Several future experiments will need to be conducted to meet these concerns.

ACKNOWLEDGMENTS

Razmik Ghukasyan helped to work out conditions for the PI4KIIIb in vitro binding assay. Giancarlo Costaguta provided technical assistance.

MATERIALS AND METHODS

Media and strains

Strains used for this study are listed in table 3-1. Yeast strains were grown in rich (YPD+ AUT) or synthetic dextrose media (SD) with the appropriate supplements. Fluorescent tags were introduced at the endogenous loci of the relevant gene using PCR to amplify the tag and then homologous recombination to insert the tag at the proper location in the genome.

Live-cell microscopy

Cells were grown in SD complete to a density of 0.1-0.3 X 10^7 cells ml^{-1}. Cells were then treated, imaged and analyzed as described in Daboussi et al., 2012 (Chapter 2). Each time-lapse movie is composed of 100 GFP/RFP frame pairs. All time-lapse movies were acquired using a 100X/1.45 NA objective on a 3i Marianas SDC confocal microscope, equipped with a Yokogawa CSU-22 confocal head and a photometrics Evolve EMCCD camera, controlled by either Slidebook 4.2 or 5.0. GFP and mRFP images were acquired by excitation at 488nm and 561 nm from a high-speed AOTF laser launch line.

Affinity Binding.

Pik1 fragments were expressed as HIS6-Fusion. Bacterial pellets containing the relevant fragments were resuspended in 1ml of 50 mM Hepes pH 7.4, 50 mM NaCl, 30mM Immidazole pH 8.0, and 2X Protease Inhibitor Cocktail (PIC) from Roche. Each suspension was then sonicated three times for 10 seconds. Lysates were then centrifuged at 4°C for 30 min at 16000g in a tabletop 5417R Eppendorf Centrifuge. Ni-NTA beads (Qiagen) were added to each of the clarified lysates and allowed to bind for 30 minutes at 4°C. Beads were then washed three

times in 50 mM Hepes pH 7.4, 50 mM NaCl, 0.05% TX-100 and then eluted three times in 50 mM Hepes pH 7.4, 50 mM NaCl, 300mM Imidazole pH 8.0 for 8 minutes per elution, at room temperature.

Eluted protein was then added to GST or GST-VHS purified constructs. GST and GST-VHS were purified by lysing in 1XPBS, 2X PIC. Sonicated and centrifuged as described above and then purified using glutathione agarose beads (GE Healthcare) applied to the clarified lysates at 4°C. Purified GST fragments were then washed three times with 50 mM Hepes pH 7.4, 50 mM NaCl, 0.05% TX-100 and applied to the purified, eluted Pik1-HIS6 fragments such that the total volume of the reaction was 1ml in a buffer that contained 50 mM Hepes pH 7.4, 50 mM NaCl, 0.05% TX-100, and allowed to bind for 1 hour at 4°C. Beads were then centrifuged, washed twice in 50 mM Hepes pH 7.4, 50 mM NaCl, 0.05% TX-100, and then twice in 50 mM Hepes pH 7.4, 50 mM NaCl. Samples were eluted with 1X LSB and boiled for 5 minutes at 100°C before being applied to an SDS page gel and subjected to a western blot analysis. Westerns are blotted for anti-HIS6 (1:1000, Qiagen).

Cells containing untagged Pik1p, or tagged HA-tagged Pik1p (wildtype, and mutant) expressed under control of the GPD promoter were grown overnight at 30°C in YPD+AUT media. 100 ODs of cells were centrifuged by a low speed spin at 3000 X g in a Sorvall centrifuge (F13S-14x50cy rotor). Yeast pellets were resuspended in 5 ml 0.1M Tris-SO4 pH 9.4 + 10mM DTT, resuspended by vortexing and then shaken for 5 minutes at 30°C. Cells were spun down at 3,000xg in a clinical centrifuge, supernatant was discarded, and then pellets were resuspended in 5ml YP, 1M sorbitol, 0.5% dextrose, 10mM Tris-HCL pH 7.4, 0.47mg / ml zymolase. Cells were vortexed briefly and then left to shake at 30°C for 30 minutes. Cells were then centrifuged at 3,000g and resuspended in ice cold lysis buffer (50mM Hepes pH 7.4, 300mM NaCl, and 1% TX-100, 2X PIC). Resuspended cells were then lysed with a dounce

homogenizer (pestle B) 30 times, lysates were then transferred to chilled eppendorf tubes and centrifuged 30 minutes on 16,000xg on the eppendorf centrifuge at 4°C. Supernatants were transferred to a new eppendorf tube and GST or GST-VHS bound glutathione agarose beads were added to each of the cleared lysates and allowed to bind for 1 hour at 4°C. Samples were then centrifuged for 10 seconds at 16,000xg and washed twice with lysis buffer. Samples were then washed with lysis buffer that did not contain TX-100. Beads were eluted in 1XLSB after boiling for 5 minutes at 100°C.

1XLSB samples were then analayzed by10% SDS-page and subsequent western blot analysis (anti-HA 1:1000 Clontech)

Arf1 pulldown assay

Pik1 (250-590)-HIS6, Arf1ΔN17p-Q71L, GST, GST-VHS, and GST-VHS-GAT were purified as described above. Affinity binding assay between Pik1p and VHS or VHS-GAT was conducted in 0.5ml total volume in a buffer containing: 25 mM HEPES, pH 7.4, 100 mM NaCl, 10 mM $MgCl_2$,,0.5 mM GTP, 1 mM DTT, and 100 µg/ml BSA. Purified Arf1ΔN17p-Q71Ladded at 20 µM final concentrations to the indicated GST, or GST-VHS samples. GST-VHS-GAT received either 2µM (low) or 20 µM (high) purified Arf1ΔN17p-Q71L. Samples were then washed twice with lysis buffer. Samples were then washed with lysis buffer that did not contain TX-100. Beads were eluted in 1XLSB after boiling for 5 minutes at 100°C and subjected to SDS-page and western blot analysis (anti-HIS, QIAGEN 1:1000).

Table 3-1

LIST OF STRAINS USED IN THIS TABLE

Name	**Genotype**	**Reference**
SEY6210	*MATα ura3–52 leu2-3112 his3- Δ200 trp1-Δ901 lys2-801 suc2-Δ9*	(Robinson et al., 1988)
GPY 404.2	*MAT**a** ura3–52 leu2-3112 his3- Δ200 trp1-Δ901 lys2-801 suc2-Δ9*	(Yeung et al., 1999)
GPY 3431	SEY 6210 *gga1Δ::HIS3 gga2Δ::HIS3*	(Costaguta et al., 2006)
GPY 2149	SEY 6210 *gga2Δ::HIS3*	(Costaguta et al., 2001)
GPY 5047	SEY 6210 *pik1^{GGA}*	This Study
GPY 5048	GPY 404.2 *pik1^{GGA}*	This Study
GPY 5049	SEY 6210 *gga2Δ::HIS3 pik1^{GGA}*	This Study
GPY 5050	GPY 404.2 *gga2Δ::HIS3 pik1^{GGA}*	This Study
GPY 5051	SEY 6210 *pik1^{GGA} Ent5-mRFP::KANMX6 Ent3-GFP::HIS3MX6*	This Study
GPY 5052	SEY 6210 *pik1^{GGA} Gga2-mRFP:: KANMX6 Apl2-GFP::HIS3MX6*	This Study
GPY 5053	SEY 6210 *pik1^{GGA} SEC7-mRFP::KANMX6 GFP-PH$^{oSH!}$::URA3*	This Study
GPY 4938	*GPY404 SEC7-mRFP::KANMX6 ura3–52::pPHO5-GFP-myc-PH^{OSH1}::URA3*	Daboussi et al., 2012
GPY 3109	SEY6210 *GGA2-mRFP::KANMX6 APL2-GFP(S65T)::HIS3MX6*	Fernandez et al., 2006
GPY 4966	GPY404 *NATNT2::GPD-HA-PIK1*	Daboussi et al., 2012
GPY 5054	GPY404 *NATNT2::GPD-HA-PIK1^{GGA}*	This Study

TABLE 3-2

LIST OF PLASMIDS USED IN THIS STUDY

Plasmid name	Cloning sites:	Reference:	Expression Conditions
Pet28a-Pik1 (80-760)-HIS	Cloned into NcoI and SalI	Daboussi et al., 2012	15°C overnight
Pet28a-Pik1 (420-760) -HIS	Cloned into NcoI and SalI	This Study	15°C overnight
Pet28a-Pik1 (250-581) -HIS	Cloned into NcoI and SalI	This Study	15°C overnight
Pet28a-Pik1 (250-548) -HIS	Cloned into NcoI and SalI	This Study	15°C overnight
Pet28a-Pik1 (250-503) -HIS	Cloned into NcoI and SalI	This Study	15°C overnight
Pet28a-Pik1 (250-425) -HIS	Cloned into NcoI and SalI	This Study	37°C 2-3 hours
Pet28a-Pik1 (250-380) -HIS	Cloned into NcoI and SalI	This Study	37°C 2-3 hours
Pet28a-Pik1 (250-330) -HIS	Cloned into NcoI and SalI	This Study	37°C 2-3 hours
Pet28a-Pik1 (330-410) -HIS	Cloned into NcoI and SalI	This Study	37°C 2-3 hours
Pet28a-Pik1 (350-425) -HIS	Cloned into NcoI and SalI	This Study	37°C 2-3 hours
Pet28a-Pik1 (350-503) -HIS	Cloned into NcoI and SalI	This Study	15°C overnight
Pet28a-Pik1 (350-548) -HIS	Cloned into NcoI and SalI	This Study	15°C overnight
Pet28a-Pik1 (290-380) -HIS	Cloned into NcoI and SalI	This Study	37°C 2-3 hours
Pet28a-Pik1 (290-380) -HIS	Cloned into NcoI and SalI	This Study	37°C 2-3 hours
Pet28a-Pik1 (283-329) -HIS	Cloned into NcoI and SalI	This Study	37°C 2-3 hours
Pet28a-HIS-Pik1 (1-258)	Cloned into BamHI and SalI	This Study	15°C overnight
Pet28a-Pik1 (160-350) -HIS	Cloned into NcoI and SalI	This Study	37°C 2-3 hours
Pet28a-Pik1 (200-350) -HIS	Cloned into NcoI and SalI	This Study	37°C 2-3 hours
Pet28a-Pik1 (220-350) -HIS	Cloned into NcoI and SalI	This Study	37°C 2-3 hours
Pet28a-Pik1 (230-350) -HIS	Cloned into NcoI and SalI	This Study	37°C 2-3 hours
Pet28a-Pik1 (240-350) -HIS	Cloned into NcoI and SalI	This Study	37°C 2-3

			hours
Pet28a-Pik1 (250-350) -HIS	Cloned into NcoI and SalI	This Study	37°C 2-3 hours
Pet28a-Pik1 (215-325-HIS; 286-291EEDEDE) K218E, K219E, T220A	Cloned into NcoI and SalI	This Study	37°C 2-3 hours
Pet28a-Pik1 (215-325-HIS; 286-291EEDEDE) S221E, R222E, S223D	Cloned into NcoI and SalI	This Study	37°C 2-3 hours
Pet28a-Pik1 (215-325-HIS; 286-291EEDEDE) S227D, S228E, S229D	Cloned into NcoI and SalI	This Study	37°C 2-3 hours
Pet28a-Pik1 (215-325-HIS; 286-291EEDEDE) K218E, K219E, R222E, K224E, R225E,	Cloned into NcoI and SalI	This Study	37°C 2-3 hours
Pet28a-Pik1 (215-325-HIS; 286-291EEDEDE) K218A, K219A, T220A	Cloned into NcoI and SalI	This Study	37°C 2-3 hours
Pet28a-Pik1 (215-325-HIS; 286-291EEDEDE) S221A, R222A, S223A	Cloned into NcoI and SalI	This Study	37°C 2-3 hours
Pet28a-Pik1 (215-325-HIS; 286-291EEDEDE) S227A, S228A, S229A	Cloned into NcoI and SalI	This Study	37°C 2-3 hours
Pet28a-Pik1 (215-325-HIS; 286-291EEDEDE) K218A, K219A, R222A, K224A, R225A,	Cloned into NcoI and SalI	This Study	37°C 2-3 hours
Pet28a-Pik1 (215-325-HIS; 286-291EEDEDE) K218E	Cloned into NcoI and SalI	This Study	37°C 2-3 hours
Pet28a-Pik1 (215-325-HIS; 286-291EEDEDE) K219E	Cloned into NcoI and SalI	This Study	37°C 2-3 hours
Pet28a-Pik1 (215-325-HIS; 286-291EEDEDE) T220D	Cloned into NcoI and SalI	This Study	37°C 2-3 hours
Pet28a-Pik1 (215-325-HIS; 286-291EEDEDE) S221D	Cloned into NcoI and SalI	This Study	37°C 2-3 hours
Pet28a-Pik1 (215-325-HIS; 286-291EEDEDE) L215A	Cloned into NcoI and SalI	This Study	37°C 2-3 hours
Pet28a-Pik1 (215-325-HIS; 286-291EEDEDE) L216A	Cloned into NcoI and SalI	This Study	37°C 2-3 hours
Pet28a-Pik1 (215-325-HIS; 286-291EEDEDE) N217A	Cloned into NcoI and SalI	This Study	37°C 2-3 hours
Pet28a-Pik1 (215-325-HIS; 286-291EEDEDE) K218A	Cloned into NcoI and SalI	This Study	37°C 2-3 hours
Pet28a-Pik1 (215-325-HIS; 286-291EEDEDE) K219A	Cloned into NcoI and SalI	This Study	37°C 2-3 hours
Pet28a-Pik1 (215-325-HIS; 286-291EEDEDE) T220A	Cloned into NcoI and SalI	This Study	37°C 2-3 hours

Pet28a-Pik1 (215-325-HIS; 286-291EEDEDE) S221A	Cloned into NcoI and SalI	This Study	37°C 2-3 hours
Pet28a-Pik1 (215-325-HIS; 286-291EEDEDE) R222A	Cloned into NcoI and SalI	This Study	37°C 2-3 hours
Pet28a-Pik1 (215-325-HIS; 286-291EEDEDE) S223A	Cloned into NcoI and SalI	This Study	37°C 2-3 hours
Pet28a-Pik1 (215-325-HIS; 286-291EEDEDE) K224A	Cloned into NcoI and SalI	This Study	37°C 2-3 hours
Pet28a-Pik1 (215-325-HIS; 286-291EEDEDE) R225A	Cloned into NcoI and SalI	This Study	37°C 2-3 hours
Pet28a-Pik1 (215-325-HIS; 286-291EEDEDE) V226A	Cloned into NcoI and SalI	This Study	37°C 2-3 hours
Pet28a-Pik1 (215-325-HIS; 286-291EEDEDE) S227A	Cloned into NcoI and SalI	This Study	37°C 2-3 hours
Pet28a-Pik1 (283-425) -HIS I283A	Cloned into NcoI and SalI	This Study	37°C 2-3 hours
Pet28a-Pik1 (283-425) -HIS K284A	Cloned into NcoI and SalI	This Study	37°C 2-3 hours
Pet28a-Pik1 (283-425) -HIS L285A	Cloned into NcoI and SalI	This Study	37°C 2-3 hours
Pet28a-Pik1 (283-425) -HIS P286A	Cloned into NcoI and SalI	This Study	37°C 2-3 hours
Pet28a-Pik1 (283-425) -HIS K287A	Cloned into NcoI and SalI	This Study	37°C 2-3 hours
Pet28a-Pik1 (283-425) -HIS R288A	Cloned into NcoI and SalI	This Study	37°C 2-3 hours
Pet28a-Pik1 (283-425) -HIS K289A	Cloned into NcoI and SalI	This Study	37°C 2-3 hours
Pet28a-Pik1 (283-425) -HIS P290A	Cloned into NcoI and SalI	This Study	37°C 2-3 hours
Pet28a-Pik1 (283-425) -HIS K291A	Cloned into NcoI and SalI	This Study	37°C 2-3 hours
Pet28a-Pik1 (283-425) -HIS Y292A	Cloned into NcoI and SalI	This Study	37°C 2-3 hours
Pet28a-Pik1 (283-425) -HIS L293A	Cloned into NcoI and SalI	This Study	37°C 2-3 hours
Pet28a-Pik1 (283-425)-HIS I283A, K284A, L285A	Cloned into NcoI and SalI	This Study	37°C 2-3 hours
Pet28a-Pik1 (283-425)-HIS P286A, K287A, R288A	Cloned into NcoI and SalI	This Study	37°C 2-3 hours
Pet28a-Pik1 (283-425)-HIS K289A, P290A, K291A	Cloned into NcoI and SalI	This Study	37°C 2-3 hours
Pet28a-Pik1 (283-425)-HIS Y292A, L293A, D294A	Cloned into NcoI and SalI	This Study	37°C 2-3 hours
Pet28a-Pik1 (283-425)-HIS N295A, S296A, Y297A	Cloned into NcoI and SalI	This Study	37°C 2-3 hours
Pet28a-Pik1 (283-425) -HIS V298A, H299A, R300A	Cloned into NcoI and SalI	This Study	37°C 2-3 hours
Pet28a-Pik1 (283-425) -HIS	Cloned into NcoI and SalI	This Study	37°C 2-3

P286A, K287A, R288A, K289A, P290A, K291A			hours
pGEX-4T-1 VHS- Gga2 (1-169)	Cloned into BamHI and SalI	Daboussi et al., 2012	15°C overnight
pGEX-4T-1 VHS-GAT Gga2 (1-313)	Cloned into BamHI and SalI	Daboussi et al., 2012	15°C overnight
Pet28a-PI4KIIIb HIS-(195-308) -HIS	cDNA containg PI4KIIIb was amplified by PCR using mouse cDNA library from. an embryonic stem cell line and cloned into BamHI and SalI	This Study	15°C overnight
pGEX4T-1 mammalian Gga2 VHS	cDNA containg Gga2 was amplified by PCR using mouse cDNA library from. an embryonic stem cell line and cloned into BamHI and SalI	This study	37°C 2-3 hours
Arf1ΔN17p-Q71L	See Reference	Rein *et al*. (2002)	24°C overnight

This is a list of all plasmids used in this study with a description of the cloning sites used for generating the plasmids as well as the expression conditions for the resulting protein fragment.

REFERENCES

Balla, A., and Balla, T. (2006). Phosphatidylinositol 4-kinases: old enzymes with emerging functions. Trends in Cell Biology *16*, 351-361.

Bonifacino, J. S. (2004). The GGA proteins: adaptors on the move. Nat Rev Mol Cell Biol *5*, 23-32.

Brodsky, F. M. (2012). Diversity of Clathrin Function: New Tricks for an Old Protein. Annual Review of Cell and Developmental Biology *28*, 309-336.

Costaguta, G., Duncan, M. C., FernÃ¡ndez, G. E., Huang, G. H., and Payne, G. S. (2006). Distinct Roles for TGN/Endosome Epsin-like Adaptors Ent3p and Ent5p. Molecular Biology of the Cell *17*, 3907-3920.

Costaguta, G., Stefan, C. J., Bensen, E. S., Emr, S. D., and Payne, G. S. (2001). Yeast Gga Coat Proteins Function with Clathrin in Golgi to Endosome Transport. Molecular Biology of the Cell *12*, 1885-1896.

Daboussi, L., Costaguta, G., and Payne, G. S. (2012). Phosphoinositide-mediated clathrin adaptor progression at the trans-Golgi network. Nat Cell Biol *14*, 239-248.

Doray, B., Ghosh, P., Griffith, J., Geuze, H. J., and Kornfeld, S. (2002). Cooperation of GGAs and AP-1 in packaging MPRs at the trans-Golgi network. Science *297*, 1700 - 1703.

Duncan, M. C., and Payne, G. S. (2003). ENTH/ANTH domains expand to the Golgi. Trends in Cell Biology *13*, 211-215.

Fuller, R. S., Sterne R. E., and Thorner J. (1988). Enzymes Required for Yeast Prohormone Processing. Annual Review of Physiology *50*, 345-362.

Godi, A., Pertile, P., Meyers, R., Marra, P., Di Tullio, G., Iurisci, C., Luini, A., Corda, D., and De Matteis, M. A. (1999). ARF mediates recruitment of PtdIns-4-OH kinase-[bgr] and stimulates synthesis of PtdIns(4,5)P2 on the Golgi complex. Nat Cell Biol *1*, 280-287.

Graham, T. R., and Burd, C. G. (2011). Coordination of Golgi functions by phosphatidylinositol 4-kinases. Trends in Cell Biology *21*, 113-121.

Hirst, J., Borner, Georg H. H., Antrobus, R., Peden, Andrew A., Hodson, Nicola A., Sahlender, Daniela A., and Robinson, Margaret S. (2012). Distinct and Overlapping Roles for AP-1 and GGAs Revealed by the Knocksideways System. Current biology : CB *22*, 1711-1716.

Hirst, J., Sahlender, D. A., Choma, M., Sinka, R., Harbour, M. E., Parkinson, M., and Robinson, M. S. (2009). Spatial and functional relationship of GGAs and AP-1 in Drosophila and HeLa cells. Traffic *10*, 1696 - 1710.

Loewen, C. J. R., Roy, A., and Levine, T. P. (2003). A conserved ER targeting motif in three families of lipid binding proteins and in Opi1p binds VAP. EMBO J *22*, 2025-2035.

Payne, G. S., and Schekman, R. (1989). Clathrin: a role in the intracellular retention of a Golgi membrane protein. Science *245*, 1358-1365.

Puertollano, R., and Bonifacino, J. S. (2004). Interactions of GGA3 with the ubiquitin sorting machinery. Nat Cell Biol *6*, 244-251.

Puertollano, R., van der Wel, N. N., Greene, L. E., Eisenberg, E., Peters, P. J., and Bonifacino, J. S. (2003). Morphology and Dynamics of Clathrin/GGA1-coated Carriers Budding from the Trans-Golgi Network. Molecular Biology of the Cell *14*, 1545-1557.

Robinson, J. S., Klionsky, D. J., Banta, L. M., and Emr, S. D. (1988). Protein sorting in Saccharomyces cerevisiae: isolation of mutants defective in the delivery and processing of multiple vacuolar hydrolases. Molecular and Cellular Biology *8*, 4936-4948.

Scott, P. M., Bilodeau, P. S., Zhdankina, O., Winistorfer, S. C., Hauglund, M. J., Allaman, M. M., Kearney, W. R., Robertson, A. D., Boman, A. L., and Piper, R. C. (2004). GGA proteins bind ubiquitin to facilitate sorting at the trans-Golgi network. Nat Cell Biol *6*, 252-259.

Shiba, Y., Katoh, Y., Shiba, T., Yoshino, K., Takatsu, H., Kobayashi, H., Shin, H.-W., Wakatsuki, S., and Nakayama, K. (2004). GAT (GGA and Tom1) Domain Responsible for Ubiquitin Binding and Ubiquitination. Journal of Biological Chemistry *279*, 7105-7111.

Strahl, T., Grafelmann, B., Dannenberg, J., Thorner, J., and Pongs, O. (2003). Conservation of Regulatory Function in Calcium-binding Proteins: HUMAN FREQUENIN (NEURONAL CALCIUM SENSOR-1) ASSOCIATES PRODUCTIVELY WITH YEAST PHOSPHATIDYLINOSITOL 4-KINASE ISOFORM, Pik1. Journal of Biological Chemistry *278*, 49589-49599.

Strahl, T., Huttner, I. G., Lusin, J. D., Osawa, M., King, D., Thorner, J., and Ames, J. B. (2007). Structural Insights into Activation of Phosphatidylinositol 4-Kinase (Pik1) by Yeast Frequenin (Frq1). Journal of Biological Chemistry *282*, 30949-30959.

Traub, L. M. (2005). Common principles in clathrin-mediated sorting at the Golgi and the plasma membrane. Biochimica et Biophysica Acta (BBA) - Molecular Cell Research *1744*, 415-437.

Yeung, B. G., Phan, H. L., and Payne, G. S. (1999). Adaptor Complex-independent Clathrin Function in Yeast. Molecular Biology of the Cell *10*, 3643-3659.

Chapter 4

The *trans*-Golgi Network in *S. cerevisiae* shares characteristics with Early Endosomes

Statement of Contribution.

I initiated and designed all experiments. Razmik Ghukasyan generated the strains and conducted the microscopy for the experiments shown in Figure 4 and 5.

Introduction

Endocytosis has an important role in several cellular processes and is tightly cooridinated with cell physiology. The diverse mechanisms of endocytosis regulate the uptake of nutrients from the extracellular space, plasma membrane dynamics during cell division cell growth, and the regulation of the signal transduction pathways (Conner and Schmid, 2003). Clathrin-mediated endocytosis, one form by which materials are delivered from the cell surface into the cell has been analyzed in detail over the past decade primarily using fluorescence microscopy, and recently comparative fluorescence and electron microscopy (Kaksonen et al., 2003; Kaksonen et al., 2005; Kaksonen et al., 2006; Kukulski et al., 2012). These analyses have demonstrated that clathrin-mediated endocytosis requires the interaction of clathrin with a large number of clathrin-related proteins. These proteins cluster cargo molecules, invaginate the membrane and enable vesicle scission at the end of vesicle biogenesis (Kaksonen et al., 2003). Each of the proteins is recruited to the plasma membrane in distinct modules. The first module that is recruited is composed of clathrin and several clathrin adaptors. Then, later modules participate in membrane bending, invagination and scission . Actin and actin binding proteins play an important role in membrane invagination and in facilitating the trafficking of the vesicle away from the plasma membrane. One well characterized actin binding protein is Abp1p. Abp1p is recruited to clathrin coated vesicles (ccvs) during the membrane bending and invagination module, 8-10 seconds before the vesicle pinches off (Kaksonen et al., 2005). It then stays associated with the ccv until the vesicle is uncoated and trafficked away from the plasma membrane.

CCVs are trafficked from the plasma membrane to the early endosome (EE). Then cargo are directed from the early endosome to the late endosome (LE)/multivesicular body (MVB) and then to the to the vacuole (Figure 1).

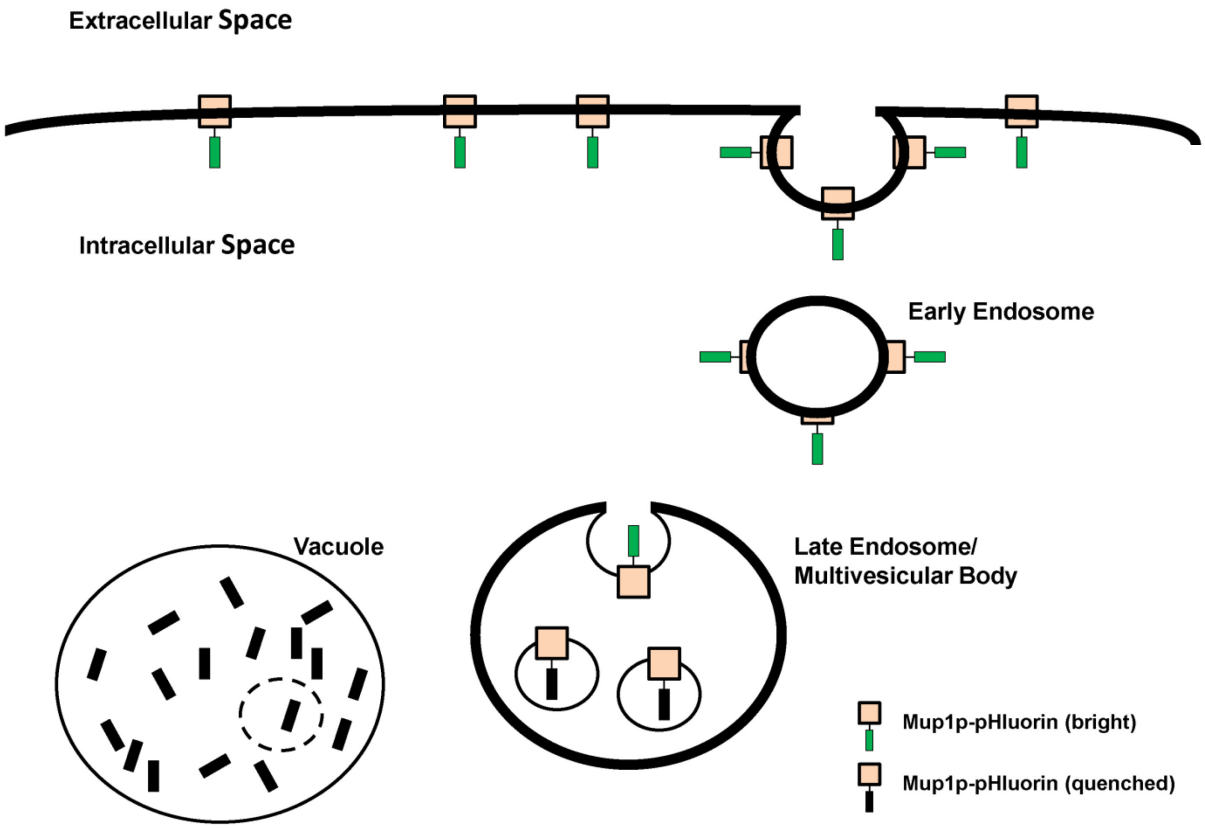

Figure 4-1. Model of Mup1p-pHluorin transport to the vacuole

Mup1p-pHluorin, an amino acid permease, travels from the ER through the Golgi and is trafficked to the plasma membrane where it stays until it binds to its ligands, methionine or cysteine. In the presence of excess methionine, Mup1p is endocytosed from the plasma membrane to the early endosome. From the early endosome it is then transported to the late endosome/ multivesicular body. Once the pHluorin fluorophore comes into contact with the low pH environment of the late endosome the fluorescence is extinguished. Mup1p-pHluorin can only be visualized in non-acidic environments. Adapted from (Prosser et al., 2010).

Machinery that assists with the biogenesis of the MVB and fusion to vacuoles has been genetically and biochemically well studied, as well as visualized by fluorescence microscopy (Hurley and Emr, 2006). In contrast, there is very little fluorescence data that consistently identifies the EE compartment, in yeast. In fact, this has been a source for much frustration for those in the trafficking field studying transport from the plasma membrane to the early endosome or those trying to identify molecules on the early endosome to serve as a stable marker for analysis of other intracellular trafficking events.

Several attempts have been made to better understand the pathway that endocytosed material takes as it travels through the endocytic pathway. Some groups have used the lipophilic dye FM4-64 which inserts itself into the lipid bilayer, and then enters the cells through bulk phase endocytosis (Wiederkehr et al., 2000). However, using this dye as a marker for endocytosed materials can be difficult as intracellular trafficking between organelles means that the dye can transfer to organelles outside of the endocytic pathway. This can make it difficult to use the dye to identify specific organelles. High temporal resolution studies to identifiy the initial organelle to which the FM4-64 material is received have not previously been reported.

In an effort to identify a fluorescent molecule that would accumulate in clathrin coated pits and then be faithfully trafficked through the endocytic pathway, one group constructed Alexa Fluor-488 C_5 or -594 C_5 conjugated α-factor, a hormone secreted from Mat α cells (Toshima et al., 2006). α-factor binds to Ste2p, its receptor at the cell surface of Mat a cells. Ste2p accumulates in ccvs, is internalized and then transported through the endocytic system to the vacuole. This research evaluated the idea that one could identify an early endosomal compartment with this fluorescent marker, and has shown that the early endosome displays interesting behavior. First, early endosomes seem to seek out newly endocytosed puncta and "consume" those puncta. Second, early endosomes may be located farther away from these

newly endocytosed ccvs, and so the ccvs seem to be directly trafficked to the them. This behavior is very interesting, and understanding it will help to characterize what machinery or markers in *S. cerevisiae* actually makes up the early endosome in *C. cerevisiae*.

S. cerevisiae do not have stacked Golgi as is found in some mammalian cells. Instead, previous studies have identified a phenomenon of Golgi maturation in yeast where markers for *cis*-Golgi (Rer1p) increase in fluorescence, then decrease. The fluorescence of the cis-Golgi marker is then replaced with fluorescence for a *medial*-Golgi marker (Gos1p). Eventually the fluorescence from the *trans*-Golgi marker (Sec7p) can be detected. These results laid the foundation for a novel maturation process, but did not consider the possibility of a a post- trans Golgi compartment (Losev et al., 2006; Matsuura-Tokita et al., 2006). We hypothesize the existence of a post *trans*-Golgi compartment that shares characteristics with the early endosome.

In an effort to identify protein markers for the EE, we have developed a novel strategy involving Mup1p. Mup1p is an integral membrane protein and methionine transporter that localizes to the plasma membrane in the absence of methioninne. In the presence of methionine, Mup1p is endocytosed and trafficked to the early endosome, and then through the remainder of the endocytic pathway- eventually reaching the yeast vacuole (Figure 4-1). Many amino acid transporters are very attractive proteins for studying the endocytic pathways because they follow a defined route (Prosser et al., 2010). To avoid confusion between Mup1p in early versus late compartments we tracked Mup1 as a fusion protein with pHluorin, a pH sensitive fluorophore. The fluorescent signal of pHluorin is greatly reduced at pH 5.5 and below, the acidity of the vacuole in wildtype yeast is predicted to be 5.45 (Brett et al., 2005; Pena et al., 1995; Plant et al., 1999). Mup1p-pHluorin can then be tracked from the plasma membrane through the early endocytic compartments.

Because GGA proteins are found on the early endosome in mammalian tissue culture cells (Puertollano et al., 2003), we hypothesized that by using a fluorescence microscopy based assay we might be able to identify GGA proteins as markers for an early endosomal compartment. We therefore present data that Golgi maturation in yeast begins with the cis-Golgi and extends to a post-TGN compartment (endocytic compartment) marked by Gga2p.

Results

Mup1 colocalizes with Gga2 at early post-endocytic compartments

We first constructed strains that expressed both Gga2-mRFP and Mup1-Phluorin from their endogenous loci. In the absence of methionine, we could detect some faint Mup1-pHluorin puncta. These puncta were never bright or numerous in the cell (Figure 4-2A). As soon as methionine was added to the media, we began imaging the cells. Upon addition of methionine to cells, internal Mup1p-Phluorin puncta become more numerous and over time (5-10 minutes), bright intracellular puncta began to appear (Figure 4-2B). This increase in early internal fluorescence also correlated well with an increased colocalization between Mup1-Phluorin and Gga2p-mRFP. Almost every Gga2-mRFP puncta colocalized with Mup1-Phluorin over its lifetime. Furthermore, membrane invaginations, marked by Mup1p-pHluorin, could be observed. These membrane invaginations showed a high degree of colocalization with Gga2-mRFP fluorescence within one to three minutes after methionine was added (Figure 4-2B, Lower Panel).

Biosynthetic Mup1-pHluorin is synthesized on ribosomes, cotranslationally inserted into the membrane of ER and then transported from the ER, through the Golgi and is eventually delivered to the plasma membrane. The exocyst complex also localizes to the Trans-Golgi Network (TGN). To determine whether the colocalization we observed was from newly endocytosed Mup1p-Phluorin, or Mup1-pHluorin that was being transported through the biosynthetic pathway, we used cyclohexamide, an inhibitor of eukaryotic translation. When we prevented the synthesis of new Mup1p and then induced endocytosis of plasma membrane Mup1p by the addition of methionine into the media, we found that Mup1p-pHluorin colocalized with Gga2p-mRFP (Figure 4-3A). This result provides evidence that that the

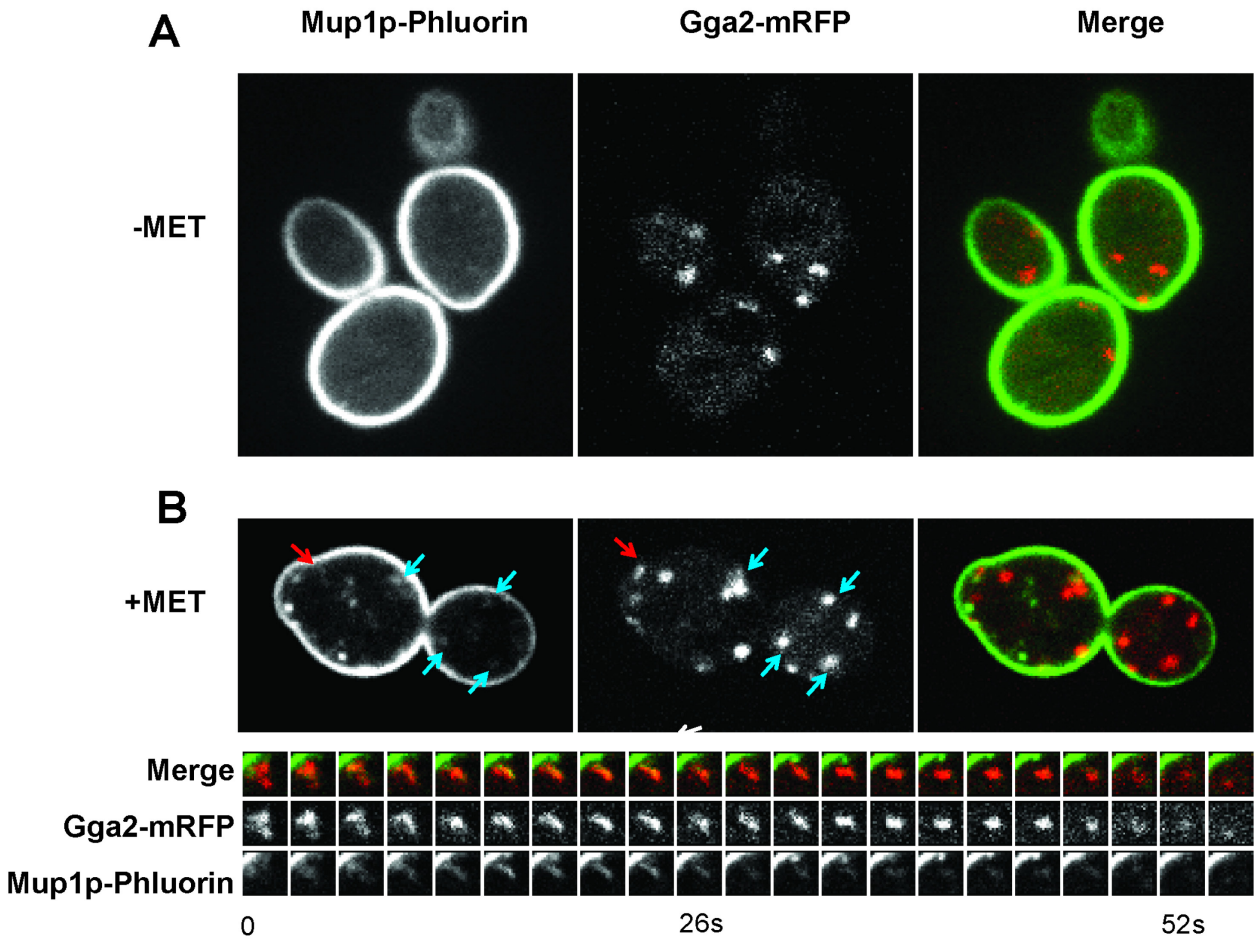

Figure 4-2. Mup1p-Phluorin colocalizes with Gga2p-mRFP

Time-lapse fluorescence microscopy of cells expressing Mup1p- Phluorin and Gga2p-mRFP expressed in cells. This movie was taken in the absence (A) or in the presence (B) of Methionine. B.) Timepoint shown is 5 minutes after the addition of Methionine. Blue arrows indicate Mup1p-GFP that colocalizes with Gga2p-mRFP. Red arrow is the area shown in the montage in the lower panel. Gga2p-mRFP does not initially colocalize with Mup1p-Phluorin, but then a membrane invagination extends towards the Gga2-mRFP puncta and eventually pinches off from the membrane, mainintaing colocalization with Gga2-mRFP.

colocalization between Mup1p and Gga2p is because recently endocytosed Mup1p is being directed to Gga2 positive puncta.

Actin polymerization is critical for clathrin dependent endocytosis in yeast. If we prevent endocytosis with Latrunculin A, an actin depolymerizing agent, we do not detect colocalization between Gga2 and Mup1. This serves as an additional indication that colocalization between Gga2 and Mup1, depends on endocytic Mup1p and not biosynthetic Mup1p, as was first speculated (Figure 4-3B).

We next sought to use a different marker of endocytosis that is exclusively associated with clathrin-coated vesicles. We fluorescently tagged Abp1p with monomeric RFP. Abp1p is an actin binding protein that has been shown to be recruited at the end of ccv formation. Typically, one can follow Abp1 fluorscence from the plasma membrane and then track it for some short distance into the cell (typically ~200-500nm). We hypothesized that if Gga2p is actually a marker for the early endosome we should detect Abp1 fluorescence being trafficked directly to Gga2p puncta. We should also detect Gga2p that is directed to Abp1 puncta that are newly pinching off from the membrane. These two types of events were observed when tracking internalized fluorescent α-factor (Toshima et al., 2006).

We found that we could reliably identify these two types of behavior. We found that Abp1 did seem to be directed to internal Gga2 puncta (Figure 4-4) and we also found that Gga2 puncta displayed a “gobbling” behavior in which they would gravitate towards those Abp1 puncta which were newly endocytosed (Figure 4-5).

These preliminary results indicate two processes that were once believe to be distinct, endocytosis, and maturation of the Golgi coalesce at the trans-Golgi compartment, which this author fondly refers to as the Golgisome. We find that endocytosed vesicles are initially directed

from the plasma membrane to these Gga2 positive puncta. Gga2 positive puncta are also generally located near to the plasma membrane, especially near burgeoning endocytic vesicles.

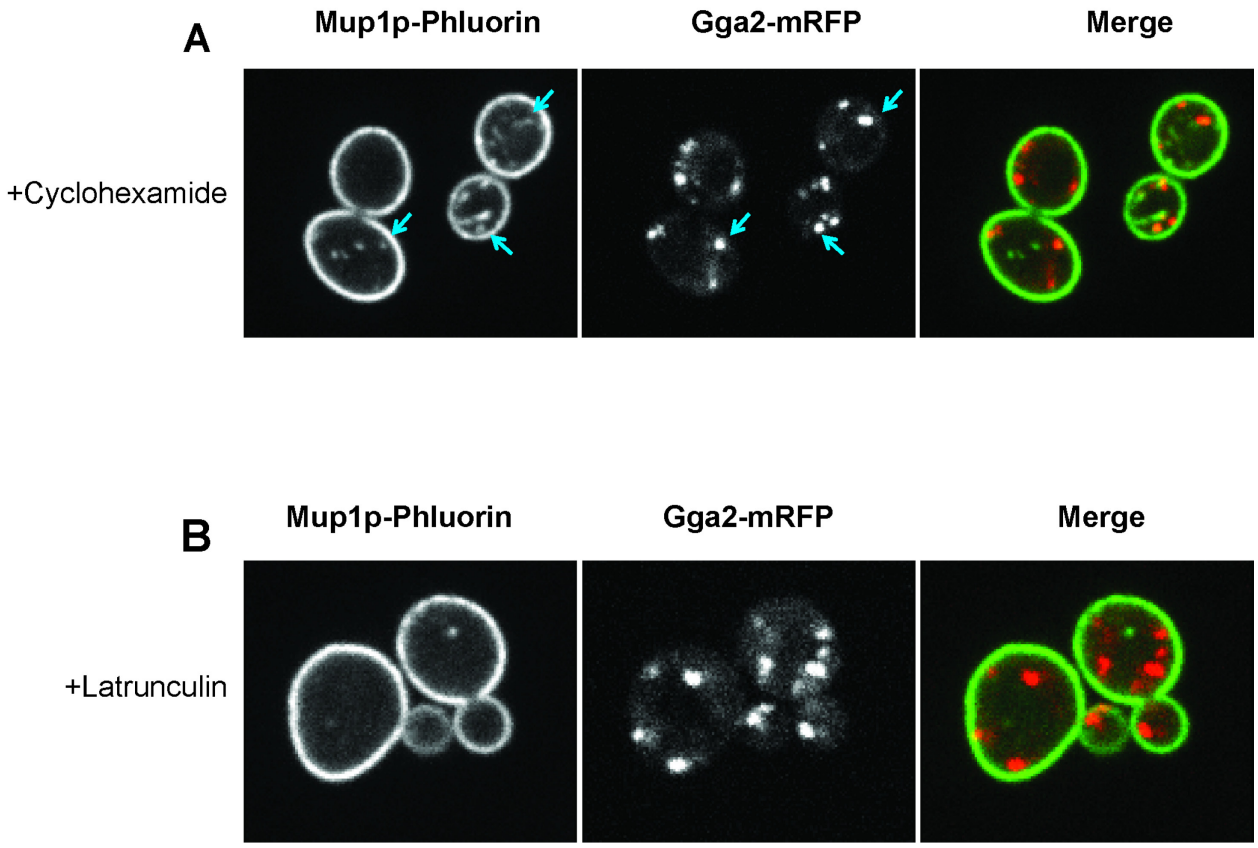

Figure 4-3. Mup1p-Phluorin that colocalizes with Gga2-mRFP originates from biosynthetic events

A.) Cells expressing Mup1p-pHluorin and Gga2p-mRFP were imaged by spinning disc confocal microscopy. Cells were incubated with 100 µg/ ml cyclohexamide, an inhibitor of eukaryotic protein synthesis for 2 hours, before the administration of methionine. Upon addition of methionine, cells were immediately imaged. Image shown is 5 minutes after methionine addition.

B.) Mup1p-Phluorin and Gga2-mRFP expressing cells in the presence of 10mM Latrunculin A. Latrunculin A was added 5 minutes before methionin. Image shown is 5 minutes after methionine addition. Under these conditions Mup1-Phluorin was not endocytosed upon addition of methionine.

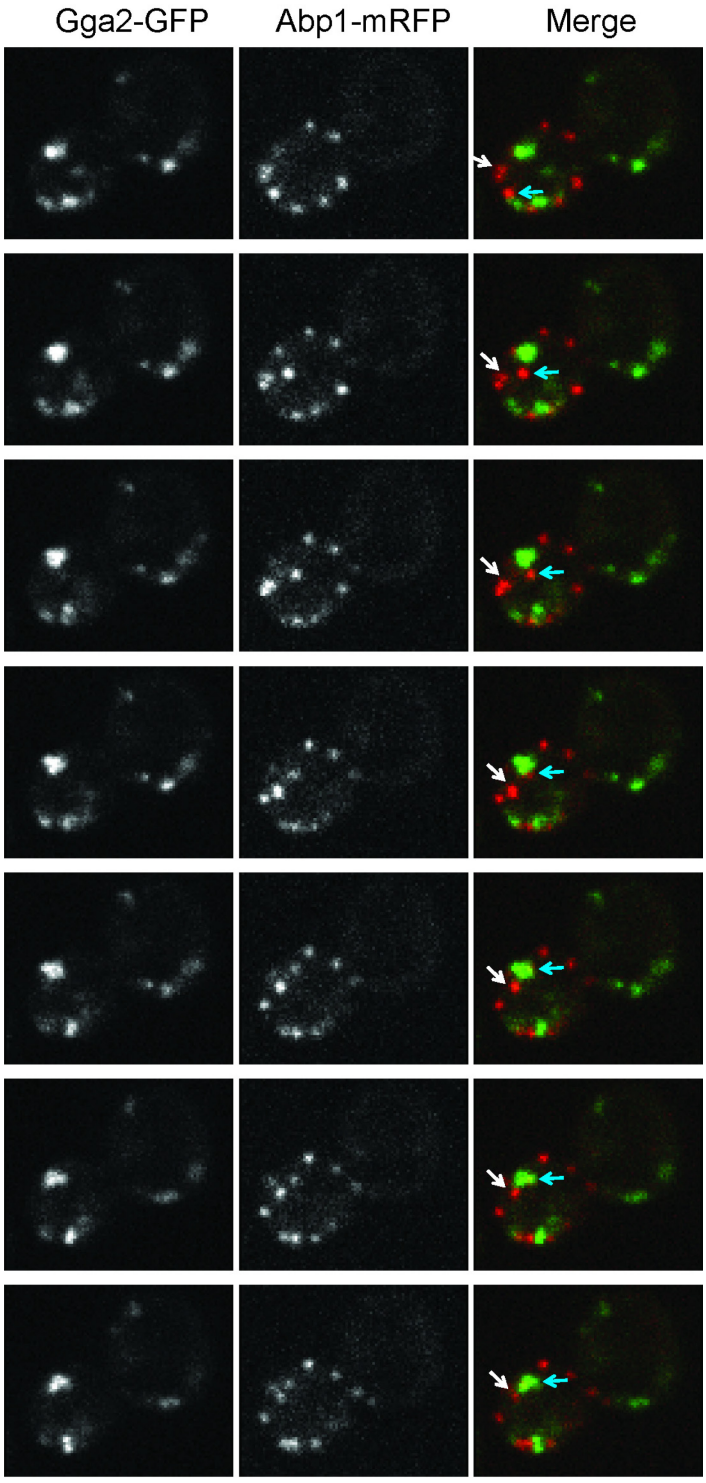
Gga2-GFP
Abp1-mRFP
Merge

Figure 4-4. Abp1p positive puncta are transported towards Gga2p positive puncta

Cells expressing Abp1p-mRFP and Gga2p-GFP were imaged by spinning disc confocal microscopy at steady state. Cells were grown to a low density (0.1 X 10^6 cells/ml). Blue and white arrowheads indicate two independent Abp1p puncta (red channel) that are directly trafficked towards the Gga2p positive puncta (green channel). Images were taken 1/sec, every third image is shown. (Experiment performed by Razmik Ghukasyan).

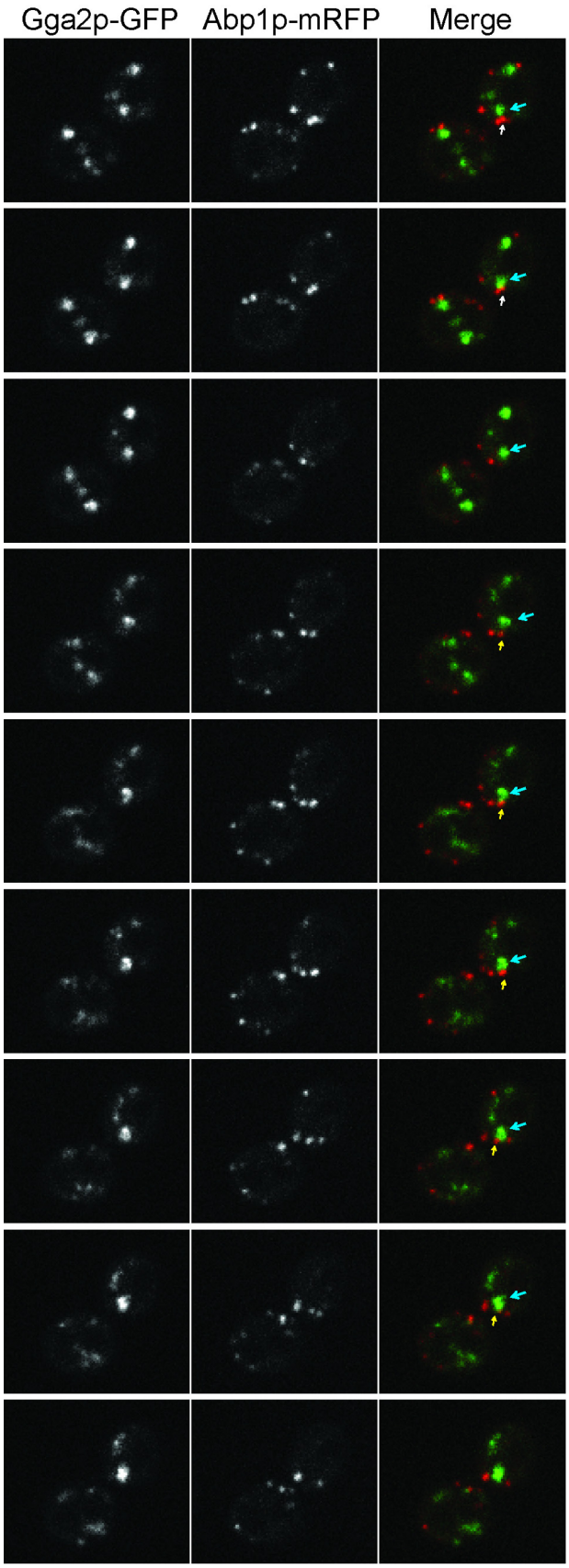
Gga2p-GFP
Abp1p-mRFP
Merge

Figure 4-5. Gga2p positive puncta are transported towards Abp1p positive puncta

Cells expressing Abp1p-mRFP and Gga2p-GFP were imaged by spinning disc confocal microscopy at steady state. Cells were grown to a low density (0.1 X 10^6 cells/ml). Blue arrowhead points towards a Gga2p positive puncta (green channel) and white and yellow arrowheads indicate two Abp1p positive puncta that disappear soon after contact with the Gga2p positive puncta. Images were taken 1/sec, every third image is shown. (Experiment performed by Razmik Ghukasyan).

Discussion

This study offers evidence that the maturation events that progress from the *cis*-Golgi to the *trans*-Golgi in yeast may also progress to a post-TGN, endosomal compartment. This compartment is the initial target of materials being endocytosed from the plasma membrane. The evidence that the TGN shares characteristics with an early endosomal compartment offers a new way to think about the trafficking pathway in yeast.

Many internal organelles are mobile without obvious directed movement, making them more difficult to track over time. One possible way to mitigate this difficulty is to image more frequently. However, as all of the tagged proteins imaged in this study are expressed from their endogenous promoters, there is a limited number of fluorophores available for imaging. Recently, EMCCD cameras have become very sensitive and now allow for very short exposure times. This capability has been important for the ability to image endogenous copy numbers of proteins at several timepoints so that a time-lapse movie can be compiled. This recent advancement in imaging technology is likely the reason why there is very little fluorescence data that consistently identifies an early endosomal compartment in yeast.

We have taken advantage of the recent availability of ultra sensitive EMCCD cameras and the development of fluorophores which are brighter than the last generation of fluorophores. Several fluorophores also have interesting capabilities, such as only fluorescent in non-acididic compartments(Giepmans et al., 2006; Pena et al., 1995; Sankaranarayanan et al., 2000). These recent developments have enabled us to employ a strategy to fluorescently identify the early endosome using a combination of fluorescently tagged endocytosed plasma membrane proteins (Mup1p and Abp1) and tagged proteins serving as markers for internal organelles (Gga2p).

We have identified Gga2p as a marker for sites of the early endosome in yeast. This result is surprising because Gga2p has previously been characterized as a protein characteristic

of the TGN. There are two likely interpretations of this data, first that the TGN and early endosome share distinct subcompartments on the same organelle or one in which the TGN and the early endosome are functionally equivalent in yeast. We favor the later model given that Gga2p participates in anterograde transport from the TGN/EE to the late endosome. It may be that there is a mechanism for Gga2p to cluster both biosynthetic cargo coming from earlier compartments of the Golgi as well as cargo received from the plasma membrane destined for later endocytic organelles.

We have identified a similar relationship between AP-1 and both Mup1p and Abp1p (data not shown). This is not surprising as previous studies have found that nearly 100% of Gga2 puncta become positive for AP-1. Also, at steady state approximately 45% of Gga2p colocalizes with AP-1in static images (Costaguta et al., 2006; Daboussi et al., 2012). However, several more questions need to be addressed. Most importantly, how is the material that is endocytosed from the plasma membrane to the Gga2 positive puncta then trafficked to later endosomal compartments. There are two possible options for transport to later endosomal compartments. The first possibility is that organellar maturation plays a role, meaning that the Gga2p positive organelle matures into these later organelles. Second, vesicle transport from Gga2p positive organelles may be the primary mode of transport to later endocytic compartments. There may also exist some combination of both possibilities. To test for the possibility of endosomal maturation, we have used fluorescence microscopy of several tagged late endosomal markers in an effort to identify a marker which might show a sequence of recruitment similar to the maturation process at the Golgi. However, we have been unsuccessful in these attempts. We have also tried the lipid markers that label PI(3)P (GFP-FYVE) which is enriched at the late endosome and vacuolar membrane (Burd and Emr, 1998). This marker showed very little colocalization with AP-1 or Gga2p. Often, a small GFP-FYVE puncta would be

detected at sites that were adjacent to Gga2p. It was unclear as to whether the puncta that did colocalize did so meaningfully or randomly ((Daboussi et al., 2012) Chapter 3- Figure S4E).

This work represents a novel strategy to fluorescently identify the early endosome in yeast. Our results suggest that Gga2p (and AP-1) puncta behave as an early endosome, in that they colocalize with newly endocytosed material (Mup1p), and colocalize near membrane invaginations which we believe represent sites of endocytosis.

Materials and Methods

Media and Strains

Strains used for this study are listed in table 4-1. Yeast strains were grown in synthetic dextrose media (SD) with the appropriate supplements. Fluorescent tags were introduced at the endogenous loci of the relevant gene using PCR to amplify the tag and then homologous recombination to insert the tag at the proper location in the genome. All strains were generated from mating haploid cells to generate diploids, sporulating and then dissecting to isolate the haploid spores.

Live- Cell Fluorescence Microscopy

Cells were grown in SD complete- methionine at room temperature to the density indicated below. GFP (pHluorin) or RFP channels were exposed for 500ms per frame, and a GFP/RFP pair was imaged every 1-2 seconds. Each time-lapse movie is composed of 100 GFP/RFP frame pairs. All time-lapse movies were acquired using a 100X/1.45 NA objective on a 3i Marianas SDC confocal microscope, equipped with a Yokogawa CSU-22 confocal head and a photometrics Evolve EMCCD camera, controlled by either Slidebook 4.2 or 5.0. GFP and mRFP images were acquired by excitation at 488nm and 561 nm from a high-speed AOTF laser launch line.

Microscopy with Cyclohexamide Treated Cells

Cells were cultured overnight as described above, at room temperature until they had reached 0.1-0.2 X 10^7 cells/ ml. Cyclohexamide that had been dissolved in water was then added to cells to a final concentration of 100 µg/ml. Cells were then allowed to incubate with the cyclohexamide for 2 hours at room temperature, while rotating. Cells were then centrifuged at 750 X g for 2 minutes and then

Microscopy with Latrunculin A Treated Cells

All strains were cultured overnight in supplemented SD media until they had reached 0.1 X 10^7 cells/ ml. Cells were then centfigued for 2 minutes at 750 X g and Latrunculin A was added to a final concentration of 10 μM/ml. Methionine was added five minutes after the addition of Latrunculin A. Cells were then immediately imaged.

Table 4-1 Strain Table

Name	Genotype	Reference
SEY6210	*MATα ura3–52 leu2-3112 his3- Δ200 trp1-Δ901 lys2-801 suc2-Δ9*	(Robinson et al., 1988)
GPY 404.2	*MAT**a** ura3–52 leu2-3112 his3- Δ200 trp1-Δ901 lys2-801 suc2-Δ9*	(Yeung et al., 1999)
GPY 5045	SEY 404.2 *Mup1-pHluorin::G418 Gga2-mRFP::G418*	This study
GPY 5046	SEY 6210 *Abp1-2xmRFP::TRP 1 Gga2-GFP::G418*	This study
BWY3818	SEY 6210 Mup1-pHluorin::KanMX	(Prosser et al., 2010)

Prosser, D. C., Whitworth, K., and Wendland, B. (2010). Quantitative Analysis of Endocytosis with Cytoplasmic pHluorin Chimeras. Traffic *11*, 1141-1150.

Robinson, J. S., Klionsky, D. J., Banta, L. M., and Emr, S. D. (1988). Protein sorting in Saccharomyces cerevisiae: isolation of mutants defective in the delivery and processing of multiple vacuolar hydrolases. Molecular and Cellular Biology *8*, 4936-4948.

Yeung, B. G., Phan, H. L., and Payne, G. S. (1999). Adaptor Complex-independent Clathrin Function in Yeast. Molecular Biology of the Cell *10*, 3643-3659.

References

Brett, C. L., Tukaye, D. N., Mukherjee, S., and Rao, R. (2005). The Yeast Endosomal Na+(K+)/H+ Exchanger Nhx1 Regulates Cellular pH to Control Vesicle Trafficking. Molecular Biology of the Cell *16*, 1396-1405.

Burd, C. G., and Emr, S. D. (1998). Phosphatidylinositol(3)-Phosphate Signaling Mediated by Specific Binding to RING FYVE Domains. Molecular Cell *2*, 157-162.
Conner, S. D., and Schmid, S. L. (2003). Regulated portals of entry into the cell. Nature *422*, 37-44.

Costaguta, G., Duncan, M. C., Fernandez, G. E., Huang, G. H., and Payne, G. S. (2006). Distinct Roles for TGN/Endosome Epsin-like Adaptors Ent3p and Ent5p. Molecular Biology of the Cell *17*, 3907-3920.

Daboussi, L., Costaguta, G., and Payne, G. S. (2012). Phosphoinositide-mediated clathrin adaptor progression at the trans-Golgi network. Nat Cell Biol *14*, 239-248.

Giepmans, B. N. G., Adams, S. R., Ellisman, M. H., and Tsien, R. Y. (2006). The Fluorescent Toolbox for Assessing Protein Location and Function. Science *312*, 217-224.

Hurley, J. H., and Emr, S. D. (2006). THE ESCRT COMPLEXES: Structure and Mechanism of a Membrane-Trafficking Network*. Annual Review of Biophysics and Biomolecular Structure *35*, 277-298.

Kaksonen, M., Sun, Y., and Drubin, D. G. (2003). A Pathway for Association of Receptors, Adaptors, and Actin during Endocytic Internalization. Cell *115*, 475-487.

Kaksonen, M., Toret, C. P., and Drubin, D. G. (2005). A Modular Design for the Clathrin- and Actin-Mediated Endocytosis Machinery. Cell *123*, 305-320.

Kaksonen, M., Toret, C. P., and Drubin, D. G. (2006). Harnessing actin dynamics for clathrin-mediated endocytosis. Nat Rev Mol Cell Biol *7*, 404-414.

Kukulski, W., Schorb, M., Kaksonen, M., and Briggs, John A. G. (2012). Plasma Membrane Reshaping during Endocytosis Is Revealed by Time-Resolved Electron Tomography. Cell *150*, 508-520.

Losev, E., Reinke, C. A., Jellen, J., Strongin, D. E., Bevis, B. J., and Glick, B. S. (2006). Golgi maturation visualized in living yeast. Nature *441*, 1002-1006.

Matsuura-Tokita, K., Takeuchi, M., Ichihara, A., Mikuriya, K., and Nakano, A. (2006). Live imaging of yeast Golgi cisternal maturation. Nature *441*, 1007-1010.

Pena, A., RamÃrez, J., Rosas, G., and Calahorra, M. (1995). Proton pumping and the internal pH of yeast cells, measured with pyranine introduced by electroporation. Journal of Bacteriology *177*, 1017-1022.

Plant, P. J., Manolson, M. F., Grinstein, S., and Demaurex, N. (1999). Alternative Mechanisms of Vacuolar Acidification in H+-ATPase-deficient Yeast. Journal of Biological Chemistry *274*, 37270-37279.

Prosser, D. C., Whitworth, K., and Wendland, B. (2010). Quantitative Analysis of Endocytosis with Cytoplasmic pHluorin Chimeras. Traffic *11*, 1141-1150.

Puertollano, R., van der Wel, N. N., Greene, L. E., Eisenberg, E., Peters, P. J., and Bonifacino, J. S. (2003). Morphology and Dynamics of Clathrin/GGA1-coated Carriers Budding from the Trans-Golgi Network. Molecular Biology of the Cell *14*, 1545-1557.

Robinson, J. S., Klionsky, D. J., Banta, L. M., and Emr, S. D. (1988). Protein sorting in Saccharomyces cerevisiae: isolation of mutants defective in the delivery and processing of multiple vacuolar hydrolases. Molecular and Cellular Biology *8*, 4936-4948.

Sankaranarayanan, S., De Angelis, D., Rothman, J. E., and Ryan, T. A. (2000). The Use of pHluorins for Optical Measurements of Presynaptic Activity. Biophysical Journal *79*, 2199-2208.
Toshima, J. Y., Toshima, J., Kaksonen, M., Martin, A. C., King, D. S., and Drubin, D. G. (2006). Spatial dynamics of receptor-mediated endocytic trafficking in budding yeast revealed by using fluorescent alpha-factor derivatives. Proceedings of the National Academy of Sciences *103*, 5793-5798.

Wiederkehr, A., Avaro, S., Prescianotto-Baschong, C., Haguenauer-Tsapis, R., and Riezman, H. (2000). The F-Box Protein Rcy1p Is Involved in Endocytic Membrane Traffic and Recycling Out of an Early Endosome in Saccharomyces cerevisiae. The Journal of Cell Biology *149*, 397-410.

Yeung, B. G., Phan, H. L., and Payne, G. S. (1999). Adaptor Complex-independent Clathrin Function in Yeast. Molecular Biology of the Cell *10*, 3643-3659.

CHAPTER 5

Yeast Irc6p is a Novel Type of Conserved Clathrin Coat Accessory Factor Related to Small G Proteins

Personal Contribution:

I contributed to the work described in Chapter 5, Gorinya et al., 2012 in Figure 1F. Strains were grown in accordance protocol found in Duncan et al., 2007 as indicated in the MATERIALS AND METHODS of this manuscript. Each strain was then imaged in the presence of calcofluor white, and then the images were compiled by strain such that representative images could be taken from each category. These results reveal that deletion of *irc6* increases chs6Δ sensitivity to calculfluor white, similar to the phenotype observed with AP-. In part, these results imply that the function of Irc6p is within the AP-1 trafficking pathway. This author also organized each of the figures presented in this manuscript.

Yeast Irc6p is a novel type of conserved clathrin coat accessory factor related to small G proteins

Sabine Gorynia[a,*], Todd C. Lorenz[a,†], Giancarlo Costaguta[a], Lydia Daboussi[a], Duilio Cascio[b,c], and Gregory S. Payne[a,b]
[a]Department of Biological Chemistry, School of Medicine, [b]Molecular Biology Institute, and [c]Department of Energy Institute of Genomics and Proteomics, University of California at Los Angeles, Los Angeles, CA 90095

ABSTRACT **Clathrin coat accessory proteins play key roles in transport mediated by clathrin-coated vesicles. Yeast Irc6p and the related mammalian p34 are putative clathrin accessory proteins that interact with clathrin adaptor complexes. We present evidence that Irc6p functions in clathrin-mediated traffic between the *trans*-Golgi network and endosomes, linking clathrin adaptor complex AP-1 and the Rab GTPase Ypt31p. The crystal structure of the Irc6p N-terminal domain revealed a G-protein fold most related to small G proteins of the Rab and Arf families. However, Irc6p lacks G-protein signature motifs and high-affinity GTP binding. Also, mutant Irc6p lacking candidate GTP-binding residues retained function. Mammalian p34 rescued growth defects in *irc6*Δ cells, indicating functional conservation, and modeling predicted a similar N-terminal fold in p34. Irc6p and p34 also contain functionally conserved C-terminal regions. Irc6p/p34-related proteins with the same two-part architecture are encoded in genomes of species as diverse as plants and humans. Together these results define Irc6p/p34 as a novel type of conserved clathrin accessory protein and founding members of a new G protein–like family.**

Monitoring Editor
Benjamin S. Glick
University of Chicago

Received: Jul 9, 2012
Revised: Aug 22, 2012
Accepted: Sep 13, 2012

INTRODUCTION

Clathrin-coated vesicles (CCV) serve as evolutionarily conserved carriers for selective transport of proteins from the plasma membrane to endosomes and between the *trans*-Golgi network (TGN) and endosomes. Assembly of a clathrin coat orchestrates CCV formation by driving membrane invagination and scission, while concomitantly selecting appropriate cargo proteins.

Clathrin, a hexamer of heavy and light chains, forms an outer polyhedral scaffold in the coat that interacts with other coat proteins but does not directly bind to membranes. Instead, clathrin associates with adaptors that help anchor the coat to the membrane through interactions with lipids and/or the cytoplasmic domains of cargo proteins (Traub, 2005; Edeling *et al.*, 2006; McMahon and Boucrot, 2011). Adaptors also function as a binding platform for recruitment of other coat-interacting proteins, termed accessory factors, that play key roles in different stages of CCV formation, including coat assembly, membrane deformation and scission, and uncoating (Traub, 2005; Edeling *et al.*, 2006; McMahon and Boucrot, 2011). Because adaptors coordinate coat formation, membrane vesiculation, and cargo collection, they are central to CCV formation.

Two related heterotetrameric adaptor complexes, AP-1 and AP-2, are major components of CCV (Robinson, 2004; Edeling *et al.*, 2006). AP-1 is associated with the TGN and endosomes, whereas AP-2 is associated with the plasma membrane. Each is composed of two large subunits (γ and β_1 in AP-1, α and β_2 in AP-2), a medium subunit (μ_1 and μ_2), and a small subunit (σ_1 and σ_2). The subunits are arranged as a core consisting of the large-subunit N-terminal regions together with the μ and σ subunits. The large-subunit C-terminal regions extend from the core as flexible

This article was published online ahead of print in MBoC in Press (http://www.molbiolcell.org/cgi/doi/10.1091/mbc.E12-07-0507) on September 19, 2012.

Present addresses: *ONCOTEST GMBH, Am Flughafen 12-14, 79108 Freiburg, Germany; †Department of Biology, University of La Verne, Los Angeles, CA 91750.

Address correspondence to: Gregory S. Payne (gpayne@mednet.ucla.edu).

Abbreviations used: CCFW, calcofluor white; CCV, clathrin-coated vesicle; CDD, Conserved Domain Database; DTT, dithiothreitol; GFP, green fluorescent protein; GST, glutathione *S*-transferase; IPTG, isopropyl β-D-1-thiogalactopyranoside; LB, Luria–Bertani broth; NTPase, nucleoside triphosphate hydrolase; PDB, Protein Data Bank; PEG, polyethylene glycol; PMSF, phenylmethylsulfonyl fluoride; TGN, *trans*-Golgi network; WCL, whole-cell lysates.

© 2012 Gorynia *et al.* This article is distributed by The American Society for Cell Biology under license from the author(s). Two months after publication it is available to the public under an Attribution–Noncommercial–Share Alike 3.0 Unported Creative Commons License (http://creativecommons.org/licenses/by-nc-sa/3.0).
"ASCB®," "The American Society for Cell Biology®," and "Molecular Biology of the Cell®" are registered trademarks of The American Society of Cell Biology.

linker regions connected to appendage domains. The AP core interacts with the membrane and cargo, while the hinge/appendage regions provide binding sites for clathrin and nearly all accessory proteins. A large number of accessory proteins have been described that bind either directly or indirectly to the AP-2 appendages, providing insights into endocytic vesicle formation at the plasma membrane (Edeling *et al.*, 2006; McMahon and Boucrot, 2011). In contrast, fewer AP-1–interacting proteins have been characterized, leaving the mechanism of TGN/endosome CCV formation less well defined (Traub, 2005).

The yeast protein Irc6p/Yfr043cp and its mammalian homologue p34 are putative clathrin coat accessory factors based on their identification as AP-1γ– and AP-2α–interacting proteins in yeast two-hybrid screens (Page *et al.*, 1999; Ito *et al.*, 2001; Yu *et al.*, 2008). Analysis of p34 revealed an unusual adaptor-binding mode involving association with the N-terminal core regions of the γ and α subunits (Page *et al.*, 1999). To investigate a possible role for these proteins in clathrin-mediated transport, we characterized the structure and function of Irc6p and tested for functional complementation by p34 in yeast. Our results indicate that Irc6p is related to G proteins, participates in clathrin-mediated TGN-endosome traffic, and can link AP-1 to the Rab Ypt31p. Mammalian p34 functionally substitutes for Irc6p in yeast. Together our findings provide evidence that Irc6p and p34 represent a novel type of evolutionarily conserved clathrin coat accessory factor.

RESULTS

Irc6p functions in clathrin-mediated TGN/endosome traffic

To test for Irc6p function in clathrin-mediated traffic, we applied an assay for genetic interaction with a temperature-sensitive allele of the clathrin heavy chain gene (*chc1-521*, referred to hereafter as *chc1-ts*; Seeger and Payne, 1992). Commonly, deletions of genes whose products act in clathrin-dependent transport pathways exacerbate *chc1-ts* growth defects, whereas the same deletions in *CHC1* cells are innocuous, likely due to redundant proteins and/or alternative pathways (Yeung *et al.*, 1999; Bensen *et al.*, 2000, 2001; Costaguta *et al.*, 2001; Fernandez and Payne, 2006). Accordingly, we compared the growth of *chc1-ts irc6*Δ double mutants with wild-type and single mutants (Figure 1A). All strains displayed similar growth rates at 24°C, and *irc6*Δ cells grew like wild-type cells at the semipermissive temperature of 30°C. However, *chc1-ts irc6*Δ cell growth at 30°C was more severely retarded than that of *chc1-ts* cells. Introduction of a low-copy plasmid expressing FLAG-tagged Irc6p into double mutant cells restored growth to the level of *chc1-ts* cells (Figure 1A).

CCVs mediate endocytosis and transport between the TGN and endosomes. Endocytosis was assayed by determining the sensitivity of cells to K28 killer toxin, which depends on AP-2–mediated endocytosis for intoxication of cells (Carroll *et al.*, 2009). In this assay, cells being tested for K28 sensitivity are spread as a lawn on an agar plate, and concentrated K28-secreting cells are spotted onto the lawn. K28 sensitivity results in a zone of cell death surrounding the K28-producing cells (Figure 1B). Based on a screen of the yeast gene deletion collection, deletion of *IRC6* was reported to confer K28 resistance (Carroll *et al.*, 2009). However, in our strain background, *irc6*Δ did not alter sensitivity to the toxin (Figure 1B). We did observe increased resistance to K28 in the *MAT*α *irc6*Δ strain from the deletion collection but not in the corresponding *MAT***a** *irc6*Δ strain (Figure S1). Furthermore, no effects on K28 sensitivity were detected when *IRC6* was deleted in the parental strain for the *MAT*α deletion collection or a completely different K28 hypersensitive strain (Figure S1). Thus our results suggest that Irc6p does not provide important function in AP-2–mediated endocytosis.

Transport between the TGN and endosomes was assessed by monitoring proteolytic maturation of the secreted pheromone α-factor. This assay provides a sensitive measure of clathrin-mediated trafficking of the maturation protease Kex2p between the TGN and endosomes (Payne and Schekman, 1989). Inhibition of clathrin function results in Kex2p mislocalization to the cell surface, which in turn causes incomplete maturation of the α-factor precursor (Payne and Schekman, 1989). Unlike clathrin mutations, inactivation of TGN/endosome clathrin adaptors, such as AP-1, often do not affect pheromone maturation. However, such mutations enhance maturation defects of *chc1-ts* cells (Phan *et al.*, 1994; Rad *et al.*, 1995; Yeung *et al.*, 1999; Costaguta *et al.*, 2001). At both 24°C and 30°C, *irc6*Δ and wild-type cells secreted only mature α-factor (Figure 1C, lanes 1, 3, 5, and 7). However, at 24°C, at which *chc1-ts* cells are not affected, combination of *irc6*Δ and *chc1-ts* resulted in secretion of precursor forms (Figure 1C, lanes 2 and 4). The double mutant also exhibited an enhanced maturation defect compared with *chc1-ts* cells at 30°C (Figure 1C, lanes 6 and 8).

Growth of cells in the presence of the chitin-binding dye calcofluor white (CCFW) provides an assay for AP-1–dependent traffic. In *chs6*Δ cells, the chitin synthase Chs3p is retained intracellularly by clathrin-dependent and AP-1–dependent cycling between the TGN and endosomes, thereby reducing cell surface chitin rings and conferring CCFW resistance. In *chs6*Δ cells, inactivation of AP-1 perturbs the intracellular cycling pathway and allows Chs3p to escape to the cell surface, restoring chitin rings and sensitivity to CCFW (Valdivia *et al.*, 2002). Deletion of *IRC6* in *chs6*Δ cells increased sensitivity to CCFW, although not to the same extent as inactivating AP-1 by deleting the β1 subunit, and restored chitin rings (Figure 1, D–F). Expression of FLAG-Irc6p in *irc6*Δ *chs6*Δ cells conferred CCFW resistance and eliminated chitin rings. There was no further increase in CCFW sensitivity when *irc6*Δ was introduced into *β1*Δ *chs6*Δ cells (Figure 1E), consistent with Irc6p function in AP-1–mediated Chs3p transport. The *irc6*Δ phenotypes provide evidence that Irc6p functions in AP-1/clathrin–mediated traffic between the TGN and endosomes. We were unable to detect Irc6p expressed at endogenous levels by immunofluorescence or using green fluorescent protein (GFP) fusions, most likely because of low expression levels. At elevated expression levels, Irc6p appeared cytoplasmic (unpublished data).

Irc6p contains a novel small G protein–like domain

Irc6p displayed no clear sequence similarity to proteins of known function in database searches. To gain insights into the molecular architecture of Irc6p, we determined the structure by x-ray crystallography. Although full-length Irc6p did not crystallize, we obtained crystals of a large, C-terminally truncated fragment (aa 1–213). Phases were determined by the selenomethionine single-wavelength anomalous dispersion method, and the final structure was refined against 1.8 Å resolution data to a crystallographic R_{work}/R_{free} = 19.7%/21.8% (Table 1 and Figures 2A and S2A). The structure revealed that amino acids 1–176 were arranged as a Rossmann fold, a structural motif involved in nucleotide binding (Rao and Rossmann, 1973). A core, six-stranded β-sheet is flanked by six α-helices (Figure 2, A and B). No electron density was detected for the C-terminal 28 residues in the fragment (aa 186-213), suggesting that this region may be flexible or absent due to proteolysis.

The Protein Data Bank (PDB) was searched with the Irc6p aa 1–176 structure using the Dali server (Holm and Rosenstrom, 2010). All significant hits were G proteins, including more than 80 with

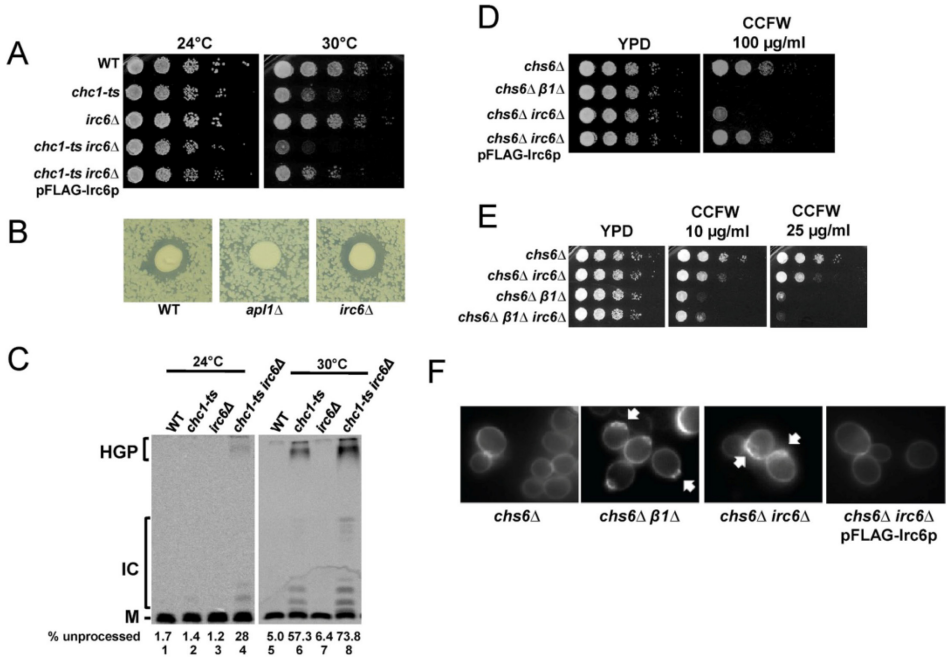

FIGURE 1: Irc6p function is associated with clathrin-mediated transport between the TGN and endosomes. (A) Genetic interactions between *irc6*Δ and *chc1-ts*. Wild-type (WT, SEY6210), *chc1-ts* (GPY1064), *irc6*Δ (GPY4986), *chc1-ts irc6*Δ (GPY3986), and *chc1-ts irc6*Δ pFLAG-Irc6p (GPY5008) strains were grown overnight at 24°C in YPD media, serially diluted, spotted onto YPD plates, and incubated for 2 d at the indicated temperatures. (B) No effect of *irc6*Δ on K28 toxin sensitivity. Indicated strains (WT, wild-type; *apl1*Δ, GPY1783-21D; *irc6*Δ, GPY4136) were grown overnight in YPD and then plated as a lawn on low-pH agar plates. Concentrated K28 toxin-secreting cells (MS300) were then spotted on the lawn, and the plates were incubated at 24°C for 2 d. The zone of clearing around the central spot of toxin-producing cells is an indicator of toxin sensitivity. (C) The α-factor maturation defect in *chc1-ts* cells is enhanced by *irc6*Δ. Wild-type and mutant strains as described in (A) were metabolically labeled at 24°C for 45 min or 30°C for 30 min. Secreted α-factor was immunoprecipitated from the media and analyzed by SDS–PAGE and autoradiography. HGP, highly glycosylated precursor; IC, intermediate cleavage products; M, mature. The amount of each form was quantified, and processing efficiency was expressed as the percentage of total present in HGP and IC forms. (D) *irc6*Δ increases CCFW sensitivity in *chs6*Δ cells. *chs6*Δ (GPY3102), *chs6*Δ *apl2*Δ (*chs6*Δ *β1*Δ; GPY3103), *chs6*Δ *irc6*Δ (GPY4042), and *chs6*Δ *irc6*Δ pFLAG-Irc6p (GPY5009) strains were grown overnight at 30°C, serially diluted, spotted onto YPD plates without (YPD) or with 100 μg/ml calcofluor white (CCFW), and incubated for 2 d at 30°C. (E) *irc6*Δ does not enhance CCFW sensitivity in *apl2*Δ *chs6*Δ cells. Cells carrying *chs6*Δ, *chs6*Δ *apl2*Δ, or *chs6*Δ *irc6*Δ as in (D) and *chs6*Δ *apl2*Δ *irc6*Δ (GPY4603) were assayed for sensitivity to the indicated CCFW concentrations as in (D). (F) Increased cell surface chitin in *irc6*Δ *chs6*Δ cells. Strains as in (D) were stained with CCFW and imaged by epifluorescence microscopy. Arrows point to bud scars.

Z-scores higher than 10. PDB structures with the strongest similarity were Arf-like GTPase 1 (Arl1, PDB ID: 1upt) and the GTPase Rab5 (PDB ID: 2efh; Figure 2B), which act in membrane trafficking (Panic *et al.*, 2003; Stenmark, 2009; Donaldson and Jackson, 2011). Irc6p aa 1–176 and Rab5 can be superimposed with a root mean-square deviation of 2.6 Å over 131 aligned Cα residues (Figure 2C).

G proteins share a common 20-kDa catalytic domain (G domain), with consensus motifs responsible for GTP binding and hydrolysis (Bourne *et al.*, 1991; Wittinghofer and Vetter, 2011). Irc6p lacks these motifs, suggesting that it does not bind GTP with high affinity. The crystals of Irc6p amino acids 1–213 were nucleotide-free, with intermolecular contacts at the putative GTP-binding site that would prevent nucleotide access. Attempts to cocrystallize Irc6p with GTP, GDP, or nonhydrolyzable analogues were unsuccessful. However, a structural comparison of Irc6p with the nucleotide-binding site of Arl1p cocrystallized with GTP identified several Irc6p residues that might participate in GTP binding (Figure 2, B, D, and E). Lys-22 and Thr-23 correspond to residues in the highly conserved P-loop motif GXXXXGK(T/S) in G domains, although the invariant glycines are absent in Irc6p (Figure 2, B and E). In G domains, the P-loop motif lysine and threonine are involved in binding to the β and γ phosphates of the nucleotide (Panic *et al.*, 2003; Donaldson and Jackson, 2011; Wittinghofer and Vetter, 2011). Specificity for GTP/GDP is typically dependent on conserved asparagine and aspartate residues in a consensus sequence NKXD that interact with the guanine base (Wittinghofer and Vetter, 2011). Irc6p has a suitably positioned glutamate (E121) in a related motif, NVNE (Figure 2, B and E).

We tested wild-type and mutant forms of Irc6p for binding to [^{35}S]GTPγS, using a standard filter-binding assay. In contrast to Arf1p, recombinant full-length Irc6p or the N-terminal domain (aa 1–213) did

	Native Irc6p	Peak (SeMet Irc6p)
Data collection		
Beamline	APS ID24-C	
Detector	ADSC Quantum Q315R	
Wavelength (Å)	0.9795	0.9793
Data processing	HKL	HKL
Space group	$P6_5$	$P6_5$
Unit cell parameters *a*,*b*,*c* (Å); α,β,γ (°)	*a* = 61.638 *b* = 61.638 *c* = 95.144 α = 90.0 β = 90.0 γ = 120.0	*a* = 61.421 *b* = 61.421 *c* = 95.008 α = 90.0 β = 90.0 γ = 120.0
Resolution (Å)	29.32–1.80	35.59–2.05
Number of observations	127,621	137,187
Unique reflections	18,511	25,501
Completeness (%)	97.4 (96.5)	99.3 (99.7)
R-merge (%)[a]	6.6 (54.1)	6.8 (39.8)
<I/σ(I)>	24.12 (3.95)	20.57 (4.23)
Number of Se atoms/ asymmetric unit		Two observed of six expected
Refinement statistics		
Resolution (Å)	53.8–1.8	
Number of reflections	17,548	
R_{work}/R_{free} (%)	19.7/21.8	
High-resolution shell	21.9/28.3	
Number of atoms	1538	
Protein	1498	
Water	40	
Average B-factor	19.3	
Wilson plot *B*	15.8	
V_m	2.1	
Estimated solvent content (%)	40.57	
RMS deviations		
Bond lengths (Å)	0.007	
Bond angles (°)	1.053	
Residues in Ramachandran	157	
Most-favored region (%)	94.6	
Additionally allowed (%)	4.8	
Generously allowed (%)	0.6	
Disallowed (%)	0.0	

[a]*R*-merge = merging *R* factor, $(\Sigma_{hkl} \Sigma_i |I_i(hkl) - \langle I(hkl)\rangle I) / (\Sigma_{hkl} \Sigma_i I(hkl)) \times 100\%$. Last shell SeMet 2.12–2.05 Å; last shell native 1.86–1.80 Å. Values in parentheses correspond to the statistics for the highest resolution.

TABLE 1: Data collection, processing, and refinement statistics.

not bind GTP in the presence (Figure 2F) or absence (unpublished data) of detergent. These findings, and the absence of consensus GTP-binding motifs, indicate that Irc6p is not a typical GTP-binding protein. However, with a sensitive UV cross-linking assay, GTPγS (but not ATPγS) associated with Irc6p but not with an unrelated protein, the lipid phosphatase Sac1p (Figure 2G; unpublished data). Two mutants, K22A and E121Q, engineered to disrupt putative GTP-binding residues, exhibited substantially reduced cross-linking to GTPγS (Figure 2G). Additionally, production of a stable C-terminally truncated fragment (residues 1–213) by limited proteolysis was slowed in the presence of GMPPNP (Figure S2B), suggesting that Irc6p may be stabilized by nucleotide.

K22A or E121Q mutations were introduced into the genomic *IRC6* locus and crossed into *chc1-ts* or *chs6*Δ strains. The GTP-binding mutants, expressed at wild-type levels (Figure S2C), did not cause defects in either strain with the standard growth assays (Figure 2, H and I). Only at high concentrations of CCFW did the mutations impair growth of the *chs6*Δ cells, but not to the extent of *irc6*Δ (Figure 2I). These findings sharply contrast with the effects of altering cognate P-loop–motif lysines in yeast Arf1p and the rab Ypt1p, which yielded severe phenotypes equivalent to complete gene inactivation (Wagner *et al.*, 1987; Click *et al.*, 2002). Thus the N-terminal domain of Irc6p differs from conventional G domains, neither binding GTP with low micromolar affinity nor exhibiting strong functional defects when mutated to prevent GTP binding.

Irc6p and p34 are members of a conserved protein family

Irc6p shares 15% sequence identity and 41% similarity with human p34. Homology-based structure-modeling programs Phyre, SWISS-MODEL, and ESyPred3D (Lambert *et al.*, 2002; Kelley and Sternberg, 2009; Kiefer *et al.*, 2009) predicted an N-terminal fold for p34 with the same topology as that of Irc6p (Figure S3A). Remarkably, expression of p34 from a multicopy plasmid completely rescued growth defects due to *irc6*Δ in either *chc1-ts* cells or in *chs6*Δ cells on CCFW (Figures 3, A and B, and S3B), revealing an unexpectedly strong functional conservation between Irc6p and p34 despite low sequence homology. Consistent with conserved function, p34 interacts with yeast AP-1 and AP-2 (Figure S3C).

A search of the Conserved Domain Database (CDD; Marchler-Bauer *et al.*, 2011) with the Irc6p sequence did not reveal the N-terminal G-like domain but did indicate a putative conserved domain in the C-terminal region (aa 162–232) that was also present in p34 (*E* value: 2.39e-07). The C-terminal region is designated as an adaptin-binding domain, although no analysis of adaptin binding by the domain has been reported. The CDD identified an additional ≈200 nonredundant eukaryotic protein sequences with putative adaptin-binding domains and, strikingly, 38 with N-terminal P-loop nucleoside triphosphate hydrolase (NTPase) domains and C-terminal adaptin-binding domains (Supplemental Table S1). G domains are a subset of P-loop NTPase domains. Among those with NTPase domains are p34 from rats, as well as sequences from humans and fish, amoeba, and plant species (Figure 4A). Some species encoded more than one Irc6-related protein. In many cases, the sequences delineated as P-loop NTPase were shorter than expected for a full Rossmann fold. A set of eight protein sequences from the 38 predicted two-domain proteins were submitted to the SWISS-MODEL three-dimensional modeling program. In every case, Rossmann fold–like domains consisting of a core of β-strands flanked by α-helices were predicted for the N-terminal regions (two examples are presented in Figure 4B). No models were predicted for the C-terminal "adaptin-binding" regions. Combined with our structural characterization of the N-terminal G-protein fold in Irc6p,

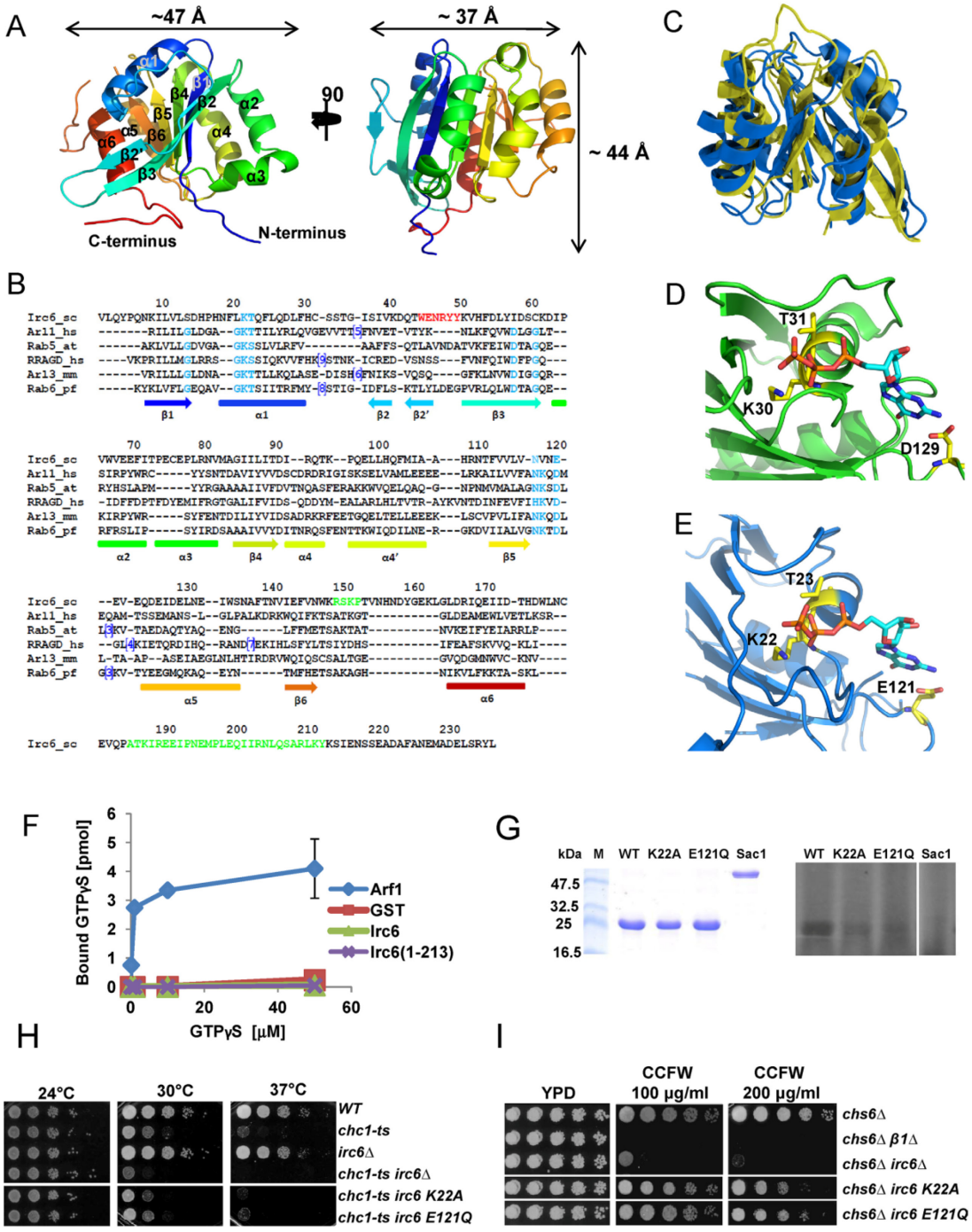

FIGURE 2: A G-like domain in Irc6p. (A) Ribbon representation of Irc6p amino acids 1–213 derived from the crystal structure determined at 1.8 Å resolution. Two perspectives are presented, rotated by 90°. Ribbon is colored in rainbow from blue at the N-terminus to red at the C-terminus, with secondary structure elements numbered. (B) Structure-based

these observations define Irc6p and p34 as founding members of a novel G protein–like family distinguished by an N-terminal G-like domain and a C-terminal region related to p34.

Sequence alignment of the 38 predicted two-domain proteins uncovered a conserved motif with the consensus sequence (I/L)(N/D)(N/T)(R/K)YY located in the accessible loop connecting β2 and β3 strands in Irc6p and the predicted p34 structure (Figure 4, C and D, and Table S1). The motif is not present in the structurally similar G proteins identified in the Dali server search (Figure 2B, motif highlighted in red). As such, the sequence appears to constitute another signature for this group of proteins. We term this motif BC-YY for the beta-strand connecting YY motif. Mutation of the BC-YY motif (YY to AA) compromised function of both Irc6p and p34 (Figure 3C). On the basis of the conservation of this motif, we suggest naming the group of Irc6p/p34-related proteins "BYGR" for BC-YY G-protein related.

The CCD search did not detect the N-terminal P-loop NTPase domain in Irc6p and consequently classified Irc6p as one of the ≈200 sequences without an N-terminal NTPase-like domain. Thus it is likely that additional members of the BYGR family are present in this set of sequences. Indeed, of the sequences with a predicted "adaptin-binding" domain but no predicted G-protein fold, ~80% carry versions of the BC-YY motif.

Our analysis suggests that Irc6p is organized into at least two regions, an N-terminal G-like domain and a conserved C-terminal region. To determine the effects of deleting one of the regions, we designed C- or N-terminal truncations based on the Irc6p structure. When combined with *chs6Δ*, deletion of the C-terminal region (aa 180–237; *irc6ΔC*) debilitated growth on CCFW more severely than full deletion of *IRC6*, even at very low CCFW concentrations (Figure 3D). This suggests that, in the absence of the C-terminal region, the G-like domain acts to inhibit Chs3p traffic between the TGN and endosomes, perhaps by nonproductive binding to a normal interaction partner. In a reciprocal experiment, expression of just the Irc6p C-terminal sequences (aa 179–237) partially complemented the growth defect in *chs6Δ irc6Δ* cells (Figure 3D). Similar results were obtained with p34 N- and C-terminal regions, although the growth effects were less pronounced than observed with Irc6p (Figure 3D). These results support the functional significance of the two-region model for Irc6p/p34.

Irc6p interacts with proteins involved in TGN/endosome traffic

We identified Irc6p-binding proteins by affinity chromatography of yeast lysate and mass spectrometry, yielding the known interactors AP-1 and AP-2, as well as novel binding partners Ypt31p and Sec4p. Sec4p and Ypt31p are Rab GTPases that function in secretory vesicle traffic between the TGN and the plasma membrane (Novick *et al.*, 1980; Benli *et al.*, 1996; Jedd *et al.*, 1997). In addition, Ypt31p functions in transport between the TGN and endosomes (Chen *et al.*, 2005, 2011). Irc6p interactions with AP-1, AP-2, Ypt31p, and Sec4p were also detected by immunoblotting of proteins isolated by Irc6p affinity chromatography (Figure 5A) and by coimmunoprecipitation of tagged Irc6p expressed from the native chromosomal locus (Figure 5B). Supporting the specificity of these interactions, Irc6p did not bind to the Arf1p GTPase or the Gga2p clathrin adaptor by affinity chromatography nor did it bind to the Rab Ypt1p by coimmunoprecipitation (Figure 5, A and B).

We tested whether purified Ypt31p and Irc6p interact directly. In the presence of GDP, Irc6p did not bind to glutathione *S*-transferase (GST)-Ypt31p (Figure 5C, lanes 5 and 6). Preincubation with a nonhydrolyzable GTP analogue, GMPPNP, stimulated Irc6p binding to GST-Ypt31p but not to GST (Figures 5C, lanes 7 and 9, and S3D). The stimulatory effect of GMPPNP still occurred when the GTP binding–defective Irc6p K22A mutant was tested for Ypt31p binding (Figure 5C, lane 10). This observation suggests that the nucleotide acts on Ypt31p to enhance the interaction. Our results establish that Irc6p binds directly to the activated form of Ypt31p.

Functional interaction of Irc6p with Ypt31p

Double mutant analysis was used to probe functional interactions between Irc6p and Ypt31p or Sec4p in vivo. No enhancement of growth defects was observed when *irc6Δ* was combined with the temperature-sensitive *sec4-8* allele, even at the semipermissive temperature of 30°C (Figure 6A). The absence of genetic interactions at

---

sequence alignment of Irc6p with similarly folded proteins identified by the Dali server. PDB codes of sequences are 1upt (Arl1), 2efh (Rab5), 2q3f (RRAGD), 3bh7 (Arl3), and 1d5c (Rab6). sc, *Saccharomyces cerevisiae*; hs, *Homo sapiens*; at, *Arabidopsis thaliana*; mm, *Mus musculus*; pf, *Plasmodium falciparum*. Conserved G-protein motifs G1, G3, and G4 are highlighted in light blue. Residues corresponding to the BC-YY motif [(L/I)(N/D)(N/T)(K/R)YY] present in the Irc6p family are in red. Residues that were present in the crystallized Irc6p construct, but lacked any electron density, are green. Dashes either correspond to residues missing in the electron density maps or gaps in the alignment. Numbers in brackets represent residues omitted to facilitate presentation of the alignment. Numbered secondary structure elements (strands β_1–β_6 and helices α_1–α_5) correspond to those shown in (A). (C) Superposition of Irc6p and atRab5. Structures of Irc6p (aa 8–177, blue) and atRab5p (aa 8–172, 2efh, gold) were superimposed with a root mean-square deviation of 2.6 Å using the program COOT (Emsley and Cowtan, 2004; Langer *et al.*, 2008). (D) GTP-binding site of Arl1 with GTP (PDB ID: 1upt). Amino acid side chains involved in GTP binding and conserved in Irc6p are shown in yellow. (E) Putative nucleotide-binding pocket in Irc6p. GTP was modeled into the Irc6p structure using the program COOT (Emsley and Cowtan, 2004). The highly conserved residues involved in GTP-binding are highlighted in yellow. (F) Irc6p does not bind GTP with high affinity. The indicated recombinant proteins (0.5 μM) were incubated with increasing concentrations of ^{35}[S]GTPγS, and bound nucleotide was measured by filter binding and rapid filtration. (G) Irc6p binds GTP by cross-linking. Purified recombinant wild-type Irc6p (WT), Irc6p K22A, and E121Q mutants and Sac1p were incubated with ^{35}[S]GTPγS, subjected to UV illumination, and analyzed for bound nucleotide by SDS–PAGE and autoradiography. Proteins were stained with Coomassie Blue (left panel) or subjected to autoradiography (right panel). M, molecular weight standard (kDa). (H) Effects of Irc6p GTP-binding mutations on *chc1-ts* cell growth. Wild-type (WT, SEY6210), *chc1-ts* (GPY1064), *irc6Δ* (GPY4986), *chc1-ts irc6Δ* (GPY3986), *chc1-ts irc6-K22A* (GPY4988), and *chc1-ts irc6-E121Q* (GPY4989) strains were analyzed for growth, as in Figure 1A. (I) Effects of Irc6p GTP-binding mutations on *chs6Δ* cell sensitivity to CCFW. *chs6Δ* (GPY3102), *chs6Δ β1Δ* (GPY3103), *chs6Δ irc6Δ* (GPY4042), *chs6Δ irc6-K22A* (GPY4990), and *chs6Δ irc6-E121Q* (GPY4991) cells were tested for sensitivity to the indicated concentrations of CCFW, as in Figure 1D.

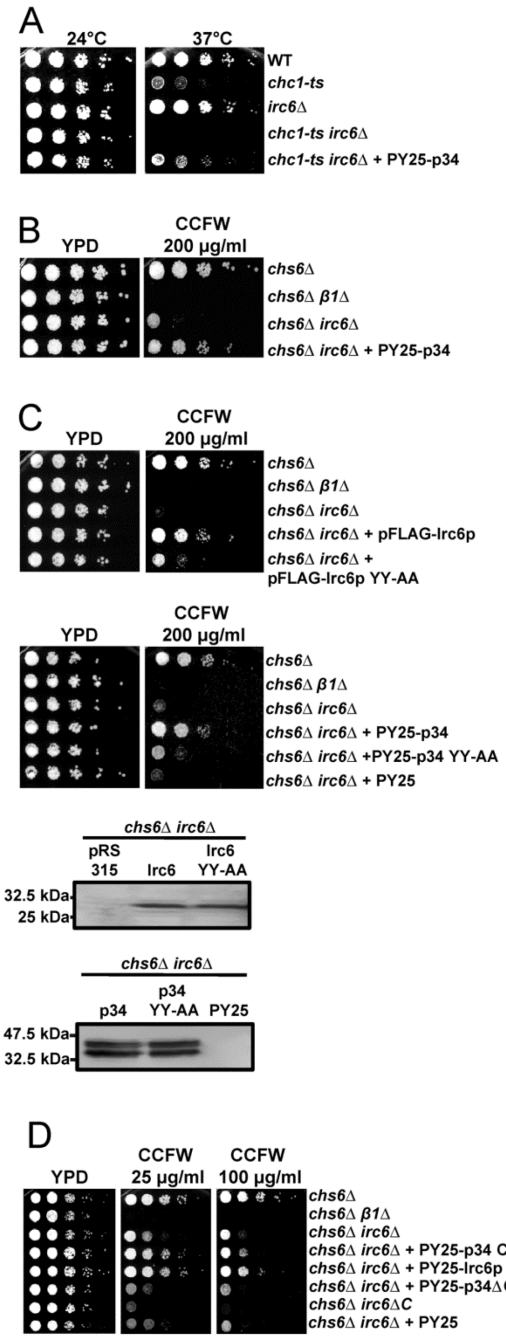

FIGURE 3: Mammalian p34 substitutes for Irc6p in vivo. (A) Indicated strains as in Figure 1A and *chc1-ts irc6Δ* cells expressing 6xHis-tagged p34 from a multicopy plasmid (PY25-p34, GPY5010) were assayed for growth, as in Figure 1A. (B) Indicated strains as in Figure 1D and *chs6Δ irc6Δ* cells expressing 6xHis-tagged p34 from a multicopy plasmid (PY25-p34, GPY5011) were assayed for sensitivity to CCFW, as in Figure 1D. (C) Indicated strains as in Figures 1D and 3B and *chs6Δ irc6Δ* cells expressing either pFLAG-Irc6p YY-AA (GPY5026) or PY25-p34 YY-AA (GPY5028) were assayed for sensitivity to CCFW, as in Figure 1D. Bottom panels show expression levels of wild-type and YY-AA mutants of Irc6p and p34 from the indicated strains detected by SDS–PAGE and immunoblotting of cell lysates. (D) *chs6Δ* (GPY3102), *chs6Δ β1Δ* (GPY3103), *chs6Δ irc6Δ* (GPY4042), *chs6Δ irc6Δ* expressing the p34 C-terminal region from a multicopy plasmid (PY25-p34 CT, GPY5014), *chs6Δ irc6Δ* expressing the Irc6p C-terminal region from a multicopy plasmid (PY25-Irc6p CT, GPY5015), *chs6Δ irc6Δ* expressing the p34 N-terminal region from a multicopy plasmid (PY25-p34ΔC, GPY5016), and *chs6Δ irc6ΔC* (GPY4993) were tested for sensitivity to the indicated concentrations of CCFW, as in Figure 1D.

any of the tested temperatures suggests that Irc6p does not functionally interact with Sec4p in secretory vesicle traffic, so this interaction was not further investigated.

Ypt31p and the related Ypt32p constitute a redundant pair of Rab GTPases that function in both secretory vesicle transport and traffic between the TGN and endosomes (Benli *et al.*, 1996; Jedd *et al.*, 1997; Ortiz *et al.*, 2002; Chen *et al.*, 2005, 2011; Sciorra *et al.*, 2005; Furuta *et al.*, 2007). Deletion of either Ypt does not cause overt growth defects, but deletion of both is lethal (Benli *et al.*, 1996; Jedd *et al.*, 1997). As one test for genetic interactions, we monitored the effect of *irc6Δ* on growth of cells harboring *ypt31Δ* and the temperature-sensitive *ypt32-A141D*^{ts} allele (Jedd *et al.*, 1997). The *ypt31Δ ypt32-ts* cells grew normally at 24°C, exhibited slowed growth at the semipermissive temperature of 33°C, and did not grow at 37°C (Figure 6B). Consistent with function of Irc6p with Ypt31/32p, *irc6Δ* dramatically inhibited the growth of *ypt31Δ ypt32-ts* cells at 33°C but did not affect growth at 24°C or at any temperature when present by itself or in combination with only *ypt31Δ* (Figure 6B).

We applied the CCFW assay to mutant combinations with *chs6Δ* to distinguish between Irc6p roles with Ypt31/32p in the secretory pathway or TGN-endosome traffic. In *chs6Δ* cells, increased sensitivity to CCFW reflects a redistribution of Chs3p from the TGN-endosome cycling pathway to the plasma membrane (Valdivia *et al.*, 2002; Copic *et al.*, 2007). Because Chs3p transport to the plasma membrane requires a functional secretory pathway, increased CCFW sensitivity in *chs6Δ* cells can be attributed to effects on TGN-endosome traffic. At 24°C, *ypt31Δ ypt32-ts* sensitized *chs6Δ* cells to CCFW more than *irc6Δ*, with effects approaching that of AP-1 inactivation (*β1Δ*; Figure 6C), supporting an important role for Ypt31/32p in TGN-endosome cycling of Chs3p. Importantly, *irc6Δ* intensified the sensitivity when introduced into *ypt31Δ ypt32-ts chs6Δ* cells, even at a low CCFW concentration (10 μg/ml) at which *irc6Δ* did not have an effect by itself in *chs6Δ* cells (Figure 6C). Similar genetic interactions were observed between *irc6Δ* and *ypt31Δ* in cells expressing the wild-type *YPT32* (Figure 6D). These results provide evidence that Irc6p functions with Ypt31/32p in Chs3p transport between the TGN and endosomes.

Irc6p links Ypt31p to AP-1

To assess the possibility that Irc6p acts to bridge AP-1 and Ypt31p, we determined whether GST-Ypt31p can bind to AP-1 in extracts from *irc6Δ* cells or *irc6Δ* cells expressing FLAG-tagged Irc6p. In cells expressing FLAG-Irc6p, both Irc6p and AP-1 bound to GST-Ypt31p but not to GST (Figure 7A). Low but specific binding to AP-2 was

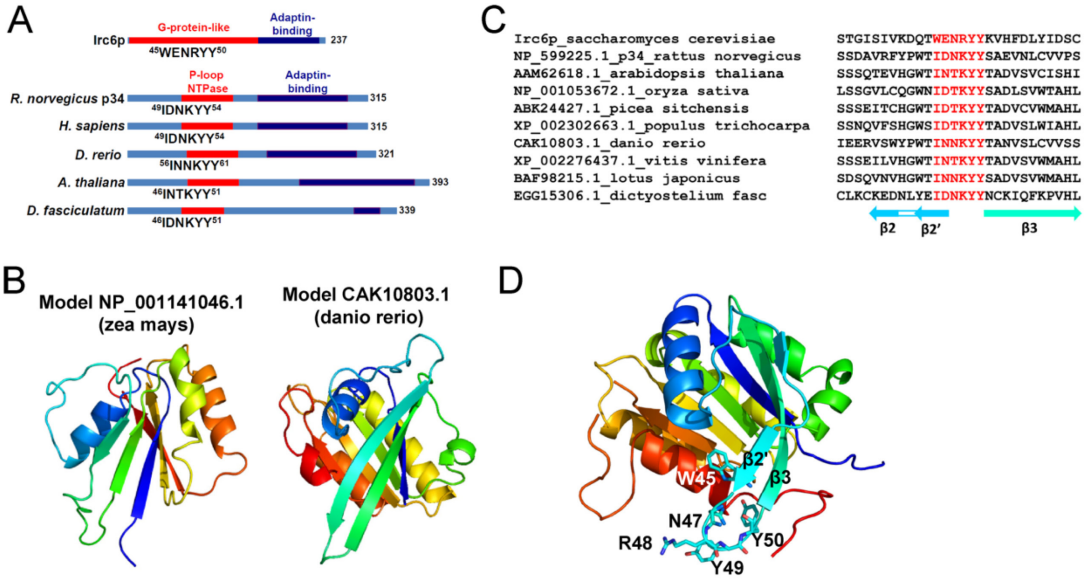

FIGURE 4: The Irc6/p34 G-protein–like family. (A) Diagrams of domain organization and conserved BC-YY motifs in selected members of the family. (B) Predicted three-dimensional structures of Irc6p/p34-related sequences from *Zea mays* and *Danio rerio*. Models were generated by the program SWISS-MODEL, and figures were made with PyMOL. (C) Clustal Omega (www.clustal.org/omega/) alignment of sequences from diverse species belonging to the novel G protein–like family. Highly conserved residues in the sequences corresponding to Irc6p amino acids 34–61 are highlighted in red. (D) Conserved BC-YY motif [(L/I)(N/D)(N/T)(K/R)YY] in Irc6p is localized in loop connecting β_2 and β_3.

also observed. Strikingly, GST-Ypt31p did not bind to AP-1 (or AP-2) in the cell extract lacking Irc6p (Figure 7A), suggesting a role for Irc6p in linking AP-1 to Ypt31p.

Binding of the two Irc6p domains to Ypt31p and AP-1 was also examined. When purified proteins were used, GST-Ypt31p (with GMPPNP) bound both Irc6p N- and C-terminal regions (Figure 7B), with an apparent preference for the C-terminal region. A similar experiment was carried out to assess AP-1 binding, but in this case the Irc6p constructs were used for affinity binding with cell extracts as a source of AP-1. As with Ypt31p, both the Irc6p N- and C-terminal regions bound AP-1, although with somewhat higher levels of AP-1 binding by the N-terminal region (Figure 7C, lanes 3–5). Taken together, the results from both physical and genetic interaction studies suggest that Irc6p and Ypt31/32p act together with AP-1 in TGN-endosome traffic.

DISCUSSION

The number and variety of clathrin coat accessory proteins confer a complexity to CCV formation that distinguishes the process from simpler mechanisms that drive biogenesis of other well-characterized classes of coated vesicles (Kirchhausen, 2000). In this study, we have identified Irc6p as a founding member of a new G protein–like family that functions with AP-1 and Ypt31p in TGN-endosome traffic. These findings define Irc6p and, by extension, its functional mammalian homologue p34, as a novel type of clathrin coat accessory factor.

The crystal structure of Irc6p amino acids 1–185 revealed an N-terminal Rossmann fold that is most similar to small G proteins of the Arf and Rab families. However, Irc6p lacks signature G-protein motifs, and both biochemical and genetic experiments provide evidence that the N-terminal region of Irc6p is not a conventional G domain that relies on GTP binding for function. Instead, our results suggest that low-affinity GTP binding might contribute to Irc6p stability. Even so, the inefficient GTP binding in vitro, the subtle in vivo defects caused by structure-based mutation of candidate GTP-binding residues, and the lack of conservation of those residues in other family members favor a view that GTP binding is not an important feature of the Irc6p/p34 family. In this way, the Irc6p/p34 N-terminal domain may represent a "pseudo-G domain" that has retained protein interaction functions but not nucleotide binding, as has been recently suggested for G-like domains in mammalian AGAP1 and LRRK (Luo *et al.*, 2012).

Our results offer several lines of evidence that Irc6p directly functions in clathrin-mediated transport between the TGN and endosomes. First, Irc6p physically interacts with AP-1 and Ypt31p, both associated with TGN-endosome traffic. Second, *IRC6* deletion affects Kex2p-dependent α-factor maturation in *chc1-ts* cells and Chs3p-dependent CCFW sensitivity in *chs6*Δ cells. Both Kex2p and Chs3p cycle between the TGN and endosomes, and defects in clathrin, AP-1, and clathrin accessory proteins yield phenotypes similar to those observed for *irc6*Δ (Seeger and Payne, 1992; Yeung *et al.*, 1999; Valdivia *et al.*, 2002; Fernandez and Payne, 2006). Third, reduced activity of Ypt31/32p caused CCFW sensitivity in *chs6*Δ cells, and *irc6*Δ enhanced this sensitivity. These results provide evidence that Ypt31/32p are involved in Chs3p cycling between the TGN and endosomes, supporting models for Ypt31/32p function in TGN-endosome traffic derived from defects in transport of other

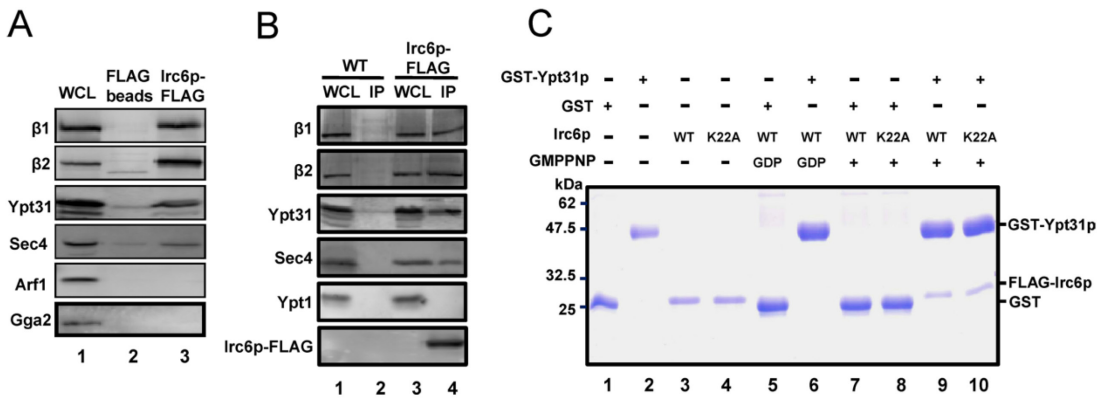

FIGURE 5: Irc6p physically interacts with AP complexes and Rab proteins. (A) Irc6p affinity binding. Purified FLAG-tagged Irc6p bound to FLAG affinity beads or FLAG affinity beads alone were incubated with WCL of wild-type cells (SEY6210). Bound proteins were separated by SDS–PAGE and analyzed using immunoblotting for the indicated proteins. Amount loaded in the WCL lane corresponds to 6% of the lysate used for affinity binding in lanes 2 and 3. (B) Irc6p coimmunoprecipitation. Wild-type cells (WT, SEY6210) or cells expressing Irc6p-FLAG from the endogenous locus (Irc6p-FLAG) were lysed under nondenaturing conditions and incubated with FLAG affinity beads. WCL and immunoprecipitated (IP) proteins were separated by SDS–PAGE and analyzed by immunoblotting for the indicated proteins and FLAG (Irc6p-FLAG). Irc6p-FLAG is difficult to detect in WCL, due to low expression levels. Amount loaded in the WCL lane corresponds to 6% of the lysate used for immunoprecipitation. (C) Direct interaction between Irc6p and Ypt31p. Purified GST (lane 1) or GST-Ypt31p (lane 2) bound to glutathione beads and purified FLAG-Irc6p (WT, lane 3) or FLAG-Irc6p-K22A (lane 4) were combined as indicated (lanes 5–10) with or without preloaded 1 mM GDP (lanes 5 and 6) or 1 mM GMPPNP (lanes 7–10). Protein interaction was analyzed by SDS–PAGE and Coomassie Blue staining. Amount of Irc6p loaded in lanes 3 and 4 corresponds to 40% of the amount used for affinity binding in lanes 5–10.

cargo (Chen *et al.*, 2005, 2011; Furuta *et al.*, 2007). Enhancement of CCFW sensitivity resulting from the combination of *irc6Δ* with *ypt31/32* mutants further supports assignment of Irc6p function to traffic between the TGN and endosomes. In contrast, although Irc6p binds to AP-2, we did not detect effects of *irc6Δ* on AP-2–mediated endocytosis. Thus a role for Irc6p in endocytosis remains to be established.

Like some other trafficking proteins (Borlido *et al.*, 2009), Irc6p has also been implicated in nuclear functions. In one report, *irc6Δ* cells displayed increased levels of recombination protein foci in nuclei, but no defects in recombination were observed (Alvaro *et al.*, 2007). In an independent study, *irc6Δ* was identified in a screen for mutations that reduced DNA double-stranded break healing by telomerase (Zhang and Durocher, 2010). Whether these phenotypes reflect a direct role for Irc6p in the nucleus or result from indirect effects of an Irc6p deficiency is not clear.

Affinity-binding experiments using Ypt31p as bait suggest that Irc6p can link Ypt31p to AP-1. Additionally, stimulation of Irc6p binding to a GTP analogue–activated form of Ypt31p indicates that Irc6p is an effector of Ypt31p. We envision that the ability of Irc6p to bind to AP-1 and serve as a Ypt31p effector provides a mechanism to bring together AP-1 and activated Ypt31p in forming CCV. CCV-associated Ypt31p could then recruit additional effectors, as has been observed for other Rab proteins (Hutagalung and Novick, 2011; Segev, 2011). In this way, Irc6p would function to expand the repertoire of coat-associated proteins during biogenesis of AP-1 clathrin coats. Whether Irc6p directly links AP-1 and Ypt31p or acts with a separate linking protein(s) will require additional investigation. The less-severe effects of *irc6Δ* compared with inactivation of AP-1 or Ypt31/32p likely reflect redundant or alternative mechanisms that can more effectively accommodate the absence of Irc6p function than a loss of the core transport functions of AP-1 or Ypt31/32p.

Results from both structural and functional analyses support a bipartite model for Irc6p organization: the N-terminal G protein–like domain and a conserved C-terminal region. Of note, the conserved C-terminal domain predicted by the CCD overlaps with the final α-helix of the G-like domain (aa 166–175). The observation that amino acids 166–175 constitute the final helix in the G-like domain crystal structure suggests that these sequences are not part of an independent C-terminal domain. Furthermore, a C-terminal fragment (aa 180–237) that does not include the final G-like domain helix was able to substitute for full-length Irc6p in vivo, indicating that amino acids 166–179 are not essential for function of the C-terminal region. On the basis of these results, we consider the conserved C-terminal region as a separate "domain" beginning after the final helix of the G-like domain. Sequences following amino acid 186 were not detected in the Irc6p crystal, leaving the structural organization of the C-terminal region unclear. Secondary-structure prediction algorithms suggest two α-helical regions between amino acid 199 and the C-terminus, as well as the possibility of a coiled coil between amino acid 199 and amino acid 212 (Figure S3E). It appears unlikely that the putative coiled coil mediates homo-dimerization, since there was no significant difference in gel filtration elution profiles of recombinant full-length Irc6p and an Irc6p fragment lacking amino acids 190–237 (unpublished data). Additional experiments will be needed to determine the structure of the C-terminal region and define the structural arrangement of the N- and C-terminal regions in full-length Irc6p.

Although the C-terminal region is designated as an "adaptin-binding domain" in the CCD database, our results indicate that both the N-terminal and C-terminal regions have the capacity to bind

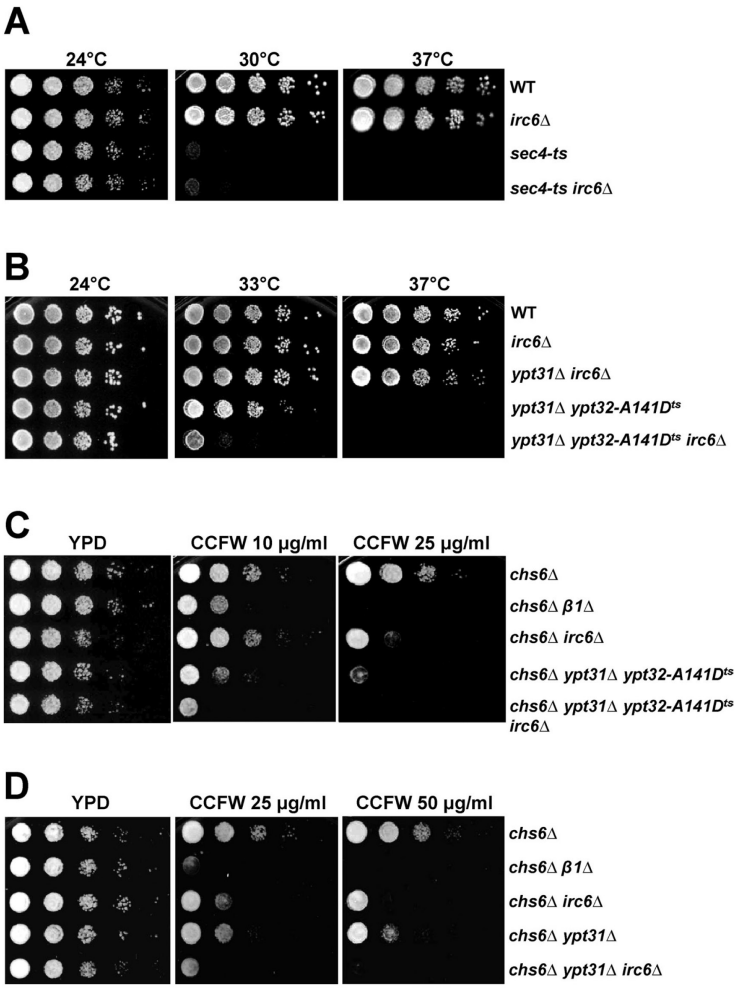

FIGURE 6: Irc6p functionally interacts with Ypt31p. (A) Absence of genetic interaction between *irc6*Δ and *sec4* by growth. Wild-type (WT, SEY6210), *irc6*Δ (GPY4986), *sec4-8* (*sec4-ts*, NY28), and *sec4-8 irc6*Δ (GPY4994) cells were analyzed for growth at the indicated temperatures, as in Figure 1A. (B) Genetic interaction between *irc6*Δ and *ypt31/32*^{ts} by growth. Wild-type (WT, SEY6210), *irc6*Δ (GPY4986), *ypt31*Δ *irc6*Δ (GPY4972-4D), *ypt31*Δ *ypt32-A141D*^{ts} (GPY4972-6D), and *ypt31*Δ *ypt32-A141D*^{ts} *irc6*Δ (GPY4972-7D) cells were analyzed for growth at the indicated temperatures, as in Figure 1A. (C) Genetic interactions between *ypt31/32*^{ts} and *irc6*Δ by CCFW sensitivity. *chs6*Δ (GPY3102), *chs6*Δ *β1*Δ (GPY3103), *chs6*Δ *irc6*Δ (GPY4042), *chs6*Δ *ypt31*Δ *ypt32-A141D*^{ts} (GPY4985-51C), and *chs6*Δ *ypt31*Δ *ypt32-A141D*^{ts} *irc6*Δ (GPY4985-8B) cells were tested for their sensitivity to the indicated concentrations of CCFW, as in Figure 1D. (D) Genetic interactions between *irc6*Δ and *ypt31*Δ by CCFW sensitivity. Strains as in Figure 6C plus *chs6*Δ *ypt31*Δ (GPY4985-79D) and *chs6*Δ *ypt31*Δ *irc6*Δ (GPY4985-6A) were assayed as in Figure 1D.

AP-1 and Ypt31p. However, the different functional consequences observed when the domains were expressed separately imply that the binding modes of the two Irc6p regions to AP-1 and Ypt31p are distinct. The ability of the C-terminal domain to bind both AP-1 and Ypt31p suggests that this domain can partly reinstate the functional interactions mediated by the full-length protein, thereby accounting for partial complementation when the C-terminal domain is expressed by itself in *irc6*Δ cells. In contrast, expression of the N-terminal domain alone was more deleterious than the complete absence of Irc6p. This finding can be explained by nonproductive, inhibitory binding of the N-terminal domain to AP-1 and/or Ypt31/32, since mutations in either of these factors yields more severe phenotypes than deletion of *irc6*Δ.

Complete complementation of *irc6*Δ growth defects by expression of full-length mouse p34 and the interaction of p34 with yeast AP-1 revealed a surprisingly strong degree of functional conservation between the yeast and mouse proteins, thereby suggesting a role for mammalian p34 in AP-1–dependent TGN-endosome traffic. The functional similarities between yeast and human proteins are likely to reflect a conserved two-region structure. Modeling algorithms predicted a Rossmann fold for the N-terminal domain of p34 similar to that of Irc6p. Database searches also predict common C-terminal regions in Irc6p and p34. Importantly, expression of the p34 C-terminal region in *irc6*Δ cells mimicked the growth-enhancing effects of the C-terminal Irc6p region. The presence of sequences encoding proteins with the same predicted domain arrangement and the conserved BC-YY motif in organisms as diverse as fungi, mammals, and plants suggest that the functions of Irc6p andp34 have been broadly conserved in evolution. On the basis of these findings, we propose that Irc6p/p34 are founding members of a previously unrecognized family related to small G proteins, constituting a novel class of conserved clathrin coat accessory factors.

MATERIALS AND METHODS

Plasmids and yeast strains

For generation of recombinant 6xHis- or FLAG-tagged Irc6p fusion proteins, DNA encoding Irc6p was amplified by PCR from yeast genomic DNA. Products were cloned in-frame into the *Nco*I/*Xho*I sites of pET-28a or the *Nco*I/*Nde*I sites of pET-15b bacterial expression vectors for 6xHis- or FLAG-tagged constructs, respectively. For generation of FLAG-Irc6p for expression in yeast, the FLAG tag was encoded in the forward primer used in PCR, such that the protein contained the sequence MGDYKDDDDKSG directly fused to Irc6p. The resulting PCR product was cloned into the *Xba*I/*Not*I sites of centromeric plasmid pRS315 containing the *PRC1* promoter and *CYC1* terminator region, and into the *Xho*I/*Bam*HI sites of multicopy PY25 containing the glyceraldehyde-3-phosphate dehydrogenase promoter (Li *et al.*, 2008). DNA encoding p34 full-length, its N-terminal–region amino acids 1–179, or the C-terminus amino acids 158–315 was amplified by PCR using mouse

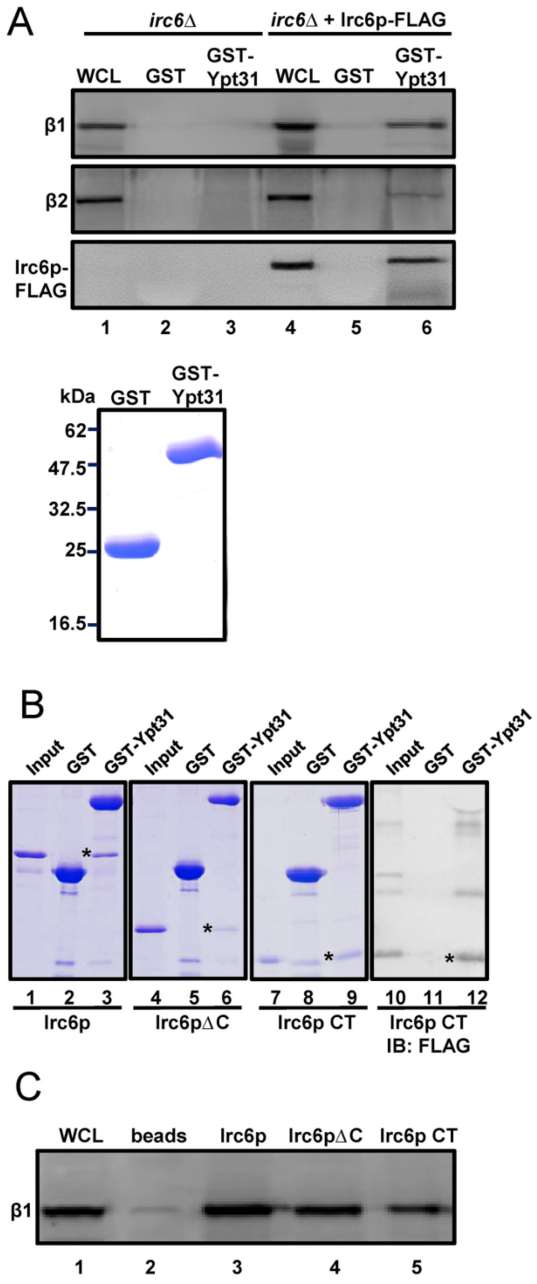

FIGURE 7: Irc6p links Ypt31p to AP-1. (A) Irc6p is necessary for Ypt31p binding to AP-1. GST or GST-Ypt31p bound to glutathione-Sepharose (bottom panel, Coomassie Blue–stained) was incubated with WCL (lanes 1 and 4) from *irc6Δ* cells (GPY4986, lanes 2 and 3) or *irc6Δ* cells expressing FLAG-Irc6p (GPY5018, lanes 5 and 6). Bound proteins were eluted, separated by SDS–PAGE, and analyzed by immunoblotting for β_1, β_2, and FLAG (top panel). (B) Ypt31p interacts with Irc6p N- and C-terminal regions. FLAG-tagged Irc6p constructs indicated at the bottom of each panel were incubated with GST or GST-Ypt31p bound to glutathione-Sepharose (in the presence of 1 mM GMPPNP). Irc6p constructs alone (input) or proteins associated with GST or GST-Ypt31p were separated by SDS–PAGE and either stained with Coomassie Blue (left three panels) or subjected to immunoblotting with FLAG antibody (right-most panel). Asterisk in each panel indicates Irc6p or Irc6p fragment associated with GST-Ypt31. (C) AP-1 interacts with N- and C-terminal regions of Irc6p. FLAG-Irc6p constructs used in (B) were bound to FLAG-affinity beads and incubated with WCL (lane 1) of wild-type cells SEY6210. Proteins associated with FLAG beads only (lane 2), wild-type FLAG-Irc6p (Irc6p, lane 3), FLAG-Irc6pΔC (lane 4) or FLAG-Irc6pCT (lane 5) were eluted, separated by SDS–PAGE, and analyzed by immunoblotting for β_1.

cDNA reverse-transcribed from 1 μg of RNA extracted from the mouse V6.5 embryonic stem cell line. For expression in yeast, p34 constructs were cloned into the *Xho*I/*Bam*HI sites of PY25, and for expression in *Escherichia coli*, p34 was cloned into the pET-15b vector using the *Nde*I and *Bam*HI sites. Irc6p K22A and E121Q mutations were introduced by site-directed mutagenesis of pET28a or pET-15b constructs using the QuikChange system (Stratagene, LalJolla, CA). All constructs were verified by sequencing.

For introduction of point mutations into endogenous *IRC6*, *irc6-K22A*, irc6-*E121Q*, or *irc6-Y49A Y50A* (YY-AA) in pET-15b was used as a template for PCR. The resulting products were cotransformed with pRS313 (*HIS3*; Sikorski and Hieter, 1989) into GPY4986. His+ colonies were replica-plated onto agar medium containing 5-fluoroorotic acid to identify cells in which the mutant sequences replaced *URA3*. C-terminal truncation (*irc6ΔC*; aa 1–179) and C-terminal tagging of Irc6p in the genomic locus were performed as described in Longtine *et al.* (1998), using the vector pFA6a-FLAG-TRP1. All alterations of genomic *IRC6* were verified by PCR and sequencing, and protein expression was evaluated by immunoblotting.

Double mutant strains were generated by standard yeast mating, sporulation, and isolation of haploid segregants. The genotypes of all strains used in this study are listed in Table S2.

Yeast media, growth assays, radiolabeling and immunoprecipitation, and fluorescence microscopy

Strains were grown in YPD (1% Bacto yeast extract [Difco, Detroit, MI], 2% Bacto peptone [Difco], 2% dextrose) or SD media (0.67% yeast nitrogen base without amino acids [Difco], 2% dextrose) with the appropriate supplements. CCFW (Sigma-Aldrich, St. Louis, MO) was added to YPD agar plates at the concentrations indicated in the figures. For growth tests, cells were diluted to 1×10^7 cells/ml and then serially diluted 10-fold before dilutions were spotted onto appropriate agar plates. K28 toxin sensitivity was assayed as described in Carroll *et al.* (2009). Radiolabeling and immunoprecipitation of α-factor was performed as described previously (Fernandez and Payne, 2006). CCFW bud-scar staining was carried out as described in Duncan *et al.* (2007).

Protein purification

For biochemical studies, pET-15b or pET-28a containing 6xHis- or FLAG-tagged Irc6p constructs were transformed into *E. coli* BL21(DE3). Protein expression was induced with 0.4 mM isopropyl β-D-1-thiogalactopyranoside (IPTG) at 0.8 OD_{600}, and cells were grown at 24°C overnight in either Luria–Bertani broth (LB) medium or M9 medium substituted with seleno-methionine. Cells were resuspended in lysis buffer (25 mM Tris–HCl, pH 7.5, 150 mM NaCl,

5% glycerol, 2 mM $MgCl_2$, 0.5% n-octyl-β-D-glucopyranoside, and protease inhibitor cocktail without EDTA [Roche Diagnostics GmbH, Mannheim, Germany]), lysed by sonication, and subjected to centrifugation at 20,000 × *g* for 30 min. 6xHis- or FLAG-tagged proteins in the soluble fraction were bound to Ni-NTA Superflow beads (Qiagen GmbH, Hilden, Germany) or anti-FLAG M2 affinity beads (Sigma-Aldrich), respectively. Beads were washed with buffer S (25 mM Tris–HCl, pH 7.5, 150 mM NaCl, 5% glycerol, 2 mM $MgCl_2$), and proteins of interest were eluted with either buffer B (buffer S + 250 mM imidazole) or FLAG elution buffer (buffer S + 150 µg/ml FLAG peptides [Sigma-Aldrich]). For the GTP-binding filter assay, pGex-4T-1, pET22b-Arf1 (Arf1-His6), pET21a-Irc6 (Irc6-His6), and pET28a-Irc6(1-213) (His6-Irc6(1-213)) in BL21(DE3) codon+ bacteria were grown to ~1 OD_{600} at 37°C, and protein expression was induced by 1 mM IPTG for 2 h at 37°C. Cells were resuspended in ice-cold lysis buffer (20 mM HEPES, pH 7.4, 100 mM NaCl, 1 mM EDTA, 2 mM $MgCl_2$, 10 mM imidazole, pH 8, 1 mM dithiothreitol [DTT]) containing 28 µl of protease inhibitor cocktail (Sigma–Aldrich), lysed, and purified as above with Ni-NTA beads or glutathione-Sepharose using elution buffers for Ni-NTA (20 mM HEPES, pH 7.4, 100 mM NaCl, 1 mM EDTA, 2 mM $MgCl_2$, 250 mM imidazole, pH 8, 1 mM DTT) or glutathione-Sepharose (20 mM HEPES, pH 7.4, 100 mM NaCl, 1 mM EDTA, 2 mM $MgCl_2$, 10 mM imidazole, pH 8, 1 mM DTT, 20 mM reduced glutathione). GST, Irc6-His6 and His6-Irc6(1-213), but not Arf1-His6, were dialyzed overnight at 4°C in 20 mM HEPES (pH 7.4), 100 mM NaCl, 1 mM EDTA, 2 mM $MgCl_2$, 1 mM DTT, and 0.5 mM phenylmethylsulfonyl fluoride (PMSF), and were further purified using a Superdex S75/H30 column.

For large-scale purification, cells were resuspended in lysis buffer and lysed using a french press. Soluble proteins were collected after centrifugation at 50,000 × *g* for 30 min. The supernatant was applied to a Ni-NTA Superflow column (Qiagen) previously equilibrated with buffer A (25 mM Tris-HCl, pH 7.5, 150 mM NaCl, 5% glycerol, 2 mM $MgCl_2$, 30 mM imidazole). The column was washed with buffer A, and Irc6p was eluted with a gradient of imidazole in buffer A. The eluted protein pool was loaded onto a HiLoad 16/60 Superdex 200 gel filtration column (GE Healthcare, Uppsala, Sweden) equilibrated in GF buffer (25 mM Tris-HCl, pH 7.5, 150 mM NaCl, 5% glycerol, 2 mM $MgCl_2$). The gel filtration peak was pooled and concentrated using an Amicon Ultra Centrifugal Filter with a 30-kDa cutoff to a final concentration of 12 mg/ml.

Crystallization and structure determination

Crystallization was performed at the University of California at Los Angeles (UCLA) Crystallization Facility using a Mosquito-TTP nanoliter dispenser. Crystals of native Irc6p and its seleno-methionine variant were obtained at 20°C using the hanging-drop vapor-diffusion technique by mixing equal volumes of protein (12 mg/ml) and reservoir solutions (0.2 M ammonium sulfate, 0.1 M MES, pH 6.5, 30% [wt/vol] polyethylene glycol [PEG] monomethyl ether 5000 or 0.2 M ammonium nitrate, pH 6.3, 20% [wt/vol] PEG 3350). Irc6p crystals belonged to the space group $P6_5$, with the following unit-cell parameters: $a = b = 61.6$; $c = 95.1$ Å; one molecule in the asymmetric unit; and an estimated solvent content of ~40.6%. Crystals of native Irc6p diffracted to 1.8 Å, and crystals of SeMet-Irc6p diffracted to 2.3 Å resolution.

Prior to data collection, crystals were frozen in a cryoprotectant consisting of 0.2 M ammonium nitrate (pH 6.3), 20% (wt/vol) PEG 3350, and 25% glycerol.

Data sets were collected at the Advanced Photon Source (Chicago, IL) at beamline 24ID-C. Both native and derivative data sets were processed using the programs Denzo and Scalepack from the HKL program suite (Otwinowski and Minor, 1997). Initial single wavelength anomalous dispersion (SAD) phases were calculated with the SHELXC/D/E and HKL2MAP program suite (Pape and Schneider, 2004; Sheldrick, 2010). Data collection and processing statistics are listed in Table 1. Density modification was performed using the DM program from the CCP4 package. Diffraction data from 27.3 to 1.8 Å were used for refinement and electron density map calculations. Graphic operations and model building were performed with ARP/wARP and COOT (Emsley and Cowtan, 2004; Langer *et al.*, 2008). For refinement and map calculations, REFMAC was used (Emsley and Cowtan, 2004; Vagin *et al.*, 2004). An overall quality factor of 99.4% was obtained using the program Errat2 (Colovos and Yeates, 1993). All structure figures were prepared using PyMOL (DeLano Scientific, San Carlos, CA). The coordinates and structure factors have been submitted to the PDB (www.rcsb.org) with the accession code 3uc9.

GTP-binding assays

The nucleotide-binding assay was performed using the rapid filtration methods described by Randazzo *et al.* (1995). Reactions were carried out in 50 µl of 25 mM HEPES (pH 7.4), 100 mM NaCl, 1 mM EDTA, 0.5 mM $MgCl_2$, 1 mM DTT, 0.1% (wt/vol) sodium cholate, and 3 mM DMPC containing 500 nM of protein and varying concentrations of [^{35}S]GTPγS (~5000 cpm/pmol; Perkin Elmer-Cetus, Boston, MA) for 2 h at 30°C. Reactions were stopped by addition of 2 ml of ice-cold TNMD buffer (25 mM Tris, pH 7.4, 100 mM NaCl, 10 mM $MgCl_2$, 1 mM DTT) and passed through BA85 filters (Millipore, Billerica, MA) using a vacuum manifold. Filters were washed with ice-cold TNMD and dried, and radioactivity was determined by scintillation counting. For cross-linking, 1 µg purified protein was incubated with 25 µCi of [^{35}S]GTPγS (Perkin Elmer-Cetus) in 50 µl reaction buffer (50 mM Tris-HCl, pH 7.5, 150 mM NaCl, 0.1% Triton X-100, 0.2 mM EDTA, 10 mM $MgCl_2$, 1 mM DTT, 10 µg/ml bovine serum albumin) in a 96-well plate placed on ice. A handheld UV lamp was placed directly on the 96-well plate, and samples were irradiated for 30 min at 254 nm. Samples were analyzed by SDS–PAGE and autoradiography.

Protein interaction studies

For obtaining whole-cell lysates (WCL), cells were converted to spheroplasts, resuspended in buffer Y (50 mM HEPES, pH 6.9, 100 mM NaCl, 1 mM $CaCl_2$, 2 mM $MgCl_2$, 2% glycerol, 0.8% n-octyl-β-D-glucopyranoside) containing protease inhibitor cocktail (Sigma-Aldrich), and lysed by agitation with glass beads. Lysates were subjected to centrifugation at 4°C for 25 min at 20,000 × *g*.

For affinity-binding studies, WCL corresponding to lysate from (5–15) × 10^9 cells was incubated with bait proteins bound to GST-Sepharose or anti-FLAG M2 affinity agarose (Sigma-Aldrich) for 1 h at 4°C. In coimmunoprecipitation experiments, WCL from wild-type cells or cells expressing FLAG-tagged Irc6p from the genomic locus were incubated with FLAG-affinity beads for 1 h at 4°C. Samples were washed in buffer Y and analyzed as in Fernandez and Payne (2006). For direct interaction tests between Ypt31p and Irc6p, purified GST or GST-Ypt31p bound to glutathione beads (10 µg) were incubated with 1 mM GDP or 1 mM GMPPNP for 30 min at room temperature. After separate preloading, FLAG-Irc6p or FLAG-Irc6p-K22A (20 µg) was added to the GST/GST-Ypt31p samples as indicated in Figure 5C. Protein-binding reactions were placed on a rotator and incubated for 30 min at 4°C. Samples were washed and analyzed using SDS–PAGE and Coomassie Blue staining.

Limited proteolysis

Irc6p was treated with chymotrypsin in 20 µl reactions containing 2.5 µg of purified Irc6p and 40 ng of protease in digest buffer (100 mM Tris-HCl, pH8, 10 mM $CaCl_2$) at 24°C. Proteolysis was stopped at different time points by adding 5 mM PMSF, and proteins were analyzed by SDS–PAGE and staining with Coomassie Blue.

ACKNOWLEDGMENTS

We thank Nava Segev, Peter Novick, and Manfred Schmitt for plasmids, strains, and antibodies; James Wohlschlegel and Ajay Vashisht for mass spectrometry; Michael Kim for technical assistance; and Michael Sawaya and Arthur Laganowsky for helpful discussions. We also thank the UCLA–U.S. Department of Energy (U.S. DOE) X-ray Crystallography Core Facility (supported by DOE grant DE-FC02-02ER63421) and the assistance team at Advanced Photon Source (APS) beamline ID24-C. Use of the APS is supported by the U.S. DOE under contract number DE-AC02-06CH11357. This work was supported by a Leopoldina Fellowship (BMBF LPD 9901/8-167) to S.G. and a National Institutes of Health grant (GM39040) to G.S.P.

REFERENCES

Alvaro D, Lisby M, Rothstein R (2007). Genome-wide analysis of Rad52 foci reveals diverse mechanisms impacting recombination. PLoS Genet 3, e228.

Benli M, Doring F, Robinson DG, Yang X, Gallwitz D (1996). Two GTPase isoforms, Ypt31p and Ypt32p, are essential for Golgi function in yeast. EMBO J 15, 6460–6475.

Bensen ES, Costaguta G, Payne GS (2000). Synthetic genetic interactions with temperature-sensitive clathrin in *Saccharomyces cerevisiae*. Roles for synaptojanin-like Inp53p and dynamin-related Vps1p in clathrin-dependent protein sorting at the *trans*-Golgi network. Genetics 154, 83–97.

Bensen ES, Yeung BG, Payne GS (2001). Ric1p and the ypt6p GTPase function in a common pathway required for localization of *trans*-Golgi network membrane proteins. Mol Biol Cell 12, 13–26.

Borlido J, Zecchini V, Mills IG (2009). Nuclear trafficking and functions of endocytic proteins implicated in oncogenesis. Traffic 10, 1209–1220.

Bourne HR, Sanders DA, McCormick F (1991). The GTPase superfamily: conserved structure and molecular mechanism. Nature 349, 117–127.

Carroll SY, Stirling PC, Stimpson HE, Giesselmann E, Schmitt MJ, Drubin DG (2009). A yeast killer toxin screen provides insights into a/b toxin entry, trafficking, and killing mechanisms. Dev Cell 17, 552–560.

Chen SH, Chen S, Tokarev AA, Liu F, Jedd G, Segev N (2005). Ypt31/32 GTPases and their novel F-box effector protein Rcy1 regulate protein recycling. Mol Biol Cell 16, 178–192.

Chen SH, Shah AH, Segev N (2011). Ypt31/32 GTPases and their F-Box effector Rcy1 regulate ubiquitination of recycling proteins. Cell Logist 1, 21–31.

Click ES, Stearns T, Botstein D (2002). Systematic structure-function analysis of the small GTPase Arf1 in yeast. Mol Biol Cell 13, 1652–1664.

Colovos C, Yeates TO (1993). Verification of protein structures: patterns of nonbonded atomic interactions. Protein Sci 2, 1511–1519.

Copic A, Starr TL, Schekman R (2007). Ent3p and Ent5p exhibit cargo-specific functions in trafficking proteins between the *trans*-Golgi network and the endosomes in yeast. Mol Biol Cell 18, 1803–1815.

Costaguta G, Stefan CJ, Bensen ES, Emr SD, Payne GS (2001). Yeast Gga coat proteins function with clathrin in Golgi to endosome transport. Mol Biol Cell 12, 1885–1896.

Donaldson JG, Jackson CL (2011). ARF family G proteins and their regulators: roles in membrane transport, development and disease. Nat Rev Mol Cell Biol 12, 362–375.

Duncan MC, Ho DG, Huang J, Jung ME, Payne GS (2007). Composite synthetic lethal identification of novel membrane traffic inhibitors. Proc Natl Acad Sci USA 104, 6235–6240.

Edeling MA, Smith C, Owen D (2006). Life of a clathrin coat: insights from clathrin and AP structures. Nat Rev Mol Cell Biol 7, 32–44.

Emsley P, Cowtan K (2004). Coot: model-building tools for molecular graphics. Acta Crystallogr D Biol Crystallogr 60, 2126–2132.

Fernandez GE, Payne GS (2006). Laa1p, a conserved AP-1 accessory protein important for AP-1 localization in yeast. Mol Biol Cell 17, 3304–3317.

Furuta N, Fujimura-Kamada K, Saito K, Yamamoto T, Tanaka K (2007). Endocytic recycling in yeast is regulated by putative phospholipid translocases and the Ypt31p/32p-Rcy1p pathway. Mol Biol Cell 18, 295–312.

Holm L, Rosenstrom P (2010). Dali server: conservation mapping in 3D. Nucleic Acids Res 38, W545–W549.

Hutagalung AH, Novick PJ (2011). Role of Rab GTPases in membrane traffic and cell physiology. Physiol Rev 91, 119–149.

Ito T, Chiba T, Ozawa R, Yoshida M, Hattori M, Sakaki Y (2001). A comprehensive two-hybrid analysis to explore the yeast protein interactome. Proc Natl Acad Sci USA 98, 4569–4574.

Jedd G, Mulholland J, Segev N (1997). Two new Ypt GTPases are required for exit from the yeast *trans*-Golgi compartment. J Cell Biol 137, 563–580.

Kelley LA, Sternberg MJ (2009). Protein structure prediction on the Web: a case study using the Phyre server. Nat Protoc 4, 363–371.

Kiefer F, Arnold K, Kunzli M, Bordoli L, Schwede T (2009). The SWISS-MODEL Repository and associated resources. Nucleic Acids Res 37, D387–D392.

Kirchhausen T (2000). Three ways to make a vesicle. Nat Rev Mol Cell Biol 1, 187–198.

Lambert C, Leonard N, De Bolle X, Depiereux E (2002). ESyPred3D: prediction of proteins 3D structures. Bioinformatics 18, 1250–1256.

Langer G, Cohen SX, Lamzin VS, Perrakis A (2008). Automated macromolecular model building for X-ray crystallography using ARP/wARP version 7. Nat Protoc 3, 1171–1179.

Li A, Liu Z, Li Q, Yu L, Wang D, Deng X (2008). Construction and characterization of bidirectional expression vectors in *Saccharomyces cerevisiae*. FEMS Yeast Res 8, 6–9.

Longtine MS, McKenzie A, Demarini DJ, Shah NG, Wach A, Brachat A, Philippsen P, Pringle JR (1998). Additional modules for versatile and economical PCR-based gene deletion and modification in *Saccharomyces cerevisiae*. Yeast 14, 953–961.

Luo R, Akpan IO, Hayashi R, Sramko M, Barr V, Shiba Y, Randazzo PA (2012). GTP-binding protein–like domain of AGAP1 is protein binding site that allosterically regulates ArfGAP protein catalytic activity. J Biol Chem 287, 17176–17185.

Marchler-Bauer A *et al*. (2011). CDD: a Conserved Domain Database for the functional annotation of proteins. Nucleic Acids Res 39, D225–D229.

McMahon HT, Boucrot E (2011). Molecular mechanism and physiological functions of clathrin-mediated endocytosis. Nat Rev Mol Cell Biol 12, 517–533.

Novick P, Field C, Schekman R (1980). Identification of 23 complementation groups required for post-translational events in the yeast secretory pathway. Cell 21, 205–215.

Ortiz D, Medkova M, Walch-Solimena C, Novick P (2002). Ypt32 recruits the Sec4p guanine nucleotide exchange factor, Sec2p, to secretory vesicles; evidence for a Rab cascade in yeast. J Cell Biol 157, 1005–1015.

Otwinowski Z, Minor W (1997). Processing of X-ray diffraction data collected in oscillation mode. Methods Enzymol 276, 307–326.

Page LJ, Sowerby PJ, Lui WW, Robinson MS (1999). γ-synergin: an EH domain-containing protein that interacts with γ-adaptin. J Cell Biol 146, 993–1004.

Panic B, Perisic O, Veprintsev DB, Williams RL, Munro S (2003). Structural basis for Arl1-dependent targeting of homodimeric GRIP domains to the Golgi apparatus. Mol Cell 12, 863–874.

Pape T, Schneider TR (2004). HKL2MAP: a graphical user interface for macromolecular phasing with SHELX programs. J Appl Crystallogr 37, 843–844.

Payne GS, Schekman R (1989). Clathrin—a role in the intracellular retention of a Golgi membrane protein. Science 245, 1358–1365.

Phan HL, Finlay JA, Chu DS, Tan PK, Kirchhausen T, Payne GS (1994). The Saccharomyces cerevisiae APS1 gene encodes a homolog of the small subunit of the mammalian clathrin AP-1 complex: evidence for functional interaction with clathrin at the Golgi complex. EMBO J 13, 1706–1717.

Rad MR, Phan HL, Kirchrath L, Tan PK, Kirchhausen T, Hollenberg CP, Payne GS (1995). *Saccharomyces cerevisiae* Apl2p, a homologue of the mammalian clathrin AP β subunit, plays a role in clathrin-dependent Golgi functions. J Cell Sci 108, 1605–1615.

Randazzo PA, Weiss O, Kahn RA (1995). Preparation of recombinant ADP-ribosylation factor. Methods Enzymol 257, 128–135.

Rao ST, Rossmann MG (1973). Comparison of super-secondary structures in proteins. J Mol Biol 76, 241–256.

Robinson MS (2004). Adaptable adaptors for coated vesicles. Trends Cell Biol 14, 167–174.

Sciorra VA, Audhya A, Parsons AB, Segev N, Boone C, Emr SD (2005). Synthetic genetic array analysis of the PtdIns 4-kinase Pik1p identifies components in a Golgi-specific Ypt31/rab-GTPase signaling pathway. Mol Biol Cell 16, 776–793.

Seeger M, Payne GS (1992). Selective and immediate effects of clathrin heavy chain mutations on Golgi membrane protein retention in *Saccharomyces cerevisiae*. J Cell Biol 118, 531–540.

Segev N (2011). Coordination of intracellular transport steps by GTPases. Semin Cell Dev Biol 22, 33–38.

Sheldrick GM (2010). Experimental phasing with SHELXC/D/E: combining chain tracing with density modification. Acta Crystallogr D Biol Crystallogr 66, 479–485.

Sikorski RS, Hieter P (1989). A system of shuttle vectors and yeast host strains designed for efficient manipulation of DNA in *Saccharomyces cerevisiae*. Genetics 122, 19–27.

Stenmark H (2009). Rab GTPases as coordinators of vesicle traffic. Nat Rev Mol Cell Biol 10, 513–525.

Traub LM (2005). Common principles in clathrin-mediated sorting at the Golgi and the plasma membrane. Biochim Biophys Acta 1744, 415–437.

Vagin AA, Steiner RS, Lebedev AA, Potterton L, McNicholas S, Long F, Murshudov GN (2004). REFMAC5 dictionary: organisation of prior chemical knowledge and guidelines for its use. Acta Crystallogr D Biol Crystallogr 60, 2284–2295.

Valdivia RH, Baggott D, Chuang JS, Schekman RW (2002). The yeast clathrin adaptor protein complex 1 is required for the efficient retention of a subset of late Golgi membrane proteins. Dev Cell 2, 283–294.

Wagner P, Molenaar CM, Rauh AJ, Brokel R, Schmitt HD, Gallwitz D (1987). Biochemical properties of the ras-related YPT protein in yeast: a mutational analysis. EMBO J 6, 2373–2379.

Wittinghofer A, Vetter IR (2011). Structure-function relationships of the G domain, a canonical switch motif. Annu Rev Biochem 80, 943–971.

Yeung BG, Phan HL, Payne GS (1999). Adaptor complex-independent clathrin function in yeast. Mol Biol Cell 10, 3643–3659.

Yu H *et al.* (2008). High-quality binary protein interaction map of the yeast interactome network. Science 322, 104–110.

Zhang W, Durocher D (2010). De novo telomere formation is suppressed by the Mec1-dependent inhibition of Cdc13 accumulation at DNA breaks. Genes Dev 24, 502–515.

Gorynia et al., Figure S1

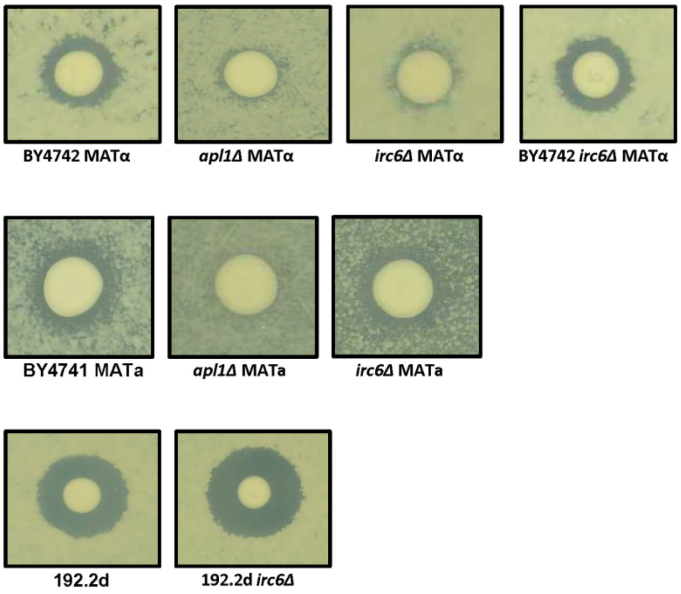

Figure S1. Irc6p does not function in AP-2-dependent endocytosis. Highly concentrated K28-producing MS300 cells were spotted onto indicated strains spread on low pH media. Cells were grown for 2-3 days at 24°C. Top row: *MAT*α parent of gene deletion collection (BY4742 *MAT*α), BY4742 *apl1*Δ (*apl1*Δ *MAT*α), *irc6*Δ*:: KanMX4* from BY4742 deletion collection (*irc6*Δ *MAT*α), *irc6*Δ*::URA3* generated for this study in BY4742 (BY4742 *irc6*Δ *MAT*α; GPY5042); Middle row: *MAT***a** parent of gene deletion collection (BY4741 *MAT***a**), BY4741 *apl1*Δ (*apl1*Δ *MAT***a**), BY4741 *irc6*Δ (*irc6*Δ *MAT***a**). Bottom row: K28-hypersensitive strain 192.2 and *irc6*Δ*::URA3* generated in 192.2 for this study (192.2 *irc6*Δ; GPY5019).

Gorynia et al., Figure S2

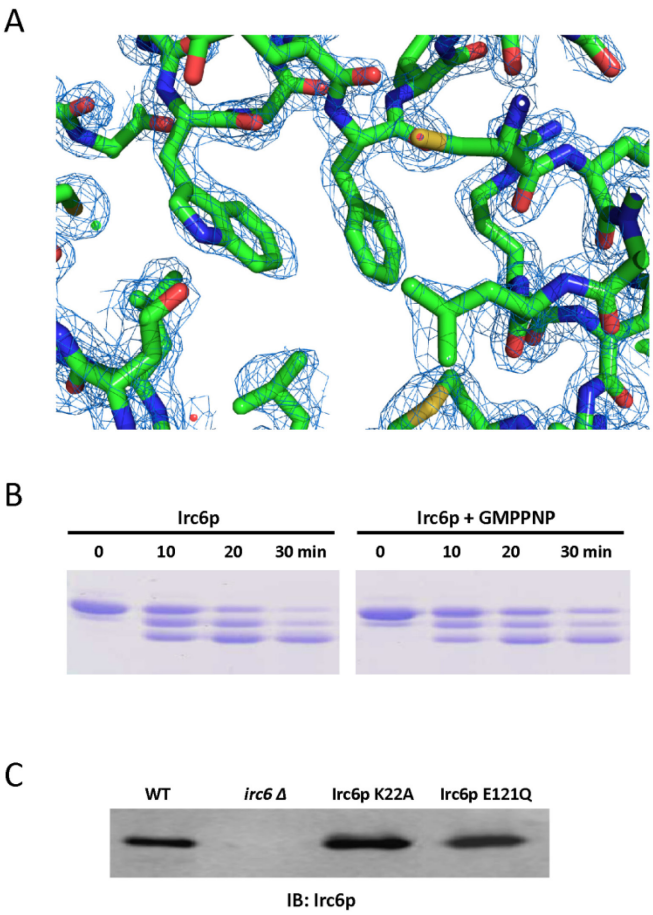

Figure S2. Irc6p contains a novel G-like domain. (**A**) Representative 2Fo-Fc electron density map around residue Phe71, superimposed with the final model of the Irc6p structure. **(B)** Binding of GMPPNP partially stabilizes Irc6p. Irc6p was incubated with chymotrypsin in the presence or absence of 1mM GMPPNP at 24°C. Reactions were stopped with PMSF at indicated time points, and the proteins were analyzed by SDS-PAGE and stained with Coomassie blue. **(C)** GTP-binding mutants of Irc6p are expressed at wild-type levels from the genomic locus. The indicated strains [SEY6210 (wt), GPY4042 (*irc6*Δ), GPY4990 (Irc6 K22A) and GPY4991 (Irc6 E121Q)] were grown overnight in YPD and lysates were prepared from 0.4 OD600 cells. Proteins were analyzed by SDS-PAGE and immunoblotting using anti-Irc6p antibody.

Gorynia et al., Figure S3

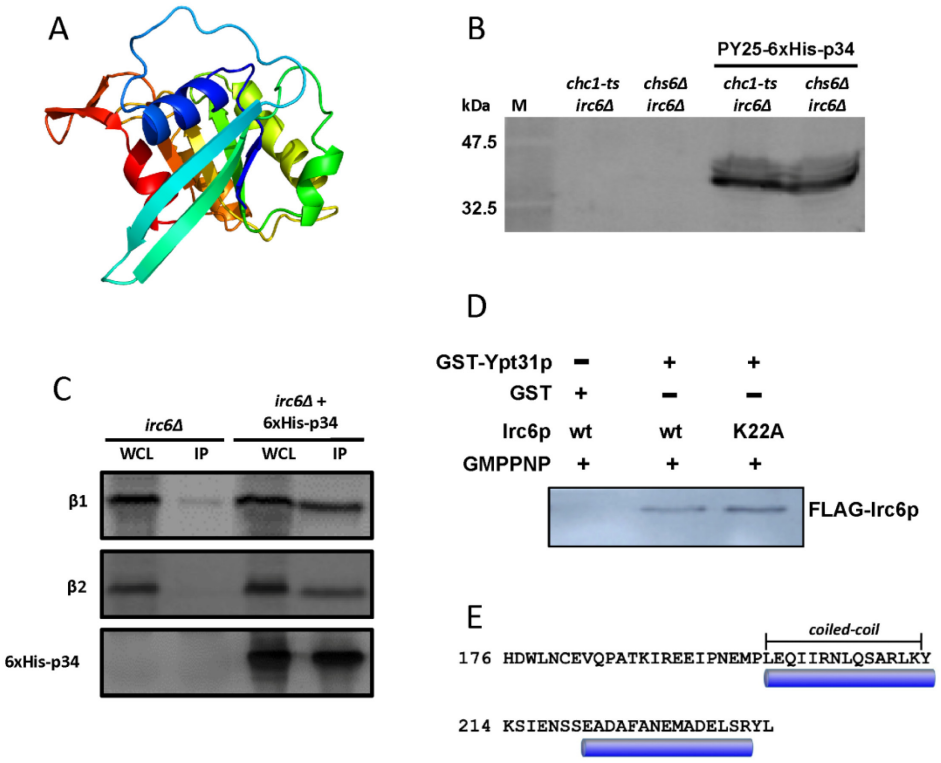

Figure S3. Mammalian p34 has a predicted N-terminal Rossmann-fold domain, can be expressed in yeast and binds yeast AP-1 and AP-2. (**A**) Predicted 3D structure of p34 derived from modeling program SwissModel. (**B**) *chc1-ts irc6*Δ (GPY3986) and *chs6 irc6*Δ (GPY4042) cells with or without the PY25 multi-copy plasmid expressing 6xHis-tagged p34. Cells were grown overnight at room temperature and lysates prepared from 0.2 OD600 cells. Lysates were analyzed by SDS-PAGE and immunoblotting using antibody against the 6xHis tag. **(C)** *irc6*Δ cells with (GPY5041) or without 6xHis-tagged p34 (GPY4986) were lysed under non-denaturing conditions and subjected to co-immunoprecipitation with antibody against the His tag. Proteins were separated by SDS–PAGE and analyzed by immunoblotting for the indicated proteins and 6xHis (6xHis-p34). WCL: whole cell lysate; IP: immunoprecipitate. **(D)** Samples from the experiment in Fig. 5, lanes 7,9, 10 were immunblotted with FLAG antibody to detect FLAG-Irc6p. **(E)** Predicted secondary structure elements in the C-terminal region of Irc6p identified by the Jpred3 server (www.compbio.dundee.ac.uk/www-jpred/). Cylinders indicate sequences with high probability for α-helical structure.

Table S1. P-loop NTPase/adaptin-binding family

Species	Accession number	BC-YY motif
Rattus norvegicus	NP_599225.1	IDNKYY
Arabidopsis thaliana	AAM62618.1	INTKYY
Arabidopsis thaliana	BAB10401.1	INTKYY
Arabidopsis thaliana	NP_569023.1	INTKYY
Oryza sativa Japonica Group	NP_001053672.1	IDTKYY
Homo sapiens	CAG38571.1	IDNKYY
Yarrowia lipolytica	XP_505351.1	IKNKYY
Danio rerio	NP_001002423.1	INNKYY
Danio rerio	CAK10803.1	INNKYY
Bos taurus	NP_001092366.1	IDNKYY
Picea sitchensis	ABK24427.1	IDTKYY
Monodelphis domestica	XP_001367559.1	IDNKYY
Monodelphis domestica	XP_001367516.1	IDNKYY
Vitis vinifera	XP_002276437.1	INTKYY
Chlamydomonas reinhardtii	XP_001696353.1	IETKYY
Physcomitrella patens	XP_001757130.1	IDTKYY
Lotus japonicus	BAF98215.1	INNKYY
Zea mays	NP_001141046.1	IETKYY
Oryza sativa Indica	EEC77867.1	IDTKYY
Populus trichocarpa	XP_002302663.1	IDTKYY
Ricinus communis	XP_002532474.1	INTKYY
Ricinus communis	XP_002526833.1	INTKYY
Sorghum bicolor	XP_002446995.1	IQTKYY
Glycine max	NP_001242087.1	INNKYY
Polysphondylium pallidum	EFA84588.1	IDTKYY
Arabidopsis lyrata	XP_002866782.1	INTKYY
Selaginella moellendorffii	XP_002984363.1	IDTKYY
Selaginella moellendorffii	XP_002972786.1	IDTKYY
Chlorella variabilis	EFN54966.1	LDNKYY
Hordeum vulgare	BAJ96675.1	IDTKYY
Anolis carolinensis	XP_003227299.1	IDNKYY
Dictyostelium fasciculatum	EGG15306.1	IDNKYY
Ornithorhynchus anatinus	XP_001516153.2	LDNKYY
Medicago truncatula	XP_003629096.1	INTKYY

Glycine max	XP_003534231.1	INNKYY
Brachypodium distachyon	XP_003580398.1	IDTKYY
Ectocarpus siliculosus	CBJ28531.1	- - - - - -
Mycosphaerella graminicola IPO323	EGP90334.1	- - - - - -

Table S2. Strains used in this study

Strain	Genotype	Source
SEY6210	*MATalpha ura3-52 leu2-3,112 his3-Δ200 trp1-Δ901 lys2-801 suc2-Δ9*	(Robinson et al., 1988)
GPY404	*MATa ura3-52 leu2-3,112 his3-Δ200 trp1-Δ901 lys2-801 suc2-Δ9*	(Yeung et al., 1999)
GPY1064	*MATalpha ura3-52 leu2-3,112 his3- Δ200 trp1- Δ901 lys2-801 suc2-Δ9 chc1-521::URA3*	(Bensen et al., 2000)
GPY1783-21D	*MATalpha ura3-52 leu2-3 his3-Δ200 trp1-Δ901 suc2-Δ9 apl1Δ::LEU2*	(Yeung et al., 1999)
GPY3102	*MATa ura3-52, leu2-3,112 his3- Δ200 trp1- Δ901 lys2-801 suc2-Δ9 chs6Δ::HIS3*	This study
GPY3103	*MATalpha ura3-52 leu2-3,112 his3-Δ200 trp1-Δ901 lys2-801 suc2-Δ9 chs6Δ::HIS3 apl2Δ::TRP1*	This study
GPY3986	*MATalpha ura3-52 leu2-3,112 his3-Δ200 trp1-Δ901 lys2-801 suc2-Δ9 irc6Δ::HIS3MX6 chc1-521*	This study
GPY4042	*MATalpha ura3-52 leu2-3,112 his3-Δ200 trp1-Δ901 lys2-801 suc2-Δ9 irc6Δ::HIS3MX6 chs6Δ::HIS3MX6*	This study
GPY4136	*MATalpha ura3-52 leu2-3,112 his3-Δ200 trp1-Δ901 lys2-801 suc2-Δ9 irc6Δ::HIS3MX6*	This study
GPY4603	*MATalpha ura3-52 leu2-3,112 his3-Δ200 trp1-Δ901 lys2-801 suc2-Δ9 irc6Δ::HIS3MX6 apl2Δ::TRP1 chs6Δ::HIS3MX6*	This study
GPY4971-1A	*MATalpha ura3-52 lys2-801 his3-Δ200 ypt31Δ::HIS3 ypt32-A141D(ts)*	This study
GPY4972-4D	*MATalpha ura3-52 lys2-801his3-Δ200 leu2-3,112 ypt31Δ::HIS3 irc6Δ::URA3*	This study
GPY4972-6D	*MATalpha ura3-52 lys2-801 his3-Δ200 leu2-3,112 ypt31Δ::HIS3 ypt32-A141D(ts)*	This study
GPY4972-7D	*MATa ura3-52 lys2-801 his3-Δ200 leu2-3,112 ypt31Δ::HIS3 ypt32-A141D(ts) irc6Δ::URA3*	This study
GPY4985-6A	*MATa ura3-52 lys2-801 his3-Δ200 trp1Δ901 leu2-3,112 ypt31Δ::HIS3 irc6Δ::URA3 chs6Δ::HIS3*	This study
GPY4985-8B	*MATa ura3-52 lys2-801 his3-Δ200 trp1Δ901 leu2-3,112 ypt31Δ::HIS3 ypt32-A141D(ts) irc6Δ::URA3 chs6Δ::HIS3*	This study
GPY4985-44A	*MATalpha ura3-52 lys2-801 his3-Δ200 trp1Δ901 leu2-3,112 irc6Δ::URA3 chs6Δ::HIS3*	This study
GPY4985-51C	*MATa ura3-52 lys2-801 trp1Δ901 leu2-3,112 ypt31Δ::HIS3 ypt32-A141D(ts) chs6Δ::HIS3*	This study
GPY4985-79D	*MATalpha ura3-52 lys2-801 his3-Δ200 trp1Δ901 leu2-3,112 ypt31Δ::HIS3 chs6Δ::HIS3*	This study
GPY4986	*MATa ura3-52 leu2-3,112 his3-Δ200 trp1-Δ901 lys2-801 suc2- Δ9 irc6Δ::URA3*	This study
GPY4987	*MATalpha ura3-52 leu2-3,112 his3-Δ200 trp1-Δ901 lys2-801 suc2-Δ9 irc6ΔC::TRP1*	This study
GPY4988	*MATa ura3-52 leu2-3,112 his3-Δ200 trp1-Δ901 lys2-801 suc2-Δ9 chc1-521::URA3 irc6-K22A*	This study
GPY4989	*MATa ura3-52 leu2-3,112 his3-Δ200 trp1-Δ901 lys2-801 suc2-Δ9 chc1-521::URA3 irc6-E121Q*	This study

GPY4990	*MATalpha ura3-52 leu2-3,112 his3-Δ200 trp1-Δ901 lys2-801 suc2-Δ9 chs6Δ::HIS3 irc6-K22A*	This study
GPY4991	*MATa ura3-52 leu2-3,112 his3-Δ200 trp1-Δ901 lys2-801 suc2-Δ9 chs6Δ::HIS3 irc6-E121Q*	This study
GPY4992	*MATalpha ura3-52 leu2-3,112 his3- Δ200 trp1- Δ901 lys2-801 suc2-Δ9 chc1-521::URA3 irc6ΔC::TRP1*	This study
GPY4993	*MATalpha ura3-52 leu2-3,112 his3-Δ200 trp1-Δ901 lys2-801 suc2-Δ9 chs6Δ::HIS3 irc6ΔC::TRP1*	This study
GPY4994	*MATalpha ura3-52 irc6Δ::URA3 sec4-8*	This study
GPY5008	GPY3986 + pFLAG-Irc6p	This study
GPY5009	GPY4042 + pFLAG-Irc6p	This study
GPY5010	GPY3986 + PY25-p34	This study
GPY5011	GPY4042 + PY25-p34	This study
GPY5012	GPY3986 + PY25	This study
GPY5013	GPY4042 + PY25	This study
GPY5014	GPY4042 + PY25-p34 CT	This study
GPY5015	GPY4042 + PY25-Irc6p CT	This study
GPY5016	GPY4042 + PY25-p34ΔC	This study
GPY5017	GPY3986 + PY25-Irc6p CT	This study
GPY5019	*MATalpha ura3-52 leu2-3,112 irc6Δ::URA3*	This study
GPY5026	GPY4042 + pFLAG-Irc6p Y49A Y50A	This study
GPY5028	GPY4042 + PY25-p34 Y49A Y50A	This study
GPY5041	GPY4986 + PY25-p34	This study
GPY5042	BY4742 *irc6Δ::URA3*	This study
BY4741	*MATa his3Δ1 leu2Δ0 ura3Δ0 met15Δ0*	(Brachmann et al., 1998)
BY4741 *apl1Δ*	*MATa his3Δ1 leu2Δ0 ura3Δ0 met15Δ0 apl1Δ::kanMX4*	(Winzeler et al., 1999)
BY4741 *irc6Δ*	*MATa his3Δ1 leu2Δ0 ura3Δ0 met15Δ0 irc6Δ::kanMX4*	(Winzeler et al., 1999)
BY4742	*MATalpha his3Δ1 leu2Δ0 ura3Δ0 met15Δ0*	(Brachmann et al., 1998)
BY4742 *apl1Δ*	*MATalpha his3Δ1 leu2Δ0 ura3Δ0 met15Δ0 apl1Δ::kanMX4*	(Winzeler et al., 1999)
BY4742 *irc6Δ*	*MATalpha his3Δ1 leu2Δ0 ura3Δ0 met15Δ0 irc6Δ::kanMX4*	(Winzeler et al., 1999)
MS300c	*MATalpha leu2-3,112 ura3-52 ski2-2* K28	(Schmitt and Tipper, 1992)
NSY348	*MATa ura3-52 lys2-801 his4-539 ypt31::HIS3 ypt32-A141D(ts)*	(Jedd et al., 1997)
NY28	*MATalpha ura3-52 sec4-8*	(Walch-Solimena et al., 1997)
192.2d	*MATalpha ura3-52 leu2-3,112*	(Schmitt et al., 1996)

Table S2 References

Bensen, E.S., Costaguta, G., and Payne, G.S. (2000). Synthetic genetic interactions with temperature-sensitive clathrin in Saccharomyces cerevisiae. Roles for synaptojanin-like Inp53p and dynamin-related Vps1p in clathrin-dependent protein sorting at the trans-Golgi network. Genetics *154*, 83-97.

Brachmann, C.B., Davies, A., Cost, G.J., Caputo, E., Li, J., Hieter, P., and Boeke, J.D. (1998). Designer deletion strains derived from Saccharomyces cerevisiae S288C: a useful set of strains and plasmids for PCR-mediated gene disruption and other applications. Yeast *14*, 115-132.

Jedd, G., Mulholland, J., and Segev, N. (1997). Two new Ypt GTPases are required for exit from the yeast trans-Golgi compartment. J. Cell Biol. *137*, 563-580.

Robinson, J.S., Klionsky, D.J., Banta, L.M., and Emr, S.D. (1988). Protein sorting in Saccharomyces cerevisiae: isolation of mutants defective in the delivery and processing of multiple vacuolar hydrolases. Mol.Cell Biol. *8*, 4936-4948.

Schmitt, M.J., Klavehn, P., Wang, J., Schonig, I., and Tipper, D.J. (1996). Cell cycle studies on the mode of action of yeast K28 killer toxin. Microbiology *142 (Pt 9)*, 2655-2662.

Schmitt, M.J., and Tipper, D.J. (1992). Genetic analysis of maintenance and expression of L and M double-stranded RNAs from yeast killer virus K28. Yeast *8*, 373-384.

Walch-Solimena, C., Collins, R.N., and Novick, P.J. (1997). Sec2p mediates nucleotide exchange on Sec4p and is involved in polarized delivery of post-Golgi vesicles. J. Cell Biol. *137*, 1495-1509.

Winzeler, E.A., Shoemaker, D.D., Astromoff, A., Liang, H., Anderson, K., Andre, B., Bangham, R., Benito, R., Boeke, J.D., Bussey, H., Chu, A.M., Connelly, C., Davis, K., Dietrich, F., Dow, S.W., El Bakkoury, M., Foury, F., Friend, S.H., Gentalen, E., Giaever, G., Hegemann, J.H., Jones, T., Laub, M., Liao, H., Liebundguth, N., Lockhart, D.J., Lucau-Danila, A., Lussier, M., M'Rabet, N., Menard, P., Mittmann, M., Pai, C., Rebischung, C., Revuelta, J.L., Riles, L., Roberts, C.J., Ross-MacDonald, P., Scherens, B., Snyder, M., Sookhai-Mahadeo, S., Storms, R.K., Veronneau, S., Voet, M., Volckaert, G., Ward, T.R., Wysocki, R., Yen, G.S., Yu, K., Zimmermann, K., Philippsen, P., Johnston, M., and Davis, R.W. (1999). Functional characterization of the S. cerevisiae genome by gene deletion and parallel analysis. Science *285*, 901-906.

Yeung, B.G., Phan, H.L., and Payne, G.S. (1999). Adaptor complex-independent clathrin function in yeast. Mol. Biol. Cell *10*, 3643-3659.

CHAPTER 6

Genome-Wide Analysis of AP-3-Dependent Protein Transport in Yeast

PERSONAL CONTRIBUTION

I contributed to the work described in Chapter 6 by conducting the experiments in Figure 3. Figure 3 provided an independent assay to test ALP traffic by the localization of GFP-ALP through fluorescence microscopy in cells that were also strained with a fluid-phase lipid marker FM4-64. A protocol was developed for these experiments so that simultaneous imaging of vacuole stained FM4-64 cells could be imaged in conjunction with steady-state GFP-ALP. These results , in part, validate the finding that β3 facilitates ALP transport to the vacuole, and that *yck3* performs a similar role, however to a lesser extent than β3. These results also confirm a role for *vac17* in vacuolar inheritance. These methods are described in the MATERIALS AND METHODS section.

Molecular Biology of the Cell
Vol. 20, 1592–1604, March 1, 2009

Genome-wide Analysis of AP-3–dependent Protein Transport in Yeast

Vikram C. Anand, Lydia Daboussi, Todd C. Lorenz, and Gregory S. Payne

Department of Biological Chemistry, David Geffen School of Medicine at UCLA, Los Angeles, CA 90095

Submitted August 8, 2008; Revised December 11, 2008; Accepted December 19, 2008
Monitoring Editor: Sandra Lemmon

The evolutionarily conserved adaptor protein-3 (AP-3) complex mediates cargo-selective transport to lysosomes and lysosome-related organelles. To identify proteins that function in AP-3–mediated transport, we performed a genome-wide screen in *Saccharomyces cerevisiae* for defects in the vacuolar maturation of alkaline phosphatase (ALP), a cargo of the AP-3 pathway. Forty-nine gene deletion strains were identified that accumulated precursor ALP, many with established defects in vacuolar protein transport. Maturation of a vacuolar membrane protein delivered via a separate, clathrin-dependent pathway, was affected in all strains except those with deletions of *YCK3*, encoding a vacuolar type I casein kinase; *SVP26*, encoding an endoplasmic reticulum (ER) export receptor for ALP; and AP-3 subunit genes. Subcellular fractionation and fluorescence microscopy revealed ALP transport defects in *yck3*Δ cells. Characterization of *svp26*Δ cells revealed a role for Svp26p in ER export of only a subset of type II membrane proteins. Finally, ALP maturation kinetics in *vac8*Δ and *vac17*Δ cells suggests that vacuole inheritance is important for rapid generation of proteolytically active vacuolar compartments in daughter cells. We propose that the cargo-selective nature of the AP-3 pathway in yeast is achieved by AP-3 and Yck3p functioning in concert with machinery shared by other vacuolar transport pathways.

INTRODUCTION

Subcellular compartmentalization by membrane-bounded organelles is a fundamental feature of eukaryotic cells. This organization allows for physical and functional segregation of subcellular processes. An important example of this compartmentalization is the lysosome, which is an acidic organelle that serves as a major site for protein degradation within eukaryotic cells. Degradative enzymes are sequestered within lysosomes ensuring that only material delivered to the organelle is subject to destruction.

Compartmentalization of lysosome functions necessitates transport pathways for lysosomal biogenesis, maintenance of function, and transfer of molecules targeted for turnover. Genetic analysis of proteins that are targeted to the lysosome-like vacuole of *Saccharomyces cerevisiae* has defined six such trafficking routes, each involving vesicle-mediated transport (Bryant and Boyd, 1993). Two of these pathways involve protein transport from the cytoplasm to the vacuole: the cytoplasm to vacuole transport pathway (CVT) and starvation-induced autophagy. A third pathway, the endocytic pathway, delivers cell surface and extracellular molecules to the vacuole. Yet another route provides for vacuole inheritance during cell division. The inheritance pathway directs vesicles derived from the maternal vacuole into the new bud where vesicle fusion seeds formation of a daughter cell vacuole. Finally, there are two vacuolar biosynthetic pathways that originate from the secretory pathway, one clathrin dependent and the other clathrin-independent. Newly synthesized vacuolar components destined for both pathways are transported from the endoplasmic reticulum (ER) to the Golgi complex. At the *trans*-Golgi network (TGN), the proteins enter into either the clathrin-dependent pathway that passes through endosomes to the vacuole or into a clathrin-independent pathway that proceeds directly to vacuole.

Clathrin-dependent transport between the TGN and endosomes relies on several evolutionarily conserved clathrin adaptors: monomeric GGA proteins and the heterotetrameric adaptor protein-1 (AP-1) complex (Bonifacino, 2004; Traub, 2005). These adaptors function as protein interaction platforms by binding to the coat protein clathrin and other coat-associated proteins, as well as recognizing sorting signals in the cytoplasmic domains of transmembrane cargo proteins. In this way, adaptors play central roles in vesicle formation by coupling cargo selection to assembly of a protein coat.

Most vacuolar proteins are transported through the clathrin-dependent pathway, including the soluble protease carboxypeptidase Y (CPY), the membrane protease carboxypeptidase S (CPS), and membrane components of the V-type H^+-ATPase responsible for acidifying the vacuole (Bowers and Stevens, 2005). This pathway flows through multivesicular endosomes, where membrane proteins destined for the lumen of the vacuole are sorted into luminal vesicles that are subsequently delivered to the vacuole. There is limited information on sorting signals for the clathrin-dependent pathway in yeast, in part because this pathway seems to act as a default route for membrane proteins lacking cytoplasmic sorting signals (Roberts *et al.*, 1992; Redding *et al.*, 1996).

The clathrin-independent pathway to the vacuole is distinguished by a requirement for the AP-3 adaptor complex, a four-subunit complex with homology to AP-1. AP-3 is evolutionarily conserved and consists of two large subunits, β3 and δ; a medium subunit μ3; and a small subunit σ3 (Odorizzi *et al.*, 1998). Only a few proteins that transit via the AP-3 pathway have been identified in yeast; among these

This article was published online ahead of print in *MBC in Press* (http://www.molbiolcell.org/cgi/doi/10.1091/mbc.E08–08–0819) on December 30, 2008.

Address correspondence to: Gregory S. Payne (gpayne@mednet.ucla.edu).

© 2009 by The American Society for Cell Biology

are alkaline phosphatase (ALP) (Cowles *et al.*, 1997a; Stepp *et al.*, 1997), the target membrane-soluble *N*-ethylmaleimide-sensitive factor attachment protein receptor (t-SNARE) Vam3p (Cowles *et al.*, 1997a), yeast casein kinase 3 (Yck3p) (Sun *et al.*, 2004), and the Niemann-Pick Type C homologue Ncr1p (Berger *et al.*, 2007). Each of these proteins is localized to the limiting vacuolar membrane rather than intravacuolar vesicles, suggesting that the AP-3 pathway bypasses multivesicular endosomes and functions as a selective and direct route from the TGN to the vacuolar membrane. Cargoes of the AP-3 pathway contain either acidic dileucine-like or YXXΦ (where Φ is a bulky hydrophobic amino acid and X is any amino acid) signals that are necessary for sorting into the pathway (Darsow *et al.*, 1998; Vowels and Payne, 1998a; Sun *et al.*, 2004).

Formation of AP-3 vesicles in yeast, unlike vesicles with AP-1 and GGA proteins, seems to be independent of clathrin. AP-3 does not strongly associate with clathrin, nor do mutations in clathrin alter the rate of ALP transport to the vacuole (Seeger and Payne, 1992; Vowels and Payne, 1998a; Yeung *et al.*, 1999). Only one other protein in yeast has been characterized with selective function in AP-3 vesicle formation in yeast, Vps41p. Vps41p is a member of the homotypic vacuole fusion and vacuole protein sorting (HOPS) complex (Nakamura *et al.*, 1997; Seals *et al.*, 2000; Wurmser *et al.*, 2000). The HOPS complex functions in tethering vesicles to the vacuole, and, in this capacity, it is necessary for delivery of both clathrin-dependent and AP-3–dependent cargo (Bowers and Stevens, 2005; Ostrowicz *et al.*, 2008). However, Vps41p also seems to play a selective role in AP-3 vesicle formation through an interaction with the AP-3 δ subunit (Rehling *et al.*, 1999; Darsow *et al.*, 2001). Vps41p has features similar to clathrin, but whether this protein is a structural component of the AP-3 coat remains unresolved (Conibear and Stevens, 1998; Ybe *et al.*, 1999).

Mammalian AP-3 also participates in protein transport to lysosomes (Robinson and Bonifacino, 2001; Di Pietro and Dell'Angelica, 2005). Much like the yeast adaptor, mammalian AP-3 seems to act in a pathway to the lysosomal limiting membrane that bypasses multivesicular late endosomes. However, in mammalian cells, AP-3 localizes predominantly at early endosomes instead of the Golgi (Peden *et al.*, 2004; Theos *et al.*, 2005), suggesting that AP-3 pathways in yeast and mammalian cells originate at distinct organelles. Another difference between yeast and mammalian AP-3 is that the mammalian adaptor binds clathrin (Dell'Angelica *et al.*, 1998), although the functional significance of this interaction has not been fully established (Newell-Litwa *et al.*, 2007).

In addition to a ubiquitous role in lysosomal protein traffic, mammalian AP-3 acts in cell type-specific pathways to specialized lysosome-related organelles such as melanosomes and platelet dense granules (Di Pietro and Dell'Angelica, 2005; Huizing *et al.*, 2008). Defects in transport to lysosomes and lysosome-related organelles caused by mutations in the AP-3 β subunit lead to the inherited human disease Hermansky–Pudlak syndrome (HPS) (Dell'Angelica *et al.*, 1999; Huizing *et al.*, 2002; Jung *et al.*, 2006), a disease characterized by oculocutaneous albinism and prolonged bleeding times (Di Pietro and Dell'Angelica, 2005; Huizing *et al.*, 2008). A disease similar to HPS is manifested in mice bearing mutations in AP-3 subunits (Di Pietro and Dell'Angelica, 2005; Newell-Litwa *et al.*, 2007; Huizing *et al.*, 2008).

Mutations in other genes also cause HPS and HPS-like diseases in both humans and mice, and the products of these genes have been associated with trafficking pathways to lysosomes and lysosome-related organelles (Di Pietro and Dell'Angelica, 2005; Huizing *et al.*, 2008). One such protein, Vps33a, is a component of the mammalian HOPS complex that also contains Vps41 (Suzuki *et al.*, 2003). Most of the other proteins do not seem to have homologues in yeast, although a recent report describes limited sequence homologies between HPS4 and the yeast Ccz1p protein involved in vacuolar protein transport (Hoffman-Sommer *et al.*, 2005). Thus, although not readily apparent by sequence conservation, there is the possibility that other HPS proteins will have functional analogues in yeast.

To more fully understand the mechanisms of transport through the AP-3 pathway and identify additional candidate disease genes, having a complete catalogue of genes/proteins involved in AP-3 pathway function would be advantageous. For this reason, we have carried out a systematic, genome-wide screen in yeast to identify genes involved in AP-3–dependent ALP transport to the vacuole. We identified a complement of genes that serve a variety of functions from processing enzymes, to vesicle budding, targeting, and vesicle fusion. Many of these genes have well established roles in protein transport through both the clathrin and AP-3 pathways. Only deletions in AP-3 subunit genes and *YCK3* selectively affected the AP-3 pathway. We also observed that the ER export receptor for ALP, Svp26p, is required for transport of a subset of type II membrane proteins. Finally, our results indicate that the vacuolar inheritance pathway is important for timely production of a proteolytically mature vacuole in newly budded cells.

MATERIALS AND METHODS

Yeast Media, Plasmids, and Strains

Yeast strains were grown in YPD (1% Bacto-yeast extract (Difco, Detroit, MI), 2% Bacto-peptone (Difco), 2% dextrose), YPD + 200 μg/ml G418, or SD (0.67% yeast nitrogen base [Difco], 2% dextrose) supplemented with 20 μg/ml L-histidine, uracil, and L-tryptophan, and 30 μg/ml L-leucine, adenine, and L-lysine. Solid media contained 2% agar. Yeast transformations were performed using the lithium acetate method (Ito *et al.*, 1983). Cell densities were measured by spectrophotometry. One OD_{600} corresponds to 10^7 cells per milliliter. Sequences of oligonucleotides used in this study are available on request.

Plasmids p*YCK3*, p*yck3-1*, and p*yck3-2* are described in Sun *et al.* (2004). *yck3-1* bears an in frame deletion of a portion of *YCK3* encoding Yck3pΔ409–462. *yck3-2* bears a substitution mutation changing amino acid 444 from tyrosine to histidine. pGFP-ALP is a multicopy plasmid encoding a fusion of GFP to the N terminus of full-length ALP (Cowles *et al.*, 1997a). pBS207, a low copy centromeric plasmid contains a fragment of chromosome XIV (coordinates 67948–78118) encoding full-length *MON2* (Jochum *et al.*, 2002).

Strains used in this study were obtained from the single gene deletion libraries constructed by the international deletion consortium (Winzeler *et al.*, 1999) constructed in BY4741 (*MAT***a** *ura3Δ0 leu2Δ0 his3Δ1 met15Δ0*) and BY4742 (*MATα ura3Δ0 leu2Δ0 his3Δ1 lys2Δ0*) (Brachmann *et al.*, 1998). Deletion of *SVP26* was performed by standard polymerase chain reaction (PCR)-based methods (Longtine *et al.*, 1998) to generate GPY4865 (*MAT***a** *ura3-52 his3Δ200 leu2-3 lys2-801 trp1Δ901 suc2Δ9 mel svp26Δ*::HIS3) in SEY6210 (Robinson *et al.*, 1988). *MAT***a** *cps1Δ pho8Δ* was generated by crossing *MATα pho8Δ* with *MAT***a** *cps1Δ* from the single gene deletion collections, sporulating, and dissecting the sporulated diploid to generate GPY4866.

Preparation of Cell Extracts from Single-Gene Deletion Libraries

The 96-well format *S. cerevisiae MAT***a** and *MATα* single gene deletion libraries were obtained from Open Biosystems (Huntsville, AL) and ResGen (now Invitrogen, Carlsbad, CA), respectively. Each plate of the 96-well format gene deletion libraries was replicated into a 96-well plate (Cole-Parmer Instrument, Vernon Hills, IL) containing 200 μl/well of YPD + 200 μg/ml G418. Cells were grown for 2 d at 30°C. Fifty microliters from each well was transferred to 2 ml of YPD in a 96-deep well plate (Matrix, Hudson, NH). Individual magnetic stir-bars (VP Scientific, San Diego, CA) were added and stirred continuously using a magnetic stir device (VP Scientific) for 5 h at 30°C. Cells were then sedimented by centrifugation at 1500 × *g* for 5 min. The supernatant was discarded, and 100 μl of cracking buffer (10% glycerol, 5% SDS, 2% β-mercaptoethanol, 50 mM Tris-Cl, pH 6.8, and 0.02% bromphenol blue) was added to each well then transferred to 96-well PCR plates (Thermo Fisher

Scientific, Waltham, MA). Plates were incubated at 99°C for 3 min, and samples were frozen at −80°C until further processing.

Immunoblotting ALP for Single-Gene Deletion Library Extracts

Five microliters of each lysed strain in cracking buffer was subjected to electrophoresis through a 10% SDS-polyacrylamide gel. Gels were transferred onto polyvinylidene difluoride (PVDF) membranes at 100 V for 60 min in 24 mM Tris base, 192 mM glycine, and 20% methanol buffer. Membranes were treated with blocking buffer (5% milk, 0.1% Tween 20 in phosphate-buffered saline [PBS; 137 mM NaCl, 2.7 mM KCl, 10 mM Na_2PO_4, 2 mM KH_2PO_4]) for 1 h and then incubated overnight at 4°C in a rabbit anti-Pho8p antibody (Seeger and Payne, 1992b) diluted in blocking buffer. Next, 25 μl/ml concentrated *cps1*Δ *pho8*Δ cell extract was added to antibody dilutions, and the mixture was preincubated for 30 min before incubation with PVDF membranes to reduce nonspecific signals. Bound rabbit antibodies were detected with goat anti-rabbit horseradish peroxidase conjugated antibody (Bio-Rad, Hercules, CA). 10 μL/ml *pho8*Δ extract was added to the secondary antibody dilution in blocking buffer and preincubated for 30 min. Membranes were washed in PBS and 0.1% Tween 20 and developed using ECL-Plus (GE Healthcare, Piscataway, NJ) according to the manufacturer's instructions. Digital images were acquired with a fluorescence imager (GE Healthcare).

To prepare concentrated *cps1*Δ *pho8*Δ extract, *MAT***a** *cps1*Δ *pho8*Δ cells were grown in YPD to 10 OD_{600}/ml, 2 l were harvested by centrifugation, and frozen in liquid nitrogen. The frozen cells were mechanically lysed in a blender, and the lysate was resuspended in 75 ml of 1% SDS and heated at 100°C for 5 min. The lysate was then clarified by centrifugation at 100,000 × *g* for 45 min at 4°C.

Cell Extract Preparation, Immunoblotting, and Immunoprecipitation for Analysis of Individual Strains

Three stationary overnight cultures in YPD from each mating type of a gene deletion strain were diluted to 0.125 OD_{600} in YPD and grown to 0.5–1 OD_{600}/ml, yielding six samples per deletion strain. Approximately 5 OD_{600} cells were harvested by centrifugation at 1500 × *g* for 3 min in 13- × 100-mm glass test tubes (Thermo Fisher Scientific). Lysates were prepared by mechanical disruption of the pellet by adding 50 μl of LSB (10% glycerol, 2% SDS, 2% β-mercaptoethanol, 50 mM Tris-Cl, pH 6.8, and 0.02% bromphenol blue) and 250 μl of 0.5-mm glass beads (Biospec, Bartlesville, OK) to the pellet and agitating with a Vortex mixer (Thermo Fisher Scientific). Lysates were resuspended in 400 μl of LSB and incubated at 100°C for 5 min. Immunoblots were performed as described above using rabbit anti-Pho8p, rabbit anti-Cps1p (generated using glutathione transferase fused to Cps1p amino acids [aa]46–576 as antigen), or rabbit anti-Gda1p (generated using 6 histidine-tagged Gda1p aa25–518). Pho8p and Cps1p antibodies and secondary antibodies were treated with concentrated *pho8*Δ *cps1*Δ extract as described above. Gda1p antibodies and secondary antibodies were treated with a concentrated *gda1*Δ cell extract prepared as described above for *pho8*Δ *cps1*Δ extract.

Radiolabeling and immunoprecipitations for ALP and CPS were performed as described in Seeger and Payne (1992b) and Costaguta *et al.* (2006).

Quantitation of Immunoblots and Immunoprecipitations

Digital images of immunoblots and immunoprecipitations were analyzed using ImageJ (http://rsb.info.nih.gov/ij/). Bands were quantified by measuring the total integrated density of a band after background subtraction. The precursor ALP (pALP) to total ALP (tALP) ratio represents the pALP band density divided by the sum of the pALP, mature ALP (mALP), and soluble ALP (sALP) band densities. A ratio of pALP/tALP was determined for each of the six samples per gene deletion strain. These six calculated ratios per strain were averaged together, and a standard deviation was calculated. Wild-type strains were also grown in sextuplicate and a pALP/tALP ratio, and standard deviation was determined. Two tailed *t* tests were performed for each deletion strain pALP/tALP ratio compared with the wild-type ratio. A strain was determined to display a processing defect if the deletion strain pALP/tALP was greater than wild-type, with $p < 0.05$. The pALP/tALP ratio for the deletion strain was then normalized to the wild-type ratio by dividing the deletion strain ratio by the wild-type ratio. The normalized pALP/tALP ratio is reported in Table 1.

Defects in CPS maturation were scored in a qualitative manner due to overlap between precursor and mature forms of the protein. Both pCPS and mCPS migrate as two differentially glycosylated forms. The lower molecular weight form of pCPS comigrates with the higher molecular weight form of mCPS—we term this the intermediate form. Thus, only the higher molecular weight precursor form can be used as a reliable diagnostic for maturation defects. Strains were scored as having no CPS maturation defect if a two band pattern corresponding to the intermediate and mature forms was detected. Strains were scored as having a severe defect if a two-band pattern was detected consisting of the higher-molecular-weight precursor and the intermediate-molecular-weight form, with little or no lower-molecular-weight mCPS. Strains were scored as having a moderate defect if three bands were detected—the higher-molecular-weight precursor form, the intermediate-molecular-weight form, and the lower-molecular-weight mature form.

Cell Lysis and Differential Centrifugation

Cell lysis and differential centrifugation was carried out as described in Yeung and Payne (2001), with the following modifications: 50 OD_{600} cells were harvested; cells were converted to spheroplasts with 0.05 U of Zymolyase (Seikagaku, Tokyo, Japan) per OD_{600} cells; and the lysis buffer was 200 mM sorbitol, 50 mM Tris, pH 6.8, 50 mM NaCl, 2 mM EDTA, and protease inhibitors.

N-[3-Triethylammoniumpropyl]-4-[p-diethylaminophenylhexatrienyl] Pyridinium Dibromide (FM4-64) Staining and Fluorescence Microscopy

The *MAT***a** wild-type strain BY4741 and *MAT***a** deletion strains *yck3*Δ, *apl6*Δ (*β3*Δ), and *vac17*Δ, all harboring pGFP-ALP were grown in liquid SD medium with appropriate supplements overnight to 0.2–0.4 OD_{600}/ml. Cells were harvested by centrifugation at 1500 × *g* for 3 min, the supernatant was decanted, and the cells resuspended in the residual liquid (200 μl). Cells were stained using 200 μM FM4-64 for 20 min, washed, and incubated for 60 min at room temperature as described in Vida and Emr (1995) and imaged using an Axioobserver Z1 1.0 spinning disk confocal microscope (Carl Zeiss, Oberkochen, Germany).

RESULTS

Genome-wide Screens for ALP Maturation Defects

To screen for AP-3 pathway defects, we monitored the proteolytic maturation of ALP. ALP, a type II membrane protein, is synthesized as a 74-kDa glycosylated zymogen (pALP) that is proteolytically processed upon delivery to the vacuole to yield a 72-kDa integral membrane mature form (mALP) and a 66-kDa soluble mature form (sALP) (Klionsky and Emr, 1989). In wild-type cells, virtually all ALP is present in the mature forms as a consequence of the rapid rate of pALP transport to the vacuole and proteolytic processing. In contrast, cells with defects in AP-3–mediated transport accumulate pALP, which is easily distinguished from the mature forms by SDS-polyacrylamide gel electrophoresis (PAGE) and immunoblotting (Lorenz *et al.*, 2007). Thus, as a systematic approach to identify genes involved in ALP trafficking, we used immunoblotting to assess pALP accumulation in the sets of haploid *MAT***a** and *MAT*α strains bearing single deletions of all nonessential genes.

Deletion strains were grown in 96-well plates to mid-logarithmic phase, and then lysates were prepared and analyzed by SDS-PAGE and immunoblotting with an ALP antibody. A strain with a partial ALP maturation defect (*yck3*Δ) was included in each 96-well plate for quality control to ensure reproducibility of the assay. Strains displaying pALP to ALP ratios significantly greater than wild-type strains, using *yck3*Δ as a general guide, were initially scored as positive. Examples of the data are presented in Figure 1, revealing pALP accumulation in *vac8*Δ, *yck3*Δ, and *apl6*Δ cells (Figure 1A, top, lane 4; and bottom, lanes 2 and 6).

Strains scored as positive in the initial screen were grown individually and retested for pALP accumulation by immunoblotting. In addition, we tested a few strains with deletions of vacuolar H^+-ATPase subunits that did not display ALP maturation defects in the genome-wide screens but that were expected to score positive because deletions of other subunits resulted in maturation defects. In total, 4848 single gene deletion strains in the *MAT***a** library and 4871 strains in the *MAT*α library were screened; 49 strains exhibited ALP maturation defects when retested (Table 1).

The specificity of the ALP maturation defect was assessed by analyzing in parallel the processing of ALP and another type II vacuolar membrane protein, CPS. CPS, like ALP, is synthesized in a precursor form that is proteolytically matured in the vacuole (Spormann *et al.*, 1992). However, CPS

Table 1. ALP maturation defects in strains from gene deletion libraries

Single gene deletion strain	Gene product function	ALP defect	CPS defect	Significance of ALP defect, p value
AP-3				
apl5Δ	δ Subunit of AP-3	3.1	—	<0.001
apl6Δ	β Subunit of AP-3	3.1	—	<0.001
apm3Δ	μ Subunit of AP-3	2.3	—	<0.001
aps3Δ	σ Subunit of AP-3	3.1	—	<0.001
Vesicle formation				
vps1Δ	Dynamin homologue	2.7	M	<0.001
arf1Δ	ARF GTPase, acts in vesicle coat assembly	2.3	M	<0.001
drs2Δ	Lipid flippase	3.2	M	<0.001
Vacuolar proteases				
pep4Δ	Vacuolar serine protease, activates other vacuolar proteases	7.2	S	<0.001
prb1Δ	Vacuolar serine protease	5.3	M	<0.001
HOPS/CORVET				
vps41Δ	HOPS subunit/AP-3 vesicle formation	6.3	S	<0.001
vam6Δ (vps39Δ)	HOPS subunit/Ypt7 guanine nucleotide exchange factor	6.5	S	<0.001
pep5Δ (vps11Δ)	HOPS/CORVET core subunit	7.2	S	<0.001
pep3Δ (vps18Δ)	HOPS/CORVET core subunit	7.4	S	<0.001
vps16Δ	HOPS/CORVET core subunit	7.5	S	<0.001
vps8Δ	CORVET subunit, interacts with Vps21p	2.3	M	<0.001
vps3Δ	CORVET subunit	3.8	S	<0.001
Rabs and vesicle targeting factors				
ypt7Δ	Rab GTPase for tethering/fusion to vacuole	5.6	S	<0.001
vps45Δ	Sec1/Munc-18 family, interacts with Pep12p	3.8	S	<0.01
vps21Δ	Rab GTPase for tethering/fusion to endosome	1.8	M	<0.001
vps9Δ	Vps21 guanine nucleotide exchange factor	3.6	S	<0.001
SNAREs and fusion				
vam3Δ	Vacuole membrane t-SNARE	6.2	S	<0.001
vam7Δ	Vacuole membrane t-SNARE	6.2	S	<0.001
pep12Δ	Endosome t-SNARE	4.6	S	<0.001
Vacuolar inheritance				
vac8Δ	Vacuolar membrane protein that binds Vac17p	3.4	M	<0.001
vac17Δ	Links Vac8p to the myosin, Myo2p	4.8	S	<0.001
Phosphatidylinositol synthesis				
fab1Δ	Phosphatidylinositol-3-phosphate 5-kinase	4.0	M	<0.01
vac14Δ	Activator of Fab1p	2.9	M	<0.001
vps15Δ	Protein kinase subunit of phosphatidylinositol 3 (PI3)-kinase complexes I and II	5.0	S	<0.001
vps34Δ	PI3-kinase	6.2	S	<0.001
vps30Δ	Subunit of PI3-kinase complexes I and II	2.9	M	<0.001
vps38Δ	Subunit of PI3-kinase complex I	3.2	M	<0.001
Retromer				
pep8Δ (vps26Δ)	Retromer subunit	1.7	M	<0.01
vps5Δ	Retromer subunit	1.6	M	=0.001
vps35Δ	Retromer subunit, cargo binding	2.3	M	<0.001
vps29Δ	Retromer subunit	2.4	M	<0.01
vps17Δ	Retromer subunit	1.4	M	=0.02
v-type H^+-A TPase				
tfp1Δ	Subunit A of V_1 domain	4.0	S	=0.02
vma2Δ[a]	Subunit B of V_1 domain	1.7	M	<0.01
vma5Δ[a]	Subunit C of V_1 domain	1.4	M	<0.001
vma8Δ[a]	Subunit D of V_1 domain	1.6	M	<0.001
vma7Δ	Subunit F of V_1 domain	3.2	S	<0.001
vma10Δ	Subunit G of V_1 domain	1.7	M	<0.05
vph1Δ	Subunit a of V_0 domain	3.3	M	<0.001
cup5Δ	Subunit c of V_0 domain	3.7	S	<0.001
ifp3Δ	Subunit c′ of V_0 domain	2.9	S	=0.1
ppa1Δ	Subunit c″ of V_0 domain	2.0	S	<0.05
vma6Δ	Subunit c‴ of V_0 domain	5.4	S	<0.05
vph2Δ	v-ATPase assembly	5.3	S	<0.01
vma22Δ	v-ATPase assembly	3.8	S	=0.01
Miscellaneous				
yck3Δ	Type I casein kinase involved in homotypic vacuole fusion	3.2	—	<0.001
svp26Δ	Adaptor for sorting ALP into COP-II vesicles at ER	4.2	—	<0.001
ccz1Δ	Acts in vesicle fusion to the vacuole in a complex with Mon1p	4.4	M	<0.001
mon1Δ	Acts in vesicle fusion to the vacuole in a complex with Ccz1p	4.4	M	<0.001

Three colonies from each mating type of a single-gene deletion strain were individually analyzed for ALP and CPS maturation defects by immunoblotting. Band densities for ALP were quantified and an average ratio of pALP to total ALP was determined for the six samples (see *Materials and Methods*). The ALP defect for a gene deletion strain is expressed as the pALP/tALP ratio of the deletion strain divided by the pALP/tALP ratio of wild-type cells. Statistical significance of the ALP defect was calculated from the values and standard deviations. CPS maturation is reported as having no defect (—), moderate defect (M), or severe defect (S) as determined by the presence or absence of precursor and mature forms of CPS (see *Materials and Methods*). Neither *MAT***a** or *MAT*α library contained valid deletion strains for *vps33Δ* (HOPS subunit), *pep7Δ* (vesicle targeting to endosomes), *vma4Δ* (subunit E of V_1 domain of ATPase), or *vma21Δ* (v-ATPase assembly) as determined by sequencing the bar codes of the relevant strains.

[a] ALP maturation defects in these strains were not detected in the genome-wide screens.

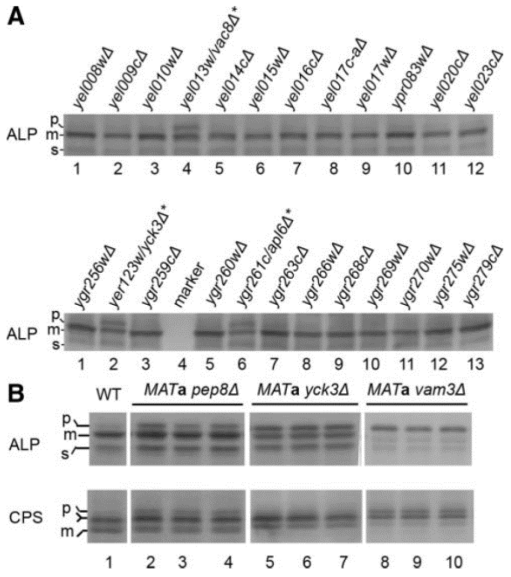

Figure 1. Example of results from analysis of ALP maturation in strains from the *MAT***a** deletion library. (A) Indicated strains were grown in YPD, extracts were prepared, and ALP maturation was assessed by SDS-PAGE and immunoblotting. Strains scored as positive for pALP accumulation are designated with an asterisk. The positions of precursor (p), mature (m), and soluble (s) forms of ALP are indicated. The abundance of the sALP form can vary between experiments depending on growth state and other undetermined factors. (B) Example of results from analysis of ALP and CPS maturation in multiple samples of each strain scored as positive in the genome-wide screen. Three individual colonies from each of the indicated gene deletion strains and WT cells were independently cultured, cell extracts were prepared, and ALP and CPS were detected by immunoblotting. Forms of ALP are indicated as in A. The position of precursor (p) and mature (m) forms of CPS are indicated. The forked line indicates the intermediate band position where pCPS and mCPS forms comigrate. Examples of strains scored in Table 1 as no defect (*yck3*Δ), moderate defect (*pep8*Δ), and severe defect (*vam3*Δ) are shown.

is transported via the clathrin-dependent pathway (Cowles *et al.*, 1997b). Consequently, defects specific for the AP-3 pathway should affect ALP but not CPS maturation. Three independent samples of each mating type of each positive strain were monitored for ALP and CPS maturation by immunoblotting (Figure 1B). Quantitation of the fraction of pALP present in each sample demonstrated that all the strains exhibited statistically significant accumulation of pALP compared with wild-type cells (Table 1). For CPS, the presence of partially overlapping glycosylated precursor and mature forms necessitated a more qualitative measure of maturation (Figure 1B and Table 1). Nevertheless, each strain exhibited reproducible patterns of CPS that could be reliably assessed for maturation defects (Table 1).

Most strains with ALP maturation defects could be grouped according to established functional categories or protein complexes (Table 1). In all cases except for AP-3 subunit gene deletions, *svp26*Δ, and *yck3*Δ, deletions of genes that affected ALP maturation also affected CPS maturation. Thus, the analysis yielded only six gene deletions with selective effects on ALP maturation, four of which were AP-3 subunits. Additionally, *vac8*Δ and *vac17*Δ strains displayed defects in both ALP and CPS maturation that have not been reported previously. Vac8p and Vac17p function in vacuole inheritance (Weisman, 2006).

Among the deletions affecting both ALP and CPS maturation are genes expected to influence ALP maturation through direct roles in either maturation or transport. These include the master vacuolar maturation proteases Pep4p and Prb1p that are required for ALP and CPS processing in the vacuole (Jones, 1984), proteins that act in vesicle formation such as Vps1p, and Arf1p (Odorizzi *et al.*, 1998; Bowers and Stevens, 2005), and components of the machinery responsible for AP-3 and endosomal pathway vesicle docking and fusion with the vacuole such as the HOPS complex, the rab GTPase Ypt7p, and SNAREs (Bowers and Stevens, 2005; Ostrowicz *et al.*, 2008).

Other gene deletions identified in the screen are likely to inhibit ALP transport/maturation indirectly. For example, proteins involved in the clathrin-dependent pathway such as Rab Vps21p, the Vps21p guanine nucleotide exchange factor Vps9p, the endosomal t-SNARE Pep12p, and the Vps34p phosphatidylinositol 3-kinase complex I, are necessary for transport of the maturation proteases Pep4p and Prb1p to endosomes (Bowers and Stevens, 2005). In these mutants, reduced levels of Pep4p and Prb1p in the vacuole can account for the ALP maturation defects. A similar explanation may apply to the weak ALP maturation defects observed in strains with deletions of genes encoding subunits of the retromer complex, which mediates endosome to Golgi retrieval of vacuolar protein sorting receptors (Seaman *et al.*, 1998). Retromer mutations could also affect ALP maturation by blocking a retrieval pathway from the vacuole membrane that passes through endosomes to the TGN (Bryant *et al.*, 1998). This pathway is involved in retrieval of the v-SNARE Vti1p that participates in ALP delivery to the vacuole (Vti1p acts in several transport steps and is essential for viability, thus *vti1*Δ is not represented in the haploid deletion mutant collection).

Deletions of *FAB1* and *VAC14* inhibit production of phosphatidylinositol 3,5 bisphosphate, resulting in perturbations in several vacuole pathways that could affect ALP and CPS maturation, including the vacuole to endosome retrieval pathway described above and the vacuolar inheritance pathway (Cooke, 2002; Shaw *et al.*, 2003; Weisman, 2006). However, we did not observe defects in ALP or CPS maturation in either *MAT***a** or *MAT*α cells lacking Vac7p, an activator of the Fab1p lipid kinase (Bonangelino *et al.*, 1997), and we also noted variable maturation defects in different *fab1*Δ strains, suggesting further analysis is needed to determine whether Fab1p and its activators are necessary for ALP and CPS maturation.

Finally, deletions of many of the genes encoding subunits or assembly factors for the V-type H^+ ATPase were identified. Acidification by the V-ATPase is required for optimal activity of the vacuolar maturation enzymes and for efficient protein transport to the vacuole, particularly through the endosomal pathway (Kane, 2006). Additionally the V_0 membrane component has been proposed to play a more direct role in vacuole membrane fusion (Peters *et al.*, 2001). Whether the variability observed between different subunit deletions reflects distinct functions will require additional investigation.

*ALP Transport Is Specifically Affected in yck3*Δ *Cells*

Our immunoblotting analysis of ALP and CPS in *yck3*Δ suggested a specific defect in ALP traffic in this strain. Yck3p

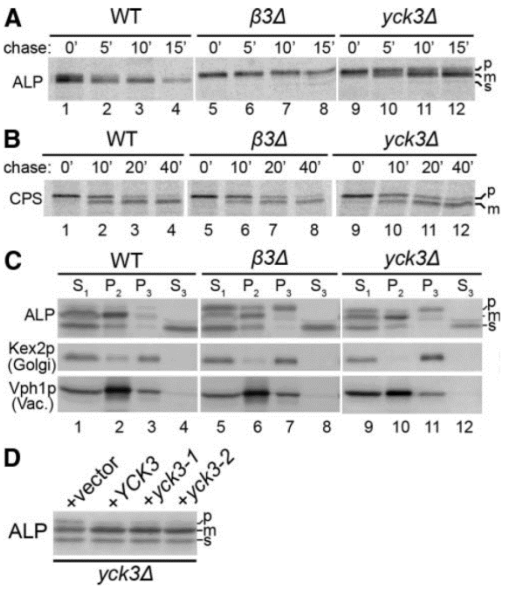

Figure 2. Specific defect in ALP transport in *yck3*Δ cells. (A) Pulse-chase immunoprecipitation of ALP. Cells from WT, *apl6*Δ-AP-3 β subunit gene deletion strain (*β3*Δ), and *yck3*Δ strains were metabolically labeled with [^{35}S]methionine for 7 min, and labeling was quenched with nonradioactive amino acids. Samples of cells were removed at the indicated times after initiation of the chase. Cells were lysed, ALP was immunoprecipitated, and the immunoprecipitates were subjected to SDS-PAGE. Gels were exposed to a phosphor screen and digitally imaged. (B) Pulse-chase immunoprecipitation of CPS. Pulse-chase analysis of CPS was performed as described in A, except that samples were removed at 0, 10, 20, and 40 min after addition of the chase. (C) Subcellular fractionation of *yck3*Δ cells. Cell lysates from wild-type (WT), *apl6*Δ (*β3*Δ), and *yck3*Δ strains were fractionated by differential centrifugation to generate low-speed (300 × *g* for 5 min) supernatant (S_1), medium-speed (10,000 × *g* for 15 min) supernatant and pellet (S_2, P_2), and high-speed (200,000 × *g* for 17 min) supernatant and pellet (S_3, P_3) fractions. Fractions were analyzed by SDS-PAGE and immunoblotted for ALP, the Golgi protein Kex2p, and the vacuole membrane (Vac) protein Vph1p. (D) ALP maturation in sorting defective Yck3p mutants. Cells from the *MAT***a** *yck3*Δ strain harboring empty vector, or plasmids containing wild-type *YCK3* or two mutant *yck3* genes (*yck3-1*, *yck3-2*) that lack a YDSI tyrosine-based AP-3 pathway sorting sequence (Sun *et al.*, 2004). Cells were cultured in selective media, cell extracts were prepared and subjected to immunoblotting for ALP.

is a type I casein kinase that is localized to the vacuole membrane and plays a role in regulating vacuole morphology and inheritance (Sun *et al.*, 2004; LaGrassa and Ungermann, 2005). A role for this kinase in protein traffic to the vacuole has not been described. To more carefully assess the specificity of the trafficking defect we characterized ALP and CPS maturation by pulse-chase immunoprecipitation. Wild-type, *yck3*Δ, and *apl6*Δ cells were pulse labeled for 10 min, and then they were subjected to chase regimens before lysis and immunoprecipitation of ALP and CPS. In wild-type cells, maturation of ALP was >50% complete after the labeling period and complete by 10 min of chase (Figure 2A, lanes 1–4). In contrast, in the *yck3*Δ cells, >50% of ALP was in the precursor form after the 5-min chase and significant levels of precursor persisted at the 15-min chase point (Figure 2A, lanes 9–12). This corresponds to roughly a threefold delay in ALP maturation in *yck3*Δ cells. By comparison, cells lacking the AP-3 β subunit (*β3*Δ) displayed a severe ALP maturation defect, with the precursor form predominant throughout the chase period (Figure 2A, lanes 5–8). These results suggest an important but not required function of Yck3p in ALP transport to the vacuole. CPS is matured more slowly than ALP in wild-type cells, presumably because of the intermediate endosome stage in the clathrin-dependent pathway (Figure 2, A and B, lanes 1–4). Maturation of CPS was not significantly delayed in *β3*Δ or *yck3*Δ cells (Figure 2B, lanes 5–12). Together, the results from immunoblotting and pulse-chase immunoprecipitation provide evidence that maturation of ALP is selectively affected in *yck3*Δ cells. This phenotype is similar to, but less severe than, those of AP-3–deficient cells, suggesting that Yck3p acts in the AP-3 pathway.

To determine whether the ALP maturation delay in *yck3*Δ cells is due to a defect in ALP transport to the vacuole, we analyzed the subcellular distribution of pALP by differential centrifugation. Extracts from wild-type, *yck3*Δ and *β3*Δ cells were first sedimented at 300 × *g* to remove unbroken cells, and then the resulting supernatant (S1) was sedimented at 13,000 × *g* to pellet larger organelles including the ER and vacuoles (P2). The 10,000 × *g* supernatant (S2) was then sedimented at 200,000 × *g* to pellet smaller organelles such as the Golgi and transport vesicles (P3). Fractions were then analyzed by immunoblotting for ALP, Kex2p (TGN/endosome marker), and Vph1p (vacuole membrane marker). In all three strains, mALP pelleted together with the Vph1p in P2 (Figure 2C, lanes 2, 6, and 10), whereas sALP was mostly present in S3 due to release from vacuoles during the lysis procedure (Figure 2C, lanes 4, 8, and 12). In *β3*Δ and *yck3*Δ cells, pALP, like Kex2p, sedimented predominantly in P3, indicating a defect in ALP transport to the vacuole in the two strains.

As an independent test of ALP traffic, localization of GFP-tagged ALP was assessed by fluorescence microscopy. To visualize vacuoles, cells were also stained with FM4-64, which is delivered to the vacuole via the endocytic pathway (Vida and Emr, 1995). In wild-type cells, GFP-ALP colocalized with FM4-64 at vacuole membranes (Figure 3, WT). In contrast, in *β3*Δ cells GFP-ALP was present both at the vacuole together with FM4-64 and also at cytoplasmic puncta that did not label with FM4-64 (Figure 3, *β3*Δ). A similar but less severe localization defect was apparent in *yck3*Δ cells (Figure 3, *yck3*Δ). The punctate distribution of GFP-ALP in *β3*Δ and *yck3*Δ cells is consistent with the pALP transport defect observed by differential centrifugation and likely reflects accumulation of pALP in Golgi and/or endosomes. Together, results from analysis of *yck3*Δ cells identify Yck3p as a factor specifically required for ALP transport between the Golgi and the vacuole.

The normal localization of Yck3p to the vacuole limiting membrane suggests a role in regulating transport vesicle targeting/fusion to the vacuole. The established role of Yck3p in controlling vacuole morphology supports this idea because many proteins involved in vacuole morphology also participate in transport vesicle targeting and fusion to the vacuole membrane (Ostrowicz *et al.*, 2008). Through such functions, these proteins are required for both the AP-3 and clathrin-dependent pathways (Bowers and Stevens, 2005). Indeed, our screen identified severe pALP and pCPS accumulation in strains lacking components of the HOPS complex and vacuole fusion machinery (Table 1). However, the

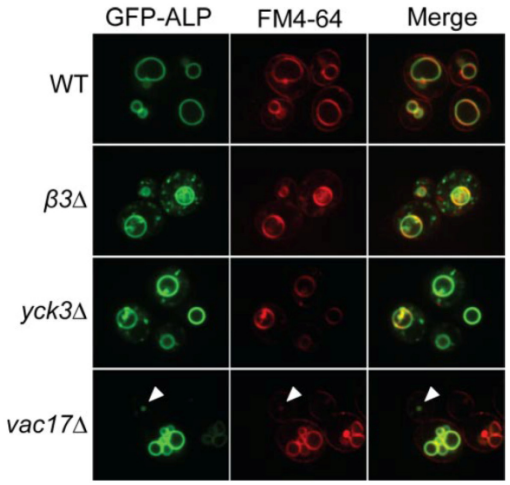

Figure 3. Mislocalization of GFP-ALP in *yck3*Δ but not *vac17*Δ cells. WT, *β3*Δ, *yck3*Δ, and *vac17*Δ cells harboring a plasmid encoding GFP-ALP were grown to early-logarithmic phase in minimal media, collected by centrifugation, and stained with FM4-64 for 20 min. The cells were then washed and allowed to internalize the dye for 60 min. Cells were imaged by confocal microscopy to visualize GFP-ALP and FM4-64 localization. Arrowhead indicates a vacuole probably generated de novo.

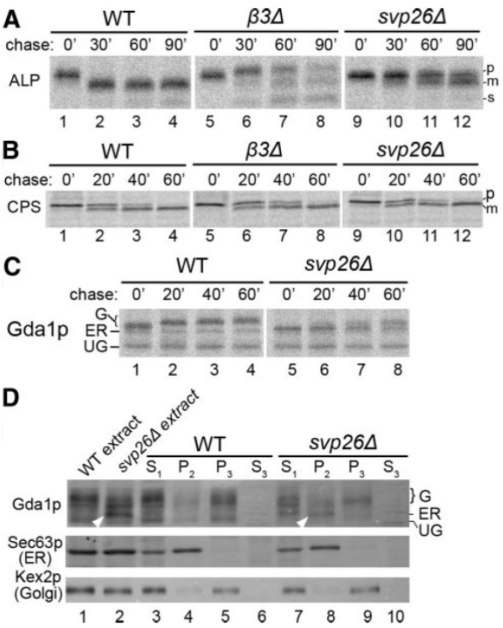

Figure 4. Selective defects in type II membrane protein transport in *svp26*Δ cells. (A) Pulse-chase immunoprecipitation of ALP. Wild-type (WT), *apl6*Δ (*β3*Δ), and *svp26*Δ cells were analyzed by pulse-chase immunoprecipitation of ALP as described in the legend to Figure 2A, except that chase samples were removed at 0, 30, 60, and 90 min. (B) Pulse-chase immunoprecipitation of CPS. Pulse-chase immunoprecipitation of CPS was performed as described in the legend to Figure 2B, except that samples were removed at 0, 20, 40, and 60 min after addition of the chase. (C) Pulse-chase immunoprecipitation of Gda1p. Pulse-chase immunoprecipitation of Gda1p from the indicated strains was performed as described in the legend to Figure 2A, except that samples were removed at 0, 20, 40, and 60 min after addition of the chase. UG, unglycosylated form of Gda1p (does not diminish in size after treatment with endoglycosidase H [data not shown]); ER, endoplasmic core glycosylated form of Gda1p; G, Golgi glycosylated forms of Gda1p (Vowels and Payne, 1998). (D) Subcellular fractionation of *svp26*Δ cells. Subcellular fractionation was performed as described in the legend to Figure 3. White arrowheads indicate the accumulated, glycosylated form of Gda1p not present in WT extract. Endoglycosidase H treatment reduces all forms of Gda1p (G, Golgi form; ER, endoplasmic reticulum form; UG, unglycosylated form) in both WT and *svp26*Δ strains to the UG form (data not shown). Fractions were immunoblotted for Gda1p, the ER protein Sec63p, and Kex2p.

selective effects of *yck3*Δ on pALP transport imply a more specific role for Yck3p in the AP-3 pathway. Yck3p is a palmitoylated, membrane-associated protein that is delivered to the vacuole through the AP-3 pathway (Sun *et al.*, 2004), raising the possibility that sorting into the pathway confers functional specificity. An example of this mechanism was recently reported for the mammalian AP-3 pathway cargo, phosphatidylinositol-4-kinase type IIα (Craige *et al.*, 2008). To test whether Yck3p function in ALP transport requires sorting into the AP-3 pathway, we analyzed ALP maturation in cells expressing mutant forms of Yck3p that carry alterations of the YDSI signal that directs sorting into the AP-3 pathway. Although these mutants are not efficiently sorted into the AP-3 pathway, they still localize to the vacuole membrane, at least in part because of default transport through the endosomal route (Sun *et al.*, 2004). As assessed by immunoblotting, cells expressing these mutants as the sole source of Yck3p displayed no accumulation of pALP (Figure 2D). These data suggest that sorting into the AP-3 pathway is not required for Yck3p function in ALP transport.

ER Export of a Subset of Type II Integral Membrane Proteins Is Delayed in svp26Δ Mutants

In addition to *yck3*Δ and AP-3 subunit deletions, *svp26*Δ affected maturation of ALP but not CPS (Table 1). A specific effect of *svp26*Δ on ALP transport was reported previously in a study that characterized Svp26p as a transmembrane adaptor required for incorporation of ALP into COP-II vesicles at the ER (Bue *et al.*, 2006). In this study, *svp26*Δ did not affect transport of CPY, a soluble luminal protein, or Gas1p, a GPI-linked membrane protein. A separate study described mislocalization of the Golgi mannosyltransferase Ktr3p to the ER in *svp26*Δ cells (Inadome *et al.*, 2005), suggesting that Svp26p may serve as an adaptor for multiple proteins. Both ALP and Ktr3p are type II membrane proteins, a feature that could be important for recognition by Svp26p. To further define the specificity of Svp26p, we assessed maturation of ALP and CPS, another type II vacuole membrane protein, in *svp26*Δ cells by pulse-chase immunoprecipitation. ALP maturation was severely hindered in *svp26*Δ cells, as expected, with a delay commensurate with that displayed in AP-3–deficient cells (Figure 4A). CPS maturation was unaffected in *svp26*Δ cells, indicating that not all type II membrane proteins require Svp26p for transport from the ER (Figure 4B).

We also examined trafficking of another type II membrane protein, the Golgi guanosine diphosphatase Gda1p. In wild-

type cells, residence of Gda1p in the Golgi complex allows continued exposure to glycosyltransferases that extend oligosaccharide chains on Gda1p, causing a progressive size increase over time (Vowels and Payne, 1998b; Figure 4C, lanes 1–4). Mutations that prevent ER-to-Golgi transport result in accumulation of a core-glycosylated form of GDPase that does not change size (Vowels and Payne, 1998b). Accordingly, the size of Gda1p over time was monitored in wild-type and *svp26*Δ cells by pulse-chase immunoprecipitation. Unlike Gda1p in wild-type cells, which gradually increased in size during the chase period (Figure 4C, lanes 1–4), Gda1p in *svp26*Δ cells did not display a size shift until 40 min after the chase and even at the 60-min chase time exhibited substantial amounts of the ER form (Figure 4C, lanes 5–8). These data are consistent with an impediment in export of Gda1p from the ER in *svp26*Δ cells.

To more directly assess Gda1p localization, the subcellular distribution of Gda1p was examined in wild-type and *svp26*Δ strains by differential centrifugation. In wild-type cell extracts, several Gda1p species were detected by immunoblotting, including a major 70-kDa form and minor 67- and 57-kDa forms (Figure 4D, Gda1p, lane 1). Treatment with endoglycosidase H reduced all forms to 57 kDa, indicating that the higher-molecular-weight forms are glycosylated (unpublished data). All Gda1p forms in wild-type cells cofractionated with the Golgi marker Kex2p in P3 (Figure 4D, Gda1p and Kex2p, lane 5). In *svp26*Δ cell extracts, a new species of ≈60 kDa was detected which corresponded in size to that expected for ER form (Figure 4D, Gda1p, lane 2, arrowhead). Additionally, there was a shift in the ratio of the higher-molecular-weight forms with the 67-kDa form most prominent. The 60-kDa form sedimented with the ER marker Sec63p (Figure 4D, Gda1p and Sec63p, lane 8), whereas the higher-molecular-weight species fractionated mostly in P3. Mislocalization of the 60-kDa Gda1p in *svp26*Δ cells is consistent with accumulation in the ER, and together with the results of the pulse-chase immunoprecipitation, provides evidence that Gda1p requires Svp26p for export from the ER. This result, combined with the earlier studies, indicates that Svp26p plays a role in transport of only a subset of type II membrane proteins from the ER to the Golgi, including Gda1p, Ktr3p, and ALP but not CPS.

ALP Maturation Is Defective in Vacuole Inheritance Mutants

Our original screen detected both ALP and CPS maturation defects in *vac8*Δ and *vac17*Δ strains. *VAC8* and *VAC17* encode proteins involved in vacuole inheritance during cell division (Weisman, 2006). Vac8p is associated with the vacuole membrane and also participates in cytoplasmic to vacuole transport and homotypic vacuole fusion (Wang *et al*., 1998, 2001). Vac17p, which acts preferentially in vacuole inheritance, links Vac8p to the type-V myosin Myo2p (Ishikawa *et al*., 2003). Myo2p directs movement of tubulovesicular vacuole inheritance structures along the actin cytoskeleton from the mother cell vacuole into the newly forming bud in which they seed formation of a new vacuole (Hill *et al*., 1996). Roles for Vac8p or Vac17p in vacuolar protein maturation and/or vesicle-mediated protein transport have not been reported.

To further evaluate the ALP and CPS maturation defects, *vac8*Δ and *vac17*Δ cells were analyzed by pulse-chase immunoprecipitation. The results of this analysis revealed an unusual maturation pattern. In the case of ALP, ~50% was mature by the 10-min chase point but the level of precursor did not decline substantially at later chase points (Figure 5A). Similar biphasic maturation kinetics were observed for CPS (Figure 5B).

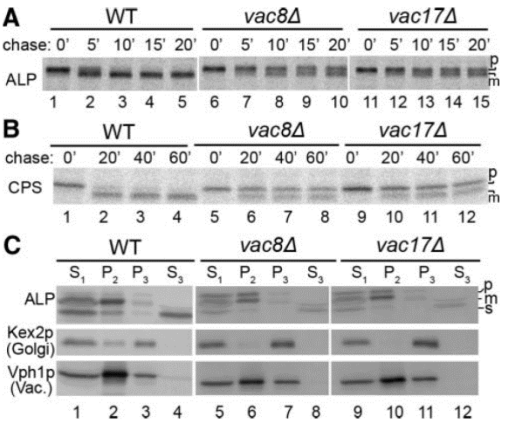

Figure 5. ALP and CPS maturation is delayed in *vac8*Δ and *vac17*Δ cells. (A) Pulse-chase immunoprecipitation of ALP. Pulse-chase immunoprecipitation of ALP from the indicated strains was performed as described in the legend to Figure 2A except that chase samples were removed at 0, 5, 10, 15, and 20 min. (B) Pulse-chase immunoprecipitation of CPS. Pulse-chase immunoprecipitation of CPS was performed as described in the legend to Figure 4B. (C) Subcellular fractionation of *vac8*Δ and *vac17*Δ cells. Subcellular fractionation *vac8*Δ and *vac17*Δ cells and immunoblotting analysis was performed as described in the legend to Figure 2C.

To determine the subcellular localization of the accumulated pALP in the inheritance mutants, we performed subcellular fractionation of *vac8*Δ and *vac17*Δ cells. Unlike pALP in trafficking mutants such as *β3*Δ and *yck3*Δ, which fractionated in P3, pALP in *vac8*Δ, and *vac17*Δ strains sedimented in P2 with mALP and the vacuolar membrane marker Vph1p (Figure 5C, ALP and Vph1p, lanes 6 and 10). Consistent with these results, GFP-ALP in *vac17*Δ cells was localized to the vacuolar limiting membrane with FM4-64 (Figure 3). These results provide evidence that pALP in *vac8*Δ and *vac17*Δ cells is transported to vacuole membranes but a portion is inefficiently matured.

The inheritance defect in *vac8*Δ and *vac17*Δ cells provides a possible explanation for the unusual maturation kinetics of ALP and CPS. Vacuole inheritance mutants can generate vacuoles de novo through an unknown mechanism (Weisman *et al*., 1987; Gomes De Mesquita *et al*., 1997). However, such vacuoles do not receive contents from the maternal vacuole that contains the active form of protease A responsible for maturation of ALP and CPS. Consequently, in contrast to inherited vacuoles, de novo-generated vacuoles are not expected to be immediately proteolytically active. Thus, the relatively stable population of pALP and pCPS in *vac8*Δ and *vac17*Δ cells may represent those precursors delivered to de novo-formed vacuoles. In contrast, newly synthesized pALP and pCPS that is delivered to the maternal vacuoles is expected to be matured with essentially normal kinetics.

Over time, vacuoles formed de novo can become proteolytically active through autocatalytic activation of proteases A and B that are delivered from the biosynthetic pathway (Woolford *et al*., 1986; Nebes and Jones, 1991). If the stable population of pALP is indeed present in de novo-generated vacuoles, then pALP should be matured once the vacuole

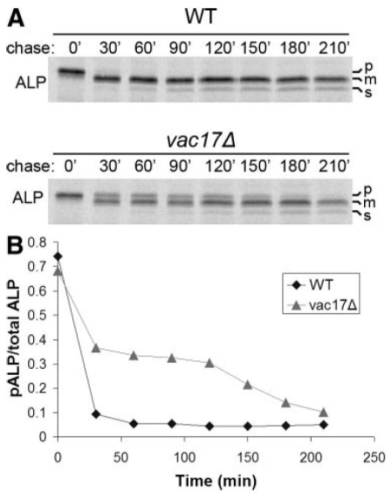

Figure 6. Accumulated pALP in *vac17*Δ cells matures after 120 min delay. (A) Pulse-chase immunoprecipitation of ALP from WT and *vac17*Δ cells was performed as described in the legend to Figure 2A except that chase samples were removed at 0, 30, 60, 90, 120, 150, 180, and 210 min. (B) Bands in A were quantified as described in *Materials and Methods*, and the ratio of pALP to total ALP was calculated.

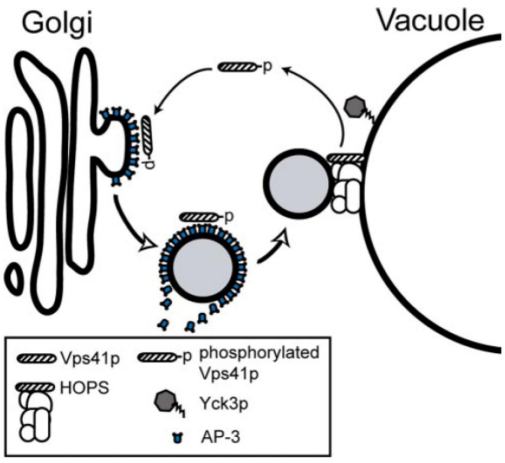

Figure 7. Model for Yck3p function. Vps41p phosphorylation by Yck3p targets Vps41p for function at the Golgi in AP-3–dependent vesicle formation. Unphosphorylated Vps41p functions as a component of HOPS in vesicle docking/fusion at the vacuole membrane. See text for details. Phosphorylated Vps41p may function at the Golgi as part of the HOPS complex although it is pictured acting independently. The site of Vps41p dephosphorylation and release from AP-3 vesicles is unknown.

acquires sufficient levels of active protease A. To test this prediction, we monitored maturation of ALP in *vac17*Δ cells by using a pulse-chase regimen that extended the chase period over 3.5 h (Figure 6). The level of pALP maturation after 30 min reached a plateau that persisted for 90 min (Figure 6, A and B). However, after 2 h ALP processing resumed, and virtually all of the pALP was mature by the 3.5-h time point. A similar result was obtained with *vac8*Δ cells (unpublished data). These data conform to the model that a percentage of pALP in *vac8*Δ and *vac17*Δ cells is transported to proteolytically inactive vacuoles formed de novo in the absence of the inheritance pathway. Our results suggest that the vacuole inheritance pathway is important for the timely biogenesis of functional vacuoles in newly forming daughter cells during cell division.

DISCUSSION

As an approach to identify the full complement of proteins required for transport through the AP-3 pathway in yeast, we have systematically surveyed collections of viable gene knockout strains by using maturation of vacuolar ALP as an indicator of AP-3 pathway function. Among the genes identified through this strategy are those that encode proteins involved in vesicle budding, targeting, and fusion, as well as other processes such as proteolytic processing in the vacuole, organelle acidification, vacuole inheritance, and protein export from the ER. Our study uncovered a selective role for the vacuolar casein kinase Yck3p in AP-3 pathway function, the only protein other than AP-3 that was required specifically for AP-3–dependent traffic.

Yck3p is one of four type I casein kinases in yeast and is unique in localizing to the vacuole (Wang *et al.*, 1996; Sun *et al.*, 2004). Recently, LaGrassa and Ungermann (2005) provided initial insight into Yck3p function, reporting that *yck3*Δ cells display a defect in maintenance of vacuole fragmentation triggered by hyperosmotic stress. The study presented evidence that the fragmentation maintenance defect results from an up-regulation of vacuole fusion driven by increased tethering activity of the HOPS complex in the absence of Yck3p. Phosphorylation of Vps41p, a HOPS subunit, was demonstrated to depend on Yck3p. Based on these findings, it was proposed that Yck3p-mediated Vps41 phosphorylation inhibits HOPS tethering activity, thereby decreasing vacuole fusion and maintaining the fragmented state in hypertonic conditions. By analogy to the role of Vps41p in AP-3 vesicle formation, the authors also speculated that Vps41p might act in vacuole fragmentation and suggested that phosphorylation could control the distribution of Vps41p functioning in vacuole fragmentation versus fusion. Our finding that *yck3*Δ cells are defective in transport of ALP to the vacuole is consistent with a role for Vps41p phosphorylation in regulating vesicle formation and, importantly, indicates that Yck3p plays a role under normal growth conditions as well as in response to hypertonic stress.

We envision a model for Yck3p function in the AP-3 pathway that integrates the mechanism proposed to control stress-induced vacuole fusion (LaGrassa and Ungermann, 2005). In this model, Yck3p serves to regulate transition of the bifunctional Vps41p between two functional states—one state involved in AP-3 vesicle formation (phosphorylated) and the other state involved in vesicle targeting/fusion (dephosphorylated) at the vacuole (Figure 7). According to this model, deletion of *YCK3* would shift the balance of Vps41p toward targeting/fusion at the vacuole. Consistent with this prediction, *yck3*Δ cells display increased levels of vacuole-associated Vps41p in vivo under normal growth conditions and more avid association of Vps41p with vacuole membrane in vitro (LaGrassa and Ungermann, 2005). Redistribu-

tion of unphosphorylated Vps41p to the vacuole would allow fusion of vesicles from both the AP-3 pathway and the clathrin-dependent pathway but would deplete the pool of Vps41p available to participate in AP-3 vesicle formation, thereby accounting for the specific defect in ALP transport in *yck3*Δ cells. To determine whether the *yck3*Δ defect can be overcome simply by increasing levels of Vps41p, ALP maturation was monitored in *yck3*Δ cells expressing *VPS41* from a multicopy plasmid (Supplemental Figure S1). However, the ALP defect persisted in these cells, suggesting that phosphorylation by Yck3p may be required for Vps41p function in AP-3 vesicle formation. Alternatively, Vps41p may function in AP-3 dependent traffic at the Golgi as part of a complex, conceivably HOPS. In this scenario, overexpression of Vps41p without other members of the complex would not increase AP-3–specific Vps41p activity.

The apparently stable membrane association of Yck3p imposes a spatial constraint on Yck3p activity that may be important for models of AP-3 pathway-specific function. As an AP-3–dependent cargo, it is possible that the pathway-specific activity of Yck3p occurs during transport through the pathway. However, our results indicate that sorting-defective Yck3p mutants supported wild-type levels of ALP maturation, making it unlikely that Yck3p transport through the AP-3 pathway confers specificity. The Yck3p sorting mutants are reported to localize primarily at the vacuole membrane, probably due to transport through the clathrin-dependent endosomal pathway (Sun *et al.*, 2004). Thus, function of the sorting mutants in ALP transport suggests that the vacuole membrane is the site from which Yck3p provides AP-3 pathway-specific activity. This possibility is compatible with the Vps41p phosphorylation model described in Figure 7—the pool of unphosphorylated Vps41p involved in tethering could serve as substrate for vacuole-localized Yck3p, thereby generating the phosphorylated form of Vps41p proposed to function in AP-3 vesicle formation.

As an approach to address the importance of membrane association in Yck3p function, we assessed ALP maturation in cells expressing a palmitoylation-defective mutant of Yck3p (Sun *et al.*, 2004). This mutant supported normal ALP maturation (Supplemental Figure S1). However, differential fractionation revealed significant but not complete mislocalization to the soluble fraction. Similarly, Vancura *et al.* (1994) reported that expression of a palmitoylation-defective mutant of the plasma membrane casein kinase I, Yck2p, rescued defects in Yck2p-deficient cells, although the mutant kinase was substantially mislocalized. It seems that, in these cases, a small fraction of properly localized kinase may be sufficient to retain function, or these kinases can provide function from the cytoplasm.

Casein kinase I activity has also been associated with AP-3 function in mammalian cells (Faundez and Kelly, 2000). In this case, however, the β3 subunit of AP-3 was identified as a kinase target. Inhibition of the kinase reduced AP-3 recruitment to synaptic vesicles in vitro and synaptic vesicle budding in vivo. In these studies, the role of Vps41 was not examined. Conversely, the possibility that AP-3 is a target of Yck3p has not been addressed in yeast. A more complete identification of kinase targets and functional tests of phosphorylation site mutants in both yeast and animal cells will be needed to define the regulatory mechanisms and determine the extent of similarity across species.

Our screen also identified Svp26p as a factor required for ALP maturation. During the course of our work, Svp26p was reported to function as an ER receptor for ALP, necessary for sorting ALP into COP II vesicles (Bue *et al.*, 2006). Another group observed that Svp26p interacted with the Golgi glycosyltransferase Ktr3p and *svp26*Δ caused mislocalization of Ktr3p to the ER, results consistent with a role for Svp26p as an ER export receptor for Ktr3p (Inadome *et al.*, 2005). Our results provide evidence that another Golgi membrane protein, Gda1p, also accumulates in the ER in *svp26*Δ cells, supporting the view that Svp26p is a general ER cargo receptor, directing multiple cargoes into COP II vesicles. It is currently unknown how Svp26p recognizes cargo. ALP, Ktr3p, and Gda1p do not share significant sequence homology, yet all are type II integral membrane proteins, raising the possibility that membrane topology could constitute part of the binding determinant for Svp26p. However, our observation that CPS, another type II membrane protein, is not affected by *svp26*Δ indicates that membrane topology is not the sole factor for Svp26p recognition. Importantly, the common topologies of CPS and the three Svp26-dependent proteins should now allow a straightforward chimeric protein approach to map the elements that target cargo to Svp26p. Single homologues of Svp26p are present in a number of eukaryotic species, including humans (Bue *et al.*, 2006). Considering the evolutionary conservation of both Svp26p and COP II proteins, analysis of Svp26p cargo recognition has the potential to provide insight into a fundamental mechanism of protein export from the ER in eukaryotic cells.

During the polarized growth of yeast cells, the vacuole inheritance pathway directs transfer of tubular/vesicular elements of the mother cell vacuole into the emerging daughter bud through an actin and myosin-based mechanism (Hill *et al.*, 1996). This pathway promotes distribution of vacuoles to both mother and daughter cells during cell division. The role of vacuole inheritance is not completely clear, because daughter cells can synthesize vacuoles de novo in vacuole inheritance mutants. Our analysis of the ALP and CPS maturation defects discovered in *vac8*Δ and *vac17*Δ cells provides evidence that the vacuole inheritance pathway is important for the timely generation of a proteolytically active vacuole. In these vacuole inheritance mutants we observed that precursor ALP is delivered to vacuole membranes but only a fraction undergoes rapid maturation. Based on these findings, we suggest that precursor vacuolar enzymes are efficiently transported to two populations of vacuoles, one population that is proteolytically active and the other population that becomes active only after several hours. Slowly activating vacuoles would arise in daughter cells through de novo biogenesis of organelles that, because of the inheritance pathway defect, would initially lack active proteases normally transferred from the mother cell vacuole. Without acquisition of preactivated forms of the master processing proteases, generation of a fully active hydrolytic compartment would be delayed until newly synthesized protease zymogens are delivered by the biosynthetic transport pathways and undergo autocatalytic activation. Thus, it seems that the vacuolar proteolytic maturation system, which restricts activation of hydrolase precursors to the appropriate compartment, imposes a significant time delay in de novo formation of active vacuoles. Our study suggests that the inheritance pathway surmounts this problem by seeding daughter cell vacuoles with preactivated maturation proteases and other vacuolar hydrolases from the maternal vacuole.

Our use of a direct screen for ALP maturation in two collections of genome-wide yeast gene deletions identified a total of forty-nine strains with maturation defects. Notably, only five of these mutants exhibited selective defects in post-ER ALP transport, those with deletions of single AP-3 subunit genes and *yck3*Δ. Does this represent the complete

set of factors required exclusively for traffic through the AP-3 pathway in yeast? In addition to our systematic screen for ALP maturation defects, several other genetic approaches have been applied to identify AP-3 pathway-specific proteins. A systematic screen of ~15% of an independent gene deletion library by immunoblotting did not reveal new AP-3 pathway-specific mutations (Avaro *et al.*, 2002). Emr and colleagues carried out two independent screens of randomly mutagenized yeast for AP-3 pathway mutants (Darsow *et al.*, 2001). These approaches were sufficiently powerful to identify an AP-3 pathway-specific allele of *VPS41* but did not yield mutations in genes other than those encoding AP-3. Finally, a systematic screen for mutants with defects in sorting through the endosomal pathway also identified AP-3 mutants, probably due to indirect effects of AP-3 mutations on the endosomal pathway (Bonangelino *et al.*, 2002). In contrast to our work, this study reported *mon2*Δ as a mutation that caused stronger defects in ALP maturation than in sorting of carboxypeptidase Y through the clathrin-dependent pathway. We specifically tested *MAT***a** and *MAT*α haploid *mon2*Δ strains but did not detect ALP maturation defects by immunoblotting and pulse-chase immunoprecipitation. However, the screen by Bonangelino *et al.* (2002) was carried out with the library of diploid strains homozygous for each gene deletion. We confirmed that the *mon2*Δ strain from the homozygous diploid collection accumulates ALP precursor. However, a plasmid expressing wild-type Mon2p that complemented the monensin sensitivity of the *mon2*Δ diploid strain did not restore ALP maturation, indicating that the ALP maturation defect in this strain is not due to the absence of Mon2p (unpublished data). These results suggest that Mon2p is not an AP-3 pathway-specific factor, a conclusion strongly supported by the recently reported role of Mon2p in Gga protein localization (Jochum *et al.*, 2002).

Considering the combined results of our direct systematic screen together with previous systematic and random screens, it is reasonable to suppose that AP-3 and Yck3p are the only proteins that function preferentially in the AP-3 pathway in yeast. Full AP-3 pathway function in yeast is therefore achieved by a very small set of pathway-specific components acting in concert with factors common to multiple trafficking pathways, some of which, like Vps41p, may be multifunctional with AP-3 pathway-specific activities. The strong evolutionary conservation of both specific and shared elements of the AP-3 pathway in yeast suggests that this set of proteins serves as a core foundation for elaboration of the machinery necessary to accommodate more complicated trafficking patterns in specialized metazoan cells.

ACKNOWLEDGMENTS

We are most grateful to Randy Schekman (University of California, Berkeley), Scott Emr (Cornell University), Nicholas Davis (Wayne State University), and Birgit Singer-Krüger (Universität Stuttgart) for gifts of antibodies, strains, and plasmids. We especially thank Giancarlo Costaguta, Mara Duncan, and Esteban Fernandez for helpful insight. This work was supported by National Institutes of Health grants R01 GM-39040 and GM-67911 (to G.S.P.), National Institutes of Health Medical Scientist Training Program T32 GM-08042 (to V.C.A.), and National Institutes of Health National Research Service Award T32 GM-007104 (to L.D.).

REFERENCES

Avaro, S., Belgareh-Touze, N., Sibella-Arguelles, C., Volland, C., and Haguenauer-Tsapis, R. (2002). Mutants defective in secretory/vacuolar pathways in the EUROFAN collection of yeast disruptants. Yeast *19*, 351–371.

Berger, A. C., Salazar, G., Styers, M. L., Newell-Litwa, K. A., Werner, E., Maue, R. A., Corbett, A. H., and Faundez, V. (2007). The subcellular localization of the Niemann-Pick Type C proteins depends on the adaptor complex AP-3. J. Cell Sci. *120*, 3640–3652.

Bonangelino, C. J., Catlett, N. L., and Weisman, L. S. (1997). Vac7p, a novel vacuolar protein, is required for normal vacuole inheritance and morphology. Mol. Cell. Biol. *17*, 6847–6858.

Bonangelino, C. J., Chavez, E. M., and Bonifacino, J. S. (2002). Genomic screen for vacuolar protein sorting genes in *Saccharomyces cerevisiae*. Mol. Biol. Cell *13*, 2486–2501.

Bonifacino, J. S. (2004). The GGA proteins: adaptors on the move. Nat. Rev. Mol. Cell Biol. *5*, 23–32.

Bowers, K., and Stevens, T. H. (2005). Protein transport from the late Golgi to the vacuole in the yeast *Saccharomyces cerevisiae*. Biochim. Biophys. Acta *1744*, 438–454.

Brachmann, C. B., Davies, A., Cost, G. J., Caputo, E., Li, J., Hieter, P., and Boeke, J. D. (1998). Designer deletion strains derived from *Saccharomyces cerevisiae* S288C: a useful set of strains and plasmids for PCR-mediated gene disruption and other applications. Yeast *14*, 115–132.

Bryant, N. J., and Boyd, A. (1993). Immunoisolation of Kex2p-containing organelles from yeast demonstrates colocalisation of three processing proteinases to a single Golgi compartment. J. Cell Sci. *106*, 815–822.

Bryant, N. J., Piper, R. C., Weisman, L. S., and Stevens, T. H. (1998). Retrograde traffic out of the yeast vacuole to the TGN occurs via the prevacuolar/endosomal compartment. J. Cell Biol. *142*, 651–663.

Bue, C. A., Bentivoglio, C. M., and Barlowe, C. (2006). Erv26p directs pro-alkaline phosphatase into endoplasmic reticulum-derived coat protein complex II transport vesicles. Mol. Biol. Cell *17*, 4780–4789.

Conibear, E., and Stevens, T. H. (1998). Multiple sorting pathways between the late Golgi and the vacuole in yeast. Biochim. Biophys. Acta *1404*, 211–230.

Cooke, F. T. (2002). Phosphatidylinositol 3,5-bisphosphate: metabolism and function. Arch. Biochem. Biophys. *407*, 143–151.

Costaguta, G., Duncan, M. C., Fernandez, G. E., Huang, G. H., and Payne, G. S. (2006). Distinct roles for TGN/endosome epsin-like adaptors Ent3p and Ent5p. Mol. Biol. Cell *17*, 3907–3920.

Cowles, C. R., Odorizzi, G., Payne, G. S., and Emr, S. D. (1997a). The AP-3 adaptor complex is essential for cargo-selective transport to the yeast vacuole. Cell *91*, 109–118.

Cowles, C. R., Snyder, W. B., Burd, C. G., and Emr, S. D. (1997b). Novel Golgi to vacuole delivery pathway in yeast: identification of a sorting determinant and required transport component. EMBO J. *16*, 2769–2782.

Craige, B., Salazar, G., and Faundez, V. (2008). Phosphatidylinositol-4-kinase type II alpha contains an AP-3-sorting motif and a kinase domain that are both required for endosome traffic. Mol. Biol. Cell *19*, 1415–1426.

Darsow, T., Burd, C. G., and Emr, S. D. (1998). Acidic di-leucine motif essential for AP-3-dependent sorting and restriction of the functional specificity of the Vam3p vacuolar t-SNARE. J. Cell Biol. *142*, 913–922.

Darsow, T., Katzmann, D. J., Cowles, C. R., and Emr, S. D. (2001). Vps41p function in the alkaline phosphatase pathway requires homo-oligomerization and interaction with AP-3 through two distinct domains. Mol. Biol. Cell *12*, 37–51.

Dell'Angelica, E. C., Klumperman, J., Stoorvogel, W., and Bonifacino, J. S. (1998). Association of the AP-3 adaptor complex with clathrin. Science *280*, 431–434.

Dell'Angelica, E. C., Shotelersuk, V., Aguilar, R. C., Gahl, W. A., and Bonifacino, J. S. (1999). Altered trafficking of lysosomal proteins in Hermansky-Pudlak syndrome due to mutations in the beta 3A subunit of the AP-3 adaptor. Mol. Cell *3*, 11–21.

Di Pietro, S. M., and Dell'Angelica, E. C. (2005). The cell biology of Hermansky-Pudlak syndrome: recent advances. Traffic *6*, 525–533.

Faundez, V. V., and Kelly, R. B. (2000). The AP-3 complex required for endosomal synaptic vesicle biogenesis is associated with a casein kinase Ialpha-like isoform. Mol. Biol. Cell *11*, 2591–2604.

Gomes De Mesquita, D. S., Shaw, J., Grimbergen, J. A., Buys, M. A., Dewi, L., and Woldringh, C. L. (1997). Vacuole segregation in the *Saccharomyces cerevisiae* vac2–1 mutant: structural and biochemical quantification of the segregation defect and formation of new vacuoles. Yeast *13*, 999–1008.

Hill, K. L., Catlett, N. L., and Weisman, L. S. (1996). Actin and myosin function in directed vacuole movement during cell division in *Saccharomyces cerevisiae*. J. Cell Biol. *135*, 1535–1549.

Hoffman-Sommer, M., Grynberg, M., Kucharczyk, R., and Rytka, J. (2005). The CHiPS Domain--ancient traces for the Hermansky-Pudlak syndrome. Traffic *6*, 534–538.

Huizing, M., Helip-Wooley, A., Westbroek, W., Gunay-Aygun, M., and Gahl, W. A. (2008). Disorders of lysosome-related organelle biogenesis: clinical and molecular genetics. Annu. Rev. Genomics Hum. Genet. *9*, 359–386

Huizing, M., Scher, C. D., Strovel, E., Fitzpatrick, D. L., Hartnell, L. M., Anikster, Y., and Gahl, W. A. (2002). Nonsense mutations in ADTB3A cause complete deficiency of the beta3A subunit of adaptor complex-3 and severe Hermansky-Pudlak syndrome type 2. Pediatr. Res. *51*, 150–158.

Inadome, H., Noda, Y., Adachi, H., and Yoda, K. (2005). Immunoisolation of the yeast Golgi subcompartments and characterization of a novel membrane protein, Svp26, discovered in the Sed5-containing compartments. Mol. Cell. Biol. *25*, 7696–7710.

Ishikawa, K., Catlett, N. L., Novak, J. L., Tang, F., Nau, J. J., and Weisman, L. S. (2003). Identification of an organelle-specific myosin V receptor. J. Cell Biol. *160*, 887–897.

Ito, H., Fukuda, Y., Murata, K., and Kimura, A. (1983). Transformation of intact yeast cells treated with alkali cations. J. Bacteriol. *153*, 163–168.

Jochum, A., Jackson, D., Schwarz, H., Pipkorn, R., and Singer-Kruger, B. (2002). Yeast Ysl2p, homologous to Sec7 domain guanine nucleotide exchange factors, functions in endocytosis and maintenance of vacuole integrity and interacts with the Arf-Like small GTPase Arl1p. Mol. Cell. Biol. *22*, 4914–4928.

Jones, E. W. (1984). The synthesis and function of proteases in *Saccharomyces*: genetic approaches. Annu. Rev. Genet. *18*, 233–270.

Jung, J. *et al.* (2006). Identification of a homozygous deletion in the AP3B1 gene causing Hermansky-Pudlak syndrome, type 2. Blood *108*, 362–369.

Kane, P. M. (2006). The where, when, and how of organelle acidification by the yeast vacuolar H+-ATPase. Microbiol. Mol. Biol. Rev. *70*, 177–191.

Klionsky, D. J., and Emr, S. D. (1989). Membrane protein sorting: biosynthesis, transport and processing of yeast vacuolar alkaline phosphatase. EMBO J. *8*, 2241–2250.

LaGrassa, T. J., and Ungermann, C. (2005). The vacuolar kinase Yck3 maintains organelle fragmentation by regulating the HOPS tethering complex. J. Cell Biol. *168*, 401–414.

Longtine, M. S., McKenzie, A., Demarini, D. J., Shah, N. G., Wach, A., Brachat, A., Philippsen, P., and Pringle, J. R. (1998). Additional modules for versatile and economical PCR-based gene deletion and modification in *Saccharomyces cerevisiae*. Yeast *14*, 953–961.

Lorenz, T. C., Anand, V. C., and Payne, G. S. (2008). High through-put protein extraction and immunoblotting analysis in *Saccharomyces cerevisiae*. Methods Mol. Biol. *457*, 13–27.

Nakamura, N., Hirata, A., Ohsumi, Y., and Wada, Y. (1997). Vam2/Vps41p and Vam6/Vps39p are components of a protein complex on the vacuolar membranes and involved in the vacuolar assembly in the yeast *Saccharomyces cerevisiae*. J. Biol. Chem. *272*, 11344–11349.

Nebes, V. L., and Jones, E. W. (1991). Activation of the proteinase B precursor of the yeast *Saccharomyces cerevisiae* by autocatalysis and by an internal sequence. J. Biol. Chem. *266*, 22851–22857.

Newell-Litwa, K., Seong, E., Burmeister, M., and Faundez, V. (2007). Neuronal and non-neuronal functions of the AP-3 sorting machinery. J. Cell Sci. *120*, 531–541.

Odorizzi, G., Cowles, C. R., and Emr, S. D. (1998). The AP-3 complex: a coat of many colours. Trends Cell Biol. *8*, 282–288.

Ostrowicz, C. W., Meiringer, C. T., and Ungermann, C. (2008). Yeast vacuole fusion: a model system for eukaryotic endomembrane dynamics. Autophagy *4*, 5–19.

Peden, A. A., Oorschot, V., Hesser, B. A., Austin, C. D., Scheller, R. H., and Klumperman, J. (2004). Localization of the AP-3 adaptor complex defines a novel endosomal exit site for lysosomal membrane proteins. J. Cell Biol. *164*, 1065–1076.

Peters, C., Bayer, M. J., Buhler, S., Andersen, J. S., Mann, M., and Mayer, A. (2001). Trans-complex formation by proteolipid channels in the terminal phase of membrane fusion. Nature *409*, 581–588.

Redding, K., Seeger, M., Payne, G., and Fuller, R. S. (1996). The effects of clathrin inactivation on localization of Kex2 protease are independent of the TGN localization signal in the cytosolic tail of Kex2p. Mol. Biol. Cell *7*, 1667–1677.

Rehling, P., Darsow, T., Katzmann, D. J., and Emr, S. D. (1999). Formation of AP-3 transport intermediates requires Vps41 function. Nat. Cell Biol. *1*, 346–353.

Roberts, C. J., Nothwehr, S. F., and Stevens, T. H. (1992). Membrane protein sorting in the yeast secretory pathway: evidence that the vacuole may be the default compartment. J. Cell Biol. *119*, 69–83.

Robinson, J. S., Klionsky, D. J., Banta, L. M., and Emr, S. D. (1988). Protein sorting in *Saccharomyces cerevisiae*: isolation of mutants defective in the delivery and processing of multiple vacuolar hydrolases. Mol. Cell. Biol. *8*, 4936–4948.

Robinson, M. S., and Bonifacino, J. S. (2001). Adaptor-related proteins. Curr. Opin. Cell Biol. *13*, 444–453.

Seals, D. F., Eitzen, G., Margolis, N., Wickner, W. T., and Price, A. (2000). A Ypt/Rab effector complex containing the Sec1 homolog Vps33p is required for homotypic vacuole fusion. Proc. Natl. Acad. Sci. USA *97*, 9402–9407.

Seaman, M. N., McCaffery, J. M., and Emr, S. D. (1998). A membrane coat complex essential for endosome-to-Golgi retrograde transport in yeast. J. Cell Biol. *142*, 665–681.

Seeger, M., and Payne, G. S. (1992). A role for clathrin in the sorting of vacuolar proteins in the Golgi complex of yeast. EMBO J. *11*, 2811–2818.

Seeger, M., and Payne, G. S. (1992b). Selective and immediate effects of clathrin heavy chain mutations on Golgi membrane protein retention in *Saccharomyces cerevisiae*. J. Cell Biol. *118*, 531–540.

Shaw, J. D., Hama, H., Sohrabi, F., DeWald, D. B., and Wendland, B. (2003). PtdIns(3,5)P2 is required for delivery of endocytic cargo into the multivesicular body. Traffic *4*, 479–490.

Spormann, D. O., Heim, J., and Wolf, D. H. (1992). Biogenesis of the yeast vacuole (lysosome). The precursor forms of the soluble hydrolase carboxypeptidase yscS are associated with the vacuolar membrane. J. Biol. Chem. *267*, 8021–8029.

Stepp, J. D., Huang, K., and Lemmon, S. K. (1997). The yeast adaptor protein complex, AP-3, is essential for the efficient delivery of alkaline phosphatase by the alternate pathway to the vacuole. J. Cell Biol. *139*, 1761–1774.

Sun, B., Chen, L., Cao, W., Roth, A. F., and Davis, N. G. (2004). The yeast casein kinase Yck3p is palmitoylated, then sorted to the vacuolar membrane with AP-3-dependent recognition of a YXXPhi adaptin sorting signal. Mol. Biol. Cell *15*, 1397–1406.

Suzuki, T., Oiso, N., Gautam, R., Novak, E. K., Panthier, J. J., Suprabha, P. G., Vida, T., Swank, R. T., and Spritz, R. A. (2003). The mouse organellar biogenesis mutant buff results from a mutation in Vps33a, a homologue of yeast vps33 and *Drosophila* carnation. Proc. Natl. Acad. Sci. USA *100*, 1146–1150.

Theos, A. C. *et al.* (2005). Functions of adaptor protein (AP)-3 and AP-1 in tyrosinase sorting from endosomes to melanosomes. Mol. Biol. Cell *16*, 5356–5372.

Traub, L. M. (2005). Common principles in clathrin-mediated sorting at the Golgi and the plasma membrane. Biochim. Biophys. Acta *1744*, 415–437.

Vancura, A., Sessler, A., Leichus, B., and Kuret, J. (1994). A prenylation motif is required for plasma membrane localization and biochemical function of casein kinase I in budding yeast. J. Biol. Chem. *269*, 19271–19278.

Vida, T. A., and Emr, S. D. (1995). A new vital stain for visualizing vacuolar membrane dynamics and endocytosis in yeast. J. Cell Biol. *128*, 779–792.

Vowels, J. J., and Payne, G. S. (1998a). A dileucine-like sorting signal directs transport into an AP-3-dependent, clathrin-independent pathway to the yeast vacuole. EMBO J. *17*, 2482–2493.

Vowels, J. J., and Payne, G. S. (1998b). A role for the lumenal domain in Golgi localization of the *Saccharomyces cerevisiae* guanosine diphosphatase. Mol. Biol. Cell *9*, 1351–1365.

Wang, X., Hoekstra, M. F., DeMaggio, A. J., Dhillon, N., Vancura, A., Kuret, J., Johnston, G. C., and Singer, R. A. (1996). Prenylated isoforms of yeast casein kinase I, including the novel Yck3p, suppress the gcs1 blockage of cell proliferation from stationary phase. Mol. Cell. Biol. *16*, 5375–5385.

Wang, Y. X., Catlett, N. L., and Weisman, L. S. (1998). Vac8p, a vacuolar protein with armadillo repeats, functions in both vacuole inheritance and protein targeting from the cytoplasm to vacuole. J. Cell Biol. *140*, 1063–1074.

Wang, Y. X., Kauffman, E. J., Duex, J. E., and Weisman, L. S. (2001). Fusion of docked membranes requires the armadillo repeat protein Vac8p. J. Biol. Chem. *276*, 35133–35140.

Weisman, L. S. (2006). Organelles on the move: insights from yeast vacuole inheritance. Nat. Rev. Mol. Cell Biol. *7*, 243–252.

Weisman, L. S., Bacallao, R., and Wickner, W. (1987). Multiple methods of visualizing the yeast vacuole permit evaluation of its morphology and inheritance during the cell cycle. J. Cell Biol. *105*, 1539–1547.

Winzeler, E. A. *et al.* (1999). Functional characterization of the *S. cerevisiae* genome by gene deletion and parallel analysis. Science *285*, 901–906.

Woolford, C. A., Daniels, L. B., Park, F. J., Jones, E. W., Van Arsdell, J. N., and Innis, M. A. (1986). The *PEP4* gene encodes an aspartyl protease implicated in the posttranslational regulation of *Saccharomyces cerevisiae* vacuolar hydrolases. Mol. Biol. Cell *6*, 2500–2510.

Wurmser, A. E., Sato, T. K., and Emr, S. D. (2000). New component of the vacuolar class C-Vps complex couples nucleotide exchange on the Ypt7 GTPase to SNARE-dependent docking and fusion. J. Cell Biol. *151*, 551–562.

Ybe, J. A., Brodsky, F. M., Hofmann, K., Lin, K., Liu, S. H., Chen, L., Earnest, T. N., Fletterick, R. J., and Hwang, P. K. (1999). Clathrin self-assembly is mediated by a tandemly repeated superhelix. Nature *399*, 371–375.

Yeung, B. G., and Payne, G. S. (2001). Clathrin interactions with C-terminal regions of the yeast AP-1 beta and gamma subunits are important for AP-1 association with clathrin coats. Traffic *2*, 565–576.

Yeung, B. G., Phan, H. L., and Payne, G. S. (1999). Adaptor complex-independent clathrin function in yeast. Mol. Biol. Cell *10*, 3643–3659.

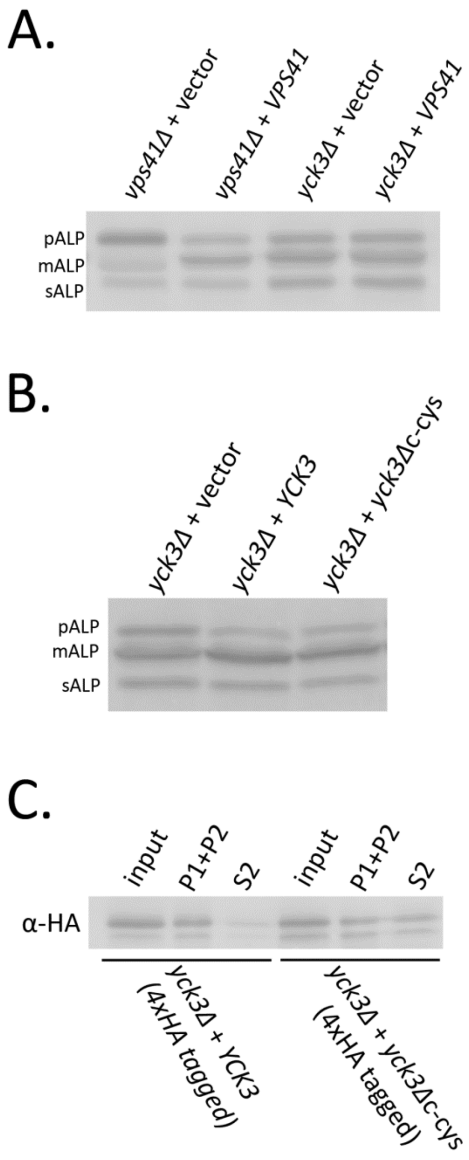
A.
vps41Δ + vector
vps41Δ + VPS41
yck3Δ + vector
yck3Δ + VPS41
pALP
mALP
sALP
B.
yck3Δ + vector
yck3Δ + YCK3
yck3Δ + yck3Δc-cys
pALP
mALP
sALP
C.
input
P1+P2
S2
input
P1+P2
S2
α-HA
yck3Δ + YCK3
(4xHA tagged)
yck3Δ + yck3Δc-cys
(4xHA tagged)

Figure S1.

A. *Overexpression of VPS41 does not rescue the ALP maturation defect in yck3Δ cells.* *VPS41* in pRS426 (+ *VPS41*) or pRS426 alone (+ vector) were transformed into *MAT*α and *MAT***a** *vps41Δ* and *yck3Δ* strains from the single gene deletion library. Three independent *MAT***a** transformants and three independent *MAT*α transformations from each strain were analyzed for ALP maturation defects by immunoblotting. A representative immunoblot from one of the six samples for each strain is shown. Note that multicopy *VPS41* reduces precursor ALP accumulation in *vps41Δ* cells but not *yck3Δ* cells. Bands were quantified in all samples as described in the methods section, a pALP/tALP ratio was determined, and an average pALP/tALP ratio and standard deviation were calculated for each strain. The difference of the ratios in *vps41Δ*+pRS426-*VPS41* compared with pRS426 was statistically significant ($p<0.001$) whereas the difference of the ratios for *yck3Δ*+pRS426 and *yck3Δ*+pRS426-*VPS41* was not ($p=0.3$).

B. *Palmitoylation of Yck3p is not essential for rescue of ALP defect in yck3Δ cells.* *MAT*α and *MAT***a** *yck3Δ* strains from the single gene deletion library were transformed with pRS316 vector alone (+ vector), 4xHA tagged *YCK3* in pRS316 (+ *YCK3*), or 4xHA tagged *yck3Δc-cys* (+ *yck3Δc-cys)* in pRS316. The *yck3Δc-cys* allele harbors a deletion of the C-terminal 8 residues (7 of which are cysteines) that prevents palmitoylation (Sun et al., 2004). As described above for panel A, six colonies from each transformation (three from each mating type) were analyzed for ALP maturation defects by immunoblotting. A representative immunoblot for ALP from one of the six samples for each strain is shown. Note that precursor ALP accumulation is reduced in cells expressing either wild-type or mutant Yck3p. Bands were quantified and pALP/tALP ratios were determined as described in A. The difference in ratios between *yck3Δ*+pRS316 and either *yck3Δ*+*YCK3* or *yck3Δ*+*yck3Δ*cys was statistically significant ($p < 0.001$ and $p < 0.002$ respectively). However the difference in ratios between *yck3Δ*+*YCK3* and *yck3Δ*+*yck3Δ*cys was not ($p = 0.14$).

C. *A fraction of palmitoylation-defective Yck3p remains sedimentable.* *MAT***a** *yck3Δ* cells expressing either 4xHA tagged wild-type (*yck3Δ + YCK3*) or palmitoylation-defective Yck3p (*yck3Δ + yck3Δc-cys*) were lysed and fractionated as described in the materials and methods with one difference. The cell lysate was subjected only to the 300xg spin to clear unbroken cells and large debris and then to the 100,000xg spin. "input" is the supernatant from the 300xg spin, "P1+P2" is the pellet from the 100,000xg spin, and "S2" is the supernatant from the 100,000xg spin. Samples were then processed as described in the materials and methods and immunoblots were performed using monoclonal α-HA antibody (Sigma). Note that about 50% of mutant Yck3p sediments in the P1 + P2 fraction.

Chapter 7

DISCUSSION

Discussion and Future Directions:

The initial observation that GFP- and RFP- tagged clathrin and clathrin adaptors localize to the Golgi in a predictable pattern, regardless of the size, shape and intensity of the puncta, has led to the underlying focus of this thesis. We initially sought to define the temporal relationship between each clathrin adaptor at the TGN, clathrin, and several TGN associated proteins (Chapter 2). Second, we dissected a detailed mechanism for adaptor recruitment, discovering that the beginning waves of clathrin adaptor recruitment are important for the correct spaciotemporal recruitment of later adaptors. Importantly, we identified Gga2p as a novel Pik1p recruitment factor. We showed that Gga2p recruits Pik1p to the TGN through a direct interaction, this interaction in turn is critical for normal PI(4)P accumulation. We have also determined that PI(4)P is a critical factor for AP-1 and Ent5p localization (Chapters 2 and 3).

Localization and stoichiometry of Pik1p at the TGN

Previous studies have identified Frq1p as essential for Pik1p localization (Strahl et al., 2003). When Frq1 is inactivated through temperature sensitivity, Pik1 is redistributed from the TGN membrane to the cytosol. In the absence of GGA proteins, Pik1p is delayed in its recruitment to the Golgi despite the presence of normally localized Frq1p. The differences in phenotypes in the absence of each of these proteins suggest that their contributions to Pik1p localization are not equivalent. What then are the relative contributions of GGA and Frq1 to Pik1p localization? Two possibilities for the differential contributions of the two proteins will be discussed. First, it is possible that Frq1p serves as a nucleating factor for the initial recruitment of Pik1p to the membrane. Pik1p would then initiate PI(4)P production which facilitates the recruitment of Gga2p to the membranes. GTP-Arf1p bound Gga2p would then be competent to

recruit additional Pik1p. The second possibility for the differential contributions of GGA and Frq1 may be accounted for by the specific subcompartmental localization of GGA and Frq1p.In this sense Pik1p would be under a two step targeting process, first to the TGN, through Frq1. Then it would be transferred laterally to a compartment specific for the generation of CCVs. In this way Pik1p could generate PI(4)P that is necessary for secretion from the TGN to the plasma membrane, and in a different subcompartment generate PI(4)P that is specific for the generation of CCVs.

We and others have also found that while Arf1 may not play a direct role in Pik1p localization, it does regulate PI(4)P production. The mechanism of PI(4)P production by Arf1p was poorly understood. We put forth data to support a model in which Arf1p modulates the conformation between the VHS and GAT domains of GGA proteins. This regulation is important because when the GAT domain is GTP-Arf1 bound, the VHS domain is then available for interacting with Pik1p (Chapter 3). We believe that it is this interaction which accounts for prior observations that Arf1p contributes to PI(4)P production (Audhya et al., 2000; Daboussi et al., 2012; Godi et al., 1999). Are there other implications for this regulatory mechanism? ARF interacts with the GAT domain solely when it is GTP bound. GTP-Arf1p undergoes a conformational change to reveal a myristoyl group which enables Arf1p association with the membrane. These data imply that Arf1p regulation of the Gga2p VHS-GAT domains occurs at the membrane and not in the cytosol. Pik1p also depends on another myristolated protein for localization to the TGN membrane, Frq1p (Graham and Burd, 2011).Taken together, these data suggest that this network of interactions occurs primarily at the membranes and not in the cytosol.

The composition of the GGA-Pik1p complex could have biological implications in vivo. Two results imply that the stoichiometry of the Pik1p-GGA interaction may not be 1:1. First, the the expression of Pik1p is lower than that of Gga2p (L.D., data not shown). Second, Pik1p has multiple Gga2p binding sites. This stoichiometry is potentially important for the localization and activity of Pik1p. If Pik1p requires multiple GGA proteins to properly localize then Pik1p would not be recruited until GGA reached a threshold concentration. The delay in Pik1p recruitment could enable GGA to interact with and cluster necessary cargo proteins, and accessory proteins. It may also be important that Pik1p is maximally recruited after Gga2p as a mechanism to delay the majority of PI(4)P production. This built in delay in Pik1p recruitment and PI(4)P production would serve to maintain the timing of AP-1 and Ent5, which are recruited after PI(4)P reaches its maximum. Biological consequences exist for AP-1 cargo proteins when the normal delay in PI(4)P production and AP-1 recruitment is removed (Daboussi et al., 2012).

Does Pik1p require Sec7p for Localization?

The TGN localizing protein, Sec7p has recently been reported to play a role in Pik1p localization. The GEF activity of Sec7p has been specifically implicated in this process. *Sec7-4*^{ts}, a temperature sensitive allele of Sec7p that specifically affects GEF activity, has been shown to disrupt Pik1p localization in vivo at the non-permissive temperature. The effects identified in vivo can arguably occur through a GGA dependent mechanism. Sec7p is a GTP exchange factor for Arf1p, GTP-Arf1p is important for opening the closed conformation of the VHS-GAT domains of GGA. GGA directly interacts with and is important for the appropriate temporal recruitment of Pik1p to the TGN. However, the authors also identified a direct interaction between the GEF domain of Sec7p and Pik1p(301-769). Based on these data, the authors argue that the Sec7p directly recruits Pik1p in vivo. These claims have not been

carefully evaluated and more work needs to be done to evaluate the role that Pik1p (301-769) plays in TGN localization.

The role of Clathrin in the Gga2p-Pik1p Interaction

Understanding the environment in which the Gga2p-Pik1p interaction takes place has implications for ccv biogenesis. One major question is whether this interaction does or does not take place under a clathrin coat. If yes, is Pik1p then included in the clathrin vesicle? If this interaction does take place at the TGN membrane, but not under a clathrin coat, how is it that clathrin is excluded from binding Gga2p? One possible answer lies in a recent report citing that in the absence of Ent5p, Gga2p does not as effectively bind clathrin in lysed cells (Hung et al.). This result suggests that cells need only exclude Ent5p to prevent effective clathrin recruitment. We have found that by live-cell microscopy only a portion of the Ent5p population is recruited with Gga2p whereas most Ent5p is recruited at a later time point with AP-1. This result is in agreement with our structured illumination microscopy data which revealed that Gga2 and Ent5 show only a small amount of colocalization. However, there are two main points of disagreement with the hypothesis that Gga2p requires Ent5p for proper clathrin binding in vivo. First, in vivo clathrin is recruited synchronously with Gga2, despite the lack of Ent5p being recruited to Gga2p positive puncta. Second, we have also found that Gga2p sets the timing for clathrin recruitment. In the absence of Gga2p clathrin recruitment is temporally delayed and assembles synchronously with AP-1. The disparity between the results in Daboussi et al., and Hung et al., may be attributable to differences observed in intact versus lysed cells, respectively. However, in the absence of a mechanism that prevents an interaction with Gga2p in vivo clathrin would be recruited to saturation. No such mechanism is currently known.

The possibility that Pik1p is recruited into vesicles so that it can be rapidly transported away from the TGN membrane could offer a mechanism to extinguish additional PI(4)P production. There is precident for this type of trafficking of kinases at the plasma membrane. For example, PI4KIIβ generates PI(4)P at the plasma membrane during ccv formation, and is also recruited into ccv vesicles. It is entirely possible that a similar mechanism may exist to include Pik1p, and PI4KIIIβ into ccvs forming at the TGN in both yeast and mammalian cells (Li et al., 2012).

Conservation of Mechanism

This process whereby the Gga2p-Pik1p interaction facilitates PI(4)P production so that AP-1 is efficiently recruited, may be conserved to humans. GGA, Arf1, Frq1 and Pik1 are conserved in higher order eukaryotes. However the *frq1* paralog, *ncs-1* is not detectably expressed in non-neuronal cell types. Therefore, it is unclear how PI4KIIIβ is recruited to membranes in the absence of this recruitment factor. Interestingly, in mammals, GTP bound Arf1p combined with cytosolic extract increases recruitment of PI4KIIIβ to membranes thereby stimulating PI(4)P production at liposomes (Godi et al., 1999). The components in the cytosol that synergize with Arf1p to cause this increase in PI4KIIIb recrutement are still unidentified. We speculate that the unidentified components in the cytosolic extract may be GGA proteins. We posit a regulatory mechanism of PI4KIIIβ by Arf1p, similar to that found in yeast given that: 1.) PI4KIIIβ directly interacts with the VHS domain of Gga2p (chapter 3) 2.) the mammalian Gga2p VHS and GAT domain directly interact (chapter 3) 3.) mammalian Arf1p also interacts with the mGAT domain . This network of known interactions is similar to those identified in yeast, and could serve as the minimum requirement of machinery necessary for PI4KIIIβ recruitment to the TGN.

Is there a hierarchy among AP-1 localization factors?

It is well established that AP-1 requires several different factors for proper localization, but is there any crosstalk between these factors that would set up a network of regulation?

Arf1p is recruited before all clathrin adaptors, when the Golgi still contains *cis*-, and *medial*- Golgi characteristics (L.D., unpublished observation). It is therefore the first known AP-1 localizing factor to be recruited to Golgi membranes. Arf1p is initially recruited at early timepoints when there is little, if any, PI(4)P at the Golgi. Sac1p, a lipid phosphatase is highly enriched in early compartments of the Golgi preventing accumulation of PI(4)P (Faulhammer et al., 2007). It is likely that Arf1p localizes to the Golgi via the ARF-GEFs Gea1p and Gea2p, which are present at the membrane at earlier stages of Golgi maturation. Transmembrane cargos also appear as puncta at the Golgi before the appearance of the clathrin adaptors. These considerations taken together suggest that it is unlikely that Arf1p localization to the TGN would be controlled by PI(4)P or is sufficient for Gga and AP-1 recruitment.

Arf1p interacts with the GAT domain of GGA proteins ((Collins et al., 2003; Puertollano et al., 2001). GAT domain bound to GTP-Arf1 regulates the interaction of the VHS domain with Pik1 (Chapter 3). Pik1p then generates PI(4)P at the membrane. In this sense Arf1p regulates the generation of PI(4)P production at the Golgi. This is consistent with previous experiments which have identified Arf1 as a PI(4)P promoting factor in vitro using mammalian proteins (Godi et al., 1999) and *arf1*Δ yeast cells as having less PI(4)P ((Audhya et al., 2000)). Presumably there is less PI(4)P because in the absence of Arf1 the Gga2p-Pik1p interaction is reduced.

Existing data points to a model in which AP-1 requires several different inputs from cargo, Arf, Laa1p and the lipid PI(4)P for optimal localization. There may be additional unknown factors that also contribute to AP-1 localization. However, of those factors which are known and

contribute to AP-1 localization, Arf1p acts as a 'master regulator,' controlling the recruitment of those factors.

Examples of Adaptor-Phosphoinositide Kinase Interactions

The idea that PIP Kinases are being enriched at specific subcellular localizations, based on how the clathrin adaptors are localized, offers a mechanism for localized generation of PIP, and then highly specific localization of vesicle related proteins that require PIP as a signal for recruitment (Craige et al., 2008). There have been several examples in which phosphoinositide kinases have been associated with clathrin adaptor complexes and incorporated into vesicles at the plasma membrane and endosomes. In mammals, at the plasma membrane PIPKIγi2 regulates AP-2 localization by directly binding to both the μ2 and γ2 subunit of AP-2. This interaction has a stimulatory effect on PIPKIγi2 activity (Kahlfeldt et al., 2010; Krauss et al., 2006). At the endosomes, AP-3 directly interacts with PI4KIIα via a dileucine sorting motif present in PI4KIIα. AP-3 and PI4KIIα show substantial colocalization in vivo. PI4KIIα has also been found to be a component of AP-3 vesicles (Craige et al., 2008; Salazar et al., 2009). Another example of PIP Kinases clathrin adaptor interdependency arises from the interaction between PIPKI γ-90 and AP-1. A three amino acid patch in μ1B is necessary for recruitment of AP-1B onto recycling endosomes containing PI(3,4,5)P3. Interestingly, a positive feedback loop may be driving accumulation of PI(3,4,5) P3, as PIPKIγ-90, the kinase that generates PIP3 depends on AP-1B for localization. Likewise, depletion of this lipid, using a PI3-Kinase inhibitor, results in the mislocalization of AP-1 from recycling endosomes and the depolarization of cargo to the apical plasma membrane. (Fields et al., 2010). Generation of PI(3,4,5)P3 may be a lipid specific for AP-1 sorting at the RE (Thompson et al., 2007).

What are the benefits of PIPkinase and adaptor protein interactions? These direct interactions offers a solution to the cell for the removal of the PIPKinase from the membrane through the incorporation of the kinase with the vesicle. The PIPKinase can also then generate a specific, highly localized pool of the phosphoinositide, promoting vesicle biogenesis. There are several outstanding questions as to how partitioning of membranes is achieved in vivo. However, these insights offer a beginning perspective on generating specificity at each type of membrane for each type of clathrin vesicle.

Endosomal Maturation in Yeast:

There are no known early endosomal markers in yeast. Biochemical and genetic data suggest that AP-1 and GGA function in between the TGN and endosomes, however the best characterized TGN marker colocalizes with both GGA and AP-1. The Golgi in yeast mature from cis-Golgi to trans-Golgi over time, and many maturation events of Golgi cisterna occurs in the same location from beginning to end. The early cis-Golgi marker GFP-Rer1, a retroviral receptor for endoplasmic retriculum membrane proteins, can be seen appearing as bright fluorescent puncta, increase in fluorescent intensity, and then disappear over time. The disappearance of the cis-Golgi marker also coincides with the appearance of later Golgi markers such as GFP-Sec7p. (Losev et al., 2006) (Matsuura-Tokita et al., 2006). Gga2 also colocalizes with the trans-Golgi marker Sec7p, in wildtype cells both of these proteins appear, disappear and reach peak fluorescent intensities synchronously. AP-1 partially colocalizes with Sec7p in still images (L.D. unpublished observation), and in live-cell imaging Sec7-mRFP is recruited first to membranes and is then followed by AP-1. Does this represent a different post-TGN compartment? If so, what is this compartment. We hypothesize that there is maturation from the TGN to the early endosomes in yeast. The TGN/ early endosomal compartment would be multi-functional, it

enables clathrin mediated trafficking, secretion to the plasma membrane, and would also act as an acceptor for newly endocytosed material, in the same manner as a traditional mammalian early endosome. Several questions still need to be addressed. What is the machinery at the TGN/EE that facilates acceptance of PM material and what machinery at these locations expedite sorting of the cargo to the correct downstream compartments?

Audhya, A., Foti, M., and Emr, S. D. (2000). Distinct Roles for the Yeast Phosphatidylinositol 4-Kinases, Stt4p and Pik1p, in Secretion, Cell Growth, and Organelle Membrane Dynamics. Molecular Biology of the Cell *11*, 2673-2689.

Collins, B. M., Watson, P. J., and Owen, D. J. (2003). The Structure of the GGA1-GAT Domain Reveals the Molecular Basis for ARF Binding and Membrane Association of GGAs. Developmental Cell *4*, 321-332.

Craige, B., Salazar, G., and Faundez, V. (2008). Phosphatidylinositol-4-Kinase Type II Alpha Contains an AP-3 sorting Motif and a Kinase Domain That Are Both Required for Endosome Traffic. Molecular Biology of the Cell *19*, 1415-1426.

Daboussi, L., Costaguta, G., and Payne, G. S. (2012). Phosphoinositide-mediated clathrin adaptor progression at the trans-Golgi network. Nat Cell Biol *14*, 239-248.

Faulhammer, F., Kanjilal-Kolar, S., Knödler, A., Lo, J., Lee, Y., Konrad, G., and Mayinger, P. (2007). Growth Control of Golgi Phosphoinositides by Reciprocal Localization of Sac1 Lipid Phosphatase and Pik1 4-Kinase. Traffic *8*, 1554-1567.

Fields, I. C., King, S. M., Shteyn, E., Kang, R. S., and Folsch, H. (2010). Phosphatidylinositol 3,4,5-trisphosphate Localization in Recycling Endosomes Is Necessary for AP-1Bâ€“dependent Sorting in Polarized Epithelial Cells. Molecular Biology of the Cell *21*, 95-105.

Godi, A., Pertile, P., Meyers, R., Marra, P., Di Tullio, G., Iurisci, C., Luini, A., Corda, D., and De Matteis, M. A. (1999). ARF mediates recruitment of PtdIns-4-OH kinase-[bgr] and stimulates synthesis of PtdIns(4,5)P2 on the Golgi complex. Nat Cell Biol *1*, 280-287.

Graham, T. R., and Burd, C. G. (2011). Coordination of Golgi functions by phosphatidylinositol 4-kinases. Trends in Cell Biology *21*, 113-121.
Hung, C.-W., Aoh, Q. L., Joglekar, A. P., Payne, G. S., and Duncan, M. C. Adaptor Autoregulation Promotes Coordinated Binding within Clathrin Coats. Journal of Biological Chemistry *287*, 17398-17407.

Kahlfeldt, N., Vahedi-Faridi, A., Koo, S. J., SchÃ¤fer, J. G., Krainer, G., Keller, S., Saenger, W., Krauss, M., and Haucke, V. (2010). Molecular Basis for Association of PIPKI gamma-p90 with Clathrin Adaptor AP-2. Journal of Biological Chemistry *285*, 2734-2749.

Krauss, M., Kukhtina, V., Pechstein, A., and Haucke, V. (2006). Stimulation of phosphatidylinositol kinase type I-mediated phosphatidylinositol (4,5)-bisphosphate synthesis by AP-2 mu cargo complexes. Proceedings of the National Academy of Sciences *103*, 11934-11939.

Li, J., Barylko, B., Johnson, J., Mueller, Joachim D., Albanesi, Joseph P., and Chen, Y. (2012). Molecular Brightness Analysis Reveals Phosphatidylinositol 4-Kinase II beta Association with Clathrin-Coated Vesicles in Living Cells. Biophysical journal *103*, 1657-1665.

Losev, E., Reinke, C. A., Jellen, J., Strongin, D. E., Bevis, B. J., and Glick, B. S. (2006). Golgi maturation visualized in living yeast. Nature *441*, 1002-1006.

Matsuura-Tokita, K., Takeuchi, M., Ichihara, A., Mikuriya, K., and Nakano, A. (2006). Live imaging of yeast Golgi cisternal maturation. Nature *441*, 1007-1010.

Puertollano, R., Randazzo, P. A., Presley, J. F., Hartnell, L. M., and Bonifacino, J. S. (2001). The GGAs Promote ARF-Dependent Recruitment of Clathrin to the TGN. Cell *105*, 93-102.

Salazar, G., Zlatic, S., Craige, B., Peden, A. A., Pohl, J., and Faundez, V. (2009). Hermansky-Pudlak Syndrome Protein Complexes Associate with Phosphatidylinositol 4-Kinase Type II Î± in Neuronal and Non-neuronal Cells. Journal of Biological Chemistry *284*, 1790-1802.

Strahl, T., Grafelmann, B., Dannenberg, J., Thorner, J., and Pongs, O. (2003). Conservation of Regulatory Function in Calcium-binding Proteins: HUMAN FREQUENIN (NEURONAL CALCIUM SENSOR-1) ASSOCIATES PRODUCTIVELY WITH YEAST PHOSPHATIDYLINOSITOL 4-KINASE ISOFORM, Pik1. Journal of Biological Chemistry *278*, 49589-49599.

Thompson, A., Nessler, R., Wisco, D., Anderson, E., Winckler, B., and Sheff, D. (2007). Recycling Endosomes of Polarized Epithelial Cells Actively Sort Apical and Basolateral Cargos into Separate Subdomains. Molecular Biology of the Cell *18*, 2687-2697.